University of Alberta

Prey–taxis and its Applications.

by

Jung Min Lee 

A thesis submitted to the Faculty of Graduate Studies and Research in partial fulfillment of the requirements for the degree of Doctor of Philosophy

in

Applied Mathematics

Department of Mathematical and Statistical Sciences

Edmonton, Alberta

Fall 2006

Your file Votre référence
ISBN: 978-0-494-23063-3
Our file Notre référence
ISBN: 978-0-494-23063-3

Abstract

A characteristic feature of living organisms is that they respond to the environment in search for food and reproductive opportunity. In particular, predators can move towards high prey density, which is called *prey–taxis*. In this thesis we investigate how predators actively react to the spatial configuration of the prey on the landscape rather than passively respond, relying on random movement. We derive carefully a prey–taxis model. For that we use a modified Kareiva–Odell approach and finally a parabolic limit gives rise to a prey–taxis model. Alternatively we derive a prey–taxis model from a model with resting stages. We incorporate prey–taxis into spatial predator–prey dynamics and study a role of prey–taxis on spreading prey population and pattern formation. We find that prey–taxis alone does not slow prey spread although it does in the presence of an Allee effect for the prey. However, prey–taxis does tend to reduce the occurrence of dispersal–induced instability in predator–prey systems, where predator diffusion is crucial to dispersal–induced instability. In a special case, a Lyapunov function can be constructed for the purpose of studying global stability. We also explore some features of a predator–prey–taxis model by means of numerical simulations. Fractional step methods are described as the framework for simulations. For each case of the diffusion, advection, and reaction terms, the Crank–Nicolson scheme, the Nessyahu–Tadmor scheme, the second–order explicit Runge–Kutta method are considered respectively.

Acknowledgement

I would like to thank my supervisors Dr. Mark Lewis and Dr. Thomas Hillen. This thesis has been greatly improved by insightful suggestions, helpful advice and passionate encouragement from Dr. Mark Lewis and Dr. Thomas Hillen. I would also like to thank my committee members Dr. Walter Allegretto, and Dr. Fangliang He, Dr. Chris Cosner, and Dr. Gerda de Vries for their insight and suggestions into the research. In particular, I would like to thank Dr. Gerda de Vries and Dr. Chris Cosner for many helpful comments on editing and revising this thesis.

I would also like to thank to all the members of the Lewis lab for your encouragement and feedback which have improved this thesis. I thank Christina Cobbold, Tomas de-Camino-Beck, Raluca Eftimie, Chris Jerde, Marty Krkosek, Frithjof Lutscher, Hannah Mckenzie, Peter Molnar, Bill Nelson, Erik Noonburg, AnneMarie Pielaat, and Thomas Robbins. In particular, I would like to thank to Caroline Bampfylde and Marjorie Wonham for kindly helping me editing this thesis and Alex Potapov for his insightful ideas and helpful suggestions. I also thank my fellow graduate students in the Department of Mathematical and Statical Sciences at University of Alberta.

I would like to thank to Ben Marchant for sending his thesis and numerical codes.

I would like to thank to my parents, my sister, my brother–in–law, and my two nieces for their their love and support. I would also like to thank my best friends in Korea.

Contents

List of Tables

List of Figures

Chapter 1

Introduction

Mathematical modeling has provided useful tools to understand biological phenomena such as disease spread, insect outbreak, animal coat patterns, wound healing, and interspecific interactions. There are three main types of interspecific interaction: predator–prey, competition, and mutualism. In a predator–prey relationship, the predator species benefits from killing and consuming the prey species, and the prey population may be regulated as a result.

Predation rates are determined to some extent by the predator's level of satiation, or gut fullness. The goal of this thesis is to investigate how predators react spatially to prey, depending on their satiation level. In particular, first, we focus on understanding the underlying mechanisms for predator dispersal towards high prey density, a phenomenon called prey–taxis. Second, we explore how these mechanisms generate spatial patterns such as traveling wave in predator–prey interactions.

This research is motivated by the interesting paper written by Kareiva and Odell [46] (1987). They investigated the phenomenon that predators (ladybugs) tend to search for food in areas of higher prey (aphids) density, and derived the mechanism for this non–random foraging. Based on this mechanism, they studied predator aggregation in high prey density areas and produced realistic aggregation simulations based on field data. Since the mechanism of modeling was analogous to chemotaxis, they coined the term prey–taxis for this phenomenon. Although their research has potential applications to various ecological phenomena, few papers have been published on prey–taxis in the two decades since the original 1987 study. One of the main reasons for this hiatus is the difficulty of collecting empirical evidence of prey–taxis. However, new technologies such as field video recording and computer motion analysis (see [96, 97]) may enable us to collect the necessary but difficult field data including moving speed and turning rates. Thus, it is an opportune moment to reintroduce the concept of prey–taxis and resume active research on it.

This research is different from that of Kareiva and Odell in several aspects. First, we use rescaling to obtain a parabolic limit to the original hyperbolic system rather than simply using a quasi–steady state assumption as in Kareiva and Odell. Second, we use Poisson processes to derive turning rates, rather than a third–degree polynomial as in Kareiva and Odell. Third, we also consider various types of functional responses, which determine the nature of local population dynamics, satiation dynamics and predator dispersal. This differs from the approach of Kareiva and Odell, who used Type II functional response and considered that local population dynamics of the predator stems only from emigration of

the predator. Fourth, we show there is another way to derive prey–taxis models from the limit of the resting models, in which we consider resting state in addition to right–and left–moving states. Fifth, using different local population dynamics of the predator, population growth corresponding to the prey density and decaying exponentially without the prey instead of the emigration in Kareiva and Odell, we look for traveling wave solutions and pattern formation.

In the following sections, we briefly describe predator–prey models, numerical simulations, travelling wave solutions, and pattern formation. Chemotaxis models which motivated the idea of prey–taxis are described. Because functional responses are an important factor in determining the population dynamics of predators interacting with prey, and regulate the mechanism for predator dispersal, we discuss them in a separate section. Finally, we give an outline of Chapters 2–7.

1.1 Predator–Prey Models

In this section, we discuss various forms of predator–prey models. Predator–prey models have been studied by numerous people using different frameworks, such as discrete models [29], ODE models [99, 5], and diffusion–reaction models [72, 73]. In spatially homogeneous models, the temporal variation in each species is considered explicitly and the effects of their movement are considered implicitly. In contrast, diffusion–reaction models describe spatial structures explicitly by means of diffusive motility of species in heterogeneous environments, and describe temporal structures via reaction terms. In these models, the effects of movement on predator–prey interactions may play an important role in generating spatial patterns (see Murray [68]). Diffusion equations have shown that the movement of insects and other animals may be very significant [71]. For example, constant diffusion may increase the chance that predators find prey and therefore survive. Models also have shown how predators aggregate around high prey density [46] and move towards stimuli [58]. Furthermore, the inclusion of directional movement towards prey–rich environments seems to increase the chance of predator survival in a heterogeneous prey distribution.

Predator–prey systems may not always be presented in a continuum model. In a patchy predator–prey model, predator and prey are assumed to recognize the environment as discrete patches. Thus, the dispersal of prey and predator is formulated in the form of migration among patches, rather than in the form of continuous diffusion or advection. In his thesis [41], Huang assumed that predator foraging activity is the main mechanism by which predators move from one patch to another instantaneously. By considering mobile and immobile states respectively as well as searching and handling states in the classical Holling time budget argument, he formulated four states of the predator population, i.e., mobile–searching state, immobile–searching state, mobile–handling state, and immobile–handling state. Immigration and emigration of the predator occur during mobile searching and mobile handling states. When the prey is also dispersing, he showed that diffusion–driven instability may occur for small predator migration rate. Huang considered how cross–migration can be generated under the assumption that the predator population has a behavioral subgroup with quick transitions between subgroups occurring on a faster time scale. This quasi–steady–state assumption in the behavioral transitions produces cross–migration in the total predator population model. A strong response of predator in the case of a cross–emigration response is shown to be able to stabilize an unstable system

rather than to generate diffusive instability.

In this thesis, we focus on the continuous environment rather than discrete patches. Specifically, we extend the diffusion–reaction model to incorporate the concept of taxis into spatial predator–prey systems. We save the remainder of this section for the development of the first prey–taxis equation and its subsequent works. We first describe the concept of taxis.

A characteristic feature of living organisms is that they respond to the environment in search for food and reproductive opportunity. One such response is movement toward or away from an external stimulus, which is called *taxis*. Taxis is facilitated by both directional behaviours– change of velocity, and turning angle (higher dimension), and nondirectional behaviours–change of speed or turning rate in response to stimulus (see Okubo [70]). Corresponding to the type of external stimulus, various types of taxis are defined, such as aerotaxis, chemotaxis, geotaxis, haptotaxis, prey–taxis and others. The purposes of taxis may be numerous, including movement toward food and fleeing from enemies. Taxis can thus provide mechanism for optimal foraging [76, 77].

Now we incorporate the concept of taxis into spatial predator–prey models. Temporal predator–prey models describe the interaction of predators with prey over a period of time. In the simplest form, it is assumed that when a predator encounters a prey, the predator may kill the prey and consume it. This may result in the growth of the predator population and decline in the prey population. Thus, predator growth depends on the prey. The prey is assumed to have self-limitation such as a logistic growth. In addition, the predator population decreases exponentially without prey. However, the above assumptions do not tell us how the predator–prey interactions occur spatio–temporally. To fully explain the spatial interaction between the two species, an important aspect is whether the predator perceives the heterogeneous spatial distribution of the prey.

In chemotaxis models, organisms respond to an external chemical stimulus. Kareiva and Odell [46] extended the idea of chemotaxis to an insect predator–prey model, in which the prey plays the role of stimulus and the predator indirectly senses the external stimulus only via internal satiation. They assumed that predators do not necessarily have the memory to recognize prey, and cannot estimate prey density. External ways by which the predator can sense prey, such as visual and olfactory abilities, were excluded. The only method by which the predator can detect the prey density is through its own gut fullness. In other words, when the predator is satiated, prey density is high and when it is not, prey density is low. Predator movement is determined by the level of satiation. Hence, it is interesting to study the direct relationships between satiety and prey density and its effects on the predator foraging strategy. To model this process, we consider the satiety as another space and time dependent compartment and investigate how satiety combined with predator motility generate foraging strategy in complex environments.

The characteristic feature of prey–taxis equations is that taxis is incorporated into dispersal terms as an advection term. This result can be obtained via approximation procedures. Predator–prey–taxis equations were successfully derived in [46] under a so–called quasi-steady state assumption, which was used both to derive the chemotaxis equations and to estimate the relevant model parameters from experimental data. Macroscopic predator–prey interaction equations are derived from the individual movement behaviours which give a spatial connection of local predator–prey interactions. There may be various approaches to obtain prey–taxis equation. One such approach is that which Hillen and Stevens [35]

used to derive chemotaxis equations from the parabolic limit of hyperbolic equations. The similarity between chemotaxis and prey–taxis comes from the fact that both share the concept of taxis. Thus, the development of the prey–taxis equation inherited those ideas from the case of chemotaxis. However,we note the main following difference between chemotaxis and prey–taxis equations. Unlike most chemicals, satiety in prey–taxis does not diffuse independent of the predator population. The movement of predator population, moreover, depends directly on satiety rather than on prey density itself. It is thus one of the topics of this thesis to extract satiety equations related to the individual movement of predators.

In contrast to the rich development of chemotaxis models, the subsequent works of prey–taxis model are quite limited. Here we review the subsequent works of prey–taxis model after Kareiva and Odell introduced their prey–taxis model in 1987. The original ideas of Kareiva and Odell were modified in [9] by Cantrell and Cosner to allow the predator and the prey to recognize the environment in different ways; relatively high motility of the predator helps the predator experience the environment as the collection of patches. Thus, the model of Cantrell and Cosner focuses on emigration and immigration of the predator between patches. The model thus includes no predator diffusion and taxis terms. It is assumed that the prey move slowly and do not jump between patches. These assumptions naturally generate multiple temporal and spatial scales; for the temporal scales, predator dispersal was considered as very fast, prey dispersal and reproduction were moderately fast, and predator reproduction was slow. For the spatial scales, the predator operates on a large spatial scale and the prey on a small scale. For the immigration and emigration rate of the predator, Cantrell and Cosner considered two aspects: the size of the patch, and the other is the average prey density with finite and infinite supply of the predator from the air around the patch. Under certain conditions, maximum and minimum patch sizes were calculated for the prey to survive without extinction.

The model in [9] was applied in [10] to the situation in which the introduced species competes with the resident species for the prey. To understand foraging strategies in the competition between two different predator species, Cantrell and Cosner investigated the role of the emigration rates. To compare foraging strategies adapted by different species, they used the net rates of energy uptake of the old and new species.

The Kareiva and Odell model was applied to estimate the mean travel time of a predator to reach a prey resource. To do so, Grünbaum [23] focused on the predator dispersal term in the absence of the predator population dynamics. He introduced two statistical indicators. One is the expected payoff of satiety per predator per unit of time as a foraging strategy, and the other is the travel time statistic of how quickly a predator finds and aggregates around a prey. He introduced a family of turning rates with one free parameter called the turning threshold λ. Then he compared the success of two predator species who used different foraging strategies by means of different turning thresholds.

In this section, we reviewed predator–prey models and introduced the development of the prey–taxis model by Kareiva and Odell [46]. In the next section, we will discuss chemotaxis models, which gave a motivation for the prey–taxis model.

1.2 Chemotaxis

In this section, we review the history of the chemotaxis equation, highlighting developments that will inform the remainder of this thesis, that is, model derivation, model approximation,

travelling wave connections, and pattern formation. We begin by describing the concept of chemotaxis which inspired the concept of prey–taxis.

In chemotaxis models, an individual's dispersal consists of two processes: the first is random motion, and the second is movement up a chemical density gradient, which is considered as chemotaxis.

In earlier work, a chemotactic interaction model was formulated for amoebae with three chemicals: acrasin, acrasinase, and a complex from the kinetic reaction between acrasin and acrasinase. Keller and Segel [47] assumed that amoebae move up the acrasin gradient. Under the assumptions that the chemical complex is at steady state and that the total concentration of enzymes is constant, they studied amoeba aggregation by finding the instability conditions driven by the diffusion and advection of amoebae and acrasin.

In 1971, this chemotaxis (Keller–Segel) model was further applied by Keller and Segel [48] to explain travelling bands of the motile bacterium *Escherichia coli*. They used a pair of coupled PDEs,

$$\frac{\partial s}{\partial t} = -kb + D\left[\frac{\partial^2 s}{\partial x^2}\right], \tag{1.1}$$

$$\frac{\partial b}{\partial t} = \frac{\partial}{\partial x}\left[\mu(s)\frac{\partial b}{\partial x}\right] - \frac{\partial}{\partial x}\left[b\chi(s)\frac{\partial s}{\partial x}\right], \tag{1.2}$$

where k is the consumption rate of the substrate, s the density of the substrate, D a constant diffusion coefficient of the substrate, b the density of bacteria, $\mu(s)$ a diffusion coefficient of bacteria, and $\chi(s)$ chemotactic sensitivity of the bacterium.

Parabolic systems such as (1.1) and (1.2) may arise from related hyperbolic models. In subsequent work, a parabolic model was approximated from a hyperbolic model in the papers [79, 80]. In the parabolic model, the organisms move in response to an external chemical signal with a quasi–steady state assumption. The external chemical signal is assumed to diffuse after it is produced from the organism.

In a similar approach, the Keller–Segel equation can also be obtained via the parabolic limit process of their hyperbolic model for chemotaxis. Hillen and Stevens [35] showed this by considering right moving and left moving subgroups whose movements are determined by a one space dimensional hyperbolic model with chemotaxis. The turning rates and velocity of the two subgroups are assumed to depend on an external stimulus, which follows the diffusion–reaction equation. They also proved existence of a unique solution for a hyperbolic chemotaxis equation with spatio–temporally variable stimulus.

Further discussion of one–dimensional hyperbolic models and a multi–dimensional transport model for chemotactic movements was carried and some known results for the Patlak–Keller–Segel model were reviewed in Hillen's review paper [33].

Independently, a chemotaxis advection term was introduced into the Lotka–Volterra equations by Pettet and McElwain [75] to describe angiogenesis and wound healing. In this model, a chemotactic sensitivity is independent of the density of the chemoattractant. Thus the capillary tip n moves in response to a gradient of chemoattractant a produced by macrophages as follows

$$\frac{\partial n}{\partial t} = f(n,a) - \chi\frac{\partial}{\partial x}\left[n\frac{\partial a}{\partial x}\right], \tag{1.3}$$

$$\frac{\partial a}{\partial t} = g(n,a), \tag{1.4}$$

where $f(n,a)$ and $g(n,a)$ are local population dynamics of n and a respectively. They found conditions for the existence of continuous travelling wave solutions, which connect the wounded state and the healed state (heteroclinic orbits). Equations (1.3) and (1.4) are transformed with travelling wave coordinates $z = x - ct$

$$f_2(n,a)\frac{\partial n}{\partial z} = f_1(n,a), \tag{1.5}$$

$$\frac{\partial a}{\partial z} = g_1(n,a), \tag{1.6}$$

where $\frac{\partial a}{\partial z}$ in (1.5) is replaced with $g_1(n,a)$. They also recognized that heteroclinic orbits may not always be connected due to a so–called 'wall of singularities' when $f_2(n,a) = 0$. No trajectory can cross this 'wall of singularities' because equation (1.5) is undefined on the 'wall'. They mentioned that when a 'wall of singularities' occurs, additional analyses other than the usual phase plane analysis are required for equations (1.5) and (1.6).

The analysis of Pettet and Mcelwain was continued by Landman et al. [52] based on the phase plane analysis and hyperbolic theory used by Marchant [64], in which a discontinuous travelling wave solution was considered. In another article, Landman et al. [53] considered how cells with chemotactic migration colonize uniformly growing domains via the chemoattractant wavefront. The mobility of each species is enhanced in an additional convection term by the local velocity of domain growth, $v(x,t)$ and the reproduction dynamics of migrating cells is assumed not to depend on a chemoattractant.

The bacteria *E. coli* and *S. typhimurium* are observed to generate patterns associated with chemotaxis toward the asparate concentration in a liquid medium, under the assumption that succinate concentration is constant. Although linear analysis of this system showed no pattern formation, Tyson et al. [94] explained how initial patterns appeared but then disappeared as the chemotactic response saturated. In another paper [93], they included the dynamics of succinate concentration in the reaction with bacteria density, and from numerical simulations found three types of patterns: (i) aggregates occur temporally in liquid medium, (ii) *S. typhimurium* generates a thin bacterial lawn and stationary rings as the lawn expands in semi–solid medium. (iii) *E. coli* forms a swarm ring initially and then aggregates in semi–solid medium.

In this section, we discussed chemotaxis models, which motivated the prey–taxis model ([46]). For chemotaxis models, discontinuous wave solutions were considered and spatial patterns have been studied analytically and numerically. In the subsequent sections, we will discuss numerical simulations, travelling wave solutions, and pattern formation.

1.3 Numerical Simulations

Here we briefly review numerical methods for the numerical simulations in this thesis. The models we study consist of three parts: reactions terms, diffusion terms, and advection term.

Models for slime molds and for bacteria in Dolak and Hillen [16], which share those three components, were analyzed numerically for pattern formation. To do this, a fractional step method was used: a one–step implicit method for the reaction terms, a standard alternating direction implicit method for the diffusion terms, and the Lax–Wendroff scheme for the advection terms. This fractional method enabled us to choose the most efficient and

accurate methods available for each component of the model. Since advection terms are treated as a hyperbolic system by the fractional step methods [95], the numerical scheme for the advection terms has to be chosen carefully.

For advection terms Tyson et al. [95] use high–resolution methods, which are based on the Godunov method, implemented in the CLAWPACK package (see [55] for details). We used high resolution central schemes rather than the Godunov method on CLAWPACK because first, we may easily extend one–dimensional codes to higher dimensional ones and two species to more than three species and second, high resolution central schemes are more easily implemented, but still show accurate simulation results.

For diffusion and reactions terms, we use the Crank–Nicolson scheme and a second order Runge–Kutta scheme, respectively.

In summary, in this research we implement efficient and accurate numerical methods for each terms via a fractional step method by using MATLAB.

1.4 Travelling Wave Solutions

So far, we have discussed the study of models: chemotaxis models and predator–prey models closely related to our own and the numerical simulations of models. We now briefly describe the two analysis approaches for our models; travelling waves in this section and pattern formation in the following section. In this thesis, travelling wave solutions represent both species invasion (prey) and territory expansion (predator).

Travelling wave fronts are solutions to partial differential equations (PDE), which have fixed shape and translate at a constant speed as time evolves. These waves are described by the so called travelling wave coordinate, $z = x - ct$ with wave velocity c. If $U(z) = u(x,t)$ denotes the solution of the PDE, then U is called the profile of the travelling wave. Murray [68] illustrates the calculations of travelling wave solutions for various equations including the Fisher equation. In the Fisher equation, the diffusion process combined with logistic population growth is used to investigate genetic propagation in one dimensional space (Fisher (1937), see [68] for detailed discussion). Since then, the Fisher equation has been studied extensively in population biology and ecology. The Fisher equation

$$\frac{\partial u}{\partial t} = ku(1-u) + D\frac{\partial^2 u}{\partial x^2}, \tag{1.7}$$

where k is an intrinsic growth rate and D a constant diffusion coefficient, is one of the simplest models that generate a biological travelling wave solution like the one shown in Figure 1.1. Travelling wave solutions can be found using the ansatz $u(x,t) = U(z)$. The PDE translates into a system of ODE's in the travelling wave coordinate z, with specific boundary conditions at $z \to \pm\infty$. In the ODE system, the travelling wave front solutions appear as heteroclinic orbits that connect a saddle point to a stable equilibrium or to a stable limit cycle. For instance, under the travelling coordinate and rescaling of time and space, the Fisher equation turns into

$$U'' + cU' + U(1-U) = 0, \tag{1.8}$$

where c is the wave speed with the boundary conditions

$$U(-\infty) = 1 \text{ and } U(\infty) = 0. \tag{1.9}$$

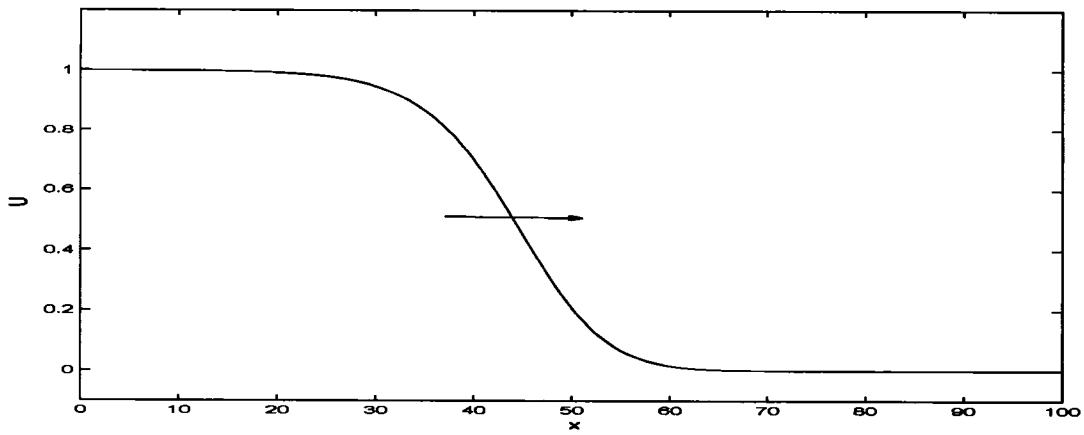

Figure 1.1: Travelling wave simulation for the Fisher equation (1.7) with $k = 0.8$ and $D = 10$.

Phase plane analysis is used to seek heteroclinic orbits (see Figure 1.2). When the wave speed c passes the threshold $c = 2$, a biologically reasonable heteroclinic orbit begins to be generated, that is, there is a non–negative population density. For the scaled Fisher equation (1.8), $c \geq 2$ guarantees a nonnegative heteroclinic orbit. Applied to predator–prey models, travelling wave front solutions represent the spatial transition of the saddle point through the unstable manifold to the stable coexistence equilibrium. They show how the predators invade an area where prey has already stabilized to its carrying capacity. Dunbar [17, 18, 19] demonstrated the existence of various travelling wave trains (travelling wave solutions which show periodic behaviours) and travelling front solutions for a diffusive predator-prey system. Huang [40] extended Dunbar's result to the case that prey has diffusion term as well. When prey dynamics are regulated by an Allee effect, predator-prey systems with constant diffusion terms for both species have a unique travelling wave solution [21]. Here an Allee effect is negative population growth at low densities due to various mechanisms such as a lower chance of finding mates, less efficient group defense, and so forth [1, 57].

1.5 Pattern Formation

We now describe the second analysis direction for our derived models, that is, pattern formation. Let us assume for now that, in the absence of dispersal, solutions of a predator–prey system converge to a coexistence steady state or a limit cycle. The first case corresponds to a spatially uniform pattern in prey and predator densities. However, the introduction of dispersal with diffusion may generate spatially non-uniform patterns. In general, diffusion terms tend to give rise to homogeneous densities over long time. In some cases, however, heterogeneous spatial patterns can result (diffusion-induced instability [70], Turing instability). Diffusion-induced instability describes the situation where, in the absence of diffusion, the homogeneous steady state is stable to small perturbations, but a diffusion process makes it unstable to small spatial perturbations. Murray [68] showed various models which exhibit diffusion–driven instability, and found necessary and sufficient conditions for pattern

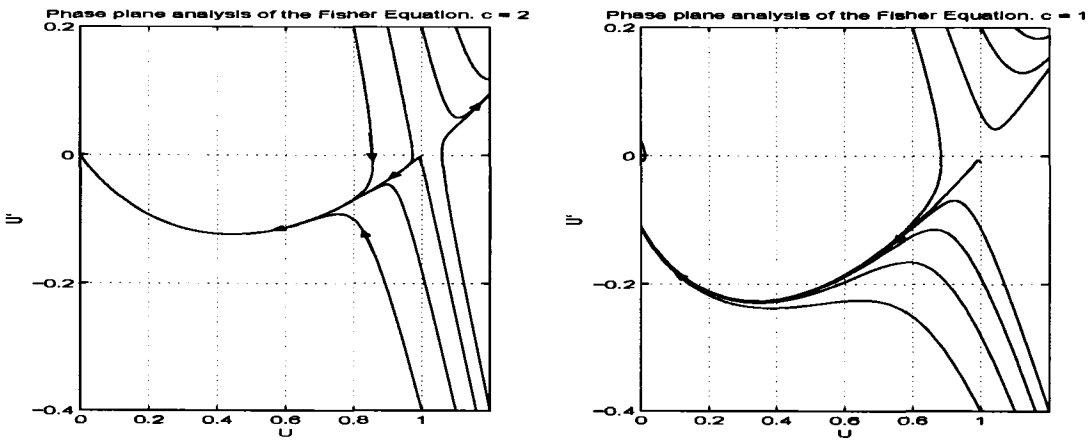

Figure 1.2: Travelling wave simulations for the Fisher equation (1.7) with $c = 2$ and $c = 1$.

formation. Zero flux boundary conditions are usually used to avoid boundary effects on the pattern. Hillen [31] found that a Turing model with correlated random walk produces a spatially unstable constant equilibrium under certain conditions for turning rates and speeds. Lewis [56] showed that a spatial pattern may occur in a plant–herbivore model, in which only herbivores are assumed to move with random motion, herbivory–taxis, and density dependent aggregation.

To analyze our models, we first look at systems that are stable to small perturbations without diffusion, but unstable to small perturbations with diffusion. Therefore, we can use the linear stability analysis, and look for solutions in the form

$$n, v \approx \exp(\lambda t), \tag{1.10}$$

where the frequency λ is an eigenvalue, n is the predator density, and v is the prey density. A positive eigenvalue, $\lambda > 0$ implies that the densities of the prey and the predator increase exponentially for a short time. We also define a time–independent solution of $n(x,t)$, $v(x,t)$ satisfying the spatial eigenvalue problem defined by

$$n_{xx} + k^2 n = 0 \text{ and } v_{xx} + k^2 v = 0 \tag{1.11}$$

with $n_x = 0$ and $v_x = 0$ on the boundary. Here, we consider a small perturbation of the system temporally and spatially around the steady state. After solving the eigenvalue problem defined above, we have eigenfunctions $n_k(x)$, $v_k(x)$ corresponding to the wavenumber k. The linearity of the problem gives the superimposed solution as follows:

$$n(x,t) = \sum_k A_k \exp(\lambda t + ikx), \tag{1.12}$$

$$V(x,t) = \sum_k B_k \exp(\lambda t + ikx), \tag{1.13}$$

where the constants A_k, B_k are determined by a Fourier expansion of the initial conditions, but these constants are not used. Substituting these $n(x,t)$ and $V(x,t)$ into the linearized

system about the steady state, we get the eigenvalues λ in terms of the wavenumber k. As time increases, modes with $\lambda(k) > 0$ grow and other modes decline exponentially to zero. Thus, we can find the range of the wavenumber k for diffusive instability and obtain the wave length corresponding to k such that if the domain is small compared to this wavelength, diffusive instability will not occur. Using this property, we can determine a critical domain size and a maximum population for persistence of the prey population (See Murray [68]). This has applications to the problem of the pest population at a refuge level (Ecological control strategy : When and where to release biological control agents to reduce the pest population).

Prey–taxis allows predators to search more actively for prey, and can generate different spatial patterns from those in models with only predator diffusion. Kareiva (1990) found (field) experimentally the spatial patterns that predator and prey distribution generate a halo of predators (ladybug) surrounding a prey (aphid) outbreak, which may not be stable. However, this pattern is generated by a diffusive component. Numerical simulations confirmed this result (see [46, 44]). Likewise, he did not explain what role the taxis term plays in the pattern formation. By studying pattern formation, we identify the role of prey–taxis in prey and predator pattern formation. Linear stability theory cannot always predict long term dynamics, but if there exists an invariant set including the unstable steady state, these linearly unstable solutions tend eventually to be balanced by the nonlinear terms and a steady state spatially inhomogeneous solution occurs [84]. Alternatively, we may use nonlinear stability analysis and numerical solutions [56]. In addition, singular perturbation analysis for the ratio of two diffusion rates near the bifurcation that initiates the pattern formation has been used to obtain a heterogeneous pattern for the nonlinear case.

1.6 Functional Response

In this section we describe the idea of functional responses. A functional response describes the prey consumption rate by an individual predator across a range of prey densities. Holling [36] suggested three functional responses based on handling time, under the assumptions that prey density is the dominating factor and that predator satiation, environmental temperature, and prey and predator motility do not significantly affect the functional responses. Thus, the number of prey consumed, $f(v)$, is proportional to searching time, T_s, times the prey density v, so we have the equation (See Holling [37]):

$$f(v) = aT_s v, \tag{1.14}$$

where a is the probability that an individual predator encounters an individual prey for a unit time interval, and a may not be a constant. The searching time, T_s is given by $T_s = T - T_h f(v)$, where T_h is the total handling time and T is the characteristic (given) time. T is now taken to be 1. Substituting this equation into (1.14) and isolating $f(v)$ on the left side gives

$$f(v) = \frac{av}{1 + T_h av}, \tag{1.15}$$

which is a type II functional response if T_h is a constant. Under the assumption that the handling time is negligible and a is a constant, we have a type I functional response:

$$f(v) = av + \mathcal{O}(T_h). \tag{1.16}$$

Note that equation (1.16) is usually called Lotka–Volterra or described as the absence of any functional response (from comment by Chris Cosner). The true form of a type I functional response is that $f(V)$ is constant for v bigger than some threshold v^*. However, for purposes of linear stability analysis near $v = 0$ and near $v = v_0$ non–zero steady state there is no difference between $f(v) = av$ and a true type I functional response. Hence, we call a type I functional response throughout this thesis without too much confusion.

In area–restricted foraging, predators search more actively in high prey density areas. If we assume that a is a linear function with respect to prey density, then a type III functional response is obtained:

$$f(v) = \frac{a_0 v^2}{1 + T_h a_0 v^2}, \tag{1.17}$$

where a_0 is a linear coefficient and T_h is a constant. The type III functional response indicates that predators search more efficiently as the prey density rises. These three functional responses are all based on the principle of mass action and a spatially uniform predator–prey density. In addition, it is assumed that the interactions between the prey and the predator do not generate spatial heterogeneity, and that predators forage independently. If the prey population is much bigger than the predator population, the above assumptions are satisfied. Cosner et al. (see [13] for details) studied various scenarios of functions a, i.e. the prey–dependent case, ratio-dependent case, predator-dependent case under different assumptions of prey and predator spatial distribution, and derived functional responses in 2- and 3- dimensions. In another study, Metz et al. [65] derived functional responses based on predator satiation in which the time for digestion, the rate of gut emptying, the effect of temperature, and the movement speed of both species were considered instead of handling time (see also [38]). In deriving these functional responses, Metz et al. used the differential equation of the predator with respect to time t and satiation s for a given prey density. For the gut emptying, a delay term with respect to satiation was used. The same method was applied for the functional responses with two different prey items, and for two–dimensional satiation state (satiation measured at the different part of gut). See [92] for detailed information on various functional responses.

Jeschke et al. [42] developed the steady–state satiation (SSS) equation of functional responses by considering five stages of the predation cycle: search, encounter, detection, attack, and eating. Classic Holling type functional responses are based on handling time, and the SSS equation considers digestion time as well. Because the SSS model takes various predation stages into account, the effects of prey defences can be included.

1.7 Outline

In this thesis, we are interested in a mechanism which explains spatial predator foraging behaviour in response to a heterogeneous prey environment, and in how foraging directly affects predator movement in response to prey density. Here the predator's satiation level is considered as an indicator of a local prey density. As a framework, we focus on the prey–taxis model introduced by Kareiva and Odell [46]. We analyze the derivation of this model, understand the assumptions used, release unnecessary assumptions, and modify some parts of the derivation procedure in a mechanistic way. Our derived prey–taxis model is applied to study the spatial predator–prey interaction. The rest of this thesis is organized as follows.

In Chapter 2, we develop a model of the interaction between prey and predators. The

model consists of a predator movement model, spatial satiation variation, turning rate, predator temporal dynamics, and prey dynamics. The directional movement of predators is described with a 1-D hyperbolic system. A satiation function is derived under the assumption that it is regulated by both prey distribution and satiation. Temporal variation in satiation is derived and combined with predator movement to approximate spatio–temporal satiation variation. Increasing the satiation level leads to frequent turning by predators, which affects predator movement. Turning rate, which is determined only by satiation, is derived mechanistically by a Poisson process and is confirmed among four candidates models via statistical selection procedures. Finally prey spatial dynamics are introduced briefly, in which prey dispersal is determined by a diffusion process and local prey population dynamics are limited by the interaction with predators. We do not derive prey dynamics rigorously.

In Chapter 3, we reduce the number of total equations derived from Chapter 2. First of all, we use rescaling and a parabolic limit to approximate the hyperbolic system of predator movement. As a result we obtain an equation in the form of (1.2). Here the counterpart of chemosensitivity $\chi(s)$ is called prey sensitivity $\chi(v)$ depending on prey density v. Prey sensitivity and diffusion rate are derived through turning rate and spatio–temporal satiation variation. An alternative derivation of prey–taxis is considered using the transition between mobile and resting states of the predator. We derive the prey–taxis equation for predator spatial variation in the form of an advection–diffusion equation, to which local population dynamics reacting to prey density are added.

In Chapter 4, we review the numerical methods used in this thesis. Numerical simulations are done using a fractional step method. For the prey–taxis term, we carefully choose high resolution central schemes, such as Nessyahu–Tadmor (NT) scheme, Kurganov and Tadmor scheme, etc. For the diffusion terms, the standard second order Crank–Nicolson method and the second order Runge–Kutta (RK) method are used.

In Chapter 5, we consider the global pattern in a predator–prey model from Chapter 3 via travelling wave connections. Here we look at the situation in which introduced predators catch up with a spreading prey. We consider two questions: 1. whether prey spread is slowed down by the predators and 2. whether it is stopped by the predators. We address these questions with diffusion–only dispersal, prey–taxis dispersal, and several other local population dynamics. We also consider that predator diffusion rate is small and prey do not have spatial mobility. We modify the model which Pettet and Mcelwain [75] considered with a nonconstant prey sensitivity $\chi(v) = \frac{b}{v}$. Without predator diffusion we consider the condition for a discontinuous travelling wave solution. Here so called 'Hole in the Wall' appears. The full model with small predator diffusion is investigated and compared with the approximate model. In the last section, we consider traveling wave speeds to the resting models derived in Section 3.6.

In Chapter 6, we consider the spatial pattern formation induced by diffusion and prey–taxis combined with various local population dynamics. We perform a mathematical analysis to find conditions for which prey can persist under the predation pressure.

In the last chapter, we summarize and discuss the results we obtained in this thesis, and talk about further research.

Chapter 2

Modelling Prey–Taxis

In this chapter, we construct mathematical models for area–restricted foraging where the foraging strategy depends on the prey density. Since we are interested in modeling directed movement of the predator depending on their satiety in detail, we begin the modeling in one spatial dimension. The resulting model for non–tumble and oriented movement of the predator is a hyperbolic model of correlated random walk for the species, which is coupled to a hyperbolic model for the satiation and coupled to a prey–diffusion equation.

Aphids are observed to actively aggregate around their own species to reduce the chance of predation [11, 90], even though their grouping strongly attracts predators. Using a mathematical model Turchin and Kareiva [90] argued that prey grouping decreases predation pressure via two components. First, the probability of prey killed per predator per unit of time is a decreasing function of an aphid colony size. Second, the expected number of predators attacking an aphid colony is an increasing function of aphid colony size but is not increasing as quickly as aphid colony growth.

Our research is motivated by the observation of area–restricted searching of the ladybug beetle *Coccinella septempunctata* in response to the goldenrod aphid (plant lice) in predator–prey models. Kareiva and Odell [46] fit their models to field data of the ladybug beetle and the goldenrod aphid and showed that the predation by lady beetles at low densities of aphid populations seems to be crucial to the control of aphid outbreaks. Therefore, time of release of ladybug is an important aspect in the control of an aphid population. Like most ladybugs, *Coccinella* beetles exhibit area–restricted foraging following the consumption of aphids. Hungry ladybug predators travel long straight paths without changing direction often. As they consume prey, their turning rate is seen to increase, and zig–zag movement is observed [46]. Ladybug predators are not able to detect prey visually at distance over 1 cm.

Predator satiation is an important factor for predator foraging behaviour, hence we begin the modeling in Section 2.2 by modeling temporal satiation dynamics. In Section 2.3, we formulate a model for spatial movement of the predator and we combine both partial models to obtain a movement model for predators that includes the satiation dynamics in Section 2.4.

We study the drift–diffusion approximation in Chapter 3, where we also extend the limit equation to more than one space dimension.

+/−	positive/ negative direction moving [N–D]
u	speed at which a predator travels [L/T]
$V(x,t)$	prey density [N/L]
$n^+(x,t)$	right–moving predator density [N/L]
$n^-(x,t)$	left–moving predator density [N/L]
$n(x,t)$	total predator density $(= n^+(x,t) + n^-(x,t))$ [N/L]
$r = R(S)$	direction–reversal probability per unit time for predator [1/T]
$S(x,t)$	degree to which a predator is satiated($[0,1]$) [N–D]
K	max density of prey [N/L]
$\mathbf{J}_P$	flux density of predators [N/T]
$S_0 = S_0(V)$	steady–state value of S [N–D]

Table 2.1: Notation and units of the predator–prey–satiation model

2.1 Notation and Units

In this section, the dependent functions that are used for our final predator–prey–satiation model are summarized in Table 2.1 (Units: L – length, T – time, N – number, and N–D – nondimensional).

2.2 Temporal Satiation Dynamics

In this section, we consider satiation dynamics. We first consider a system where there is no space dependence. Hence the satiation of a predator $S(t)$ and the prey density $V(t)$ vary with time t only. The satiation $S(t)$ increases each time the predator consumes a victim and decreases as the predator digests and excretes. The predation rate depends on the prey density $V(t)$ experienced by the predators, and on the satiation $S(t)$, since stomach fullness clearly influences a predator's inclination toward further predation. The rate of digestion, which is the rate at which $S(t)$ decreases in the absence of feeding, also depends on $S(t)$. Thus, we assume the existence of a differentiable function $f(S,V)$ that determines the satiation dynamics of each predator as follows

$$\frac{dS(t)}{dt} = f(S(t), V(t)). \tag{2.1}$$

Here $f(S,V)$ can be understood as the foraging strategy (foraging intensity) of the predator, depending on the satiation S and available food V.

We assume the following condition that is derived from biological reasoning

$$\frac{\partial f}{\partial S} < 0. \tag{2.2}$$

It describes the situation that, as gut-fullness increases, satiation growth rate is slowed. In other words, increased satiation makes the predator less efficient in searching for more food . This situation may occur because predators tend to kill less prey or because predators change the consumption pattern to partial consumption of prey killed [82].

We also assume that

$$f(0,V) \geq 0 \text{ and } f(1,V) < 0, \tag{2.3}$$

which says that, for a fixed prey population, an empty gut drives predator to consume prey and increase its satiation level, and that, for a fixed prey population, a full gut restricts predator from higher satiation.

In Section 2.5 we relate the turning rates to the predator satiation and to the prey density. In the final section of this chapter we derive the coupled predator–prey–satiation model.

We normalize satiation $S(t)$ to be within $D = [0,1]$. Assumption (2.3) is sufficient to prove that D is positively invariant for (2.1).

Lemma 2.1 *Assume condition (2.3) and let $V(t)$ be a given continuous non-negative prey density, then the region $D = [0,1]$ is positively invariant for the solutions of (2.1).*

Proof. We prove that D is positive invariant by showing that $S(t)$ starting inside of D does not cross the boundary of D. Assume that D is not positively invariant. Then there exists a solution of (2.1) such that initially $S(0)$ is in D but for some $T > 0$, $S(T)$ is not in D. It means that $S(t)$ crosses the boundary of D for some $t > 0$. At $S = 0$, we first consider the case of $f(0,V) > 0$ in condition (2.3) so that we have $dS/dt = f(0,V) > 0$, which means that the solution of (2.1) is increasing at $S = 0$, hence it cannot cross the boundary of D through $S = 0$. Now we consider the case of $f(0,V) = 0$ in condition (2.3) so that we have $dS/dt = f(0,V) = 0$. Here we consider $S_1 = -\epsilon$ for small positive constant ϵ. For such S_1, we can see that $f(S_1,V) > 0$ from the assumption (2.2). Thus a trajectory starting on $S = 0$ cannot decrease any further. Similarly at $S = 1$, we find $dS/dt = f(1,V) < 0$, which means that the solution of (2.1) is decreasing at $S = 1$. In addition, a trajectory starting on $S = 1 + \epsilon$ should decrease due to the assumption (2.2), hence a satiation starting at $S = 1$ cannot grow any further . Therefore D is shown to be positively invariant (see [89]). □

When the prey density is held constant for a long time, it will be shown that the satiation $S(t)$ approaches the steady–state solutions of equation (2.1) that satisfy $f(S,V) = 0$. With assumption (2.2), the implicit–function theorem [4] is used to show that S is expressed uniquely as a function of V. We denote this steady–state value of S by $S_0(V)$.

Since $f(S,V)$ is the rate at which satiation of predator varies, we need to consider two processes to express $f(S,V)$. The one is the rate of satiation increase through consumption of prey, and the second is the rate of the satiation decreasing by activity and energy intake, such as searching for prey and digesting and excreting eaten prey. For the case of increasing satiation, we need to consider the rate of consuming prey with variable satiation, because the rate of consuming prey has been observed to vary with respect to predator satiation [46]. Therefore, $f(S,V)$ consists of energy intake and energy decay terms. The energy intake is expressed as a classical killing rate in the form of a functional response $g(V)$ times the conversion of killed prey into energy $e(S)$. The second is an energy decay which may be proportional to satiation level or may follow a functional response form if we take into account an increased energy level due to the partial consumption of prey [82].

In this model, we assume that energy decay is proportional to satiation and does not depend on prey density. Then, we have

$$f(S,V) = C_1 e(S) g(V) - C_2 S, \tag{2.4}$$

where C_1 converts units of prey into satiation units, and C_2 is an energy decay coefficient. Besides three types of functional responses $g(V)$ introduced by Holling [36], we consider a fourth functional form, which has been introduced by several researchers [14, 49]. The prototypes of the functional responses that we show in Figure 2.1 are

$$\begin{aligned} \text{Type I}\,, g_I(V) &= \begin{cases} \frac{b}{a}V & \text{for } 0 \le V \le c \\ \frac{bc}{a} & \text{for } V > c \end{cases} \\ \text{Type II}\,, g_{II}(V) &= \frac{aV}{1+bV} \\ \text{Type III}\,, g_{III}(V) &= \frac{aV^2}{1+bV^2} \\ \text{Type IV}\,, g_{IV}(V) &= \frac{aV}{b+V+V^2/c}, \end{aligned} \tag{2.5}$$

where a, b, and c are positive constants. We define $e(S) = (1-S)^\gamma$, which describes how satiation regulates the intention of partial consuming prey. $(1-S)$ indicates that as predator is satiated more, an energy intake occurs more slowly for the same prey density. As γ approaches zero, $e(S)$ approaches 1 for all satiation S except for high satiation $S = 1$, so that predators show the same foraging behaviour with respect to varying satiation (See Figure 2.2).

To find a steady state relationship between S_0 and V, we need to understand the relationship $g(V) = \frac{C_2 S}{C_1 e(S)}$ from equation (2.4) for the four functional responses defined above.

Let $S_0(V)$ be a solution to $g(V) = \frac{C_2 S_0}{C_1 e(S_0)} = \Phi(S_0)$ providing it exists. Then we have

Lemma 2.2 *(i). $\Phi(S_0)$ is monotonically increasing. (ii). $\Phi(S_0)$ is continuously differentiable in* $[0, 1)$.

Proof. (i) When we take a derivative of $\Phi(S_0)$ with respect to S_0, we have $\Phi'(S_0) = \frac{C_2}{C_1}(1-S_0)^{-\gamma-1}(1-S_0+\gamma S_0)$, which is always positive for $S_0 < 1$ and nonnegative γ. Therefore $\Phi(S_0)$ is monotonically increasing. (ii) $\Phi(S_0)$ is product of two functions (let, $\Phi_1(S_0) = \frac{C_2}{C_1} S_0$ and $\Phi_2(S_0) = (1-S_0)^{-\gamma}$). $\Phi_1(S_0)$ and $\Phi_2(S_0)$ are all infinitely differentiable in $[0, 1)$, hence the product of two infinitely differentiable functions is infinitely differentiable. □

Thus, $\Phi(S_0)$ is a one–to–one function on its domain, which implies that the inverse function of $\Phi(S_0)$ exists [4].

Lemma 2.3 *Under the assumption that $g'(V)$ exists, let $S_0(V) = \Phi^{-1}(g(V))$, then*

$$\begin{aligned} S_0'(V) &> 0 \text{ iff } g'(V) > 0 \\ S_0'(V) &< 0 \text{ iff } g'(V) < 0 \\ S_0'(V) &= 0 \text{ iff } g'(V) = 0. \end{aligned} \tag{2.6}$$

Proof. When we differentiate both sides of $g(V) = \Phi(S_0(V))$ with respect to V, we have $\frac{dg(V)}{dV} = \frac{d\Phi(S_0)}{dS_0}\frac{dS_0}{dV}$, in which $\frac{d\Phi(S_0)}{dS_0}$ is always positive by Lemma 2.2. Thus, $\frac{dg(V)}{dV}$ and $\frac{dS_0}{dV}$ have the same sign, which shows (2.6). Hence $S_0(V)$ and $g(V)$ have the same extremal points. □

Note that for Type I, $\frac{dg}{dV}$ does not exist at $V = c$. We use Matlab to show the behaviour of the curve $S_0(V)$ as γ decreases to zero (See Figure 2.3). As γ approaches zero, we can

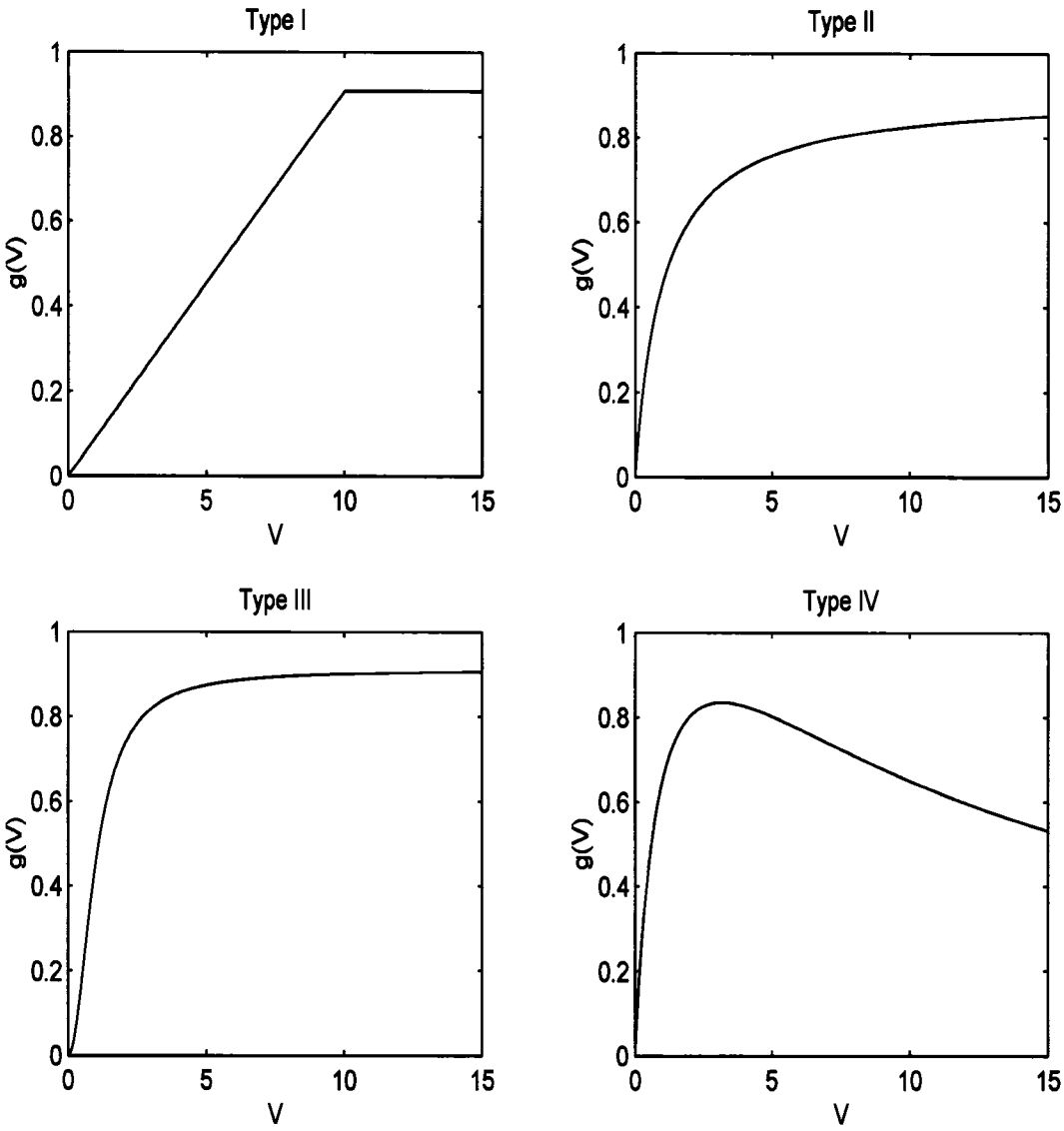

Figure 2.1: Four types of functional response dependent on prey density (V). Type I–IV are shown in formula (2.5) and the parameters are: Type I) $a = 11$, $b = 1$ and $c = 10$, Type II) and Type III) $a = 10/11$ and $b = 1$,Type IV) $a = 15/11$, $b = 1$ and $c = 10$.

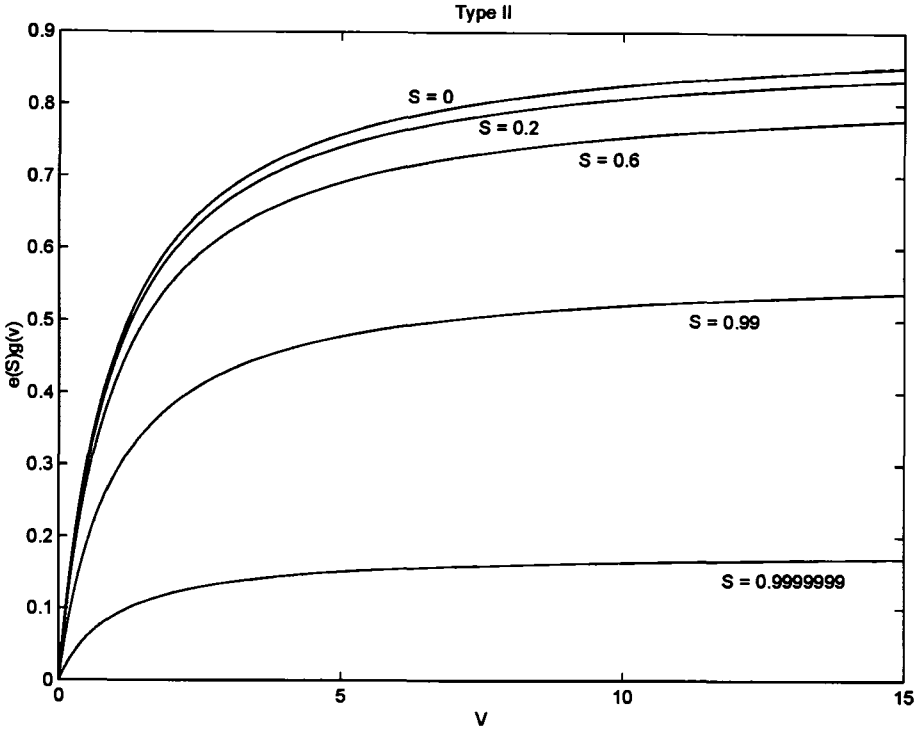

Figure 2.2: As satiation S increases, food consuming expressed by $e(S)g(V)$ is shown to decrease. The parameters are: $\gamma = 0.1$, $a = 10/11$ and $b = 1$.

see that $S_0(V)$ has classical functional response forms corresponding to $g(V)$. In addition to condition (2.2), Kareiva and Odell [46] assumed the following condition

$$\frac{\partial f}{\partial V} \geq 0, \tag{2.7}$$

which describes the situation that as there are more prey, the predator has a higher inclination to consume prey and it takes shorter time to search for prey so that satiation increases more quickly.

Type I, II and III satisfy all required conditions (2.2–2.7) for $f(S,V)$ but Type IV fails to satisfy condition (2.7) for large prey density. We have the following property for Type I, II and III functional responses

$$\frac{\partial S_0(V)}{\partial V} \geq 0, \tag{2.8}$$

which means that, when V is held fixed, the equilibrium satiation of the predator's gut should be larger for larger values of prey density. But Type IV functional response does not show this kind property of predator. However, releasing condition (2.7) in this thesis, we may include Type IV functional response. Without condition (2.7), $S_0(V)$ is not a one–to–one function, but the above three Lemmas 2.1–2.3 still hold. For Type IV curve, $S_0(V)$ is decreasing for large prey density, which can be explained with the concept of implicit prey defense or predator resting for mating or reproduction. The resting for mating or reproduction might increase with prey consumption. $S_0(V)$ is the solution that should be observed in predators that forage in a fixed constant–prey density, V, for a long time. Indeed we find

Lemma 2.4 *Under conditions (2.2) and (2.3) , the equilibrium $S_0(V)$ of equation (2.4) is unique and it is asymptotically stable.*

Proof. By the way that $S_0(V)$ is defined, we can see it is assigned uniquely with V. It implies that $f(S,V)$ can be zero only one time at any fixed prey density. Under condition (2.3) ($f(0,V) \geq 0$), and condition (2.2) ($\partial f/\partial S < 0$), $f(S,V)$ is a function of S that starts nonnegative at $S = 0$ and is monotonically decreasing with respect to S. By equation (2.1), we can see that for $S < S_0(V)$, $S(t)$ is monotonically increasing and approaching $S_0(V)$, and for $S > S_0(V)$, $S(t)$ is monotonically decreasing and approaching $S_0(V)$ (Figure 2.4). Thus when V is held fixed at any value, that equation (2.1) has a unique steady–state solution–namely, $S_0(V)$– and as $t \to \infty$, S approaches $S_0(V)$, i.e. $S_0(V)$ is globally asymptotically stable. □

A functional response is a per predator consumption rate as a function of prey density. In our case, satiation can be interpreted in two ways. The first is to directly account for the killed prey, as described by the functional response curves. The second is to assume implicitly an energy conversion with a constant energy conversion rate from the killed prey to satiation.

Kareiva and Odell used $e(S) = 1 - S$ and $g(V) = \frac{V}{1+V/\nu}$. They estimated $C_1 = 0.018632$ m/day, $\nu = 711.2$/m, and $C_2 = 2.3384$/day. The relation between S and V at equilibrium is shown in Figure 2.5. As prey increase, the killing rate approaches a plateau of value ν. When the killing rate is near this plateau, the satiation equation (2.1) can be expressed as a function of satiation only as follows,

$$\frac{dS}{dt} = C_1\nu - (C_1\nu + C_2)S. \tag{2.9}$$

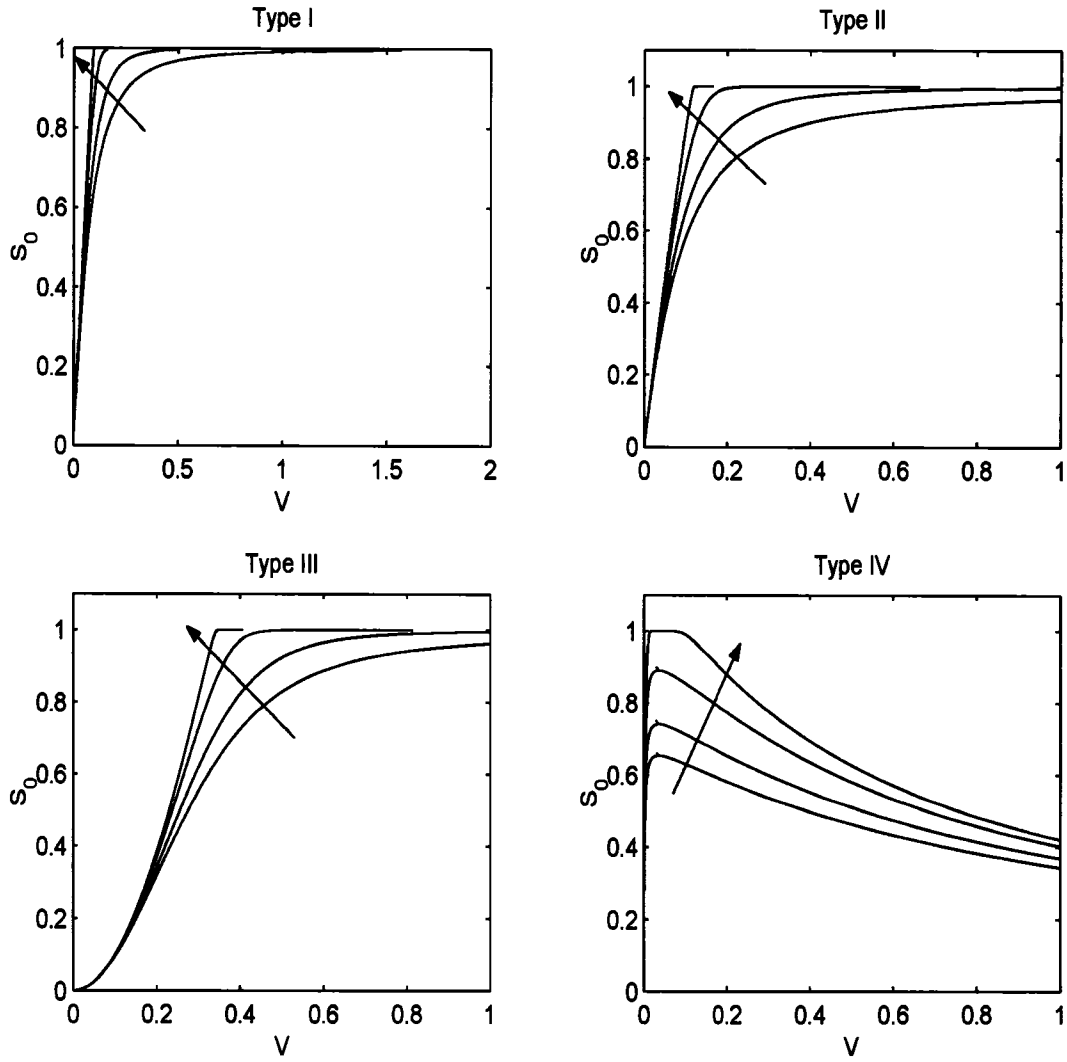

Figure 2.3: As γ decreases to zero, $S_0(V)$ shows similar behaviour corresponding to four functional responses ($g(V)$). With γ closer to zero, the steady satiation level for a fixed prey density increases. The parameters are: $\gamma = 0.5$, 0.3, 0.1 and 0.01, $C_0 = 1/11$, Type I) $a = 11$, $b = 1$, $c = 10$ and $C_1 = 1/11$, Type II) and Type III) $a = 10/11$, $b = 1$, and $C_1 = 1/11$, Type IV) $a = 15/10$, $b = 1$, $c = 1/2$, and $C_1 = 13/11$. The arrows show the direction of decreasing γ.

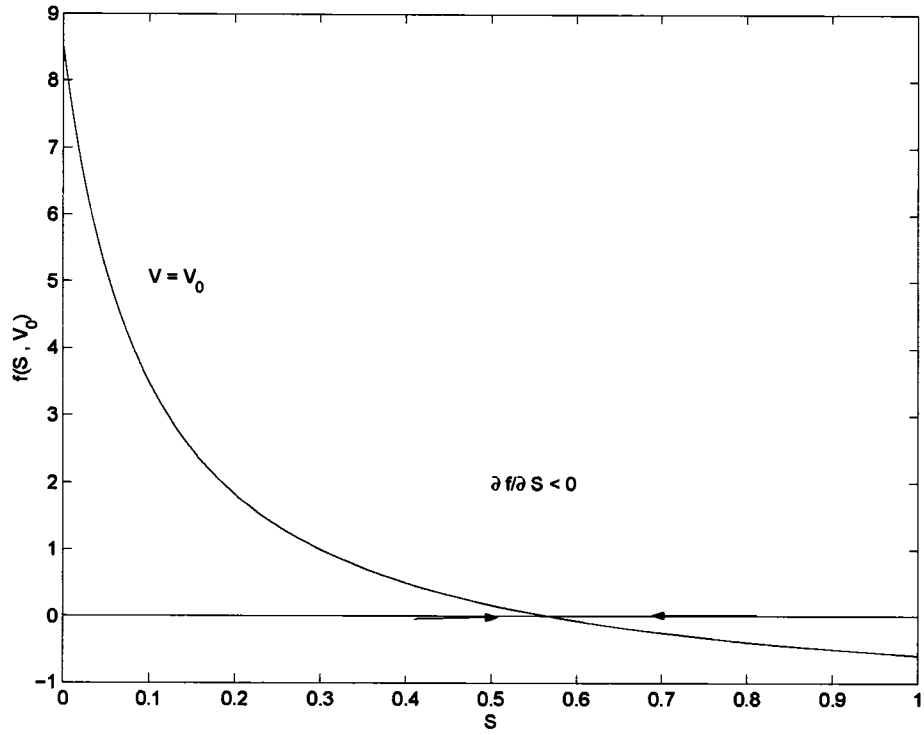

Figure 2.4: With condition (2.2) and (2.3), for the fixed prey density, all initial values of S approach $S_0(V)$.

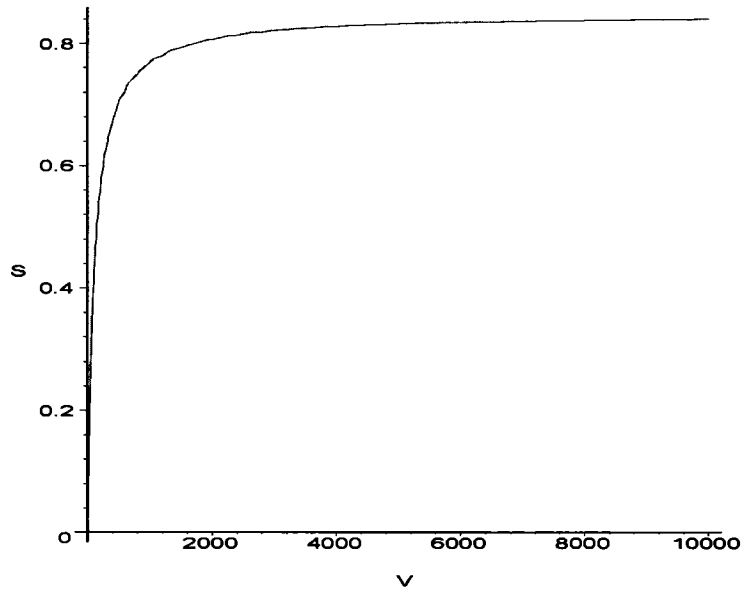

Figure 2.5: Satiation equilibrium using the Kareiva and Odell [46] functional form and parameters: $S_0 = \frac{C_1 g(v)}{C_1 g(v) + C_2}$. $C_1 = 0.018632$, $\nu = 711.2$, and $C_2 = 2.3384$

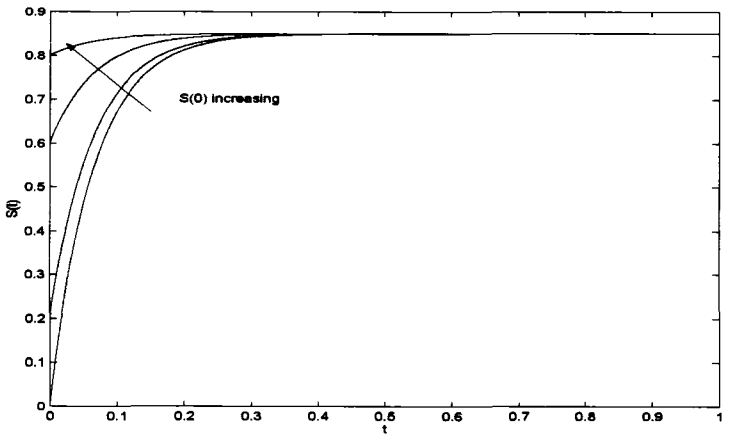

Figure 2.6: $S = \frac{(C_1\nu-(C_1\nu+C_2)S(0))\exp(-(C_1\nu+C_2)t))-C_1\nu}{-(C_1\nu+C_2)}$. $C_1 = 0.018632$, $\nu = 711.2$, and $C_2 = 2.3384$. With different initial satiation, satiation approaches the plateau quickly.

The analytical solutions of equation (2.9) are shown in Figure 2.6 for increasing initial satiation $S(0)$ from 0 to 0.8.

To summarize, it is seen that when the prey density is held constant for a long time, the satiation $S(t)$ is expressed uniquely as a function of V, $S_0(V)$.

2.3 Predator Movement Model

In this section, we derive predator movement model in two ways; the conservation law and a discrete random walk.

2.3.1 Derivation of Predator Movement Model

Here we derive a mathematical model for predator movement by using the conservation law. To motivate the general movement rules we consider a cylinder of fixed cross–sectional area A, oriented along the x–axis (Figure 2.7). Assuming that all quantities of right– and left–moving predators vary with x, let us examine the rate at which the number of right–moving predators n^+ changes in a slice of the cylinder that extends from some fixed x to $x + \Delta x$, where Δx is a small constant spatial increment.

The total amount of the right–moving predator n^+ in this slice is $n^+ A\Delta x$. We assume that n^+ changes (i) due to the fact that a left–moving predator become right–moving and vice–versa, and (ii) through flux across the boundaries of the slice. Written as an equation we obtain

$$\frac{\partial(n^+ A\Delta x)}{\partial t} = (i) + (ii). \tag{2.10}$$

The volume factor $A\Delta x$ converts densities into the total number of predators in the "slice".

To obtain (i), consider that a directional turning rate of the right–moving predator r^+ is the probability per unit of time that a right–moving predator reverses. Thus $\int_x^{x+\Delta x} r^+ n^+ A dx$ is the expected number of right–moving predators within the slice that reverse per unit time. Similarly $\int_x^{x+\Delta x} r^- n^- A dx$ is the expected number of left–moving

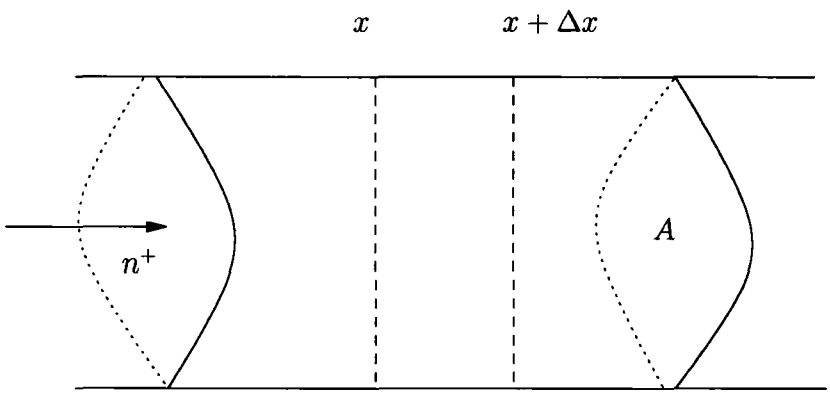

Conservation Law

Figure 2.7: Equations of balance are derived for flow of predators [concentration $n(x,t)$] with constant velocity, u, along a cylinder with uniform cross–sectional area A.

predators within the slice that reverse per unit time. Then $(i) = \int_x^{x+\Delta x} r^- n^- A dx - \int_x^{x+\Delta x} r^+ n^+ A dx$. Derivation of (ii) begins with the observation that the rate at which right–moving predator move into the "slice" from the left is $uAn^+(x,t)$. Because the density of predator varies with x, the predators generally leave the slice at a different rate from that at which they enter, that is $uAn^+(x+\Delta x,t)$. The net rate at which n^+ flows into the slice through its two sides is therefore

$$uAn^+(x+\Delta x,t) - uAn^+(x,t) = uA[n^+(x+\Delta x,t) - n^+(x,t)]. \tag{2.11}$$

Putting everything together, we have

$$\frac{\partial(n^+ A\Delta x)}{\partial t} = \int_x^{x+\Delta x} r^- n^- A dx - \int_x^{x+\Delta x} r^+ n^+ A dx - uA[n^+(x+\Delta x,t) - n^+(x,t)]. \tag{2.12}$$

Dividing by $A\Delta x$, and then letting Δx approach zero we obtain the equation

$$\frac{\partial n^+}{\partial t} = r^- n^- - r^+ n^+ - u\frac{\partial n^+}{\partial x}, \tag{2.13}$$

which is rearranged as

$$\frac{\partial n^+}{\partial t} + u\frac{\partial n^+}{\partial x} = r^- n^- - r^+ n^+. \tag{2.14}$$

Similarly we can derive a left–moving predator movement equation using left–moving velocity with $-u$ as follows

$$\frac{\partial n^-}{\partial t} - u\frac{\partial n^-}{\partial x} = -(r^- n^- - r^+ n^+). \tag{2.15}$$

where $r^+(x,t)$ is the turning rate of the right–moving predator at time t and position x and similarly $r^-(x,t)$ can be assigned for left–moving predators.

A more rigorous derivation can be made without the assumption of small Δx and with nonhomogeneous cylinder. Alternatively, (2.14)–(2.15) can be derived as conservation laws using the divergence theorem (see [49]) or from correlated random walk (see [100, 91, 24, 35]).

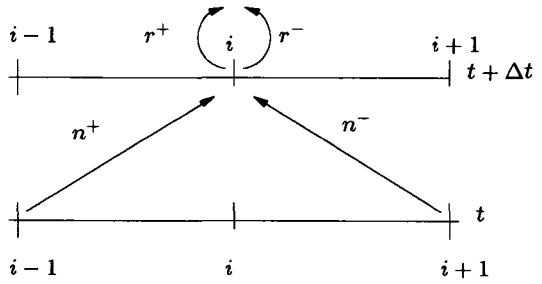

Figure 2.8: Change of locations on a discrete grid due to the moving and turning values described in the text.

For the hyperbolic system (2.14–2.15) on an interval $0 < x < l$ zero Dirichlet boundary conditions are

$$n^+(0,t) = 0,\ n^-(l,t) = 0. \tag{2.16}$$

No predator can enter at $x = 0$ and $x = l$ into the domain [24]. However the right–moving predators can leave through $x = l$ and the left–moving ones through $x = 0$.

No–flux boundary conditions on an interval are

$$n^+(0,t) = n^-(0,t),\ n^-(l,t) = n^+(l,t). \tag{2.17}$$

The left–moving predators arriving at $x = 0$ turn into the right–moving predators and similarly the right–moving predators arriving at $x = l$ turn into the left–moving predators.

Moreover, we consider travelling waves on unbounded domains $-\infty \leq x \leq \infty$.

2.3.2 Derivation from Discrete Model

In this section, we provide an alternative derivation of the predator movement model that is based on a discrete random walk [100].

We discretize an one dimensional domain with stepsize Δx and denote the grid points by $i-1$, i, and $i+1$ and so forth, Right–moving predators move from location $i-1$ to location i in one time step and left–moving predators move from location $i+1$ to location i. We assume that a predator's turning can occur immediately after the predator's arrival at a location i, and no turning happens while predators move (see Figure 2.8). The number of right–moving predators at location i increases by the immigration of right–moving predators from the $i-1$ location, but decreases by the immediate turning of some right–moving predators after their arrival at location i from the location $i-1$, i.e. $r^+_{i-1}(t)\Delta t n^+_{i-1}(t)$, and increases by the immediate turning of some left–moving predators after their arrival at location i from the location $i+1$, i.e. $r^-_{i+1}(t)\Delta t n^-_{i+1}(t)$. Hence we have a discrete right–moving predator movement equation as follows

$$n^+_i(t+\Delta t) = n^+_{i-1}(t) + r^-_{i+1}(t)\Delta t n^-_{i+1}(t) - r^+_{i-1}(t)\Delta t n^+_{i-1}(t), \tag{2.18}$$

and with the similar argument, we can derive the following equation for the left–moving predators

$$n^-_i(t+\Delta t) = n^-_{i+1}(t) + r^+_{i-1}(t)\Delta t n^+_{i-1}(t) - r^-_{i+1}(t)\Delta t n^-_{i+1}(t). \tag{2.19}$$

Moving $n^{\pm}_{i\mp1}(t)$ to the left–hand side by subtraction and dividing both terms by Δt produce

$$\frac{n^+_i(t+\Delta t)-n^+_i(t)}{\Delta t}+\frac{n^+_i(t)-n^+_{i-1}(t)}{\Delta x/u}= \frac{\Delta t(r^-_{i+1}(t)n^-_{i+1}(t)-r^+_{i-1}(t)n^+_{i-1}(t))}{\Delta t}, \tag{2.20}$$

$$\frac{n^-_i(t+\Delta t)-n^-_i(t)}{\Delta t}+\frac{n^-_i(t)-n^-_{i+1}(t)}{\Delta x/u}= \frac{\Delta t(r^+_{i-1}(t)n^+_{i-1}(t)-r^-_{i+1}(t)n^-_{i+1}(t))}{\Delta t}, \tag{2.21}$$

where $\Delta t=\Delta x/u$ and Δt can be canceled out from the right term. As Δt and $\Delta x\to 0$, we have

$$\frac{\partial n^+(x,t)}{\partial t}+u\frac{\partial n^+(x,t)}{\partial x}=r^-(x(t),t)n^-(x(t),t)-r^+(x(t),t)n^+(x(t),t), \tag{2.22}$$

$$\frac{\partial n^-(x,t)}{\partial t}-u\frac{\partial n^-(x,t)}{\partial x}=-(r^-(x(t),t)n^-(x(t),t)-r^+(x(t),t)n^+(x(t),t)). \tag{2.23}$$

Thus equations (2.22)–(2.23) are equivalent with equations (2.14)–(2.15).

2.4 Spatio–Temporal Satiation Dynamics

In Section 2.2, we looked at satiation dynamics inside of a predator that is not moving. As predators move around for searching food, the satiation variable varies spatially as well. Here we extend the derivation from a discrete model to derive a model for spatio–temporal satiation dynamics.

Spatial satiation variation is a change of satiation due to a spatial predator movement. Indeed, Spatio–temporal satiation varies due to the moving behaviour of predators, the turning behaviour of predators, i.e. the satiation level of right–moving predators S^+ and the satiation level of left–moving predators S^- interchange. The variable n^+S^+ describes the satiation (or total amount of eaten food) as transported to the right by right–moving predators. Note that we assume here that each right–moving predator has the average satiation S^+. The moving behaviour and the turning behaviour of predators cause the total satiation level of right–moving predators at location i to change. It increases by the immigration of right–moving predators from location $i-1$ to location i by $(n^+S^+)_{i-1}(t)$. It decreases by the immediate turning of some right–moving predators after their arrival at location i, $-r^+_{i-1}(t)\Delta t(n^+S^+)_{i-1}(t)$. It also increases by the immediate turning of some left–moving predators after their arrival at location i, $+r^-_{i+1}(t)\Delta t(n^-S^-)_{i+1}(t)$. In addition, satiation changes due to the predator activities, such as searching, handling, and digesting prey so that satiation variation should be included approximately as $n^+_i(t+\Delta t)\Delta t f(S^+_i(t+\Delta t),V)$. Hence we have a spatio–temporal satiation dynamics inside of right–moving predators as follows

$$(n^+S^+)_i(t+\Delta t)=(n^+S^+)_{i-1}(t)+r^-_{i+1}(t)\Delta t(n^-S^-)_{i+1}(t) - r^+_{i-1}(t)\Delta t(n^+S^+)_{i-1}(t)+n^+_i(t+\Delta t)\Delta t f(S^+_i(t+\Delta t),\cdot). \tag{2.24}$$

With a similar argument, we can derive the following equation for a spatio–temporal satiation dynamics inside of left–moving predators

$$(n^-S^-)_i(t+\Delta t) = (n^-S^-)_{i+1}(t) + r^+_{i-1}(t)\Delta t(n^+S^+)_{i-1}(t) \\ - r^-_{i+1}(t)\Delta t(n^-S^-)_{i+1}(t) + n^-_i(t+\Delta t)\Delta t f(S^-_i(t+\Delta t),\cdot). \quad (2.25)$$

We move $(n^+S^+)_{i-1}(t)$ and $(n^-S^-)_{i+1}(t)$ to the left–hand side by subtraction, divide both terms by Δt, and rearrange equations (2.24–2.25) as follows

$$\frac{(n^+S^+)_i(t+\Delta t) - (n^+S^+)_i(t)}{\Delta t} + \frac{(n^+S^+)_i(t) - (n^+S^+)_{i-1}(t)}{\Delta x/u} \\ = \frac{\Delta t(r^-_{i+1}(t)(n^-S^-)_{i+1}(t) - r^+_{i-1}(t)(n^+S^+)_{i-1}(t))}{\Delta t} + n^+_i(t+\Delta t)f(S^+_i(t+\Delta t),\cdot), \quad (2.26)$$

$$\frac{(n^-S^-)_i(t+\Delta t) - (n^-S^-)_i(t)}{\Delta t} + \frac{(n^-S^-)_i(t) - (n^-S^-)_{i+1}(t)}{\Delta x/u} \\ = \frac{\Delta t(r^+_{i-1}(t)(n^+S^+)_{i-1}(t) - r^-_{i+1}(t)(n^-S^-)_{i+1}(t))}{\Delta t} + n^-_i(t+\Delta t)f(S^-_i(t+\Delta t),\cdot). \quad (2.27)$$

Here $\Delta t = \Delta x/u$ and Δt can be canceled out from the right term. As Δt and $\Delta x \to 0$, we arrive at the hyperbolic model

$$\frac{\partial(n^+S^+)}{\partial t} + u\frac{\partial(n^+S^+)}{\partial x} = r^-n^-S^- - r^+n^+S^+ + n^+f(S^+,V), \quad (2.28)$$

$$\frac{\partial(n^-S^-)}{\partial t} - u\frac{\partial(n^-S^-)}{\partial x} = -r^-n^-S^- + r^+n^+S^+ + n^-f(S^-,V). \quad (2.29)$$

In particular, if we regard the satiation level of moving predators $S^\pm$ as constant variables and the local saitaion dynamics as $f(S^\pm,V) = 0$, then we can see that equations (2.14) and (2.15) are considered as a special case of equations (2.28) and (2.29) respectively. Thus when we look at the more detailed mechanism such as including satiation dynamics to a predator movement, we may understand the more realistic phenomena.

The term $n^\pm S^\pm$ denotes the total satiety (or total gut content) of right and left–moving predators respectively at location x and time t. Thus $un^\pm S^\pm$ is the flux of gut fullness as transported by the moving predator. $r^\pm n^\pm S^\pm$ describes a change in the transport of gut contents due to a change of direction of predators. $n^\pm f(S^\pm,V)$ describes uptake, decay, and consumption of food during the walk of a predator.

The product rule applied to equations (2.28–2.29) and combination with equations (2.14–2.15) leads to the following equations for the effective dynamics of satiation, divided into gut content transported right/left respectively:

$$\frac{\partial S^+}{\partial t} + u\frac{\partial S^+}{\partial x} = -(r^-n^-/n^+)(S^+ - S^-) + f(S^+,V), \quad (2.30)$$

$$\frac{\partial S^-}{\partial t} - u\frac{\partial S^-}{\partial x} = (r^+n^+/n^-)(S^+ - S^-) + f(S^-,V) \quad (2.31)$$

2.5 Turning Rate

As we saw in the derivations of the predator movement model (Section 2.3) and spatio–temporal satiation dynamics, directional turning rates of predators r^+ and r^- are key

parameters for the model. In the following we assume that turning is only influenced by the satiation and we write $r^+ = R(S^+)$ and $r^- = R(S^-)$. The turning function $R(S)$ will be derived from experimental data. Kareiva and Odell [46] measured the turning rate of ladybug as a function of mean satiation. They fitted the data using a third order polynomial $R_1(S) = \hat{A} + \hat{B}S + \hat{C}S^2 + \hat{D}S^3$. In the fitting process, they estimated additional parameters simultaneously, such as moving speed u, and parameters for the functional repsonse. We propose a mechanistic model for the turning behaviour and fit it to the data. To derive a mechanistic model for turning events, we assume that turning events follow a Poisson process with rate λ . Then $e^{-\lambda t}$ is the probability of not changing direction in a time interval $(0,t)$, or $1 - e^{-\lambda t}$ is the probability of changing direction in $(0,t)$. We assume that the rate $\lambda(S)$ depends on the satiation S. We assume that the probability to change direction in one unit of time δt is proportional to the relative satiation, so that $1 - e^{-\lambda(S)} = \frac{S}{S_{max}}$, where S_{max} denotes a hypothetical maximum satiation and can be obtained by parameter estimates as a free parameter. Thus $\lambda(S) = -\ln\left(\frac{S_{max}-S}{S_{max}}\right)$. We consider S_{max} as an unknown parameter which we fit from the data. Hence as a second candidate for a turning function we assume $R_2(S) = -B\ln\left(\frac{S_{max}-S}{S_{max}}\right)$ where B is the strength of this effect. Here it is the case that $R_2(0) = 0$. We may generalize to a different situation so that $R_2(0) = A$ for a positive constant A, which results in $R_3(S) = A - B\ln\left(\frac{S_{max}-S}{S_{max}}\right)$. The third candidate for a turning function is the third order polynomial $R_4(S) = A + BS + CS^2 + DS^3$. We will take the number of free parameters into account and we will use the corrected Aikaike information criterion (AICc) to choose the best model from the data of Kareiva and Odell. To summarize the candidates for turning functions are:

1. Kareiva and Odell: $R_1(S) = \hat{A} + \hat{B}S + \hat{C}S^2 + \hat{D}S^3$, parameters $\hat{A}$, $\hat{B}$, $\hat{C}$, $\hat{D}$, predator velocity u, functional response parameters.
2. $R_2(S) = -B\ln\left(\frac{S_{max}-S}{S_{max}}\right)$, parameters B, S_{max}.
3. $R_3(S) = A - B\ln\left(\frac{S_{max}-S}{S_{max}}\right)$, parameters A, B, S_{max}.
4. $R_4(S) = A + BS + CS^2 + DS^3$, parameters A, B, C, D.

To fit the turning rates as a function of satiation, we use least squares approximation of all four candidates to the data of Kareiva and Odell (Fig. 1. [46]).

We can summarize Table 2.2 by saying that model 4 would be more likely than model 1, model 2, and model 3 if we only consider the maximum likelihood. However, the models have different number of parameters and we use AIC test to compare the models.

$$\mathrm{AIC} = -2\log(\mathcal{L}(\hat{\theta}|y)) + 2K, \tag{2.32}$$

where K is the number of parameters and $\mathcal{L}(\hat{\theta}|y)$ the maximum likelihood, given the data y. Note that AIC test considers the penalty of models from the number of parameters and a smaller AIC indicates a better model. Especially, the small number of data (13) requires using AICc.

$$\mathrm{AIC}_c = \mathrm{AIC} + \frac{2K(K+1)}{n-K-1}, \tag{2.33}$$

where n is sample size (see [8] for detail).

In this section, we considered the turning function $R(S)$ from experimental data. Thus, the lowest value of AICc gives the best model. Figure 2.9 and Table 2.2 indicate that

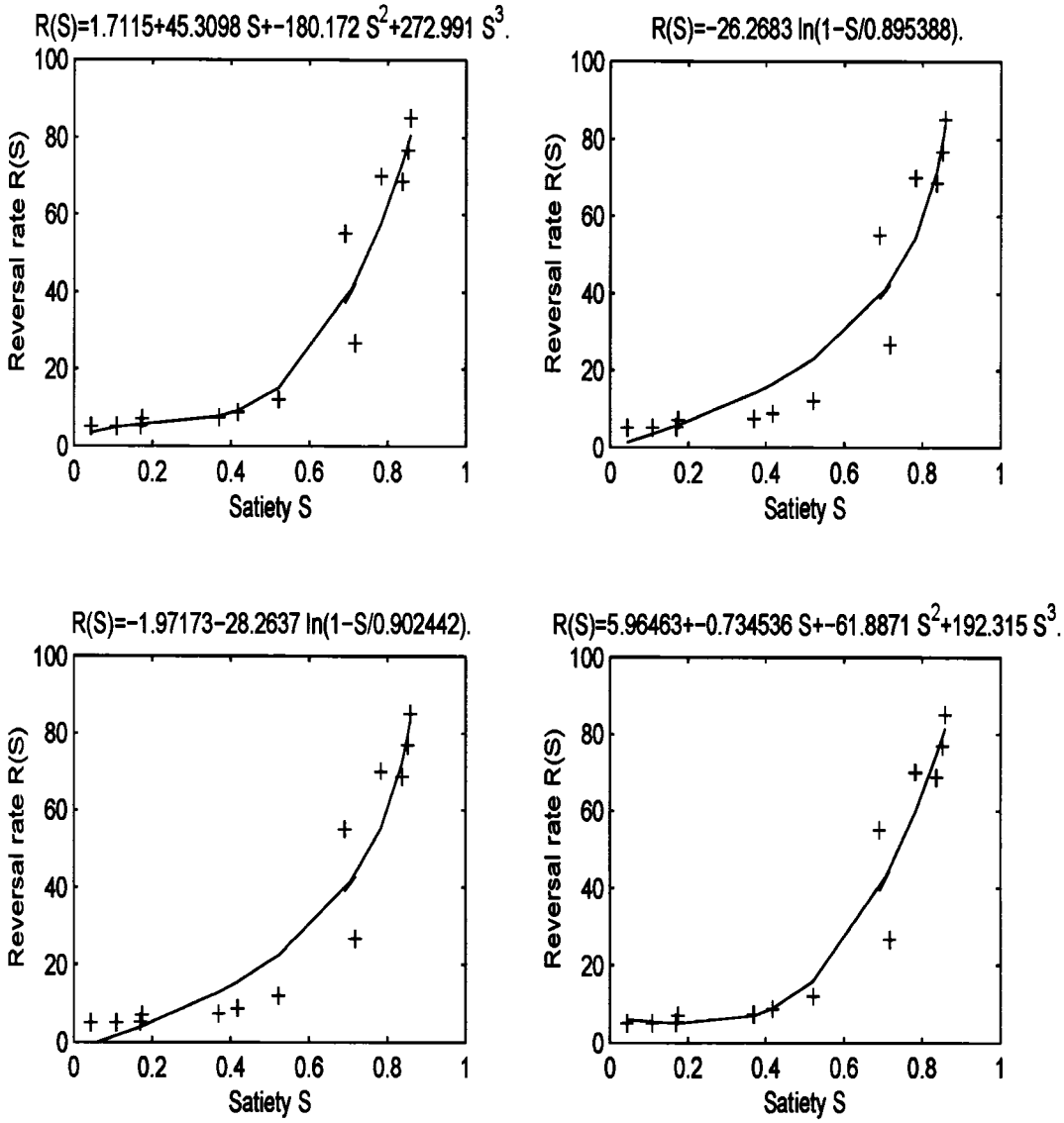

Figure 2.9: Turning rate vs Satiation. Four models of turning rates from Table 2.2 are plotted with data from Kareiva and Odell [46]. The parameters of four models are obtained from the best fit to experimental data (Fig. 1. [46]).

Model equation	Lmax	AIC	AICc
$R_1 = \hat{A} + \hat{B}S + \hat{C}S^2 + \hat{D}S^3$	0.0034	19.3957	24.3957
$R_2 = -B\ln(1 - S/S_{max})$	5.7784e-04	18.9124	20.1124
$R_3 = A - B\ln(1 - S/S_{max})$	6.4754e-04	20.6847	23.3513
$R_4 = A + BS + CS^2 + DS^3$	0.0041	19.0072	24.0072

Table 2.2: To compare four models of the predator turning rate $R(S)$, a Likelihood ratio test and the Aikaike information criterion (AIC) are used. In addition, since the number of data is less than 40, a correction term to the AIC is added (AICc).

$R_2 = -B\ln\left(1 - \frac{S}{S_{max}}\right)$ gives the best model (see Table 2.2 and Figure 2.9). It is interesting to see that a mechanistic model is as good as or slightly better than other types of models.

2.6 Summary: Formulation of the Predator–Prey–Satiation Model

In this chapter we derived the predator–prey–satiation model. For that, we considered each component of the predator–prey–satiation model except the prey model. The complete predator–prey–satiation model consists of three components; 1. the predator movement model (Section 2.3), 2. the spatio–temporal satiation dynamics (Section 2.4), and 3. the prey model.

First of all, the predator movement model is derived in Section 2.3 and reads

$$\frac{\partial n^+}{\partial t} + u\frac{\partial n^+}{\partial x} = r^- n^- - r^+ n^+, \tag{2.34}$$

$$\frac{\partial n^-}{\partial t} - u\frac{\partial n^-}{\partial x} = -(r^- n^- - r^+ n^+), \tag{2.35}$$

where the turning rates $R(S^{\pm})$ depending on the satiation is obtained by comparing four models in Section 2.5. Here we do not consider birth–death terms for predators in equations (2.34)–(2.35) because equations (2.34)–(2.35) are not the final form of a model we analyze in this thesis. In the next chapter, equations (2.34)–(2.35) are approximated with a parabolic type single equation and a reaction term is added to the parabolic equation. The spatial satiation transport through predators is derived in Section 2.4 and reads

$$\partial(n^+S^+)/\partial t + u\partial(n^+S^+)/\partial x = r^- n^- S^- - r^+ n^+ S^+ + n^+ f(S^+, V), \tag{2.36}$$

$$\partial(n^-S^-)/\partial t - u\partial(n^-S^-)/\partial x = -r^- n^- S^- + r^+ n^+ S^+ + n^- f(S^-, V). \tag{2.37}$$

Instead of equations (2.36)–(2.37), we could use equations (2.30)–(2.31). Applying the product rule to equations (2.36)–(2.37) and cancelling the results with equations (2.34)–(2.35) lead to equations (2.30)–(2.31). Similarly equations (2.34)–(2.35) can be obtained from equations (2.36)–(2.37) and equations (2.30)–(2.31).

For the prey we assume that they move randomly with local population dynamics related to predation,

$$V_t = \epsilon V_{xx} + V(h(V) - \frac{(n^+ + n^-)}{V}g(V)), \tag{2.38}$$

where $h(V)$ is a prey growth function and $g(V)$ is a predator functional response (see (2.5)) as used for temporal satiation dynamics.

For n^+ and n^- zero Dirichlet boundary conditions were described in (2.16) and (2.17). For S^+ and S^- on an interval $0 < x < L$, zero Dirichlet boundary conditions are

$$S^+(0,t) = 0,\ S^-(L,t) = 0. \tag{2.39}$$

For the prey dynamics, zero Dirichlet boundary condition is

$$V(0,t) = 0,\ V(L,t) = 0. \tag{2.40}$$

No–flux boundary conditions come from

$$n^+(0,t)S^+(0,t) = n^-(0,t)S^-(0,t) \tag{2.41}$$

$$n^-(L,t)S^-(L,t) = n^+(L,t)S^+(L,t). \tag{2.42}$$

With boundary condition (2.17) we have

$$S^+(0,t) = S^-(0,t),\ S^-(L,t) = S^+(L,t). \tag{2.43}$$

For the prey dynamics, no–flux boundary condition is

$$\frac{\partial V}{\partial x}(0,t) = 0,\ \frac{\partial V}{\partial x}(L,t) = 0 \tag{2.44}$$

Furthermore, we consider travelling waves on unbounded domains $-\infty \leq x \leq \infty$.

The significance of this chapter is that we derived the predator movement model (2.34–2.35) and the spatio–temporal satiation dynamics (2.36)–(2.37). Hence we now understand the difference and similarity between prey–taxis and chemotaxis. The predator movement model is common for both prey–taxis and chemotaxis. However, the spatio–temporal satiation dynamics are different. In chemotaxis, chemical stimulus move randomly independent of amoebae or bacteria. However, in prey–taxis, the dispersal of the level of satiation occurs by the dispersal of predators. Hence, different temporal satiation dynamics predict different predator–prey interactions. This opens a further research direction.

In the following chapter we will derive a simpler approximation for the model equations (2.34)–(2.35) and (2.36)–(2.37).

Chapter 3

Drift–Diffusion Approximation

In the previous chapter, we derived the prey–predator satiation model. Equations (2.34)–(2.35) and (2.36)–(2.37) describe spatial predator dynamics induced by movement and spatial satiation dynamics caused by both movement and the interaction with the prey, respectively. In this chapter, we find a drift–diffusion approximation for equations (2.34)–(2.35) and (2.36)–(2.37).

In order to obtain an approximation, various approaches may be taken. Quasi–steady state assumption is one of such approaches. Kareiva and Odell [46] applied the quasi–steady state assumption to find a parabolic type of the prey–taxis approximation. The purpose of this chapter is to eliminate unnecessary assumptions and derive an approximation more rigorously. Here we adapt different approaches from that by Kareiva and Odell [46]. In Sections 3.1, 3.2, and 3.3, we consider constant, symmetric spatially dependent, and nonsymmetric spatially dependent turning rates, respectively. With rescaling variables and parameters, we approximate the hyperbolic predator movement equations (2.34)–(2.35) with the parabolic type of a drift–diffusion equation. The parabolic limit is also used to obtain the spatial dynamics of the total predator population composed of the right and left moving predators. This parabolic limit procedure provides the main body of the drift–diffusion approximation in Section 3.4. The coefficients of the drift–diffusion approximation are obtained in Section 3.5 from the spatial satiation dynamics (2.36)–(2.37). As a result, this drift–diffusion approximation gives a prey–taxis equation. Alternative derivations of prey–taxis equations are achieved from resting models in Section 3.6.

3.1 Constant Turning Rates

In Section 2.5, we considered a spatially homogeneous turning rate. In Section 2.3, it was seen that predator movement equations are determined by a general turning rate. In this section, we consider constant turning rates and investigate an approximation of (2.34)–(2.35). In next several sections, spatially general turning rates are considered. We restate equations (2.34)–(2.35)

$$\frac{\partial n^+}{\partial t} + u\frac{\partial n^+}{\partial x} = \hat{r}^- n^- - \hat{r}^+ n^+, \tag{3.1}$$

$$\frac{\partial n^-}{\partial t} - u\frac{\partial n^-}{\partial x} = -(\hat{r}^- n^- - \hat{r}^+ n^+). \tag{3.2}$$

For some characteristic time scale T and length scale L, let $\epsilon = \frac{L}{uT}$ be a small parameter. We assume that the turning rates can be written as $r^{\pm} = \hat{r}^{\pm}\rho^{\pm}(x,t)$ with $\hat{r}^{\pm}$ constant and $\rho^{\pm}(x,t) = \mathcal{O}(1)$ with respect to ϵ. First of all, we consider the case that $\rho^{\pm}(x,t) = 1$, that is, a spatially homogeneous turning rate. We introduce $t^* = \frac{t}{T}$, $\delta = \frac{u^2T}{(\hat{r}^+ + \hat{r}^-)L^2}$, $x^* = \frac{x}{L}$, $\omega = \hat{r}^+T$ and $\phi = \frac{L(\hat{r}^- - \hat{r}^+)}{u}$. Then equations (3.1)–(3.2) are expressed as follows,

$$\epsilon^2\delta\frac{\partial n^+}{\partial t^*} + \epsilon\delta\frac{\partial n^+}{\partial x^*} = ((1-\omega\delta\epsilon^2)n^- - \omega\delta\epsilon^2 n^+), \tag{3.3}$$

$$\epsilon^2\delta\frac{\partial n^-}{\partial t^*} - \epsilon\delta\frac{\partial n^-}{\partial x^*} = -((1-\omega\delta\epsilon^2)n^- - \omega\delta\epsilon^2 n^+). \tag{3.4}$$

We assume that turning rates $\hat{r}^+$ and $\hat{r}^-$ are constant so that ω, ϕ and δ are constants as well. Later we handle the case where ω, ϕ and δ depend on x and t.

For the simplicity of analysis, from now on we use n_t instead of $\partial n/\partial t$, and so forth. We also rename t^* and x^* with t and x respectively. We define $n = n^+ + n^-$ and $v = n^+ - n^-$, and cancel ϵ on both sides of equations (3.3)–(3.4). Addition and subtraction of equations (3.3)–(3.4) yields

$$\epsilon n_t + v_x = 0 \tag{3.5}$$

$$\epsilon^2\delta v_t + \epsilon\delta n_x = \epsilon\phi\delta n - v. \tag{3.6}$$

We assume that the parameter $0 < \epsilon \ll 1$ is small and that the other parameters δ and ϕ are $\mathcal{O}(1)$ with respect to ϵ. What does this mean? There are three possible scenarios:
Case 1. We let the time scale of interest get large (T large) and let the average turning rate $\frac{\hat{r}^+ + \hat{r}^-}{2}$ get large but assume that $\hat{r}^+$ and $\hat{r}^-$ are similar ($\hat{r}^+ - \hat{r}^-$ is $\mathcal{O}(1)$) with spatial scale, $L = \mathcal{O}(1)$.
Case 2. We consider the spatially and temporally bounded case (T and L are $\mathcal{O}(1)$). Instead, we let velocity get large (u large) and we let the average turning rate $\frac{\hat{r}^+ + \hat{r}^-}{2}$ get large with assuming that the difference between $\hat{r}^+$ and $\hat{r}^-$ is large ($\hat{r}^+ - \hat{r}^-$ is $\mathcal{O}(\frac{1}{\epsilon})$).
Case 3. We consider spatially and temporally unbounded case; we let the time and spatial scale of interest get large (T and L large) with the relationship of $\frac{L^2}{T} = \mathcal{O}(1)$, and let $\hat{r}^+$ and $\hat{r}^-$ are very similar ($\hat{r}^+ - \hat{r}^-$ is $\mathcal{O}(\epsilon)$) with $u = \mathcal{O}(1)$ and $\hat{r}^{\pm} = \mathcal{O}(1)$.

Among these three scenarios the second case refers to the parabolic limit. In addition to the assumptions we mentioned above, we assume that $v_t = \mathcal{O}(1)$. The second scenario says that movement speed is large relative to the ratio of characteristic length and time scales and turning rates are fast relative to the time scale. In this case, we can study the quasi–steady state approximation of equation (3.6). We differentiate once with respect to x and get

$$v_x = \epsilon\delta(\phi n_x - n_{xx}), \tag{3.7}$$

which is put into equation (3.5) to yield

$$\epsilon n_t + \epsilon\delta(\phi n_x - n_{xx}) = 0. \tag{3.8}$$

By dividing both sides with ϵ, we have

$$n_t - \delta n_{xx} + \phi\delta n_x = 0. \tag{3.9}$$

With rescaling variables and parameters, we here approximate the hyperbolic predator movement equations (3.1)–(3.2) with a parabolic type equation (3.9).

3.2 Symmetric Spatially Dependent Turning Rates

In the previous section, we assume the condition $\rho^{\pm}(x,t) = 1$ so that δ, ϕ and ω are constant with respect to x and t in *Case 2*. Here we tackle the more general case of non–homogeneous $\rho^{\pm}(x,t)$ so that δ, ϕ and ω are functions of x and t. We like to keep δ, ϕ and ω as constants, hence we introduce new paramter functions as with new naming, $d(x,t) = \frac{u^2T}{(r^+(x,t)+r^-(x,t))L^2}$, $\Phi(x,t) = \frac{(r^-(x,t)-r^+(x,t))L}{u}$, and $\Omega(x,t) = r^+(x,t)T$. We restrict to the case where $\rho(x,t) = \rho^+(x,t) = \rho^-(x,t)$, that is, right turning and left turning have the same spatial distribution with different amplitude. Then we have $d(x,t) = \frac{\delta}{\rho(x,t)}$, $\Phi(x,t) = \phi\rho(x,t)$ and $\Omega(x,t) = \omega\rho(x,t)$, where δ, ϕ and ω are constants defined as before, and equation (3.7) is turned into

$$v_x = -\epsilon(d(x,t)n_x)_x + \epsilon(\Phi(x,t)d(x,t)n)_x. \tag{3.10}$$

Since $\Phi(x,t)d(x,t) = \phi\delta$ and $d(x,t) = \frac{\delta}{\rho(x,t)}$, we have

$$v_x = -\epsilon\delta\left(\frac{n_x}{\rho(x,t)}\right)_x + \epsilon\phi\delta n_x, \tag{3.11}$$

which is put into equation (3.5). With dividing both sides by ϵ, we get

$$n_t - \delta\left(\frac{n_x}{\rho(x,t)}\right)_x + \phi\delta n_x = 0. \tag{3.12}$$

With expanding each term, we have

$$n_t + \left(\delta\frac{\rho_x(x,t)}{\rho^2(x,t)} + \phi\delta\right)n_x - \frac{\delta}{\rho(x,t)}n_{xx} = 0, \tag{3.13}$$

which is equivalent to

$$n_t + \left(d(x,t)\frac{\rho_x(x,t)}{\rho(x,t)} + \Phi(x,t)d(x,t)\right)n_x - d(x,t)n_{xx} = 0, \tag{3.14}$$

In addition to $d(x,t) = \mathcal{O}(1)$ and $\Phi(x,t) = \mathcal{O}(1)$, we assume $\rho_x(x,t) = \mathcal{O}(\epsilon)$.
Thus we have a similar result with equation (3.9)

$$n_t - d(x,t)n_{xx} + \Phi(x,t)d(x,t)n_x = 0. \tag{3.15}$$

The only difference is that equation (3.15) has $d(x,t)$ and $\Phi(x,t)$ instead of δ and ϕ respectively.

Steady State Analysis of equation (3.12)

As time approaches infinity, we assume $n_t = 0$ so that the steady state solution of equation (3.12) can be considered. Setting $n_t = 0$ and dividing by δ changes equation (3.12) into

$$-\left(\frac{n_x(x)}{\rho(x)}\right)_x + \phi n_x(x) = 0. \tag{3.16}$$

After integrating, we have

$$-\frac{n_x(x)}{\rho(x)} + \phi n(x) = C, \tag{3.17}$$

where C is determined by initial or boundary conditions. Assuming $n(\infty) = 0$ and $n_x(\infty) = 0$, that is, predator density at the right end edge of the domain is zero, leads to

$$n_x(x) = \rho(x)\phi n(x) = \Phi(x)n(x). \tag{3.18}$$

This equation is solved by

$$n(x) = n_0(x)\exp(\int_0^x \Phi(s)ds), \tag{3.19}$$

where $n_0(x)$ is an initial predator distribution. This solution is expressed in detail as

$$n(x) = n_0(x)\exp\Big\{\int_0^x \frac{(r^-(s) - r^+(s))L}{u}ds\Big\}. \tag{3.20}$$

Under constant turning rates, $\hat{r}^{\pm} = r^{\pm}$ the steady state solution (3.20) is

$$n(x) = n_0(x)\exp\Big\{\frac{(\hat{r}^- - \hat{r}^+)L}{u}x\Big\}. \tag{3.21}$$

With $\hat{r}^- = \hat{r}^+$, the solution is $n(x) = n_0(x)$. However, if we adopt a different boundary condition, we may have a different steady state solution (recall that we assumed that $n(\infty) = 0$ and $n_x(\infty) = 0$). Multiplying equation (3.17) by $\rho(x)$ yields

$$n_x(x) - \Phi(x)n(x) + C\rho(x) = 0. \tag{3.22}$$

If $\rho(x)$ is continuous on the domain, then there exists a unique solution of equation (3.22) [6]. Letting $\mu(x) = \exp(\int -\Phi(s)ds)$, then the solution of equation (3.22) is

$$n(x) = \frac{\int \mu(s)C\rho(s)ds + c}{\mu(x)}, \tag{3.23}$$

for some integral constant c, which can be determined by an initial condition.

In summary, in this section, it was assumed that turning rates are symmetric and spatially dependent. Then an approximation (3.15) of (2.34)–(2.35) was obtained.

3.3 Nonsymmetric Spatially Dependent Turning Rates

In this section, we consider spatially general turning rates for an approximation of (2.34)–(2.35). We now consider $r^{\pm} = \hat{r}^{\pm}\rho^{\pm}(x,t)$ where $\rho^+ \neq \rho^-$ so that $d(x,t) = \frac{u^2T}{(r^+(x,t)+r^-(x,t))L^2}$, $\Phi(x,t) = \frac{(r^-(x,t)-r^+(x,t))L}{u}$ and $\Omega(x,t) = r^+(x,t)T$. This case is important for the application to the satiation based model, since we assume $\rho^{\pm} = R(S^{\pm})$ and $S^+(x,t)$ and $S^-(x,t)$ are spatio–temporal functions. Again we assume that $d(x,t)$ and $\Phi(x,t)$ are $\mathcal{O}(1)$, then equation (3.7) is turned into

$$v_x = -\epsilon(d(x,t)n_x)_x + \epsilon(\Phi(x,t)d(x,t)n)_x. \tag{3.24}$$

We substitute this into equation (3.5) with dividing both sides by ϵ to get

$$n_t - (d(x,t)n_x)_x + (\Phi(x,t)d(x,t)n)_x = 0. \tag{3.25}$$

With expanding each term, we have

$$n_t + (d_x(x,t) - \Phi(x,t)d(x,t))n_x - d(x,t)n_{xx} + (\Phi(x,t)d(x,t))_x n = 0. \tag{3.26}$$

In addition to $d(x,t) = \mathcal{O}(1)$ and $\Phi(x,t) = \mathcal{O}(1)$, we assume $\rho_x^{\pm}(x,t) = \mathcal{O}(\epsilon)$ as before, which implies that $d_x(x,t) = \Phi_x(x,t) = \mathcal{O}(\epsilon)$ from the following calculations:

$$d_x(x,t) = -\frac{\hat{r}^+\rho_x^+(x,t) + \hat{r}^-\rho_x^-(x,t)}{\hat{r}^+\rho^+(x,t) + \hat{r}^-\rho^-(x,t)}d(x,t), \tag{3.27}$$

and

$$\Phi_x(x,t) = \frac{(\hat{r}^-\rho_x^-(x,t) - \hat{r}^+\rho_x^+(x,t))L}{u}. \tag{3.28}$$

Thus we have a similar result with equation (3.9) up to the order $\mathcal{O}(\epsilon)$

$$n_t - d(x,t)n_{xx} + \Phi(x,t)d(x,t)n_x = 0. \tag{3.29}$$

3.4 Parabolic Limit

In this section, we approximate the hyperbolic system (3.1)–(3.2) with a parabolic equation by applying the parabolic limit process.

Addition and subtraction of equations (3.1)–(3.2) lead to the following hyperbolic system.

$$n_t + uv_x = 0 \tag{3.30}$$

$$v_t + un_x = -\xi n - \eta v, \tag{3.31}$$

where $n = n^+ + n^-$, $v = n^+ - n^-$, $\xi = r^+ - r^-$ and $\eta = r^+ + r^-$. In this section, we focus on a general relation among u, ξ and η in order to lead equations (3.1)–(3.2) to a parabolic equation like (3.8).

We first differentiate the first equation with respect to t and the second one with respect to x. Rearranging the second equation after the differentiation, we have

$$\begin{aligned} uv_{xt} &= -u^2 n_{xx} - u(\xi n)_x - u\eta_x v - \eta u v_x \\ &= -u^2 n_{xx} - u(\xi n)_x - u\eta_x v + \eta n_t, \end{aligned} \tag{3.32}$$

with $uv_x = -n_t$. By using the result of differentiating the first equation, i.e. $uv_{xt} = -n_{tt}$, we get

$$n_{tt} - u^2 n_{xx} - u(\xi n)_x - u\eta_x v + \eta n_t = 0. \tag{3.33}$$

If the term including v in (3.33) vanishes, we obtain an equation for n alone. For the scaling below we assume that this term $u\eta_x v$ is of low order. To obtain the desired parabolic limit we assume that there exist a small parameter ϵ, (for example u^{-1}) such that the following quantities scale as $u \sim \frac{1}{\epsilon}$, $\xi \sim \frac{1}{\epsilon}$, and $\eta \sim \frac{1}{\epsilon^2}$. It is important to note that the sum η and the difference ξ of the turning rates scale differently with respect to $\epsilon \to 0$. Other scalings are possible too but it turns out that the above scaling leads to the most general diffusion limit (that includes a drift term). We give examples where the above scaling is reasonable

later. To be specific we assume the model parameters, u, η, and ξ are replaced by u_ϵ, η_ϵ, and ξ_ϵ which scale as

$$u_\epsilon = \frac{1}{\epsilon}u,\ \xi_\epsilon = \frac{1}{\epsilon}\xi \text{ and } \eta_\epsilon = \frac{1}{\epsilon^2}\eta, \tag{3.34}$$

where u, η, and ξ are terms of order one. In addition we assume that

$$\epsilon^2 u_\epsilon (\eta_\epsilon)_x v \to 0 \text{ as } \epsilon \to 0. \tag{3.35}$$

That is, even though η_ϵ is order of $\frac{1}{\epsilon^2}$, the order of $(\eta_\epsilon)_x$ is less than $\frac{1}{\epsilon}$. Otherwise we would keep a term including v.

When replacing u, ξ and η in (3.33) by u_ϵ , ξ_ϵ and η_ϵ, we get

$$n_{tt} - u_\epsilon^2 n_{xx} - u_\epsilon(\xi_\epsilon n)_x - u_\epsilon(\eta_\epsilon)_x v + \eta_\epsilon n_t = 0. \tag{3.36}$$

Then using equation (3.34), we get

$$\epsilon^2 n_{tt} - u^2 n_{xx} - u(\xi n)_x + \eta n_t - \epsilon u(\eta_\epsilon)_x v = 0. \tag{3.37}$$

If $n_{tt} = \mathcal{O}(1)$, then we get the following parabolic equation.

$$n_t = \frac{u^2}{\eta}n_{xx} + \frac{1}{\eta}u(\xi n)_x + \mathcal{O}(\epsilon^\gamma), \tag{3.38}$$

with $\gamma > 0$ As $\epsilon \to 0$,

$$\begin{aligned} n_t &= \frac{u^2}{\eta}n_{xx} + \frac{1}{\eta}u(\xi n)_x \\ &= \frac{u^2}{\eta}n_{xx} + u\left(\frac{\xi}{\eta}n\right)_x \\ &= \frac{u^2}{\epsilon^2(r^+ + r^-)}n_{xx} + u\left(\frac{\epsilon(r^+ - r^-)}{\epsilon^2(r^+ + r^-)}n\right)_x \\ &= \frac{u^2}{\epsilon^2(r^+ + r^-)}n_{xx} + u\left(\frac{r^+ - r^-}{\epsilon(r^+ + r^-)}n\right)_x \\ &= \frac{u_\epsilon^2}{r^+ + r^-}n_{xx} + u_\epsilon\left(\frac{r^+ - r^-}{r^+ + r^-}n\right)_x. \end{aligned} \tag{3.39}$$

This equation is of divergence form. Dropping ϵ from u_ϵ for simplicity, we define a total predator flux as

$$\mathbf{J}_n = -\left(\frac{u^2}{r^- + r^+}\right)\frac{\partial n}{\partial x} + n\left(\frac{r^- - r^+}{r^- + r^+}\right)u, \tag{3.40}$$

Example 1. Especially with the example of $r^\pm = \frac{A}{2\epsilon^2} \mp \frac{A\chi}{2\epsilon}\frac{\partial V}{\partial x}$, we have $\lim_{\epsilon\to 0}\epsilon^2(r^- + r^+) = A$ and $\lim_{\epsilon\to 0}\frac{(r^+ - r^-)}{\epsilon(r^+ + r^-)} = \frac{1}{A}\lim_{\epsilon\to 0}\epsilon(r^+ - r^-) = \frac{1}{A}(-A\chi\frac{\partial V}{\partial x})$. Here A is some constant and V is a prey density. After borrowing chemotactic notation, for $\epsilon \to 0$, we formally get

$$n_t = (Dn_x - \chi n \partial V/\partial x)_x, \tag{3.41}$$

with

$$D = \frac{u^2}{A}. \tag{3.42}$$

The above formal calculation of a parabolic limit allows two interpretations. Firstly if $r^{\pm}$ and u are known from experimental data then we derive expressions for the diffusion coefficient D and preytactic sensitivity χ of the whole population. Secondly if D and χ of the parabolic system are given then we choose turning rates $r_{\epsilon}^{\pm}$ and speed u_{ϵ} such that the hyperbolic model (2.14) and (2.15) converges formally to the parabolic equation (3.41)

Now we consider the boundary conditions of (3.41). A Dirichlet boundary condition is obtained from equations (3.30)–(3.31) by using a limit process. In section 2.6 the zero Dirichlet boundary condition for the hyperbolic system is

$$n^+(0,t) = 0,\ n^-(l,t) = 0, \tag{3.43}$$

which leads to $n(0,t) = n^-(0,t) = -v(0,t)$ and $n(l,t) = n^+(l,t) = v(l,t)$. At $x = 0$, the above statement gives $n_t(0,t) = -v_t(0,t)$ and equation (3.30) $n_t(0,t) = -uv_x(0,t)$. In addition, equation (3.31) isolates $-v_t(0,t)$ with $un_x(0,t) + \xi n(0,t) + \eta v(0,t)$. Thus we have one equation

$$-uv_x(0,t) = un_x(0,t) + \xi n(0,t) + \eta v(0,t). \tag{3.44}$$

By using the limiting process (3.34), equation (3.44) gives $v(0,t) = 0$, which leads to $n(0,t) = 0$. Similarly we have $n(l,t) = 0$.

The no–flux boundary condition for the hyperbolic system is

$$n^+(0,t) = n^-(0,t),\ n^-(l,t) = n^+(l,t). \tag{3.45}$$

Thus for all t we have $v(0,t) = n^+(0,t) - n^-(0,t) = 0$ and $v(l,t) = n^+(l,t) - n^-(l,t) = 0$, which yield that $v_t(0,t) = 0$ and $v_t(l,t) = 0$. At $x = 0$ equation (3.31) leads to

$$v_t(0,t) + un_x(0,t) = -\xi n(0,t) \tag{3.46}$$

since $v(0,t) = 0$ and $v_t(0,t) = 0$. Therefore $n_x(0,t) = -\frac{\xi}{u} n(0,t)$. Similarly we have $n_x(l,t) = -\frac{\xi}{u} n(l,t)$.

In this section, we approximated the hyperbolic system (3.1)–(3.2) with a parabolic equation by applying the parabolic limit process. We also considered the boundary condition for the parabolic equation based on the boundary condition for the hyperbolic system (3.1)–(3.2). In the next section, we will consider the two coefficients of the parabolic equation (3.41).

3.5 Prey Sensitivity and Diffusion Rate Approximation

In this section, we consider two coefficients of the parabolic equation (3.41). In the last section, one example of $r^{\pm}$ was introduced. In this section, we consider turning rates as derived in Sections 2.4–2.5. We will approximate $r^- + r^+$ and $r^- - r^+$ in equation (3.40) to find prey sensitivity and diffusion rate in terms of average turning rate and satiation related functions. We begin with the assumption of $S^+ = S_0 - g$ and $S^- = S_0 + g$, in which S_0 is a temporal equilibrium state of satiation at a given location (see Section 2.2 for detail) and g is a small variable (much smaller than 1). Then Taylor expansions of r^+ and r^- are

$$r^+ = R(S^+) = R(S_0 - g) = R(S_0) - \frac{dR}{dS}(S_0)g + \mathcal{O}(g^2)$$
$$r^- = R(S^-) = R(S_0 + g) = R(S_0) + \frac{dR}{dS}(S_0)g + \mathcal{O}(g^2)$$

From these expansions, we get

$$r^- + r^+ \approx 2R(S_0) + \mathcal{O}(g^2), \tag{3.47}$$

and

$$r^- - r^+ \approx 2\frac{dR}{dS}(S_0)g + \mathcal{O}(g^3). \tag{3.48}$$

g here can be identified with ϵ in the parabolic limit formulation. If we now assume that $R(S_0) \sim \mathcal{O}(1/g^2)$ and $\frac{dR}{dS}(S_0) \sim \mathcal{O}(1/g^2)$ and in addition $u \sim \mathcal{O}(1/g)$ then we find $r^- + r^+ \sim \mathcal{O}(1/\epsilon^2)$ and $r^- - r^+ \sim \mathcal{O}(1/\epsilon)$ as was assumed in the parabolic limit. Thus the next step is the identification of g to complete the approximation of the prey sensitivity. To estimate g, we use spatial satiation variation equations (2.30)–(2.31). Plugging $S^- = S_0 + g$ and $S^+ = S_0 - g$ into equations (2.30)–(2.31), we have

$$\frac{\partial S_0}{\partial t} + u\frac{\partial S_0}{\partial x} - \left(\frac{\partial g}{\partial t} + u\frac{\partial g}{\partial x}\right) = -\frac{r^- n^-}{n^+}(-2g) + f(S_0, V) - \frac{\partial f}{\partial S}(S_0, V)g, \tag{3.49}$$

$$\frac{\partial S_0}{\partial t} - u\frac{\partial S_0}{\partial x} + \frac{\partial g}{\partial t} - u\frac{\partial g}{\partial x} = \frac{r^+ n^+}{n^-}(-2g) + f(S_0, V) + \frac{\partial f}{\partial S}(S_0, V)g, \tag{3.50}$$

Since S_0 is a temporal equilibrium state of satiation, $\partial S_0/\partial t = 0$ and $f(S_0, V) = 0$. Thus equations (3.49–3.50) are simplified as

$$u\frac{\partial S_0}{\partial x} - \left(\frac{\partial g}{\partial t} + u\frac{\partial g}{\partial x}\right) = -\frac{r^- n^-}{n^+}(-2g) - \frac{\partial f}{\partial S}(S_0, V)g, \tag{3.51}$$

$$-u\frac{\partial S_0}{\partial x} + \frac{\partial g}{\partial t} - u\frac{\partial g}{\partial x} = \frac{r^+ n^+}{n^-}(-2g) + \frac{\partial f}{\partial S}(S_0, V)g. \tag{3.52}$$

With the additional assumptions of $\partial g/\partial t \ll 1$ and $r^\pm = R(S_0) + \mathcal{O}(g)$, we have

$$u\frac{\partial S_0}{\partial x} - u\frac{\partial g}{\partial x} = -\frac{R(S_0)n^-}{n^+}(-2g) - \frac{\partial f}{\partial S}(S_0, V)g, \tag{3.53}$$

$$-u\frac{\partial S_0}{\partial x} - u\frac{\partial g}{\partial x} = \frac{R(S_0)n^+}{n^-}(-2g) + \frac{\partial f}{\partial S}(S_0, V)g. \tag{3.54}$$

Subtracting equation (3.54) from equation (3.53), we have

$$2u\frac{\partial S_0}{\partial x} = 2(R(S_0)\left(\frac{n^-}{n^+} + \frac{n^+}{n^-} - \frac{\partial f}{\partial S}(S_0, V)\right)g. \tag{3.55}$$

Therefore, g is isolated as

$$g = \frac{u\frac{\partial S_0}{\partial x}}{(R(S_0)(\frac{n^-}{n^+} + \frac{n^+}{n^-}) - \frac{\partial f}{\partial S}(S_0, V))}, \tag{3.56}$$

where $\frac{\partial S_0}{\partial x} = \frac{dS_0}{dV}\frac{\partial V}{\partial x}$ is expanded. From (3.48) we find,

$$r^- - r^+ \approx 2\frac{u\frac{dR}{dS}(S_0)\frac{\partial S_0}{\partial x}}{(R(S_0)(\frac{n^-}{n^+} + \frac{n^+}{n^-}) - \frac{\partial f}{\partial S}(S_0, V))} + \mathcal{O}(g^3). \tag{3.57}$$

We plug all results into the predator flux (3.40) and borrow the idea of prey sensitivity from equation (3.41). Then prey sensitivity is approximated as follows:

$$\chi(V,n^+,n^-) = \frac{u^2 \frac{dR}{dS}[S_0(V)]\frac{dS_0}{dV}(V)}{\Big(R[S_0(V)]\Big\{R[S_0(V)](n^-/n^+ + n^+/n^-) - \frac{\partial f}{\partial S}[S_0(V),V]\Big\}\Big)}. \tag{3.58}$$

Note that $\chi(V,n^+,n^-)$ is a little different from the approximation by Kareiva and Odell [46], who chose

$$\chi_{KO}(V) = \frac{u^2 \frac{dR}{dS}[S_0(V)]\frac{dS_0}{dV}(V)}{\Big(R[S_0(V)]\Big\{2R[S_0(V)] - \frac{\partial f}{\partial S}[S_0(V),V]\Big\}\Big)}. \tag{3.59}$$

If we assume that $\frac{dR}{dS}[S_0(V)]\frac{dS_0}{dV}(V) \geq 0$ then we can use the inequality $\frac{n^-}{n^+} + \frac{n^+}{n^-} \geq 2$ to observe that $0 \leq \chi(V,n^+,n^-) \leq \chi_{KO}(V)$. It is seen that $\chi_{KO}(V)$ is the maximum of $\chi(V,n^+,n^-)$. In addition, the formula of Kareiva and Odell has the advantage, that is, $\chi_{KO}(V)$ does not depend explicitly on the predator populations n^+ and n^-. Thus we use $\chi_{KO}(V)$ as a prey sensitivity $\chi(V)$ throughtout this thesis.

Example 2. For specific choices of $S(V) = \frac{\gamma V}{\lambda + V(\gamma+\lambda/\nu)}$, $f(S,V) = \frac{\gamma(1-S)V}{1+V/\nu} - \lambda S$, and $R(S) = -a_1 \log(1 - S/b_1)$, we analytically calculated prey sensitivity $\chi(V)$ for small prey density V. We have

$$\chi(V) = \frac{A}{V} + B + \mathcal{O}(V), \tag{3.60}$$

where $A = \frac{u^2}{\lambda}$ and $B = -\frac{A}{2}\frac{(4\lambda b_1\gamma\nu + 2\lambda^2 b_1 - \lambda\gamma\nu + 4\gamma\nu a_1)}{b_1\lambda^3\nu}$ with $\lambda = 2.3384$/day, $\gamma = 0.018632$, $\nu = 711.2$/m and $u = 5.87$m/day from [46] and a_1 and b_1 from the best fit of the turning rate (see section 2.5).

In general, the diffusion rate is $\frac{u^2}{r^+ + r^-}$ and from the Taylor expansion (3.47)

$$D(V) \approx \frac{u^2}{2R[S_0(V)]}. \tag{3.61}$$

For the above example 1, we have the following approximation of order O(1):

$$D(V) = \frac{C}{V} + E + \mathcal{O}(V). \tag{3.62}$$

where $C = \frac{u^2\lambda b_1}{2a_1\gamma}$ and $E = \frac{u^2(2b_1\gamma\nu + 2b_1\lambda - \gamma\nu)}{4\gamma a_1\nu}$. Thus, we have

$$\frac{\chi(V)}{D(V)} = 2\frac{\gamma a_1}{\lambda^2 b_1} + \mathcal{O}(V). \tag{3.63}$$

Kareiva and Odell [46] estimated parameters in the prey sensitivity (3.59) and diffusion rate (3.61) (see Table 3.5), where $R(S) = \beta_0 + \beta_1 S + \beta_2 S^2 + \beta_3 S^3$, $S_0(V) = \frac{\gamma V}{\lambda + V(\gamma+\lambda/\nu)}$, and $\frac{\partial f}{\partial S} = -(\lambda + \frac{\gamma V}{1+V/\nu})$. The diffusion rate $D(V)$ and the prey sensitivity functions $\chi_{KO}(V)$ are shown in Figures 3.1 and 3.2 as functions of prey density V, respectively. According to the estimation of the diffusion rate and the prey sensitivity functions from Kareiva and Odell, the diffusion rate is much bigger than the prey sensitivity. To compute the prey sensitivity function (3.59), we need to know four functions; $\frac{\partial f}{\partial S}[S_0(V),V]$, $R[S_0(V)]$,

parameter	value	parameter	value
u	5.87 m/day	β_0	1.7115
β_1	45.3098/day	β_2	-180.172/day
β_3	272.991/day	γ	0.018632
λ	2.3384/day	ν	711.2/m

Table 3.1: Parameters used to compute the prey sensitivity (3.59) and diffusion rate (3.61) in [46]

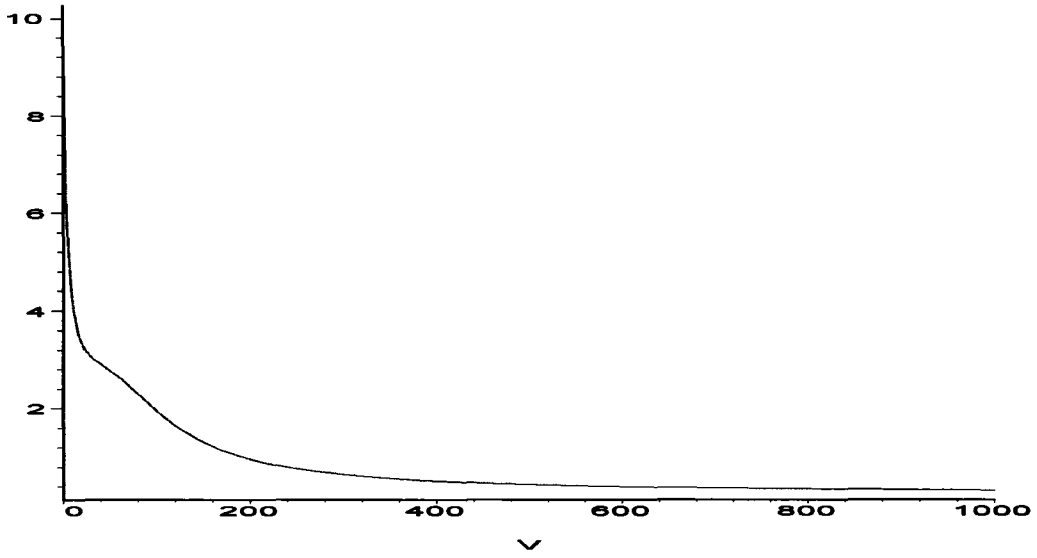

Figure 3.1: The diffusion rate approximated by Kareiva and Odell [46].

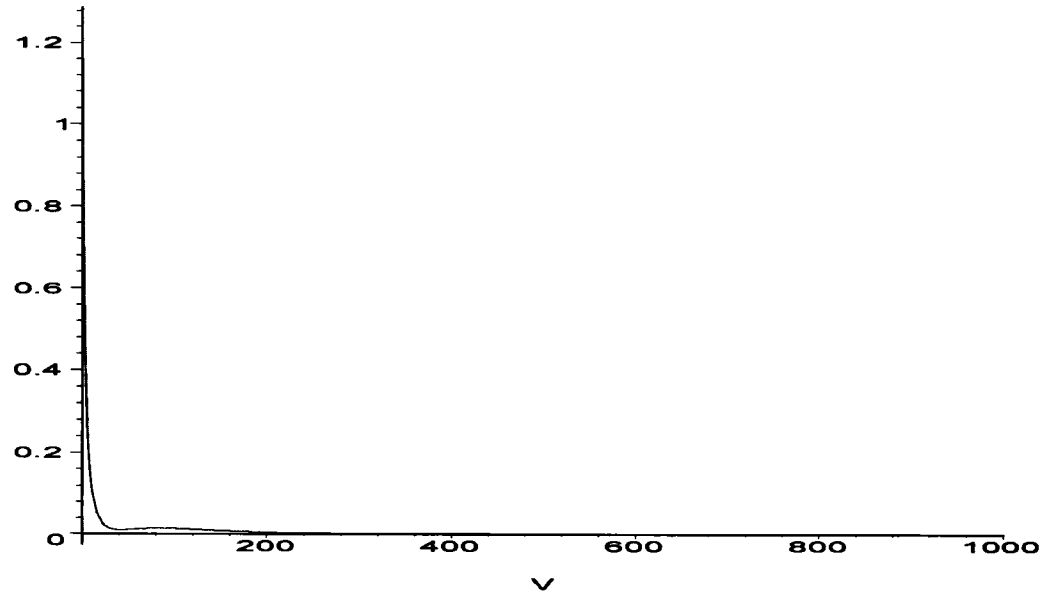

Figure 3.2: The prey sensitivity approximated by Kareiva and Odell [46].

$\frac{dR}{dS}[S_0(V)]$, and $\frac{dS_0}{dV}(V)$. In Figure 3.3 we plot these four functions with parameters from Kareiva and Odell. In section 2.5, we compared four turning rate models to find the best fit to the data from Kareiva and Odell. Those four models are substituted into the prey sensitivity function (3.59) of Kareiva and Odell and plotted in Figure 3.4. The best fit of the turning rate model (model 2) shows qualitatively similar features with model 1 which Kareiva and Odell used. Model 3 and model 4 show negative quantative when prey density is low. In particular, when prey density is low, Model 3 show two singular points because $R[S_0(V)] = 0$ and $2R[S_0(V)] - \frac{\partial f}{\partial S}(S_0, V) = 0$ make the denominator of $\chi(V)$ zero (see the form of $\chi(V)$ (3.59)). It is noted that the prey sensitivity may be negative if we use different functional response. With the type IV functional response, $\frac{dR}{dV}[S_0(V)]$ is negative for a large prey density so that in the prey sensitive functions, (3.58) or (3.59), for any turning rate models $\chi(V)$ becomes negative as prey density increases over some threshold density.

In this section, we approximated two coefficients of the parabolic equation (3.41); the prey sensitivity and the diffusion rate. The results were compared with the prey sensitivity and the diffusion rate found by Karieva and Odell [46].

3.6 Alternative Derivation of Prey–Taxis Equations from Resting–Model

We now derive prey–taxis equations from models interchanging between resting state and directional moving state. Hillen [34] considered the exchange between resting phase and directional moving state in n spatial dimensions to derive taxis equations in a scaling limit. Here, as before, we consider a one–dimensional setting. We are interested in the effect of a resting compartment for the predators on the overall population dynamics. In the following sections we introduce a resting compartment $q(x,t)$ where the transition rates for stopping

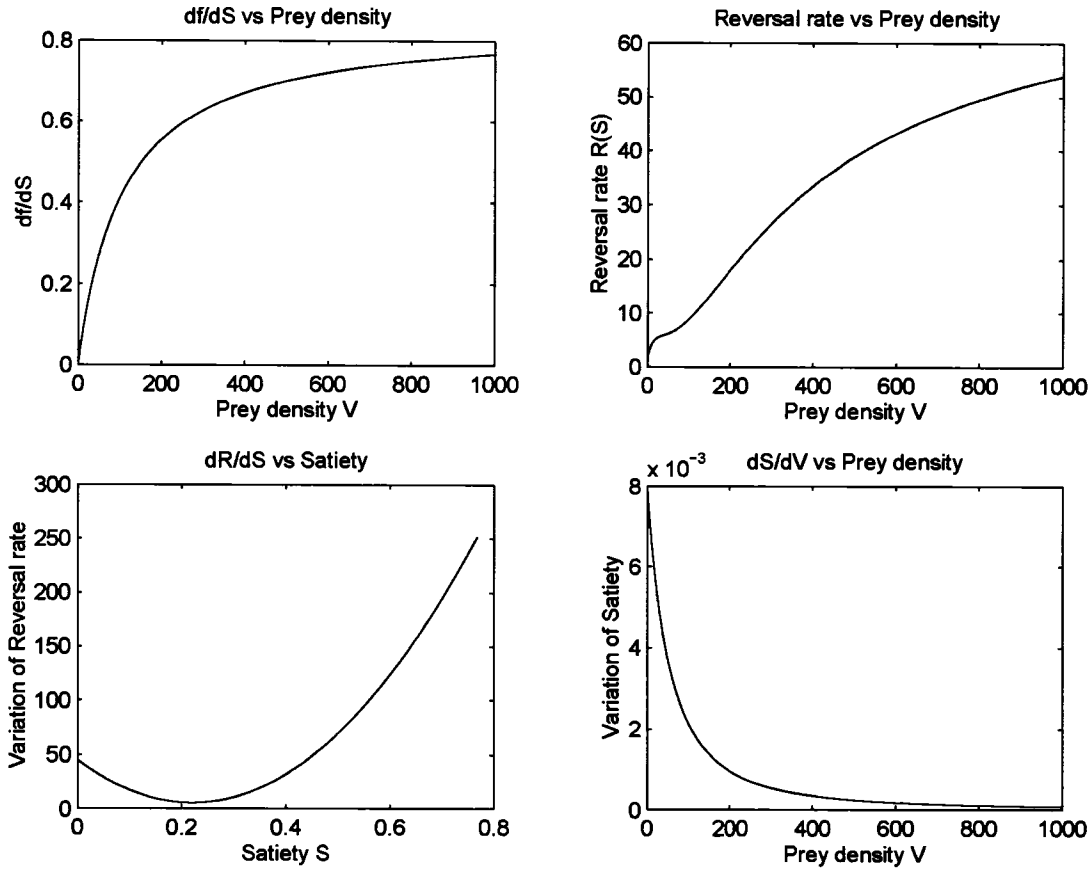

Figure 3.3: Various functions, $\frac{\partial f}{\partial S}[S_0(V), V]$, $R[S_0(V)]$, $\frac{dR}{dS}[S_0(V)]$, and $\frac{dS_0}{dV}(V)$, used for approximating prey sensitivity and diffusion rate are displayed vs prey density or satiety for the Kareiva–Odell case.

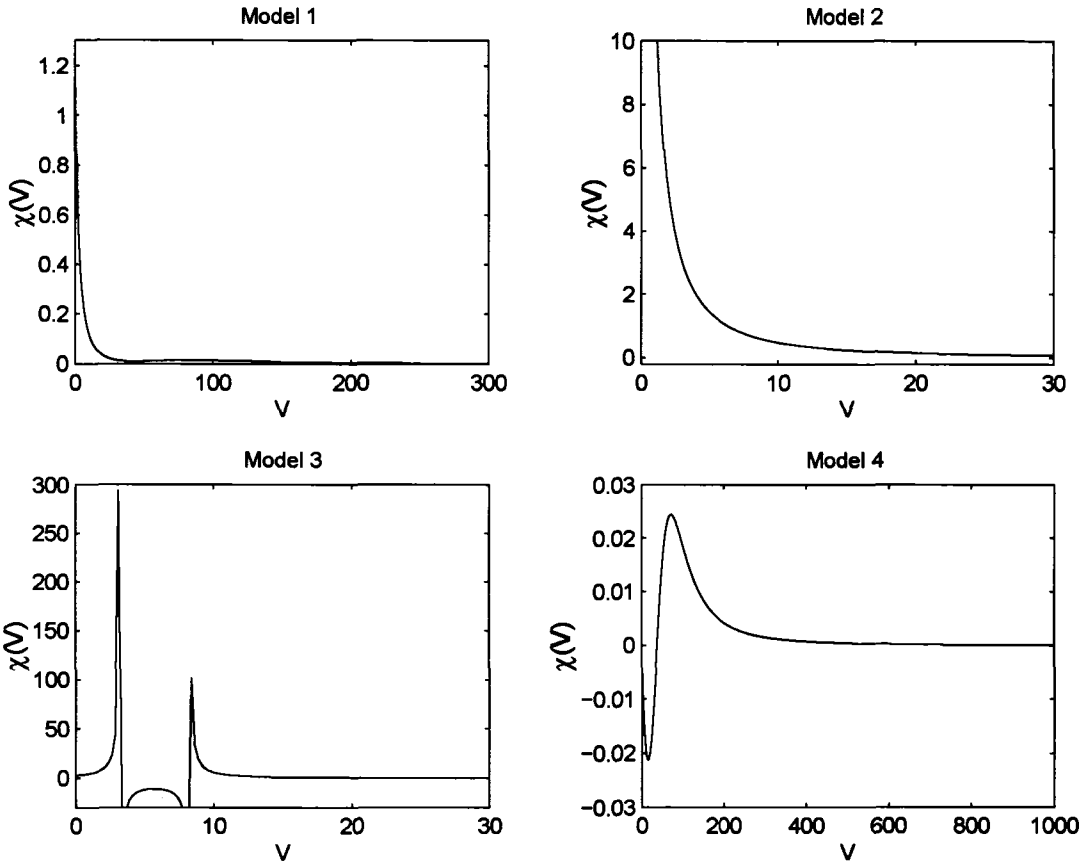

Figure 3.4: Four turning rate models in Section 2.5 are applied for the prey sensitivity $\chi(V)$ in response to prey density V.

and resuming moving depend on a given prey density $V(x,t)$.

In section 3.6.1 we focus on the moving–resting dynamics without random directional changes and without population dynamics. We introduce the method of asymptotic expansions in macroscopic time and space scales. In section 3.6.2 we extend the model to include random directional changes and birth and death events in the moving compartment. In section 3.6.3 we consider birth and death events in the quiescent compartment and in section 3.6.4 we study a combination of the previous models.

It turns out that the diffusion and taxis coefficients are scaled by the mean fraction of moving predators. The effective population kinetics is given as a convex combination of the birth and death terms of the moving and resting phases, respectively. The relative weights are given by the mean fraction of the population at resting or moving state.

3.6.1 Moving–Resting Dynamics

In this section, for right moving and left moving predators, we introduce a resting state of predators. It is assumed that transitions between right– and left–moving states occur via the resting state, that is, there is no direct transition between right– and left–moving states. The dynamics of the total predator population will be expressed in a parabolic equation.

$$\frac{\partial n^+}{\partial t} + u\frac{\partial n^+}{\partial x} = -\alpha(V,S)n^+ + \frac{\beta(S)}{2}q, \tag{3.64}$$

$$\frac{\partial n^-}{\partial t} - u\frac{\partial n^-}{\partial x} = -\alpha(V,S)n^- + \frac{\beta(S)}{2}q, \tag{3.65}$$

$$\frac{\partial q}{\partial t} = \alpha(V,S)(n^+ + n^-) - \beta(S)q, \tag{3.66}$$

where $q(t)$ is a density of resting predators, $\alpha(V,S)$ a stopping rate from moving state to resting state, and $\beta(S)$ a transition rate from resting state to moving state. We assume that predators that enter the moving state choose either direction with probability $\frac{1}{2}$.

Setting $n = n^+ + n^-$ and $v = n^+ - n^-$ and adding and subtracting equations (3.64–3.65), we have

$$n_t + uv_x = -\alpha(V,S)n + \beta(S)q, \tag{3.67}$$

$$v_t + un_x = -\alpha(V,S)v, \tag{3.68}$$

$$q_t = \alpha(V,S)n - \beta(S)q. \tag{3.69}$$

We now introduce the scaling of $\tau = \epsilon^2 t$ and $\xi = \epsilon x$ for small $0 < \epsilon \ll 1$. Then equations (3.67– 3.69) turn into

$$\epsilon^2 n_\tau + u\epsilon v_\xi = -\alpha(V,S)n + \beta(S)q, \tag{3.70}$$

$$\epsilon^2 v_\tau + u\epsilon n_\xi = -\alpha(V,S)v, \tag{3.71}$$

$$\epsilon^2 q_\tau = \alpha(V,S)n - \beta(S)q. \tag{3.72}$$

We consider series expansions:

$$n(\tau,\xi) = n_0(\tau,\xi) + \epsilon n_1(\tau,\xi) + \epsilon^2 n_2(\tau,\xi) + \mathcal{O}(\epsilon^3) \tag{3.73}$$

$$v(\tau,\xi) = v_0(\tau,\xi) + \epsilon v_1(\tau,\xi) + \epsilon^2 v_2(\tau,\xi) + \mathcal{O}(\epsilon^3) \tag{3.74}$$

$$q(\tau) = q_0(\tau) + \epsilon q_1(\tau) + \epsilon^2 q_2(\tau) + \mathcal{O}(\epsilon^3). \tag{3.75}$$

We introduce these expansions into equations (3.70– 3.72) and collect orders of ϵ:
ϵ^0:

$$\alpha(V,S)n_0 - \beta(S)q_0 = 0 \tag{3.76}$$
$$\alpha(V,S)v_0 = 0, \tag{3.77}$$

ϵ^1:

$$uv_{0\xi} = -\alpha(V,S)n_1 + \beta(S)q_1 \tag{3.78}$$
$$un_{0\xi} + \alpha(V,S)v_1 = 0, \tag{3.79}$$

ϵ^2:

$$n_{0\tau} + uv_{1\xi} = -\alpha(V,S)n_2 + \beta(S)q_2 \tag{3.80}$$
$$v_{0\tau} + un_{1\xi} = -\alpha(V,S)v_2, \tag{3.81}$$
$$q_{0\tau} = \alpha(V,S)n_2 - \beta(S)q_2. \tag{3.82}$$

From equation (3.76), we have $q_0 = \frac{\alpha(V,S)}{\beta(S)}n_0$, and equation (3.77) gives $v_0 = 0$ so that $v_{0\xi} = v_{0\tau} = 0$. Using the result from equation (3.82) and equation (3.79), that is, $v_1 = -\frac{u}{\alpha(V,S)}n_{0\xi}$, equation (3.80) is rewritten as

$$n_{0\tau} + u\left(-\frac{u}{\alpha(V,S)}n_{0\xi}\right)_\xi = -q_{0\tau} = -\left(\frac{\alpha(V,S)}{\beta(S)}n_0\right)_\tau, \tag{3.83}$$

which leads to

$$\left(n_0\left(1+\frac{\alpha(V,S)}{\beta(S)}\right)\right)_\tau = \left(\frac{u^2}{\alpha(V,S)}n_{0\xi}\right)_\xi. \tag{3.84}$$

Defining $a = n_0\frac{(\beta+\alpha)}{\beta} = n_0 + q_0$, we have $n_0 = \frac{\beta}{\beta+\alpha}a$. Plugging this into equation (3.84), we have an equation for the total population (resting population plus moving population) as follows:

$$a_\tau = \left(\frac{u^2}{\alpha}\left(\frac{\beta}{\beta+\alpha}a\right)_\xi\right)_\xi. \tag{3.85}$$

The expansion of the right hand side of the above equation gives

$$a_\tau = \left(\frac{u^2}{\alpha}\frac{\beta}{\beta+\alpha}a_\xi + \frac{u^2}{\alpha}\left(\frac{\beta}{\beta+\alpha}\right)_\xi a\right)_\xi. \tag{3.86}$$

Here $\frac{u^2}{\alpha}\frac{\beta}{\beta+\alpha}a_\xi$ term is interpreted as a diffusion term and $\frac{u^2}{\alpha}(\frac{\beta}{\beta+\alpha})_\xi a$ as a taxis term.

Example 3: We assume specifically that predators tend to change into a resting state as energy input increases, e.g. $\alpha(V,S) = \kappa S$. Resting predators resume moving as the satiation related energy level decreases, e.g. $\beta(S) = (1-S)$. That is, as a predator is satiated, it tends to move into a resting state and as satiation level diminishes, a predator tends to resume its mobility for searching food. We recall the notation of S_0 in Section 2.2 that $S_0(V)$ is a solution to $(1-S)g(V) - \kappa S = 0$. Then we have $\alpha(V,S_0) = (1-S_0)g(V)$

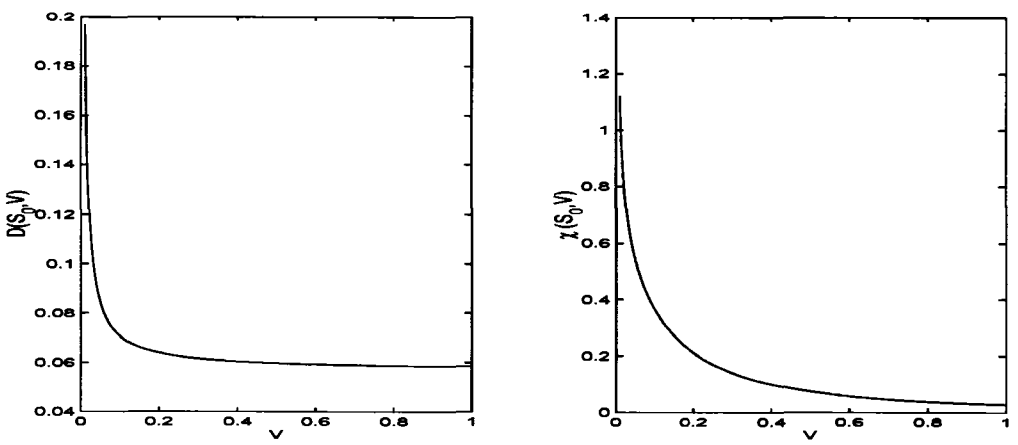

Figure 3.5: In Example 2, the prey sensitivity $\chi(S_0, V)$ and the diffusion rate $D(S_0, V)$ are calculated with rescaled functional response $g(V)$, i.e. $V \in [0, 1]$, and moving speed u used by Kareiva and Odell [46].

and $\beta(S_0) = (1 - S_0)$. As a result, a diffusion rate, $D(S_0, V)$, and a taxis term, $\chi(S_0, V)$, are defined,

$$D(S_0, V) = \frac{u^2}{(1 - S_0)g(V)(g(V) + 1))} = \frac{u^2(g(V) + \kappa}{\kappa g(V)(g(V) + \kappa))}, \text{ and} \tag{3.87}$$

$$\chi(S_0, V) = \frac{u^2}{(1 - S_0)g(V)} \left(\frac{1}{1 + g(V)} \right)_V = -\frac{u^2 g_V(V)}{\kappa g(V)(g(V) + 1)^2}, \tag{3.88}$$

so that equation (3.86) is expressed as follows:

$$a_\tau = \left(D(S_0, V)a_\xi - \chi(S_0, V)\frac{\partial V}{\partial \xi}a \right)_\xi . \tag{3.89}$$

With rescaling prey density, we used the functional response $g(V)$ by Kareiva and Odell [46] to draw the graphs of a diffusion rate, $D(S_0, V)$, and a taxis term, $\chi(S_0, V)$. Figure 3.5 demonstrates that both diffusion rate and prey sensitivity are inversely proportional to the prey density V.

3.6.2 The Resting–Model Including Reproduction and Death in Moving State Only

In this section, we consider that there are direct transitions between right– and left–moving states. We also include reproduction and death of predators in moving state (we will

consider reproduction and death of predators in resting state in the next section) as follows

$$\frac{\partial n^+}{\partial t} + u\frac{\partial n^+}{\partial x} = -\alpha(V,S)n^+ + \frac{\beta(S)}{2}q - rn^+ + rn^- + \epsilon^2\left(\frac{b(n,S)}{2}n - m(n,S)n^+\right), \tag{3.90}$$

$$\frac{\partial n^-}{\partial t} - u\frac{\partial n^-}{\partial x} = -\alpha(V,S)n^- + \frac{\beta(S)}{2}q + rn^+ - rn^- + \epsilon^2\left(\frac{b(n,S)}{2}n - m(n,S)n^-\right), \tag{3.91}$$

$$\frac{\partial q}{\partial t} = \alpha(V,S)(n^+ + n^-) - \beta(S)q, \tag{3.92}$$

where $q(t)$, $\alpha(V,S)$, and $\beta(S)$ are defined as before. $b(n,S)$ is a birth rate of total moving predator population and $m(n,S)$ a death rate of total moving predator population.

Setting $n = n^+ + n^-$ and $v = n^+ - n^-$, and adding and subtracting equations (3.90)–(3.91), we have

$$n_t + uv_x = -(\alpha(V,S) + \epsilon^2(m(n,S) - b(n,S))n + \beta(S)q, \tag{3.93}$$

$$v_t + un_x = -(\alpha(V,S) + 2r + \epsilon^2 m(n,S))v, \tag{3.94}$$

$$q_t = \alpha(V,S)(n^+ + n^-) - \beta(S)q. \tag{3.95}$$

We now introduce the scaling of $\tau = \epsilon^2 t$ and $\xi = \epsilon x$ for small $0 < \epsilon \ll 1$. Then equations (3.93– 3.95) turn into

$$\epsilon^2 n_\tau + u\epsilon v_\xi = -(\alpha(V,S) + \epsilon^2(m(n,S) - b(n,S))n + \beta(S)q, \tag{3.96}$$

$$\epsilon^2 v_\tau + u\epsilon n_\xi = -\alpha(V,S)v - 2rv - \epsilon^2 mv, \tag{3.97}$$

$$\epsilon^2 q_\tau = \alpha(V,S)(n^+ + n^-) - \beta(S)q. \tag{3.98}$$

We consider series expansions as before:

$$n(\tau,\xi) = n_0(\tau,\xi) + \epsilon n_1(\tau,\xi) + \epsilon^2 n_2(\tau,\xi) + \mathcal{O}(\epsilon^3) \tag{3.99}$$

$$v(\tau,\xi) = v_0(\tau,\xi) + \epsilon v_1(\tau,\xi) + \epsilon^2 v_2(\tau,\xi) + \mathcal{O}(\epsilon^3) \tag{3.100}$$

$$q(\tau) = q_0(\tau) + \epsilon q_1(\tau) + \epsilon^2 q_2(\tau) + \mathcal{O}(\epsilon^3). \tag{3.101}$$

We introduce these expansions into equations (3.96– 3.98) and collect orders of ϵ:
ϵ^0:

$$\alpha(V,S)n_0 - \beta(S)q_0 = 0 \tag{3.102}$$

$$(\alpha(V,S) + 2r)v_0 = 0, \tag{3.103}$$

ϵ^1:

$$uv_{0\xi} = -\alpha(V,S)n_1 + \beta(S)q_1 \tag{3.104}$$

$$un_{0\xi} + (\alpha(V,S) + 2r)v_1 = 0, \tag{3.105}$$

ϵ^2:

$$n_{0\tau} + uv_{1\xi} = -\alpha(V,S)n_2 + \beta(S)q_2 - (m-b)n_0 \tag{3.106}$$

$$v_{0\tau} + un_{1\xi} = -(\alpha(V,S) + 2r)v_2 - mv_0, \tag{3.107}$$

$$q_{0\tau} = \alpha(V,S)n_2 - \beta(S)q_2 \tag{3.108}$$

From equation (3.102), we have $q_0 = \frac{\alpha(V,S)}{\beta(S)}n_0$, and equation (3.103) gives $v_0 = 0$ due to $r \geq 0$ so that $v_{0\xi} = v_{0\tau} = 0$. Using the result from equation (3.108) and equation (3.105), that is, $v_1 = -\frac{u}{(\alpha(V,S)+2r)}n_{0\xi}$, equation (3.106) is rewritten as

$$n_{0\tau} + u\left(-\frac{u}{(\alpha(V,S)+2r)}n_{0\xi}\right)_\xi = -q_{0\tau} - (m-b)n_0 = -\left(\frac{\alpha(V,S)}{\beta(S)}n_0\right)_\tau - (m-b)n_0, \tag{3.109}$$

which leads to

$$\left(n_0\left(1 + \frac{\alpha(V,S)}{\beta(S)}\right)\right)_\tau = \left(\frac{u^2}{(\alpha(V,S)+2r)}n_{0\xi}\right)_\xi + (b-m)n_0. \tag{3.110}$$

Defining $a = n_0\frac{(\beta+\alpha)}{\beta} = n_0 + q_0$, we have $n_0 = \frac{\beta}{\beta+\alpha}a$. Plugging this into the equation (3.110), we have a equation of total population (resting population plus moving population) as follows:

$$a_\tau = \left(\frac{u^2}{(\alpha+2r)}\left(\frac{\beta}{\beta+\alpha}a\right)_\xi\right)_\xi + (b-m)\frac{\beta}{\beta+\alpha}a. \tag{3.111}$$

The expansion of the right hand side of the above equation gives

$$a_\tau = \left(\frac{u^2}{(\alpha+2r)}\frac{\beta}{\beta+\alpha}a_\xi + \frac{u^2}{(\alpha+2r)}\left(\frac{\beta}{\beta+\alpha}\right)_\xi a\right)_\xi + (b-m)\frac{\beta}{\beta+\alpha}a. \tag{3.112}$$

Here $\frac{u^2}{(\alpha+2r)}\frac{\beta}{\beta+\alpha}a_\xi$ term is interpreted as a diffusion term, $\frac{u^2}{(\alpha+2r)}(\frac{\beta}{\beta+\alpha})_\xi a$ as a taxis term, and $(b-m)\frac{\beta}{\beta+\alpha}a$ a population dynamics term. It is noted that including reproduction and death does not change the diffusion term and prey sensitivity but affects total population dynamics. Here we encounter reproduction term $(b-m)\frac{\beta}{\beta+\alpha}a$, which is interpreted as product of population growth rate $(b-m)$ and the relative population of reproduction in the total population $\frac{\beta}{\beta+\alpha}a$.

3.6.3 The Resting–Model Including Reproduction and Death in Resting State Only

In the previous case the population dynamics was happenning only in the moving compartment. Here we assume the opposite, that is, we include reproduction and death in resting state only again on a slow time scale.

$$\frac{\partial n^+}{\partial t} + u\frac{\partial n^+}{\partial x} = -\alpha(V,S)n^+ + \frac{\beta(S)}{2}q - rn^+ + rn^-, \tag{3.113}$$

$$\frac{\partial n^-}{\partial t} - u\frac{\partial n^-}{\partial x} = -\alpha(V,S)n^- + \frac{\beta(S)}{2}q + rn^+ - rn^-, \tag{3.114}$$

$$\frac{\partial q}{\partial t} = \alpha(V,S)(n^+ + n^-) - \beta(S)q + \epsilon^2(b-m)q, \tag{3.115}$$

where $q(t)$, $\alpha(V,S)$, $\beta(S)$, $m(q,S)$, and $b(q,S)$ are defined as before.

An asymptotic analysis as done above, an asymptotic analysis for $n = n^+ + n^-$ and $v = n^+ - n^-$ with respect to transformed time and space scales $\tau = \epsilon^2 t$ and $\xi = \epsilon x$ leads to a leading order approximation of

$$n_{0\tau} + u\left(-\frac{u}{(\alpha(V,S)+2r)}n_{0\xi}\right)_\xi = -\left(\frac{\alpha(V,S)}{\beta(S)}n_0\right)_\tau - (m-b)\frac{\alpha}{\beta}n_0, \tag{3.116}$$

which leads to

$$\left(n_0\left(1+\frac{\alpha(V,S)}{\beta(S)}\right)\right)_\tau = \left(\frac{u^2}{(\alpha(V,S)+2r)}n_{0\xi}\right)_\xi + (b-m)\frac{\alpha}{\beta}n_0. \tag{3.117}$$

Defining $a = n_0\frac{(\beta+\alpha)}{\beta} = n_0 + q_0$, we have $n_0 = \frac{\beta}{\beta+\alpha}a$. Plugging this into equation (3.110), we have an equation of total population (resting population plus moving population) as follows:

$$a_\tau = \left(\frac{u^2}{(\alpha+2r)}\left(\frac{\beta}{\beta+\alpha}a\right)_\xi\right)_\xi + (b-m)\frac{\alpha}{\beta+\alpha}a. \tag{3.118}$$

The expansion of the right hand side of the above equation gives

$$a_\tau = \left(\frac{u^2}{(\alpha+2r)}\frac{\beta}{\beta+\alpha}a_\xi + \frac{u^2}{(\alpha+2r)}\left(\frac{\beta}{\beta+\alpha}\right)_\xi a\right)_\xi + (b-m)\frac{\alpha}{\beta+\alpha}a. \tag{3.119}$$

Here $\frac{u^2}{(\alpha+2r)}\frac{\beta}{\beta+\alpha}a_\xi$ term is interpreted as a diffusion term, $\frac{u^2}{(\alpha+2r)}(\frac{\beta}{\beta+\alpha})_\xi a$ as a taxis term, and $(b-m)\frac{\alpha}{\beta+\alpha}a$ a population dynamics. As we saw in the previous section, it is noted that including reproduction and death in a resting state does not change the diffusion term and prey sensitivity but affect only total population dynamics. But it changes the reproduction term because the relative population of reproduction in the total population is $\frac{\alpha}{\beta+\alpha}a$.

3.6.4 The Resting–Model Including Reproduction and Death in Resting and Moving State

In a last case we introduce reproduction and death in all compartments. The result is a combination of the effects found in the previous sections. As before we include reproduction and death on a slow time scale in resting and moving states as follows

$$\begin{aligned}\frac{\partial n^+}{\partial t} + u\frac{\partial n^+}{\partial x} &= -\alpha(V,S)n^+ + \frac{\beta(S)}{2}q - rn^+ + rn^- \\ &\quad + \epsilon^2\left(\frac{b(n,S)}{2}n - m(n,S)n^+\right),\end{aligned} \tag{3.120}$$

$$\begin{aligned}\frac{\partial n^-}{\partial t} - u\frac{\partial n^-}{\partial x} &= -\alpha(V,S)n^- + \frac{\beta(S)}{2}q + rn^+ - rn^- \\ &\quad + \epsilon^2\left(\frac{b(n,S)}{2}n - m(n,S)n^-\right),\end{aligned} \tag{3.121}$$

$$\frac{\partial q}{\partial t} = \alpha(V,S)(n^+ + n^-) - \beta(S)q + \epsilon^2(b_1 - m_1)q, \tag{3.122}$$

where $q(t)$, $\alpha(V,S)$, $\beta(S)$, $m(q,S)$, and $b(q,S)$ are defined as before. $b_1(q,S)$ and $m_1(q,S)$ are a birth rate and a death rate of resting population respectively. Then after similar computations as before, we have the following result

$$a_\tau = \left(\frac{u^2}{(\alpha+2r)} \frac{\beta}{\beta+\alpha} a_\xi + \frac{u^2}{(\alpha+2r)} \left(\frac{\beta}{\beta+\alpha} \right)_\xi a \right)_\xi + \frac{(b_1-m_1)\alpha + (b-m)\beta}{\beta+\alpha} a. \quad (3.123)$$

Here $\frac{u^2}{(\alpha+2r)} \frac{\beta}{\beta+\alpha} a_\xi$ term is interpreted as a diffusion term, $\frac{u^2}{(\alpha+2r)} (\frac{\beta}{\beta+\alpha})_\xi a$ as a taxis term, and $\frac{(b_1-m_1)\alpha+(b-m)\beta}{\beta+\alpha} a$ as population dynamics. The population growth rate is expressed as a convex combination of the moving population growth rate and the resting population growth rate

$$\frac{(b_1-m_1)\alpha + (b-m)\beta}{\beta+\alpha} = \frac{\alpha}{\beta+\alpha}(b_1-m_1) + \frac{\beta}{\beta+\alpha}(b-m). \quad (3.124)$$

Thus the total population growth rate lies on a straight line between the growth rates of resting group and moving group. In addition, the location of the total population growth rate is proportional to the fraction of time that an individual stays in the moving states and in the resting states. Especially, if $b = b_1$ and $m = m_1$, then we can see the population dynamics $(b-m)a$.

3.7 Summary

In this chapter we derived a drift–diffusion approximation for equations (2.34)–(2.35) and (2.36)–(2.37) by rescaling parameters and taking the parabolic limit. Alternatively, we also approximated a drift–diffusion equation from the resting models in Section 3.6.

In Chapter 2 the predator movement model is expressed in two equations (2.34)–(2.35). The spatial satiation dynamics of the predator corresponding to prey density are also described in two equations (2.36)–(2.37). By the use of approximations, these four equations can be collapsed into one equation

$$n_t = (Dn_x - \chi n \partial v/\partial x)_x, \quad (3.125)$$

where D is a diffusion coefficient, χ is a prey–sensitivity, n is the total population density of the predator, and v is the population density of the prey.

With local population dynamics related to predation, we formulate the complete predator–prey–taxis model

$$v_t = \epsilon v_{xx} + v\left(f(v) - \frac{n}{v}h(v)\right), \quad (3.126)$$

$$n_t = n_{xx} - (\chi(v) v_x n)_x + \gamma n(h(v) - \delta), \quad (3.127)$$

where $f(v)$ is a prey growth function and $h(v)$ is a predator functional response.

The zero Dirichlet boundary condition for (3.126)–(3.127) is

$$n(0,t) = 0, \quad n(L,t) = 0, \quad v(0,t) = 0, \quad v(L,t) = 0. \quad (3.128)$$

The no–flux boundary condition for (3.126)–(3.127) is

$$n_x(0,t) = -\frac{\xi}{u} n(0,t), \quad n_x(L,t) = -\frac{\xi}{u} n(L,t), \quad v_x(0,t) = 0, \quad v_x(L,t) = 0, \quad (3.129)$$

where u is moving speed of the predator.

The significance of this chapter is that we derived a prey–taxis model mechanistically. Hence, we understand what determines the coefficients of the prey sensitivity $\chi(v)$. That is, a different functional response results in a different prey sensitivity. As a result, a prey sensitivity could be different from one species to the other.

We obtained prey–taxis models by two approaches by using a parabolic limit (rescaling) and considering resting and moving. This gave some idea that a prey–taxis equation does not occur by a unique source.

The speed of the predator was assumed to be a constant. However, leg length, which differs among species, is one factor to determine the speed of movement [15]. Thus, under the assumption of a constant turning rate we may investigate the role of leg length in prey–taxis in the future.

The prey–taxis model is the system of two nonlinear advection–diffusion–reaction equations. Thus analysis of this system will be challenging. We will use numerical simulations to support the results of the analysis and demonstrate what analysis may fail to show. We consider numerical methods in the next chapter.

Chapter 4

Numerical Methods

In Chapter 3 we derived a drift–diffusion approximation from a hyperbolic system. In later chapters, we will use this drift–diffusion approximation to study traveling wave solutions and pattern formations to the predator–prey model.

In this chapter we study numerical methods for the predator–prey equations which include diffusion, advection, and reactions terms. These diffusion terms, advection terms, and reaction terms may be handled by applying one method–an unsplitting method. A simple example is the forward–time central–space scheme (FC). That is, it uses the forward difference operator in time and the centered difference operator in space. The scheme is known to give oscillations near a sharp front [2, 88]. Another example is the scheme FB, which uses upwind differencing of the advection term. This scheme is known to smear near the sharp front. Kurganov and Tadmor introduced a second order semi–discrete scheme, which was applied for the advection term with the central differencing of the diffusion term to obtain high resolution for convection–diffusion equations [51]. However, it was noted that the ODE solver has to be chosen carefully for unsplit methods unless we can afford very small time steps. In general, an unsplit method may more closely model the correct equations, but it is harder to obtain high resolution when handling sharp front problems [55]. Thus to be able to use high resolution methods for discontinuous problems, we adapt a fractional step method, which allows us to choose a scheme for each of the diffusion, advection, and reaction terms.

In Section 4.1 we review fractional step methods. In Section 4.2 we discuss several methods for numerically solving hyperbolic equations for the advection term. The Crank–Nicolson scheme is described in Section 4.3. In Section 4.4, some numerical methods are considered for the reaction terms.

4.1 Fractional Step Methods

In this section, two fractional step methods are described: Godunov and Strang fractional step methods. A fractional step method is applied to find the numerical solutions of systems of predator–prey equations of the form,

$$v_t = \epsilon v_{xx} + g(n, v), \tag{4.1}$$

$$n_t = n_{xx} - (\chi(v) v_x n)_x + f(n, v), \tag{4.2}$$

where $f(n,v)$ and $g(n,v)$ are the local population dynamics of n and v, respectively, and ϵ is small, $\epsilon \ll 1$. $\chi(v)$ is constant or $\sim \frac{1}{v}$. Our full predator–prey model consists of diffusion terms for both species, an advection term for the predator population, and reaction terms for both species. Thus we adapt a fractional step method, in which diffusion, advection and reaction terms are handled independently and individually with the most efficient and effective scheme for each case. An approximation process for the full model occurs via three split steps. Here the full model can be expressed in the form

$$U_t = \mathcal{A}(U) + \mathcal{D}(U) + \mathcal{R}(U), \tag{4.3}$$

where $\mathcal{A}$ is an advection operator, $\mathcal{D}$ is a diffusion operator, and $\mathcal{R}$ is a reaction operator. An operator has the following meaning: if v is any function, then an operator $\mathcal{L}$ converts v into a new function $\mathcal{L}v$. For instance, $\mathcal{L} = \frac{\partial^2}{\partial x^2}$ is the diffusion operator that transforms v into its second partial derivative v_{xx}. Numerical operators are defined as algebraic analogs of differential operators. These numerical (advection, diffusion, and reaction) operators are obtained by applying three numerical methods for the advection term, the diffusion term, and the reaction term, respectively. For instance, we consider a constant diffusion rate, say D, and apply the classic explicit scheme under Neumann boundary condition. Then the numerical diffusion operator is

$$\mathcal{D} = \begin{bmatrix} 1-r & r & & \\ r & 1-2r & r & \\ & & \ddots & \\ & & r & 1-r \end{bmatrix}, \tag{4.4}$$

with $r = D\frac{k}{h^2}$. the time step size is $k = \delta t$ and the mesh grid size is $h = \delta x$.

In the first step, only the advection term is approximated, i.e. $U_t = \mathcal{A}(U)$, and transferred to the (second) diffusion process. Various numerical schemes may be applied for approximating the advection equation [55]. Secondly, diffusion terms, $U_t = \mathcal{D}(U)$, are implemented by numerical methods and the new data are passed to the (third) reaction process. Finally, reaction terms are handled, i.e. $U_t = \mathcal{R}(U)$ to completely update U at the next time step (Godunov splitting [55]), that is,

$$U^{j+1} = \tilde{\mathcal{R}}(\Delta t)\tilde{\mathcal{D}}(\Delta t)\tilde{\mathcal{A}}(\Delta t)(U^j), \tag{4.5}$$

where $\tilde{\mathcal{A}}$ is a numerical advection operator, $\tilde{\mathcal{D}}$ is a numerical diffusion operator, and $\tilde{\mathcal{R}}$ is a numerical reaction operator. For the case of Godunov splitting, the length of time step, Δt, is identical for all three processes. The splitting error was evaluated via Taylor series expansions for a general linear PDE with a time step, Δt, in [55]. LeVeque showed that there is no splitting error for the simple case: $n_t + un_x = -\mu n$, which includes an advection term and a reaction term, but not a diffusion term. It is, however, not generally true, even with slight modification to the simple example case. Linear PDEs may generate splitting error. For instance, $n_t = (\mathcal{A} + \mathcal{B})n$ with differential operators $\mathcal{A}$ and $\mathcal{B}$ may have splitting error unless the differential operators $\mathcal{A}$ and $\mathcal{B}$ commute.

Generally the fractional step method gives second order accurate approximation, i.e. $\mathcal{O}(\Delta t^2)$ in each time step and a first order accuracy for an accumulated time period, $\frac{T}{\Delta t}$ for some fixed T. The Strang splitting takes different combinations of splitting operators used in (4.3) in order to give second order accuracy for an accumulated time period, $\frac{T}{\Delta t}$ for some

fixed T. In the first step, the Strang splitting updates data using the advection term with a half time step, i.e. $\Delta t/2$. Approximating diffusion terms are followed with a half time step as well. In the third step, reaction terms take the full time step. Then the Strang splitting procedure applies to diffusion operator for another half time step, followed by the advection term to update new data, U^{j+1} (see [95] for details).

$$U^{j+1} = \tilde{\mathcal{A}}(\Delta t/2)\tilde{\mathcal{D}}(\Delta t/2)\tilde{\mathcal{R}}(\Delta t)\tilde{\mathcal{D}}(\Delta t/2)\tilde{\mathcal{A}}(\Delta t/2)(U^j). \tag{4.6}$$

Although the Godunov splitting and the Strang splitting are formally first order and second order accurate, respectively, the Godunov splitting actually often gives as accurate results as the Strang splitting does [55]. It was shown numerically that the Godunov splitting generates slightly less accurate results than the Strang splitting if both fractional methods adapt the second order Lax–Wendroff method for the advection equation and the second order two stage Runge–Kutta method for the reaction equation. The Godunov splitting generates much more accurate results than the Strang splitting if the first one uses the second order Lax–Wendroff method for the advection equation and the second one uses the first order upwind method for the advection equation. Note that for the scalar advection equation $u_t + au_x = 0$ with advection speed a, the first order upwind method is written as

$$U_i^{j+1} = U_i^j - |a|\frac{k}{h}(U_i^j - U_{i-1}^j), \tag{4.7}$$

where i indicates the location of a mesh point, and the second order Lax–Wendroff method is

$$U_i^{j+1} = U_i^j - \frac{ak}{2h}(U_{i+1}^j - U_{i-1}^j) + \frac{k^2}{2h^2}a^2(U_{i+1}^j - 2U_i^j + U_{i-1}^j). \tag{4.8}$$

Furthermore, the Godunov splitting is easier and more efficient to apply. Therefore in this thesis high resolution methods for the advection equation are used via the Godunov Splitting. For more details on fractional step methods, see [55].

4.2 Advection Terms

Here we consider several numerical methods for the advection term of the predator–prey equations (4.1) and (4.2). A typical form of a system of non–linear advection equations is as follows

$$\frac{\partial U}{\partial t} + \frac{\partial f(U)}{\partial x} = 0, \tag{4.9}$$

where U is a vector of species (in this thesis, U are two or three variables) and $f(U)$ is a flux function of U. We briefly describe Godunov–type schemes and delve into central difference schemes in order to solve system (4.9).

Courant, Friedrichs, and Lewy recognized in 1928 a necessary condition for convergence of the numerical solution to a solution of (4.9) [54], that is, a necessary condition for the convergence of a finite–difference approximation to an initial–value problem is that the numerical domain of dependence, $D_k(x_i, t_j)$, at any grid point contains the exact domain of dependence, $D(\bar{x}, \bar{t})$, at that point, i.e. $D(\bar{x}, \bar{t}) \subset D_k(x_i, t_j)$. This condition has been known as the CFL Condition since then.

For a non–linear system, the CFL condition requires that

$$|\frac{\lambda_p k}{h}| \leq 1, \tag{4.10}$$

for each eigenvalue λ_p of the Jacobian matrix of $f(U)$ where k is the time step size and h the spatial mesh size. Here the Courant number is naturally defined by $\frac{\lambda_p k}{h}$. For stability of a numerical scheme, the Courant number is required to be less than 1, which is adapted as an important restriction for computing advection terms of the simulations in this thesis.

For nonlinear problems the discontinuous solution may cause the numerical schemes to converge to a solution that is not a weak solution even though the CFL condition is satisfied. Thus keeping a conservation form for the numerical methods is necessary for the solution to converge to a weak solution, which satisfies the integral form of the system (4.9)

$$\begin{aligned}\int_{x_{i-1/2}}^{x_{i+1/2}} U(x,t_{j+1})dx = &\int_{x_{i-1/2}}^{x_{i+1/2}} U(x,t_j)dx \\ &- \left[\int_{t_j}^{t_{j+1}} f(U(x_{i+1/2},t))dt - \int_{t_j}^{t_{j+1}} f(U(x_{i-1/2},t))dt\right].\end{aligned} \tag{4.11}$$

Dividing both sides by the spatial mesh size h, then we have

$$\overline{U}_i^{j+1} = \overline{U}_i^j - \frac{1}{h}\left[\int_{t_j}^{t_{j+1}} f(U(x_{i+1/2},t))dt - \int_{t_j}^{t_{j+1}} f(U(x_{i-1/2},t))dt\right], \tag{4.12}$$

where $\overline{U}_i^j$ is a cell average on the ith cell, i.e. $\overline{U}_i^j = \int_{x_{i-1/2}}^{x_{i+1/2}} U(x,t_j)dx$. If we know the right hand side of (4.12), we can update a cell average on the ith cell at the $j+1$ time step. However generally it is not possible to compute the time integrals on the right hand side of (4.12). Thus the cell averages, $\overline{U}_i^j$, and the average flux along $x = x_{i+1/2}$, i.e. $\frac{1}{k}\int_{t_j}^{t_{j+1}} f(U(x_{i+1/2},t))dt$, should be numerically approximated, namely, $\bar{u}_i^j$ and $F_{i+1/2}^j$, respectively. This provides the numerical method of the conservation form

$$\bar{u}_i^{j+1} = \bar{u}_i^j - \lambda(F_{i+1/2}^j - F_{i-1/2}^j), \tag{4.13}$$

with $\lambda = k/h$.

This way of using an integral form to get approximations is called a Finite Volume Method. Equation (4.13) says that the i th cell average $\bar{u}$ at the $j+1$ time step is determined by the i th cell average $\bar{u}$ at the j time step and the difference of two numerical flux functions at two cell edges, i.e. $x = x_{i-1/2}$ and $x = x_{i+1/2}$. In order to approximate a solution of (4.9) numerically, Godunov–type schemes are widely used. To approximate the numerical flux function $F_{i+1/2}^j$ from the ith cell average $\frac{1}{k}\int_{t_j}^{t_{j+1}} f(U(x_{i+1/2},t))dt$, $U(x_{i+1/2},t)$ are replaced with a piecewise polynomial approximation $\tilde{u}(x,t_j) \approx u(x_{i+1/2},t)$ of the form

$$\tilde{u}(x,t_j) = \sum_i p_i(x)\mathbf{1}_X(x), \tag{4.14}$$

where $p_i(x)$ are piecewise polynomials defined at the discrete cells, $X = [x_{i-1/2}, x_{i+1/2}]$ and $\mathbf{1}_X(x)$ is the characteristic function of X defined by $\mathbf{1}_X(x) = 1$ for $x \in X$, otherwise $\mathbf{1}_X(x) = 0$. Generally Godunov–type schemes follow the three steps algorithm [55]:

Algorithm (Godunov's method).

1. Given cell average $\bar{u}_i^j$, construct a function $\tilde{u}(x,t_j)$ for $x \in [x_{i-1/2}, x_{i+1/2}]$. Godunov himself used a piecewise constant $\tilde{u}(x,t_j)$, i.e. $\tilde{u}(x,t_j) = \bar{u}_i^j$ for all $x \in [x_{i-1/2}, x_{i+1/2}]$

.

2. Solve the conservation law exactly or approximately with this data to obtain $\tilde{u}(x, t_{j+1})$ for $x \in [x_{i-1/2}, x_{i+1/2}]$. A Riemann solver is involved in this process.

3. Compute cell averages at the resulting solution to obtain $\bar{u}_i^{j+1} = \frac{1}{h}\int_{x_{i-1/2}}^{x_{i+1/2}} \tilde{u}(x, t_j)dx$.

Here we describe how Godunov's method works with a simple example. With a piecewise constant $\tilde{u}(x, t_j) = \bar{u}_i^j$ and Courant number less than 1, the flux function is $F_{i+1/2,j} = \frac{1}{k}\int_{t_j}^{t_{j+1}} f(\tilde{u}(x_{i+1/2}, t))dt = \frac{1}{k}f(\bar{u}(x_i, t_j))k = f(\bar{u}_{i,j})$, if we assume that the Jacobian matrix $f'(\bar{u}_{i,j})$ has only nonnegative eigenvalues for all $\bar{u}_{i,j}$. Dropping the bars, a first order upwind method for the hyperbolic system (4.9) is expressed as

$$u_i^{j+1} = u_i^j - \lambda(f(u_i^j) - f(u_{i-1}^j)), \tag{4.15}$$

here we interpret u_i^j as the cell average at the jth time step on the ith cell with Courant number less than 1 rather than approximations on the grids. Thus for the general hyperbolic systems, eigenvalue computations are required for upwind–style methods.

Among Godunov types methods, central difference schemes have an advantage over upwind–style methods for nonlinear advection terms due to the relative simplicity of application. The first order central–difference scheme of the Lax–Friedrichs (LxF) method for a nonlinear system (4.9) takes the form

$$u_i^{j+1} = \frac{1}{2}(u_{i-1}^j + u_{i+1}^j) - \frac{\lambda}{2}(f(u_{i+1}^j) - f(u_{i-1}^j)). \tag{4.16}$$

In the conservation form of (4.13), the LxF method takes the numerical flux function with

$$F_{i-1/2}^j = \frac{1}{2}(f(u_{i-1}^j) + f(u_{i+1}^j)) - \frac{1}{2\lambda}(u_i^j - u_{i-1}^j). \tag{4.17}$$

Due to its simplicity (no Riemann solvers involved), the LxF scheme is straightforward to implement compared to Godunov type methods, which require Riemann solvers as the second step in the above algorithm (Godunov's method). On the other hand, due to $\frac{1}{2\lambda}(u_i^j - u_{i-1}^j)$ interpreted as numerical diffusion, the LxF scheme produces large numerical dissipation so that this scheme generates poor resolution of shock discontinuous solutions. Thus several high resolution schemes based on LxF type schemes have been presented. Nessyahu and Tadmor [69] introduced one of such schemes (the second order NT scheme), which inherited the simplicity of the LxF framework –Riemann solver free– but still gained high resolution. To improve the resolution, the NT scheme looks for cell averages, $\bar{u}_i^j$, rather than point values, u_i^j. Since the cell average of u over the interval $I_x = [x_i, x_{i+1}]$ is $\bar{u}_{i+1/2}^{j+1} = \frac{1}{I_x}\int_{I_x} u(\xi, t)d\xi$, the NT scheme actually computes $\bar{u}_{i+1/2}^{j+1}$ on the staggered grids, which can be identified with the point values, $u_{i+1/2}^{j+1}$, up to second order accuracy. $\bar{u}_{i+1/2}^{j+1}$ is approximated as follows

$$\bar{u}_{i+1/2}^{j+1} = \frac{1}{2}(\bar{u}_i^j + \bar{u}_{i+1}^j) + \frac{\Delta x}{8}((u_x)_i^j - (u_x)_{i+1}^j) - \lambda[f(u_{i+1}^{j+1/2}) - f(u_i^{j+1/2})], \tag{4.18}$$

where $u_i^{j+1/2}$ is estimated by a Taylor expansion as

$$u_i^{j+1/2} = \bar{u}_i^j - \frac{\Delta t}{2}(f_x)_i^j, \tag{4.19}$$

and $(u_x)_i^j$ is obtained via the minmod limiter,

$$(u_x)_i^j = \text{minmod}\left(\frac{u_i^j - u_{i-1}^j}{\Delta x}, \frac{u_{i+1}^j - u_i^j}{\Delta x}\right), \tag{4.20}$$

with $\text{minmod}(a,b) = \frac{1}{2}[\text{sgn}(a) + \text{sgn}(b)] \cdot \min(|a|, |b|)$. $(f_x)_i^j$ can be computed from the Jacobian matrix of $f(u)$ or from a discrete approximation based on neighboring values of $f(\bar{u}_{i-1}^j)$, $f(\bar{u}_i^j)$, and $f(\bar{u}_{i+1}^j)$ without loss of high resolution [60]. With $(u_x)_i^j = 0$ and $(f_x)_i^j = 0$, the NT scheme collapses into a staggered form of the LxF scheme.

$$\bar{u}_{i+1/2}^{j+1} = \frac{1}{2}(\bar{u}_i^j + \bar{u}_{i+1}^j) - \lambda[f(\bar{u}_{i+1}^j) - f(\bar{u}_i^j)]. \tag{4.21}$$

The second–order NT scheme shows high resolution due to the considerably lower amount of numerical dissipation compared to the amount of the dissipation by the first–order LxF scheme. The dissipation in the NT and LxF schemes has an amplitude of $\mathcal{O}((\Delta x)^{2r}/\Delta t)$, where r is an order of accuracy. Even though the second–order NT scheme produces relatively less dissipation, a small time step Δt leads to large dissipation. In the case that small time steps are required, the second–order NT scheme loses high resolution due to its accumulated numerical dissipation (see [51, 69] for details).

Thus, to deal with this loss of resolution, Kurganov and Tadmor introduced Kurganov–Tadmor schemes that have smaller numerical dissipation and admit a semi–discrete form [51]. For (4.9), the fully discrete second–order central scheme by Kurganov and Tadmor is

$$\begin{aligned} u_i^{j+1} &= \lambda a_{i-1/2}^j w_{i-1/2}^{j+1} + [1 - \lambda(a_{i-1/2}^j + a_{i+1/2}^j)] w_i^{j+1} \\ &\quad + \lambda a_{i+1/2}^j w_{i+1/2}^{j+1} + \frac{\Delta x}{2}[(\lambda a_{i-1/2}^j)^2 (u_x)_{i-1/2}^{j+1}) - (\lambda a_{i+1/2}^j)^2 (u_x)_{i+1/2}^{j+1})], \end{aligned} \tag{4.22}$$

with

$$a_{i+1/2}^j = \max\left(\rho\left(\frac{\partial f}{\partial u}(u_{i+1/2}^-)\right), \rho\left(\frac{\partial f}{\partial u}(u_{i+1/2}^+)\right)\right), \tag{4.23}$$

where $u_{i+1/2}^+ = u_{i+1}^j - \frac{\Delta x}{2}(u_x)_{i+1}^j$ and $u_{i+1/2}^- = u_i^j + \frac{\Delta x}{2}(u_x)_i^j$ are the intermediate values of $\tilde{u}(x, t_j)$ at $x_{i+1/2}$, and $\rho(A)$ is the absolute value of the largest eigenvalues of matrix A. $(u_x)_i^j$ is defined in (4.20).

Here $w_{i+1/2}^{j+1}$ and w_i^{j+1} are defined as follows

$$\begin{aligned} w_{i+1/2}^{j+1} &= \frac{u_i^j + u_{i+1}^j}{2} + \frac{\Delta x - a_{i+1/2}^j \Delta t}{4}((u_x)_i^j - (u_x)_{i+1}^j) \\ &\quad - \frac{1}{2a_{i+1/2}^j}[f(u_{i+1/2,r}^{j+1/2}) - f(u_{i+1/2,l}^{j+1/2})], \end{aligned} \tag{4.24}$$

$$\begin{aligned} w_i^{j+1} &= u_i^j + \frac{\Delta t}{2}(a_{i-1/2}^j - a_{i+1/2}^j)(u_x)_i^j \\ &\quad - \frac{\lambda}{1 - \lambda(a_{i-1/2}^j + a_{i+1/2}^j)}[f(u_{i+1/2,l}^{j+1/2}) - f(u_{i-1/2,r}^{j+1/2})], \end{aligned} \tag{4.25}$$

where

$$u^{j+1/2}_{i+1/2,l} = u^j_{i+1/2,l} - \frac{\Delta t}{2} f(u^j_{i+1/2,l})_x \tag{4.26}$$

$$u^{j+1/2}_{i+1/2,r} = u^j_{i+1/2,r} - \frac{\Delta t}{2} f(u^j_{i+1/2,r})_x \tag{4.27}$$

$$u^j_{i+1/2,l} = u^j_i + \Delta x (u_x)^j_i (\frac{1}{2} - \lambda a^j_{i+1/2}) \tag{4.28}$$

$$u^j_{i+1/2,r} = u^j_{i+1} - \Delta x (u_x)^j_{i+1} (\frac{1}{2} - \lambda a^j_{i+1/2}). \tag{4.29}$$

We can use the Jacobian of f directly or a componentwise evaluation based on neighboring values of $f(\bar{u}^j_{i-1})$, $f(\bar{u}^j_i)$, and $f(\bar{u}^j_{i+1})$ for computing f_x terms. Finally $(u_x)^{j+1}_{i+1/2}$ is approximated by

$$(u_x)^{j+1}_{i+1/2} = \frac{2}{\Delta x} \text{minmod} \left(\frac{w^{j+1}_{i+1} - w^{j+1}_{i+1/2}}{1 + \lambda(a^j_{i-1/2} - a^j_{i+3/2})}, \frac{w^{j+1}_{i+1/2} - w^{j+1}_i}{1 + \lambda(a^j_{i+1/2} - a^j_{i-1/2})} \right). \tag{4.30}$$

Setting $(u_x)^{j+1}_{i+1/2} = 0$ and $(u_x)^j_i = 0$, we obtain a first order Rusanov scheme.

$$u^{j+1}_i = u^j_i - \frac{\lambda}{2}(f(u^j_{i+1}) - f(u^j_{i-1})) + \frac{1}{2}[\lambda a^j_{i+1/2}(u^j_{i+1} - u^j_i) - \lambda a^j_{i-1/2}(u^j_i - u^j_{i-1})], \tag{4.31}$$

where $a^j_{i+1/2}$ are the maximal local speeds. The Kurganov–Tadmor fully discrete scheme gives high resolution, but it is complicated to implement as shown from (4.22–4.31). On the contrary, the semi–discrete version of the Kurganov–Tadmor scheme is relatively easy to apply,

$$\frac{d}{dt} u_i(t) = -\frac{H_{i+1/2}(t) - H_{i-1/2}(t)}{\Delta x}, \tag{4.32}$$

where the numerical flux on the edge of each cell is

$$H_{i+1/2}(t) = \frac{f(u^+_{i+1/2}(t)) - f(u^-_{i+1/2}(t))}{2} - \frac{a_{i+1/2}(t)}{2}[u^+_{i+1/2}(t) - u^-_{i+1/2}(t)], \tag{4.33}$$

with $u^+_{i+1/2}(t) = u_{i+1}(t) - \frac{\Delta x}{2}(u_x)_{i+1}(t)$ and $u^-_{i+1/2}(t) = u_i(t) + \frac{\Delta x}{2}(u_x)_i(t)$. To compute (4.32), any ODE solver may be used. Here we use the explicit Euler method or a two step RK method. However, due to a stability restriction, a very small time step is required. In order to release this restriction, implicit or explicit–implicit ODE solvers can be used. Kurganov and Tadmor use the explicit embedded integration methods introduced by Medovikov (see [51] for details).

When $(u_x)^j_i = 0$, the NT, and semi–discrete and fully discrete Kurganov and Tadmor schemes become the first order schemes, which generally show better resolution than the first order Lax–Friedrichs scheme, but the assumption of $(u_x)^j_i = 0$ leads to the zero flux function in our model because the flux function in the predator equation depends on the gradient of the prey density. Therefore, in this thesis, a second NT scheme is mainly used and fully–discrete or semi–discrete schemes are used to validate the results from the second NT scheme.

When we apply conservative methods, such as Gonunov type methods, the following Lax and Wendroff theorem gives confidence in a solution, which is a good approximation

to some weak solution.

Theorem (Lax and Wendroff). Consider a sequence of grids indexed by $i = 1, 2, \cdots$, with mesh parameters k_i, $h_i \to 0$ as $i \to \infty$. Let $u^{(i)}(x,t)$ denote the numerical approximation computed with a consistent and conservative method on the ith grid. Suppose that $u^{(i)}$ converges to a function u as $i \to \infty$, in the sense made precise below. Then $u(x,t)$ is a weak solution of the conservation law [54].

Over every bounded set $\Omega = [a,b] \times [0,T]$ in $x - -t$ space

$$\int_0^T \int_a^b |u^{(i)}(x,t) - u(x,t)| dx dt \to 0 \text{ as } i \to \infty.$$

We now use Burgers' equation to compare the numerical methods discussed in this section. The conservative form of Burgers' equation is

$$u_t + \left(\frac{1}{2}u^2\right)_x = 0. \tag{4.34}$$

Figures 4.1 show numerical solutions to Burgers' equation computed with the six methods described in this section. With $k/h = 0.5$, the numerical results are plotted at time $t = 1$ with the solid line of the exact solution. The first order Lax–Friedrichs scheme is shown to give the most smeared solution while the second order Lax–Wendroff scheme produces oscillations, which occur behind the discontinuity. The second order non–oscillatory schemes, that is, semi–discrete Kurganov–Tadmor, and NT, show very similar results, but Figure 4.2 shows that the fully–discrete Kurganov–Tadmor scheme has a better resolution than the NT scheme.

4.3 Diffusion Terms

Here we consider the numerical schemes for the diffusion terms. Both predator and prey equations have diffusion terms, but there is no cross diffusion term, so we can apply one numerical scheme twice for the diffusion terms with the different diffusion coefficients. A typical form of a system of diffusion equations is

$$\frac{\partial U}{\partial t} = D\frac{\partial^2 U}{\partial x^2}, \tag{4.35}$$

where D is a diffusion coefficient and U is the species we are concerned with. Computationally a simple classic explicit method, which employs a forward difference operator for the temporal derivative operator and a centered difference operator for the spacial derivative operator, requires a very small time step since its accuracy is $\mathcal{O}(k + h^2)$. Here k stands for a time step and h for a spatial mesh size. Furthermore the condition for the convergence is severe due to $k \leq \frac{h^2}{2D}$. On the contrary, the Crank–Nicolson scheme approximates the diffusion equation at the mid–point of t_n and t_{n+1} temporal points, that is, $(\frac{\partial U}{\partial t})_i^{j+1/2} = (D\frac{\partial^2 U}{\partial x^2})_i^{j+1/2}$. It employs centered difference operators for both the temporal derivative and the spatial derivative, that is,

$$\frac{u_i^{j+1} - u_i^j}{k} = \frac{1}{2}D\left(\frac{u_{i+1}^{j+1} - 2u_i^{j+1} + u_{i-1}^{j+1}}{h^2} + \frac{u_{i+1}^j - 2u_i^j + u_{i-1}^j}{h^2}\right). \tag{4.36}$$

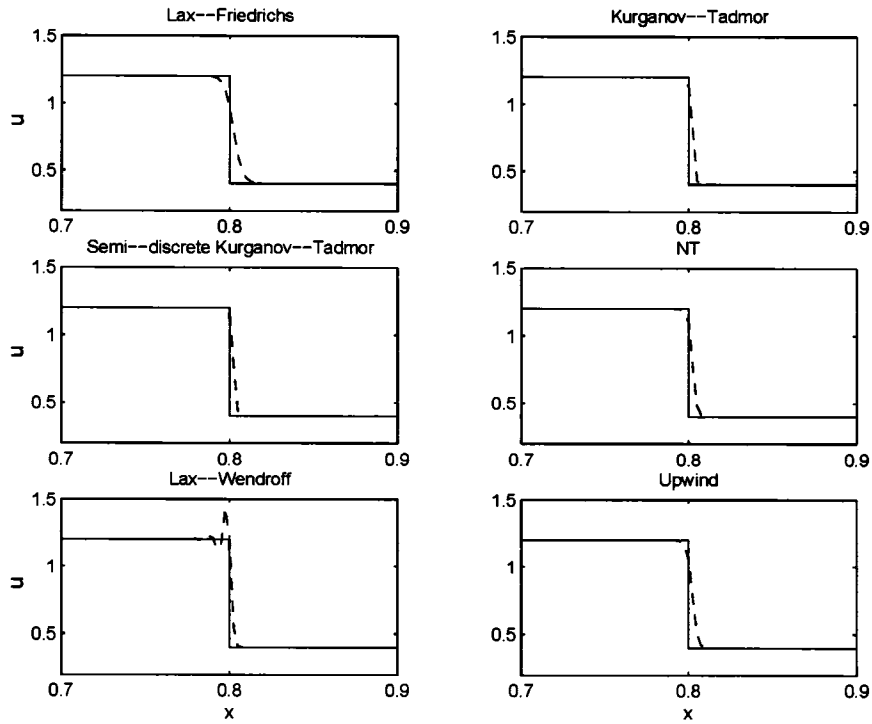

Figure 4.1: Numerical solutions and exact solutions to (4.34) are dashed and solid lines, respectively, with $h = 0.0025$, $k = 0.00125$, and at time $t = 1$. The following numerical methods are used: (a) staggered Lax–Friedrichs, (b) (Fully–discrete) Kurganov–Tadmor, (c) Semi–discrete Kurganov–Tadmor, (d) NT, (e) Lax–Wendroff, (f) Upwind.

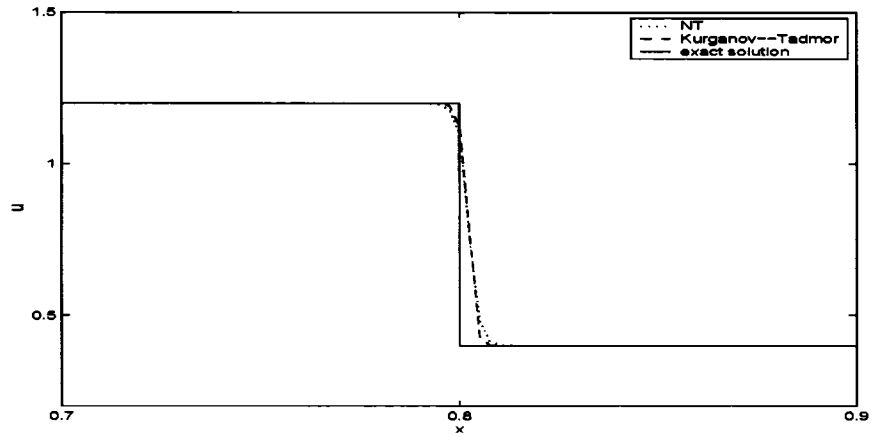

Figure 4.2: Comparison of NT and (Fully discrete) Kurganov–Tadmor along with exact solution to (4.34). Exact solution is a solid line, the numerical solution using the Kurganov–Tadmor scheme is a dashed line, and the numerical solution using NT scheme is a dotted line with $h = 0.0025$, $k = 0.00125$, and at time $t = 1$.

Rearranging the above algebraic expression with $r = \frac{kD}{h^2}$ gives

$$-ru_{i-1}^{j+1} + (2+2r)u_i^{j+1} - ru_{i+1}^{j+1} = ru_{i-1}^{j} + (2-2r)u_i^{j} + ru_{i+1}^{j}, \tag{4.37}$$

where u_i^j is an approximate solution at the point $\{ih, jk\}$. If there are N internal mesh points along each time step, then the diffusion equation can be approximated with N coupled linear equations of u_i^j at each time step with $i = 1, \cdots, N$ as follows.

$$\begin{bmatrix} 2+2r & -r & & \\ -r & 2+2r & -r & \\ & & \ddots & \\ & & -r & 2+2r \end{bmatrix} \begin{bmatrix} u_1^{j+1} \\ u_2^{j+1} \\ \vdots \\ u_N^{j+1} \end{bmatrix} = \begin{bmatrix} 2-2r & r & & \\ r & 2-2r & r & \\ & & \ddots & \\ & & r & 2-2r \end{bmatrix} \begin{bmatrix} u_1^{j} \\ u_2^{j} \\ \vdots \\ u_N^{j} \end{bmatrix}$$

which is a generic expression of the C–N scheme in matrix form, namely $AU^{j+1} = BU^j$ with the vector $U^j = (u_1^j, \cdots, u_N^j)^T$. Boundary conditions may change the first and last rows of matrix A and B or the format of $AU^{j+1} = BU^j$. For example, under the fixed boundary condition, such as $U(0) = a$ and $U(L) = b$, then $u_0^j = a$ holds for all $j \geq 1$ and $u_{N+1}^j = b$ for all $j \geq 1$ so that we know approximate values of U at two boundary points for all time. Therefore there are N unknown variables left to be computed, that is, $u_1, u_2, \cdots, u_N$ so matrices A and B are now $N \times N$ matrices. For the fixed boundary condition such as $U(0) = a$ and $U(L) = b$, there is an extra vector, $R = (2a, \cdots, 2b)^T$ in the matrix form of the C–N scheme so that the matrix equation form is now $AU^{j+1} = BU^j + R$ with $U = (u_1, u_2, \cdots, u_N)$. With zero boundary condition the vector R becomes zero. When we handle the zero flux boundary condition, i.e. $\partial U/\partial x = 0$ at the boundary points, the first row and last row of A are modified to $(2+2r, -2r, \cdots)$ and $(\cdots, -2r, 2+2r)$, respectively. Similarly the first row and last row of B are modified to $(2-2r, 2r, \cdots)$ and $(\cdots, 2r, 2-2r)$, respectively. Here u_{-1}^j and u_{N+2}^j are replaced with u_1^j and u_N^j, respectively for second order accuracy on the boundaries. For the zero flux boundary condition, the matrices A and B are $(N+2) \times (N+2)$ matrices and U^j is a size $(N+2)$ vector of $(u_0^j, u_1^j, \cdots, u_{N+1}^j)^T$.

When we have $AU^{j+1} = BU^j$ or $AU^{j+1} = BU^j + R$, we need to convert $AU^{j+1} = BU^j$ and $AU^{j+1} = BU^j + R$ into $U^{j+1} = A^{-1}BU^j$ and $U^{j+1} = A^{-1}BU^j + A^{-1}R$, respectively by computing an inverse matrix of A, that is A^{-1}. Since the tridiagonal matrix A is symmetric and positive definite, the system is guaranteed to have an inverse matrix A^{-1} at each time step computation. Gaussian elimination requires only $\mathcal{O}(N^3)$ to compute an exact inverse matrix A^{-1}, which is acceptable compared with expensive advection solvers. We thus use direct methods, such as Gaussian elimination or LU (LDL^T) factorization rather than iterative methods.

The C–N scheme is of $\mathcal{O}(k^2 + h^2)$ meaning that temporal and spatial approximations for the diffusion equations show second order accuracy. In addition, although large value of $r = \frac{kD}{h^2}$, such as 40, can generate oscillations in the numerical solution, the C–N scheme is unconditionally stable in the sense that the errors approach zero as j gets larger [83]. Thus throughout this thesis the C–N scheme is applied to approximate diffusion terms (prey and predator diffusion). For more detailed explanations and examples of numerical scheme for parabolic equations you are referred to [2, 83, 88].

4.4 Reaction Terms

In this section we consider the numerical schemes for the reaction terms. In equations (4.1) and (4.2), local predator– prey population dynamics are described in the form of ODEs. A typical form of a system of first order non–linear ordinary equations is

$$\frac{dU}{dt} = f(U), \tag{4.38}$$

where f is a function of U and the unknown U is a differentiable function with respect to time, t.

To handle reaction terms, we replace temporal differential equations with approximate difference equations. A simple form is the explicit one–step Euler method as follows

$$u^{j+1} = u^j + kf(u^j), \tag{4.39}$$

where u^j is a numeric approximation of U at the jth time step and k is the step size. We here use a uniform step size rather than an adaptive one for the simplicity of computing the full equations. The explicit Euler scheme is easy to implement to approximate differential equations, but it requires very small step sizes to exhibit sufficiently accurate results since its accuracy is $\mathcal{O}(k)$. Therefore improvements on the Euler method have been suggested by replacing $f(u^j)$ in (4.39) with modified functions, say $\Phi_k(u^j)$. Indeed the generic form of the explicit one step scheme is

$$u^{j+1} = u^j + k\Phi_k(u^j). \tag{4.40}$$

The Runge–Kutta method is one of the explicit one–step methods, which produce higher accuracy than the explicit Euler scheme (4.39).

For example in a fourth order Runge–Kutta method, $\Phi_k(u^j)$ is expressed by

$$\Phi_k(u^j) = \frac{1}{6}(f_1 + f_2 + f_3 + f_4), \tag{4.41}$$

where $f_1 = f(u^j)$, $f_2 = f(u^j + \frac{1}{2}kf_1)$, $f_3 = f(u^j + \frac{1}{2}kf_2)$, and $f_4 = f(u^j + kf_3)$. As a result, the RK4 scheme presents fourth order accuracy in time. However, fourth order accuracy is not necessary for the simulations in this thesis due to the lower accuracy of the schemes used for diffusion and advection terms. Therefore, Runge–Kutta second order scheme is adapted for computing reaction terms. The second order Runge–Kutta method used in this thesis is expressed by

$$u^{j+1} = \frac{1}{2}(u^* + u^{**}), \tag{4.42}$$

where

$$u^* = u^j + kf(u^j) \tag{4.43}$$

$$u^{**} = u^* + kf(u^*), \tag{4.44}$$

so that a modified function, $\Phi_k(u^j) = \frac{1}{2}(2f(u^j) + f(u^j + f(u^j)))$.

When the RK2 scheme is implemented as one of schemes for computing the full equation, (4.42), it needs to be applied repeatedly at each spatial grid point i from 1 to N (or 0 to $N+1$ depending on the boundary conditions) as follows

$$u_i^{j+1} = \frac{1}{2}(u_i^* + u_i^{**}), \tag{4.45}$$

where

$$u_i^* = u_i^j + kf(u_i^j) \tag{4.46}$$
$$u_i^{**} = u_i^* + kf(u_i^*), \tag{4.47}$$

for $i = 1, \cdots, N$ or $i = 0, 1, \cdots, N, N+1$.

The explicit one–step method for (4.38) with a function f satisfying the Lipschitz condition is defined to converge if the global error, $\varepsilon_k(t_j) = U(t_j) - u^j$ approaches zero as $k \to 0$ for every t concerned. Here $U(t_j)$ is an exact solution of the equation (4.38) at the time t_j and u^j an approximate solution computed from (4.40). How well a difference scheme approximates the original ODE is defined as follows. The one–step scheme (4.40) for the IVP (4.38) is said to be consistent with order p if the truncation error (or local discretization error), $\tau_k(u) = \mathcal{O}(k^p)$ as $t \to 0$, that is, if there are positive constants C and $\bar{k}$ independent of k, such that $\| \tau_k(u) \| < Ck^p$ whenever $k < \bar{k}$ and $f \in C^{p+1}$ in a given domain [2].

4.5 Summary

In this chapter we reviewed numerical methods for solving spatial predator–prey models of reaction–diffusion–advection equations (4.1)–(4.2). Finding numerical solutions of the advection part is challenging especially when steep gradients occur [95]. Thus we use a fractional step method, which allows us to choose a efficient and accurate scheme for each case of the diffusion, advection, and reaction terms.

Fractional step methods were described in Section 4.1. The Strang splitting method provides better accuracy than the Godunov Splitting does. However, the difference is not quite obvious. The fact that the first requires more computations than the second makes us use the Godunov Splitting over the Strang splitting. As a result in the following sections we considered numerical schemes for each case of the diffusion, advection, and reaction terms. In Section 4.2 we discussed several methods for numerically solving hyperbolic equations for the advection term. The NT scheme provides high resolution and is easy to implement, so we use the NT scheme for the advection term. The Crank–Nicolson scheme, which is well known as a second order method, is described in Section 4.3. In Section 4.4, some numerical methods are considered for the reaction terms. Indeed the RK2 scheme is used for the reaction terms.

The significance of this chapter is that a fractional step method will be the cornerstone of the intensive numerical simulations in the future. We considered eight different schemes for an advection term. In further researches we will consider not only different schemes for an advection term but also a different combination of three schemes for advection–diffusion–reaction terms to reduce numerical errors and increase resolution. To understand the efficiency and accuracy of fractional step methods, unsplitting methods need to be studied and compared with fractional step methods.

Chapter 5

Travelling Waves

In this chapter, we consider travelling wave solutions to prey–taxis models. In particular, we study the effect of a predator on a spreading prey population, and a discontinuous travelling wave solution. We also consider the spread rate of resting models derived in Section 3.6.

Owen and Lewis [72] showed that in some cases the predator catching up to the prey is not sufficient to slow down the prey spread. To show this the following system is used

$$v_t = \epsilon v_{xx} + v(f(v) - \frac{n}{v}h(v)), \tag{5.1}$$

$$n_t = n_{xx} + \gamma n(h(v) - \delta), \tag{5.2}$$

where ϵ, γ and δ are positive dimensionless quantities. It is also assumed that $\epsilon \ll 1$. Here v and n are prey density and predator density respectively for consistency. $f(v)$ is the prey population dynamic per prey without the predator, $h(v)$ is the functional response per predator, and $\gamma\delta$ is the decaying rate of the predator without the prey. They linearized this system about the leading edge of the wave where the densities of the prey and the predator are both zero and found that the population dynamics of prey only plays a dominant role in the spatial feature of the predator, slowing down (even reversing) the prey invasion. Without loss of generality, it was assumed that the diffusion rate of the predator is much faster than that of the prey. When the prey dynamics were developed under an Allee effect, they applied a singular perturbation analysis to consider the coexistence wavefront after the front of the predator arrives at that of the prey and found two conditions for stopping the prey invasion. We observe that it may be an interesting topic to see what kinds of effects on the predator–prey relationship can be expected by the introduction of prey-taxis in the spatial predator–prey interactions. That is, whether it can play a role in stopping the prey invasion. Here, we add the prey–taxis term $-(\chi(v)v_x n)_x$ to equations (5.1)–(5.2). The prey-sensitivity, $\chi(v)$, is a nonnegative decreasing function of the prey density.

5.1 Prey Dynamics with a Logistic Growth and Type I or II Functional Responses

Here, we study the wavefront after the predators catch up with the prey and achieve coexistence. In this section, we consider logistic growth, $f(v) = 1 - v$, and a Type I functional response, $h(v) = v$ or a Type II functional response, $h(v) = \frac{(a+1)v}{a+v}$. Here we consider various forms of the prey sensitivity, $\chi(v) = \chi$, $\chi(v) = \frac{b}{v}$ and $\chi(v) = \frac{b}{v^2}$.

Slow movement of the prey generates a sharp transition in prey population from the coexistence steady state to zero population on the right. In this section we consider type I and II functional responses, and ratio–dependent functional responses for the local prey population dynamics. The dispersals of predators are of three types: zero prey–taxis ($\chi(0) = 0$), bounded prey–taxis ($\chi(0) < \infty$), and unbounded prey–taxis ($\chi(0) = \infty$). The first case is the same as the diffusion–only case. However, we may consider the first and the second cases under the bounded prey–taxis ($\chi(0) < \infty$).

The system is considered as follows

$$v_t = \epsilon v_{xx} + v(f(v) - \frac{n}{v}h(v)), \tag{5.3}$$

$$n_t = n_{xx} - (\chi(v)v_x n)_x + \gamma n(h(v) - \delta), \tag{5.4}$$

where ϵ, γ and δ are positive dimensionless quantities. It is assumed that $\epsilon \ll 1$. $f(v) = 1-v$ is the prey population dynamic per prey without the predator as a part of logistic growth. $h(v)$ is the type I or II functional response per predator, i.e. $h(v) = v$ and $h(v) = \frac{(a+1)v}{a+v}$, respectively. $\gamma\delta$ is the decaying rate of the predator without the prey.

First, we consider the case where prey sensitivity is bounded at zero prey density, i.e. $\chi(0) < \infty$. We transform equations (5.3)–(5.4) with travelling coordinate, $z = x - ct$ (with wave speed c) to get

$$0 = cV' + \epsilon V'' + V(f(V) - \frac{N}{V}h(V)), \tag{5.5}$$

$$0 = cN' + N'' - (\chi(V)V'N)' + \gamma N(h(V) - \delta), \tag{5.6}$$

with $N(z) = n(x,t)$ and $V(z) = v(x,t)$. We consider the travelling wave connection between the coexistence steady state $(\hat{n}, \hat{v}) = (n_0, v_0)$ and trivial steady state $(\hat{n}, \hat{v}) = (0,0)$ with the conditions that $\lim_{z\to\infty} N(z) = \lim_{z\to\infty} V(z) = 0$, $\lim_{z\to-\infty} N(z) = n_0$, and $\lim_{z\to-\infty} V(z) = v_0$, which describes the situation where an established prey population begins to spread along the positive direction and newly introduced predators follow prey spreading. Since predator density changes via diffusion and local population dynamics induced by the existence of prey density, initially predators may easily catch up with prey spread. However, as soon as predators reach a frontier of spreading prey, predator spreading speed is slowed down due to the lack of prey density.

We consider whether travelling waves of prey go slower due to the interaction with predators. We use linear analysis for this. In a small neighborhood of a hyperbolic equilibrium $(\hat{v}, \hat{u}) = (0,0)$ for (5.3)–(5.4), flow of the nonlinear system is topologically equivalent with that of its linearization [28]. The linearized equations of equations (5.5)–(5.6) are,

$$0 = cV' + \epsilon V'' + (\hat{v}f'(\hat{v}) + f(\hat{v}) - \hat{n}h'(\hat{v})V - h(\hat{v})N, \tag{5.7}$$

$$0 = cN' + N'' - (\chi(\hat{v})\hat{n})V'' + \gamma\hat{n}h'(\hat{v})V + \gamma(h(\hat{v}) - \delta)N. \tag{5.8}$$

The linearized prey–taxis term can be obtained by

$$\begin{aligned}(\chi(v)v_x n)_x &= ((\chi(\hat{v}) + \chi'(\hat{v})V)V_x(\hat{n} + N))_x \\ &= \chi(\hat{v})\hat{n}V_{xx} + \chi'(\hat{v})\hat{n}(VV_x)_x + \chi(\hat{v})(NV_x)_x + \chi'(\hat{v})(NVV_x)_x \\ &= \chi(\hat{v})\hat{n}V_{xx},\end{aligned} \tag{5.9}$$

up to the order V^2 approximation.

We now look for solutions in the form

$$N, V \propto exp(\lambda z), \tag{5.10}$$

where λ is the eigenvalue. λ having negative real parts implies that the steady state $(\hat{n}, \hat{v}) = (0,0)$ is linearly stable, since, after small perturbation, $(\hat{n}, \hat{v}) \to (0,0)$ as $t \to \infty$. Substitution of (5.10) into (5.7)–(5.8) gives that the eigenvalues satisfy

$$\begin{vmatrix} \epsilon\lambda^2 + c\lambda + \hat{v}f'(\hat{v}) + f(\hat{v}) - \hat{n}h'(\hat{v}) & -h(\hat{v}) \\ -\chi(\hat{v})\hat{n}\lambda^2 + \gamma\hat{n}h'(\hat{v}) & \lambda^2 + c\lambda + \gamma(h(\hat{v}) - \delta) \end{vmatrix} = 0. \tag{5.11}$$

Since we are interested in the predator–prey–free steady state, i.e. $(\hat{n}, \hat{v}) = (0,0)$, (5.11) becomes

$$\begin{vmatrix} \epsilon\lambda^2 + c\lambda + f(0) & -h(0) \\ 0 & \lambda^2 + c\lambda + \gamma(h(0) - \delta) \end{vmatrix} = 0. \tag{5.12}$$

Hence, λ can be computed from two quadratic equations. That is,

$$\epsilon\lambda^2 + c\lambda + f(0) = 0, \text{ or } \lambda^2 + c\lambda + \gamma(h(0) - \delta) = 0. \tag{5.13}$$

Analysis about the leading edge of the wave $(\hat{v}, \hat{n}) = (0,0)$ yields

$$\lambda_{\pm}^{V} = \frac{-c \pm \sqrt{c^2 - 4\epsilon f(0)}}{2\epsilon}, \tag{5.14}$$

and

$$\lambda_{\pm}^{N} = \frac{-c \pm \sqrt{c^2 - 4\gamma(h(0) - \delta)}}{2}, \tag{5.15}$$

in which $\lambda_{\pm}^{N}$ is always negative if $h(0) > \delta$. Indeed $h(0) = 0$ for any speed c, guarantees that predators have non-negative density from equation (5.15). Thus, from (5.14), the linear analysis gives a necessary condition

$$c^2 \geq 4\epsilon f(0). \tag{5.16}$$

Without predator interruption, prey spread with the Fisher rate of $2\sqrt{\epsilon f(0)}$, which provides an upper limit of prey spread when prey population is regulated by predator interactions. Hence with the bounded prey sensitivity, predators cannot slow down the prey spread in the form of travelling waves. Since $h(0) = 0$, for any speed c predators have non-negative density from equation (5.15). It is shown in Figure 5.1 and Figure 5.2 that predators, whose prey sensitivity is bounded at zero prey density with type I functional response to prey of logistic growth, cannot slow down prey spread. In this case predators slow down and adjust their own spread rate to the prey's spread rate. Thus predators with bounded prey sensitivity function are the same as predators with diffusion–only case for their dispersal.

We now consider the case that prey sensitivity is unbounded at zero prey, i.e. $\chi(v) = \frac{b}{v}$ or $\chi(v) = \frac{b}{v^2}$.

We first consider the prey sensitivity $\chi(v) = \frac{b}{v}$ in system (5.5)–(5.6). The linearization of equations (5.5)–(5.6) about $(\hat{v}, \hat{n}) = (0,0)$ is,

$$0 = cV' + \epsilon V'' + f(0)V - h(0)N, \tag{5.17}$$

$$0 = cN' + N'' - \left(b\frac{V'N}{V}\right)' + \gamma(h(0) - \delta)N., \tag{5.18}$$

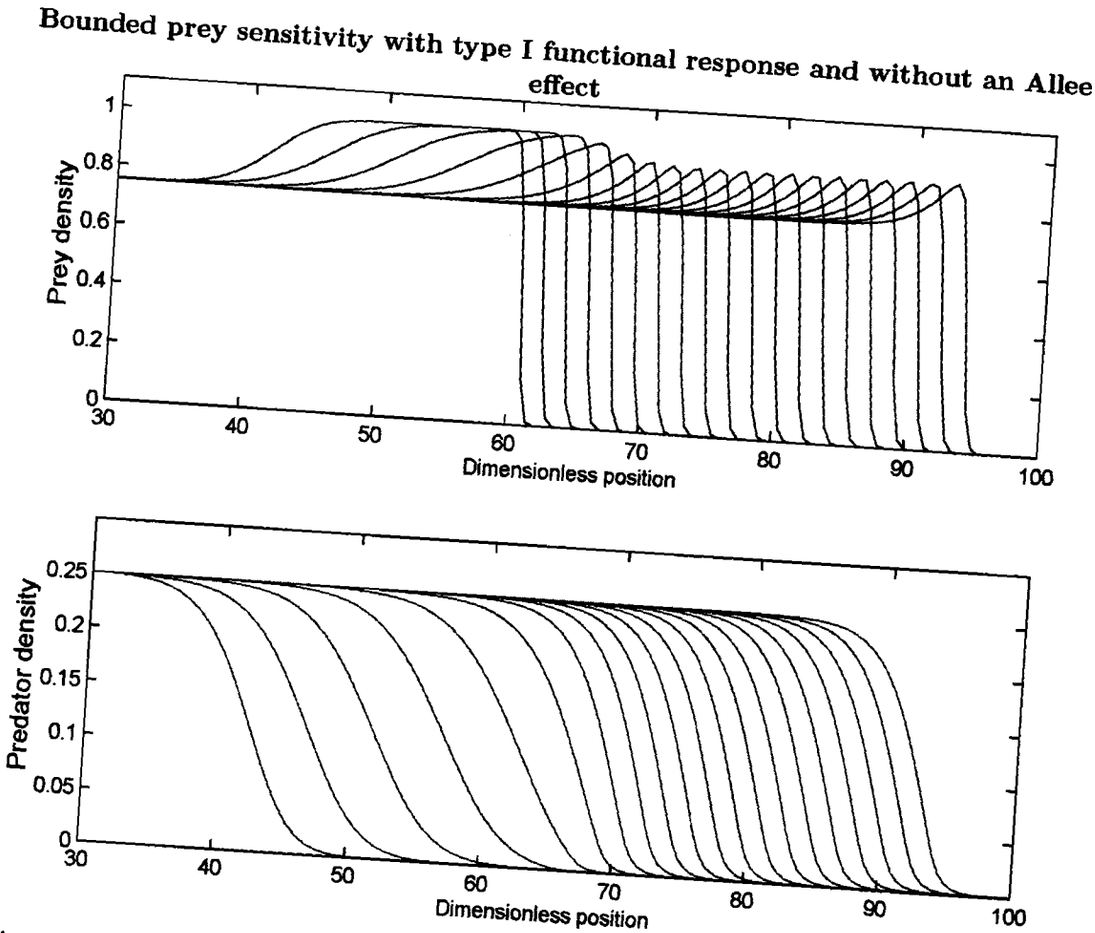

Figure 5.1: With logistic growth, $f(v) = 1 - v$, type I functional response, $h(v) = v$, and zero prey sensitivity ($\chi = 0$), introduced predators, which catch up with prey spread, do not slow it down. Here $\delta = 0.75$, $\gamma = 1$, and $\epsilon = 0.01$. Dashed lines show initial conditions, solid lines show solutions up to t=100 at intervals of 5 dimensionless time units.

Bounded prey sensitivity with type I functional response and without an Allee effect

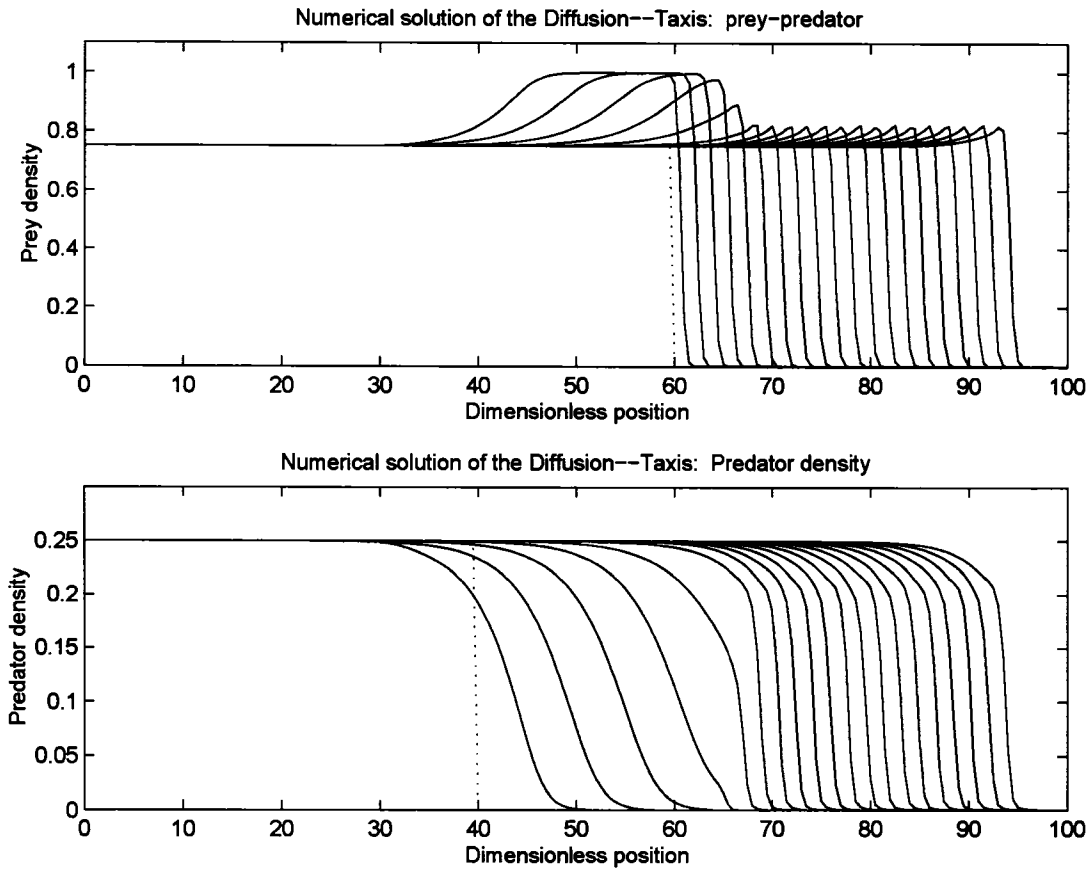

Figure 5.2: With logistic growth, $f(v) = 1 - v$, type I functional response, $h(v) = v$, and constant prey sensitivity ($\chi = 7.0$), introduced predators, which catch up with prey spread, do not slow it down. Here $\delta = 0.75$, $\gamma = 1$, and $\epsilon = 0.01$. Dashed lines show initial conditions, solid lines show solutions up to t=100 at intervals of 5 dimensionless time units.

We look for solutions in the form of

$$V = k_1 \exp(\lambda z), \quad N = k_2 \exp(\lambda z), \tag{5.19}$$

Substitution of (5.19) into (5.17–5.18) gives that the eigenvalues satisfy

$$\begin{aligned}
0 &= c\lambda k_1 \exp(\lambda z) + \epsilon\lambda^2 k_1 \exp(\lambda z) + f(0)k_1 \exp(\lambda z) - h(0)k_2 \exp(\lambda z), \\
0 &= c\lambda k_2 \exp(\lambda z) + \lambda^2 k_2 \exp(\lambda z) - \left(b\frac{\lambda k_1 \exp(\lambda z) k_2 \exp(\lambda z)}{k_1 \exp(\lambda z)} \right)' \\
&\quad + \gamma(h(0) - \delta)k_2 \exp(\lambda z).
\end{aligned}$$

After cancelation in the prey–taxis term, we have

$$\begin{aligned}
0 &= c\lambda k_1 \exp(\lambda z) + \epsilon\lambda^2 k_1 \exp(\lambda z) + f(0)k_1 \exp(\lambda z) - h(0)k_2 \exp(\lambda z), \\
0 &= c\lambda k_2 \exp(\lambda z) + \lambda^2 k_2 \exp(\lambda z) - (b\lambda k_2 \exp(\lambda z))' \\
&\quad + \gamma(h(0) - \delta)k_2 \exp(\lambda z).
\end{aligned}$$

Dividing the above equations by $\exp(\lambda z)$ leads to

$$0 = c\lambda k_1 + \epsilon\lambda^2 k_1 + f(0)k_1 - h(0)k_2, \tag{5.20}$$

$$0 = c\lambda k_2 + \lambda^2 k_2 - b\lambda^2 k_2 + \gamma(h(0) - \delta)k_2.. \tag{5.21}$$

We now look for non-zero k_1 and k_2 so that with $h(0) = 0$ we have the following equation

$$\begin{vmatrix} \epsilon\lambda^2 + c\lambda + f(0) & 0 \\ 0 & \lambda^2 - b\lambda^2 + c\lambda + \gamma(-\delta) \end{vmatrix} = 0. \tag{5.22}$$

Hence, λ can be computed from two quadratic equations as before,

$$\epsilon\lambda^2 + c\lambda + f(0) = 0, \quad \text{or} \quad (1-b)\lambda^2 + c\lambda + \gamma(-\delta) = 0. \tag{5.23}$$

The first equation for λ is the same as the case of bounded prey sensitivity. When $b < 1$, the second equation gives one negative root and one positive root. For $b > 1$ we have a necessary condition for the existence of positive eigenvalues λ. The second equation above is rewritten as follows

$$(b-1)\lambda^2 - c\lambda + \gamma\delta = 0, \tag{5.24}$$

where $b > 1$, and $\gamma, \delta > 0$. Complex λ leads to negative prey density, so

$$c^2 \geq 4(b-1)\gamma\delta \tag{5.25}$$

is a condition for prey density to remain non–negative. Thus $\lambda = \frac{c \pm \sqrt{c^2 - 4(b-1)\gamma\delta}}{2(b-1)}$ guarantees at most two positive roots. In addition to condition (5.25), condition (5.16) has to be satisfied for non–negative density. While $c^2 = 4\epsilon f(0)$ gives a upper bound of prey spread, condition (5.16) may give a lower bound. Thus, prey spread rate should be

$$4(b-1)\gamma\delta \leq c^2 \leq 4\epsilon f(0). \tag{5.26}$$

If $(b-1)\gamma\delta > \epsilon f(0)$, there may be no travelling wave connection. This may indicate that as predators approach the tip of prey spread they adjust their catching-up speed not to exceed

the tip of the prey's spread. In other words, predators change their catching–up speed in order not to suffer from the insufficient prey density due to the prey sensitivity. Through a series of simulations it is seen that as constant b decreases, the tip of predators catching up with prey retreats behind the tip of prey spread, so a predator free zone appears near the tip of the prey spread. A diffusion process of the predator tend to make predators smear into the tip of the prey spread, but strong prey–taixs makes predators move back. Thus, at some distance from the tip of the prey spread, the tip of the predator catching up may be formulated. Then predators passively follow the prey spread and eat enough prey behind the tip of the prey spread.

We now consider the prey sensitivity $\chi(v) = \frac{b}{v^2}$ in system (5.5)–(5.6). Then the eigenvalues satisfy

$$\begin{aligned}
0 &= c\lambda k_1 \exp(\lambda z) + \epsilon\lambda^2 k_1 \exp(\lambda z) + f(0)k_1 \exp(\lambda z) - h(0)k_2 \exp(\lambda z), \\
0 &= c\lambda k_2 \exp(\lambda z) + \lambda^2 k_2 \exp(\lambda z) - \left(b\frac{\lambda k_1 \exp(\lambda z) k_2 \exp(\lambda z)}{k_1^2 \exp(2\lambda z)} \right)' \\
&\quad + \gamma(h(0) - \delta)k_2 \exp(\lambda z).
\end{aligned}$$

After cancelation in the prey–taxis term, we have

$$\begin{aligned}
0 &= c\lambda k_1 \exp(\lambda z) + \epsilon\lambda^2 k_1 \exp(\lambda z) + f(0)k_1 \exp(\lambda z) - h(0)k_2 \exp(\lambda z), \\
0 &= c\lambda k_2 \exp(\lambda z) + \lambda^2 k_2 \exp(\lambda z) - (b\lambda\frac{k_2}{k_1})' + \gamma(h(0) - \delta)k_2 \exp(\lambda z).
\end{aligned}$$

Thus the prey–taxis term becomes zero. Dividing the above equations by $\exp(\lambda z)$ leads to

$$0 = c\lambda k_1 + \epsilon\lambda^2 k_1 + f(0)k_1 - h(0)k_2, \tag{5.27}$$

$$0 = c\lambda k_2 + \lambda^2 k_2 + \gamma(h(0) - \delta)k_2., \tag{5.28}$$

which is the same as the case of the bounded prey sensitivity. Thus we cannot expect the case that predators slow down prey spread.

In this section, we investigated a combination of a logistic growth and a Type I functional response and a combination of a logistic growth and a Type II functional response with various forms of the prey sensitivity $\chi(v)$. We found that the predators fail to slow down and stop the prey spread. Hence, we conclude that for Type I and II functional responses prey–taxis may not play any role in stopping the prey spread. We will consider different functional responses next.

5.2 Prey Dynamics with Logistic Growth and Ratio–Dependent Functional Responses

Here, we consider hyperbolic ratio dependent and linear ratio dependent functional responses in order to examine whether predators may slow down prey spread. In the previous section, we found that prey–taxis did not play any role in stopping the prey spread. We here consider only a diffusion process for the predator. Hyperbolic ratio dependent functional response is $h(v,n) = \frac{\mu v}{dn+v}$ and linear ratio dependent functional response $h(v,n) = \frac{\nu v}{n}$ for some positive constant μ, ν, and d. What $h(v,n)$ approaches as $(v,n) \to (0,0)$ seems to be crucial and will be considered during the computation.

Unbounded prey sensitivity with type I functional response and without an Allee effect

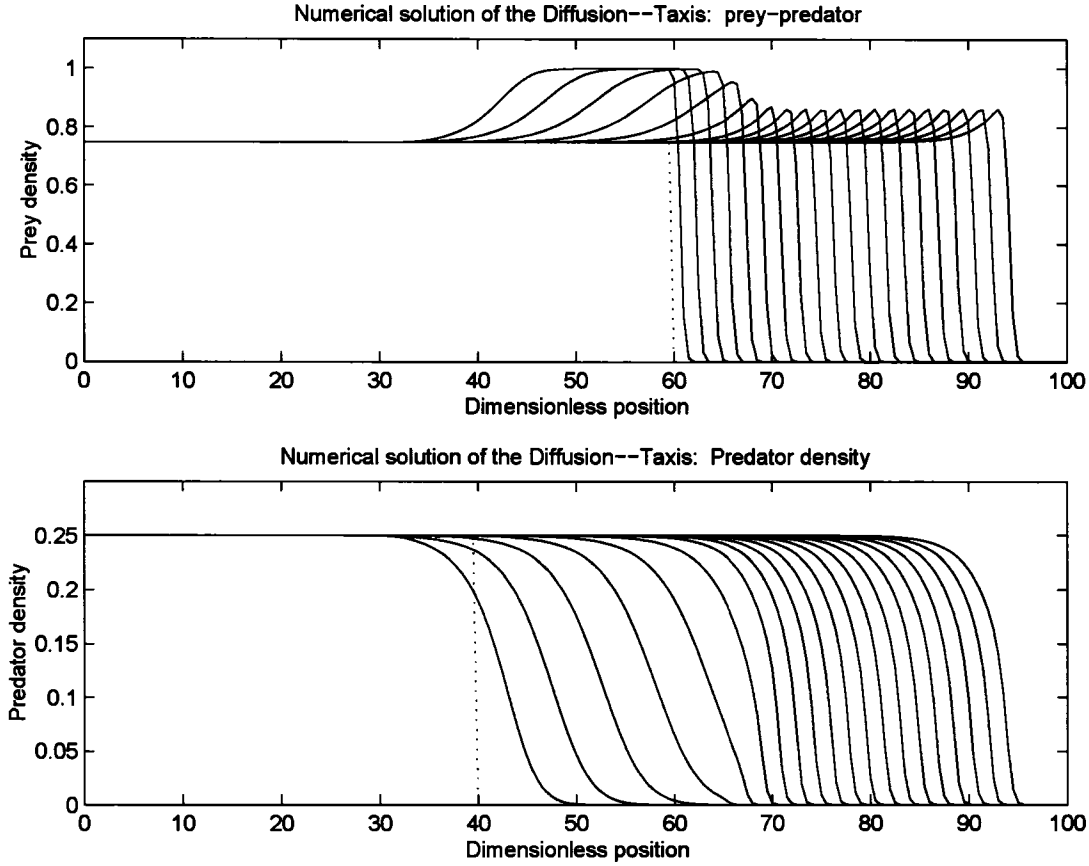

Figure 5.3: With logistic growth, $f(v) = 1 - v$, type I functional response, $h(v) = v$, and constant prey sensitivity ($\chi(V) = 1.5/V$), introduced predators, which catch up with prey spread, do not slow down prey spread. Here $\delta = 0.75$, $\gamma = 1$, and $\epsilon = 0.01$. Dashed lines show initial conditions, solid lines show solutions up to t=100 at intervals of 5 dimensionless time units.

We are thus interested in the following system

$$v_t = \epsilon v_{xx} + v(f(v) - \frac{n}{v}h(v,n)), \tag{5.29}$$

$$n_t = n_{xx} + \gamma n(h(v,n) - \delta), \tag{5.30}$$

We transform equations (5.29)–(5.30) with travelling coordinate, $z = x - ct$ (with wave speed c) to get

$$0 = cV' + \epsilon V'' + V(f(V) - \frac{N}{V}h(V,N)), \tag{5.31}$$

$$0 = cN' + N'' + \gamma N(h(V,N) - \delta), \tag{5.32}$$

where $N(z) = n(x,t)$ and $V(z) = v(x,t)$. We consider the travelling wave connection between the coexistence steady state $(\hat{n}, \hat{v}) = (n_0, v_0)$ and trivial steady state $(\hat{n}, \hat{v}) = (0,0)$ with the conditions that $\lim_{z\to\infty} N(z) = \lim_{z\to\infty} V(z) = 0$, $\lim_{z\to-\infty} N(z) = n_0$, and $\lim_{z\to\infty} V(z) = v_0$. We now consider the diffusion-only system of equations (5.31)–(5.32) to show whether prey travelling waves can go slower due to the interaction with predators. Here we do not consider the prey–taxis because in the previous sections we saw that prey–taxis had no effect. We use linear analysis to elucidate what happens at the wavefront. In a small neighborhood of the hyperbolic equilibrium $(\hat{v}, \hat{u}) = (0,0)$ of equations (5.29)–(5.30), flow of the nonlinear system is topologically equivalent with the one of its linearization. Before linearizing equations (5.31)–5.32), we need to consider linear and hyperbolic ratio dependent functional response individually and plug each case into equations (5.31)–(5.32) to get

$$0 = cV' + \epsilon V'' + V(f(V) - \nu), \tag{5.33}$$

$$0 = cN' + N'' + \gamma\nu V - \gamma\delta N, \tag{5.34}$$

and

$$0 = cV' + \epsilon V'' + V(f(V) - \frac{\mu N}{dN + V}), \tag{5.35}$$

$$0 = cN' + N'' + \gamma N(h(V,N) - \delta), \tag{5.36}$$

for linear and hyperbolic ratio dependent functional response, respectively. The linearized equations of the linear ratio dependent functional response case are

$$0 = cV' + \epsilon V'' + (\hat{v}f'(\hat{v}) + f(\hat{v}) - \nu)V, \tag{5.37}$$

$$0 = cN' + N'' + \gamma\nu V - \gamma\delta N. \tag{5.38}$$

We look for solutions in the form of (5.10). Substitution of (5.10) into (5.37–5.38) gives that the eigenvalues satisfy

$$\begin{vmatrix} \epsilon\lambda^2 + c\lambda + \hat{v}f'(\hat{v}) + (f(\hat{v}) - \nu) & 0 \\ \gamma\nu & \lambda^2 + c\lambda - \gamma\delta \end{vmatrix} = 0. \tag{5.39}$$

Since we are interested in the predator–prey–free steady state, i.e. $(\hat{n}, \hat{v}) = (0,0)$, (5.39) becomes

$$\begin{vmatrix} \epsilon\lambda^2 + c\lambda + f(0) - \nu & 0 \\ \gamma\nu & \lambda^2 + c\lambda - \gamma\delta \end{vmatrix} = 0. \tag{5.40}$$

Hence, λ can be computed from two quadratic equations, that is,

$$\epsilon\lambda^2 + c\lambda + f(0) - \nu = 0, \text{ or } \lambda^2 + c\lambda - \gamma\delta = 0. \tag{5.41}$$

Analysis about the leading edge of the wave $(\hat{v}, \hat{n}) = (0, 0)$ yields

$$\lambda_{\pm}^{V} = \frac{-c \pm \sqrt{c^2 - 4\epsilon(f(0) - \nu)}}{2\epsilon}, \tag{5.42}$$

and

$$\lambda_{\pm}^{N} = \frac{-c \pm \sqrt{c^2 + 4\gamma\delta}}{2}. \tag{5.43}$$

Thus, linear analysis gives a necessary condition

$$c^2 \geq 4\epsilon(f(0) - \nu), \tag{5.44}$$

for non-negative prey density. Hence when the predator follows ratio dependent functional response, it may slow down or stop the prey spread with diffusion as a searching strategy depending on the parameter ν. Without predators prey dynamics follow logistic growth, but introduced predators lead to a different prey population growth about the leading edge of the wave. The main cause of prey slowing down is that prey intrinsic growth rate becomes smaller due to the potential interactions with predators at the leading edge of the wave, i.e. $f(0) - \nu$.

The linearized equations of the hyperbolic ratio dependent functional response case are more complicated than the ones of the linear ratio case, so we need to consider three different N/V, i.e. $N/V = 0$, N/V is constant, and $N/V = \infty$ as $(V, N) \to (0, 0)$. For $N/V = 0$, the linearized equations of (5.35)–(5.36) are

$$0 = cV' + \epsilon V'' + (\hat{v}f'(\hat{v}) + f(\hat{v}))V, \tag{5.45}$$

$$0 = cN' + N'' + \gamma\mu N - \gamma\delta N. \tag{5.46}$$

Substitution of (5.10) into (5.45)–(5.46) gives that the eigenvalues satisfy

$$\begin{vmatrix} \epsilon\lambda^2 + c\lambda + \hat{v}f'(\hat{v}) + f(\hat{v}) & 0 \\ 0 & \lambda^2 + c\lambda + \gamma\mu - \gamma\delta \end{vmatrix} = 0. \tag{5.47}$$

Since we are interested in the predator–prey–free steady state, i.e. $(\hat{n}, \hat{v}) = (0, 0)$, (5.47) becomes

$$\begin{vmatrix} \epsilon\lambda^2 + c\lambda + f(0) & 0 \\ 0 & \lambda^2 + c\lambda + \gamma\mu - \gamma\delta \end{vmatrix} = 0. \tag{5.48}$$

Hence, λ can be computed from two quadratic equations, that is,

$$\epsilon\lambda^2 + c\lambda + f(0) = 0, \text{ or } \lambda^2 + c\lambda + \gamma\mu - \gamma\delta = 0. \tag{5.49}$$

Analysis about the leading edge of the wave $(\hat{v}, \hat{n}) = (0, 0)$ yields

$$\lambda_{\pm}^{V} = \frac{-c \pm \sqrt{c^2 - 4\epsilon f(0)}}{2\epsilon}, \tag{5.50}$$

and

$$\lambda_{\pm}^{N} = \frac{-c \pm \sqrt{c^2 - 4\gamma(\mu - \delta)}}{2}. \tag{5.51}$$

Thus, linear analysis gives a necessary condition

$$c^2 \geq 4\epsilon f(0), \text{ and } c^2 \geq 4\gamma(\mu - \delta) \tag{5.52}$$

for non-negative prey density. Hence when predators follow a ratio dependent functional response with the assumption that $n/v \to 0$ as $(v,n) \to 0$, they do not slow down or stop the prey spread with diffusion.

For N/V constant, say θ, the linearized equations are

$$0 = cV' + \epsilon V'' + (\hat{v}f'(\hat{v}) + f(\hat{v}) - \frac{\mu\theta}{d\theta+1})V, \tag{5.53}$$

$$0 = cN' + N'' + \gamma\frac{\mu}{d\theta+1}N - \gamma\delta N. \tag{5.54}$$

Substitution of (5.10) into (5.53)–(5.54) gives that the eigenvalues satisfy

$$\begin{vmatrix} \epsilon\lambda^2 + c\lambda + \hat{v}f'(\hat{v}) + f(\hat{v}) - \frac{\mu\theta}{d\theta+1} & 0 \\ 0 & \lambda^2 + c\lambda + \gamma\frac{\mu}{d\theta+1} - \gamma\delta \end{vmatrix} = 0. \tag{5.55}$$

Since we are interested in the predator–prey–free steady state, i.e. $(\hat{n},\hat{v}) = (0,0)$, (5.55) becomes

$$\begin{vmatrix} \epsilon\lambda^2 + c\lambda + f(0) - \frac{\mu\theta}{d\theta+1} & 0 \\ 0 & \lambda^2 + c\lambda + \gamma\frac{\mu}{d\theta+1} - \gamma\delta \end{vmatrix} = 0. \tag{5.56}$$

Hence, λ can be computed from two quadratic equations, that is,

$$\epsilon\lambda^2 + c\lambda + f(0) - \frac{\mu\theta}{d\theta+1} = 0, \text{ or } \lambda^2 + c\lambda + \gamma\frac{\mu}{d\theta+1} - \gamma\delta = 0. \tag{5.57}$$

Analysis about the leading edge of the wave $(\hat{v},\hat{n}) = (0,0)$ yields

$$\lambda_{\pm}^V = \frac{-c \pm \sqrt{c^2 - 4\epsilon(f(0) - \frac{\mu\theta}{d\theta+1})}}{2\epsilon}, \tag{5.58}$$

and

$$\lambda_{\pm}^N = \frac{-c \pm \sqrt{c^2 - 4\gamma(\frac{\mu}{d\theta+1} - \delta)}}{2}. \tag{5.59}$$

Thus, linear analysis gives a necessary condition

$$c^2 \geq 4\epsilon(f(0) - \frac{\mu\theta}{d\theta+1}), \text{ and } c^2 \geq 4\gamma(\frac{\mu}{d\theta+1} - \delta) \tag{5.60}$$

for non-negative prey density. Hence when predator follows ratio dependent functional response with assumption $\frac{N}{V}$ = constant, it can slow down or stop the prey spread with diffusion as a searching strategy depending on the parameters μ, d, and θ.

For $N/V = \infty$, $V/N = 0$ so that the linearized equations are

$$0 = cV' + \epsilon V'' + (\hat{v}f'(\hat{v}) + f(\hat{v}) - \frac{\mu}{d})V, \tag{5.61}$$

$$0 = cN' + N'' + \gamma\frac{\mu}{d}V - \gamma\delta N. \tag{5.62}$$

Substitution of (5.10) into (5.61–5.62) gives that the eigenvalues satisfy

$$\begin{vmatrix} \epsilon\lambda^2 + c\lambda + \hat{v}f'(\hat{v}) + f(\hat{v}) - \frac{\mu}{d} & 0 \\ \gamma\frac{\mu}{d} & \lambda^2 + c\lambda - \gamma\delta \end{vmatrix} = 0. \tag{5.63}$$

Since we are interested in the predator–prey–free steady state, i.e. $(\hat{n}, \hat{v}) = (0, 0)$, (5.63) becomes

$$\begin{vmatrix} \epsilon\lambda^2 + c\lambda + f(0) - \frac{\mu}{d} & 0 \\ \gamma\frac{\mu}{d} & \lambda^2 + c\lambda - \gamma\delta \end{vmatrix} = 0. \tag{5.64}$$

Hence, λ can be computed from two quadratic equations, that is,

$$\epsilon\lambda^2 + c\lambda + f(0) - \frac{\mu}{d} = 0, \text{ or } \lambda^2 + c\lambda - \gamma\delta = 0. \tag{5.65}$$

Analysis about the leading edge of the wave $(\hat{v}, \hat{n}) = (0, 0)$ yields

$$\lambda_{\pm}^{V} = \frac{-c \pm \sqrt{c^2 - 4\epsilon(f(0) - \frac{\mu}{d})}}{2\epsilon}, \tag{5.66}$$

and

$$\lambda_{\pm}^{N} = \frac{-c \pm \sqrt{c^2 + 4\gamma\delta}}{2}. \tag{5.67}$$

Thus, linear analysis gives a necessary condition

$$c^2 \geq 4\epsilon(f(0) - \frac{\mu}{d}), \tag{5.68}$$

for non-negative prey density. Hence when predator follows ratio dependent functional response with assumption $\frac{N}{V} = \infty$, it can slow down or stop the prey spread with diffusion as a searching strategy depending on the parameters μ and d.

In summary, the case of $N/V = 0$ is described as predator population decreasing much faster than prey population. Because of that, predators may stay a little distance from the tip of prey spread. That is, at the leading edge of prey spread, prey enjoy the non–predator environment so that prey intrinsic growth rate is preserved. The case of $N/V = \theta$ (constant) is that the decreasing rate of predator population is proportional to the decreasing rate of prey population at the leading edge of prey spread. In this case prey and predator coexist near the prey and predator zero state. Thus the new intrinsic rate of prey population dynamics related to predator interruption is $f(0) - \frac{\mu\theta}{d\theta+1}$, a combination of μ, d and θ. For instance, bigger μ tends to slow down or even stop the prey spread under the fixed d and θ. For the case of $V/N = 0$, predators still patrol the area near the head of the tip of prey spread. In other words, predators roam around the prey free area and prepare to attack the front of prey invasion so that the intrinsic rate of prey population decreases due to the predators' ambush, i.e. $f(0) - \frac{\mu}{d}$. Therefore increasing μ tends to restrict prey spread. Figures 5.4 and 5.5 demonstrate prey spreads with $\mu = 0.1$ and $\mu = 0.95$, respectively. It is noted that the case of $\mu = 0.95$ shows slower prey spread than that of $\mu = 0.1$.

5.3 Prey Dynamics with an Allee Effect

In the previous sections, we used linear analysis to find the prey spread rate. However, when the prey dynamics include an Allee effect we cannot use linear analysis (see [57]).

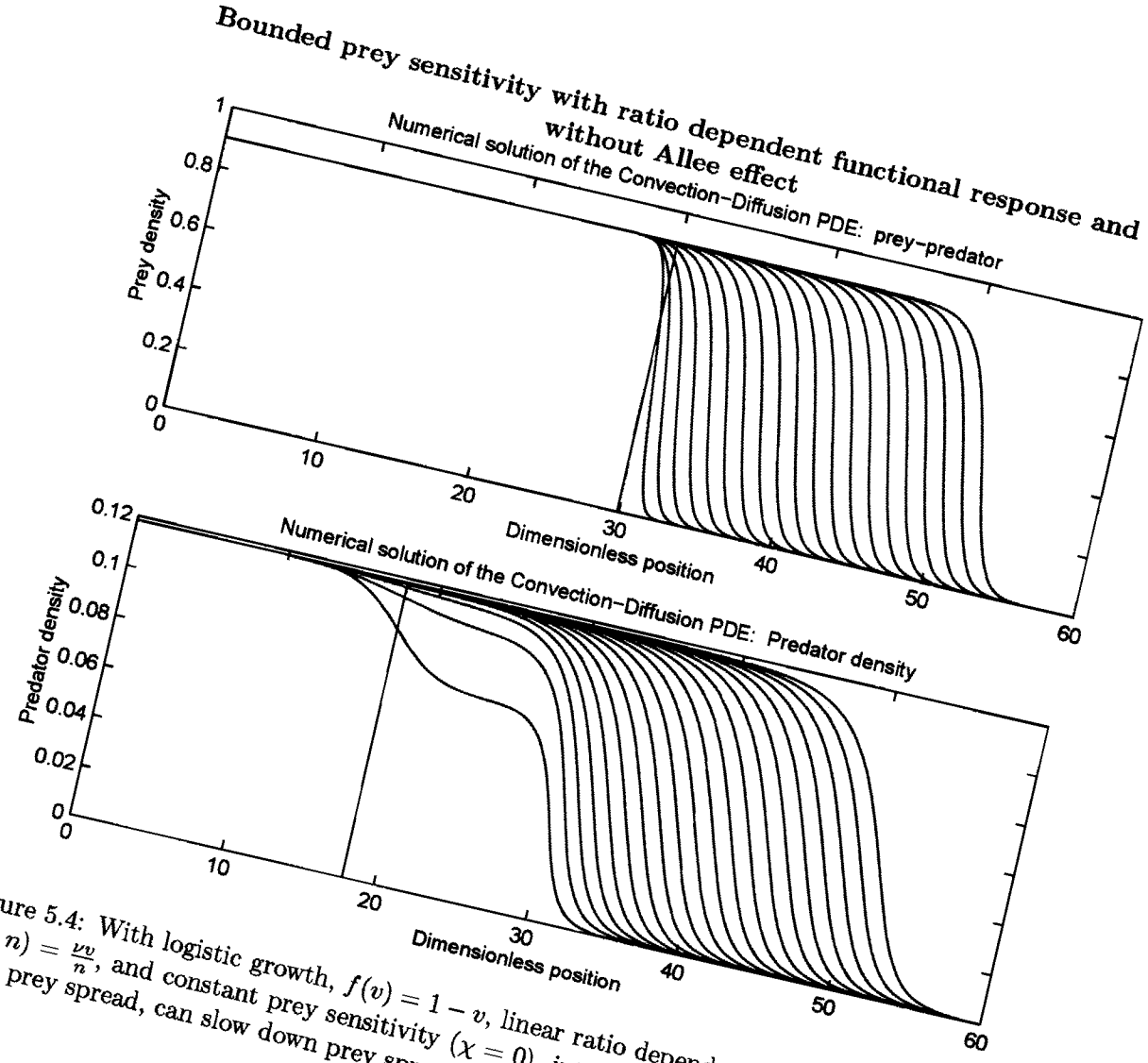

Figure 5.4: With logistic growth, $f(v) = 1 - v$, linear ratio dependent functional response, $h(v, n) = \frac{\nu v}{n}$, and constant prey sensitivity ($\chi = 0$), introduced predators, which catch up with prey spread, can slow down prey spread. Here $\nu = 0.1$.

Bounded prey sensitivity with ratio dependent functional response and without Allee effect

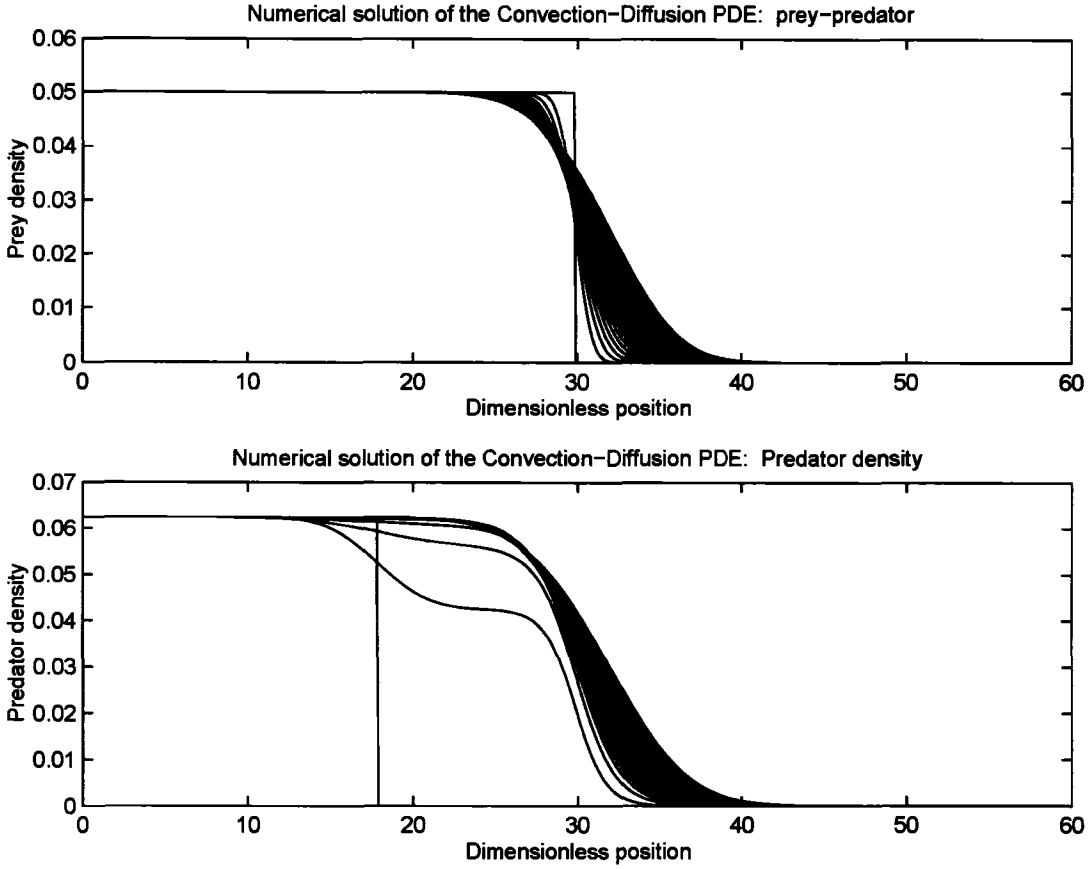

Figure 5.5: With logistic growth, $f(v) = 1 - v$, linear ratio dependent functional response, $h(v,n) = \frac{\nu v}{n}$, and constant prey sensitivity ($\chi = 0$), introduced predators, which catch up with prey spread, can slow down prey spread. Here $\nu = 0.95$.

Instead of linear analysis, Owen and Lewis [72] used a singular perturbation analysis of the wavefront for the diffusion–only case. In this section, we follow the analysis of Owen and Lewis [72] to find a necessary condition for the predator to stop the prey spread, i.e. $c = 0$. They require the following two conditions in order to have zero wave speed solutions. The conditions restrict the values of v_0 and δ.

$$\int_0^{v_0} v(f(v) - \frac{g(v_0)}{v}h(v))dv = 0, \tag{5.69}$$

$$\int_{v_0}^{v_s} vf(v)g'(v)dv = \frac{1}{2}\delta g(v_s)^2. \tag{5.70}$$

Here v_s is the value of v at the coexistence steady state and $g(v) = \frac{f(v)v}{h(v)}$ (see Appendix D for detailed analysis). The meaning of two conditions (5.69)–(5.69) will be considered in subsequent paragraphs.

A singular perturbation analysis of the wavefront consists of two steps and each step ends up with one condition. The first step is finding the stationary wave solution of a completely immobile prey. The temporal steady state of system (5.3)–(5.4) with $\chi = 0$, and zero wave speed leads to

$$0 = v(f(v) - \frac{n}{v}h(v)), \tag{5.71}$$

$$0 = n_{xx} + \gamma n(h(v) - \delta). \tag{5.72}$$

Figure 5.6 A shows the initial distributions of the predator and prey density. Predators spread forward and eventually they stop moving forward since there are no prey to sustain the population for $x > 20$. Figure 5.6 B shows the distributions of the predator and prey density after 500 time units, which is regarded as a stationary wave solution to equations (5.71) and (5.72). In Figure 5.6 B, there is one point at which the predator curve crosses the prey curve. At this point, the predator density is $n = n_0$ and the prey is $v = v_0 = g^{-1}(n_0)$. The value v_0 is in the condition (5.70) and this v_0 can be computed from equation (5.70). In this case v_0 is the peak of the prey curve.

Now we consider the meaning of condition (5.69). When prey move slowly compared to their predators, a transition layer appears at the front (see Figure 5.7. B). Condition (5.69) says that in the transition layer predator density is assumed to be constant, say $n = n_0$, rather than slowly decreasing as we can see in Figure 5.7 B. Then in the transition layer, the prey equation is

$$0 = v_{xx} + v(f(v) - \frac{n_0}{v}h(v)),. \tag{5.73}$$

The sign of wave speed c is determined by the sign of

$$\int_0^{v_0} v(f(v) - \frac{n_0}{v}h(v))dv \tag{5.74}$$

(see [68] for details). Thus zero wave speed occurs when $\int_0^{v_0} v(f(v) - \frac{n_0}{v}h(v))dv = 0$ for nonzero v_0. However, the logistic growth $f(v) = 1 - v$ gives positive $\int_0^{v_0} v(f(v) - \frac{n_0}{v}h(v))dv$ for non–zero v_0, which gives the same result from the linear analysis, that is, positive wavespeed. In contrast, when considering an Allee effect, for example, $f(v) = k(1-v)(v-a)$ may give $\int_0^{v_0} v(f(v) - \frac{n_0}{v}h(v))dv = 0$, which is shown as condition (5.69).

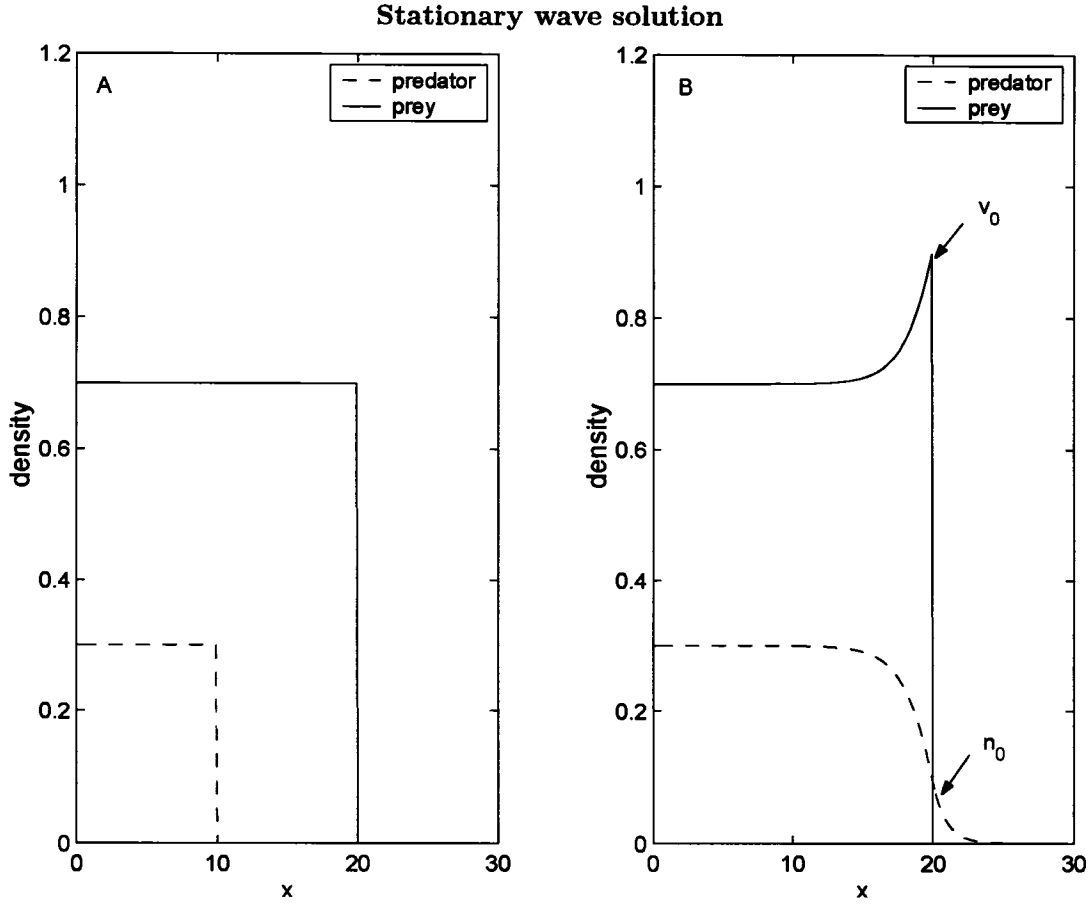

Figure 5.6: Stationary wave solution to equations (5.71) and (5.72) with logistic growth, $f(v) = 1 - v$, type I functional response and $h(v) = v$. Here $\delta = 0.7$, $\epsilon = 0$, and $\gamma = 1$. In A, dashed and solid lines show initial predator and prey distribution, respectively. In B, dashed and solid lines show predator and prey distribution, respectively, at t=500.

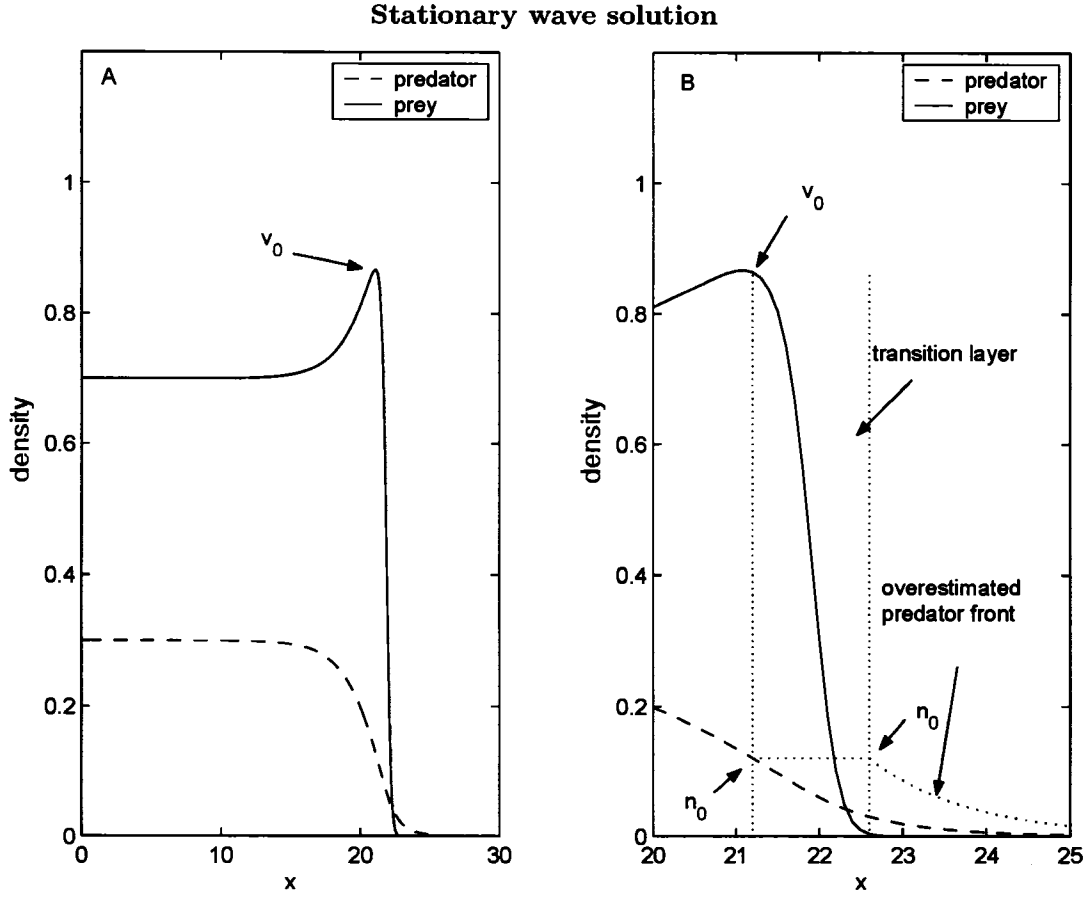

Figure 5.7: Stationary wave solution to equations (5.71) and (5.72) with logistic growth, $f(v) = 1 - v$, type I functional response and $h(v) = v$. Here $\delta = 0.7$, $\epsilon = 0.01$, and $\gamma = 1$. In A, dashed and solid lines show initial predator and prey distribution, respectively. In B, dashed and solid lines show predator and prey distribution, respectively, at t=10.

In summary, when we examine whether predators can slow down or stop the prey spread, we need to consider two steps. First, we need to find v_0 and n_0. Second, we put these v_0 and n_0 into condition (5.69) and see whether this n_0 and v_0 satisfy the equality (5.69).

Before we derive a necessary condition for stopping prey in the predator–prey model with prey–taxis, we note that a singular perturbation analysis of the wavefront can be applied for the case without an Allee effect. We now use an example to see how a singular perturbation analysis of the wavefront can be used for the case with an Allee effect.

We now consider $f(v) = k(v-a)(1-v)$ and $h(v) = v$. Substituting $g(v) = f(v)$, $h(v) = v$, and $f(v) = k(v-a)(1-v)$ into condition (5.69),

$$\begin{aligned}&\int_0^{v_0} kv((v-a)(1-v) - (v_0-a)(1-v_0))dv\\ &= -k\frac{v_0^3(-3v_0+2+2a)}{12} = 0.\end{aligned}$$

Thus v_0 is 0 or $\frac{2+2a}{3}$ from the condition (5.69).

First, we substitute $v_0 = 0$ into (5.70) with $v_s = \delta$, which leads to

$$\begin{aligned}&\int_0^{v_s} vf(v)g'(v)dv - \frac{1}{2}\delta g(v_s)^2\\ &= k^2\left(\int_0^{v_s} v(-1+v)(v-a)(2v-a-1)dv - \frac{\delta(1-\delta)^2(\delta-a)^2}{2}\right)\\ &= -k^2\delta\frac{(6\delta^4 - 15\delta^3 - 15\delta^3 a + 40\delta^2 a + 10\delta^2 + 10a^2\delta^2 - 30\delta a - 30a^2\delta + 30a^2)}{60}\\ &= 0.\end{aligned}$$

The last equation shows that $\delta = 0$ or $6\delta^4 - 15\delta^3 - 15\delta^3 a + 40\delta^2 a + 10\delta^2 + 10a^2\delta^2 - 30\delta a - 30a^2\delta + 30a^2 = 0$, which can be expressed as a polynomial in a as follows

$$(10\delta^2 - 30\delta + 30)a^2 + (-15\delta^3 + 40\delta^2 - 30\delta)a + 6\delta^4 - 15\delta^3 + 10\delta^2 = 0, \qquad (5.75)$$

which is quadratic with respect to a so that we can find the roots. The coefficient of a^2, $10\delta^2 - 30\delta + 30$, is positive for all δ and the constant term, $6\delta^4 - 15\delta^3 + 10\delta^2$ is positive for all δ except for $\delta = 0$, in which case the constant term also becomes zero. The coefficient of a, $-15\delta^3 + 40\delta^2 - 30\delta$ is negative for $\delta > 0$. Therefore we can expect two positive a's in terms of δ for $\delta > 0$. However, the determinant, $(-15\delta^3 + 40\delta^2 - 30\delta)^2 - 4(10\delta^2 - 30\delta + 30)(6\delta^4 - 15\delta^3 + 10\delta^2)$, is negative so that there is no real root. Thus v_0 cannot be zero.

Second, we substitute $v_0 = \frac{2+2a}{3}$ into (5.70) with $v_s = \delta$, yielding

$$\begin{aligned}&\int_{v_0}^{v_s} vf(v)g'(v)dv - \frac{1}{2}\delta g(v_s)^2\\ &= \quad k^2\left(\int_{v_0}^{v_s} v(-1+v)(v-a)(2v-a-1)dv - \frac{\delta(1-\delta)^2(\delta-a)^2}{2}\right) = 0.\end{aligned}$$

We can rearrange the above equation into

$$\begin{aligned}&-k^2\delta\frac{(6\delta^4 - 15\delta^3 - 15\delta^3 a + 40\delta^2 a + 10\delta^2 + 10a^2\delta^2 - 30\delta a - 30a^2\delta + 30a^2)}{60}\\ &= 2k^2\frac{(1+a)^3(2-11a+2a^2)}{1215}.\end{aligned}$$

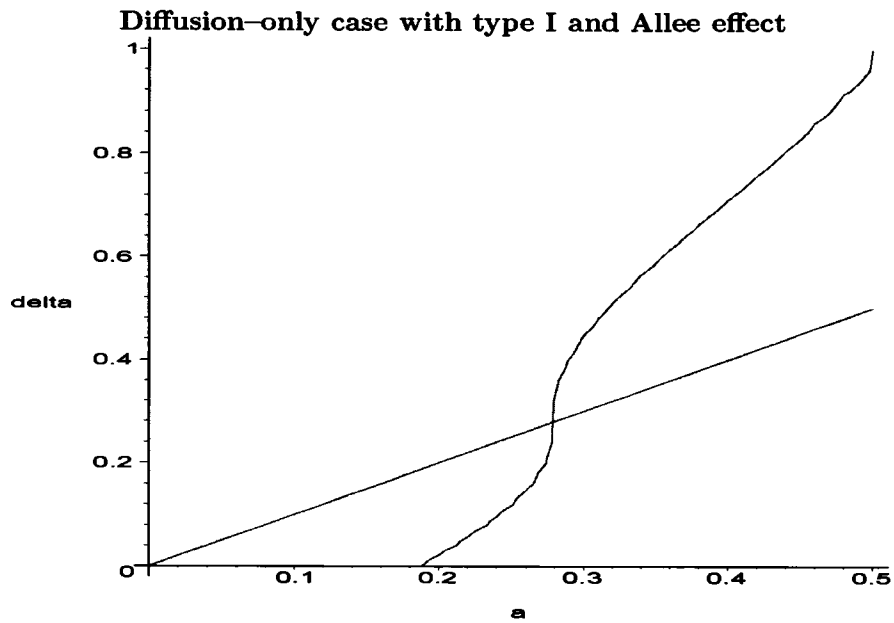

Figure 5.8: When $v_0 = \frac{2+2a}{3}$, the relation between δ and a to satisfy equation (5.76) is drawn with the straight line $\delta = a$.

We can simplify to get

$$-\delta((10\delta^2 - 30\delta + 30)a^2 + (-15\delta^3 + 40\delta^2 - 30\delta)a + 6\delta^4 - 15\delta^3 + 10\delta^2)$$
$$= \frac{8}{81}(1+a)^3(2 - 11a + 2a^2). \tag{5.76}$$

When we consider the condition for the existence of the coexistence state, that is, $a < \delta < 1$, Figure 5.8 shows that there exist pairs of (a, δ) to satisfy the condition that predators with diffusion–only dispersal and a type I functional response on the prey may stop the prey spread with an Allee effect. a is approximately located between 0.28 and 0.5 while δ is between 0.28 and 0.91. δ determines a, say a_0, for prey stopping. For $a > a_0$, the prey retreats, and for $a < a_0$, the prey spread slows down.

It is noted that when we apply these two conditions (5.69)–(5.70) to the situation where the prey population growth is logistic or shows an Allee effect, the predator density is slightly overestimated in the transition area (see Figure 5.7. B). With logistic growth, the overestimated predators fail to stop the prey spread. Therefore the predators from the exact solution cannot stop the prey spread. In contrast, with an Allee effect, the overestimated predators stop the prey spread, however it does not guarantee that the predators from the exact solution may stop the prey spread. As the prey diffusion rate ϵ increases, the error estimate increases. Thus, the parameter a shown in the Allee effect would have to increase for predators to stop the prey spread as ϵ increases.

We now resume finding the stopping conditions for the case of prey–taxis. Recall that a key difference between our model and the model of Owen and Lewis is that prey–taxis is added in our model. To find a spread rate, we study the wavefront after the predators catch up with the prey and the coexistence is observed. Slow movement of the prey generates a

sharp transition in prey population from the coexistence steady state to the zero population on the right.

We now want to find out whether predators with a prey–taxis strategy stop prey spread, i.e. $c = 0$. First we consider a constant prey sensitivity, i.e. $\chi(v) = \chi$. Here we aim to find two conditions like (5.69)–(5.70) for predators with prey–taxis. Basically, we follow the steps in Appendix D.

Due to the zero wave speed we consider the temporal steady state of the following system

$$v_t = \epsilon v_{xx} + v\left(f(v) - \frac{n}{v}h(v)\right), \tag{5.77}$$

$$n_t = n_{xx} - (\chi v_x n)_x + \gamma n(h(v) - \delta), \tag{5.78}$$

where the constant χ is the prey sensitivity of the predator and ϵ, γ, δ, $f(v)$, and $h(v)$ are the same as before (see (5.1)–(5.2). Later we will consider various forms of $f(v)$, and $h(v)$). The stationary system is as follows

$$0 = \epsilon v_{xx} + v\left(f(v) - \frac{n}{v}h(v)\right), \tag{5.79}$$

$$0 = n_{xx} - (\chi v_x n)_x + \gamma n(h(v) - \delta). \tag{5.80}$$

Transition layer. Rescaling the spatial coordinate to $\xi = \frac{x}{\sqrt{\epsilon}}$, equations (5.79)–(5.80) are written as

$$0 = v_{\xi\xi} + v\left(f(v) - \frac{n}{v}h(v)\right), \tag{5.81}$$

$$0 = n_{\xi\xi} - (\chi v_\xi n)_\xi + \epsilon\gamma n(h(v) - \delta), \tag{5.82}$$

which is the stationary front solutions of (5.77)–(5.78)). In addition, the boundary conditions are: $\lim_{\xi\to\pm\infty} v_\xi(\xi) = 0$, $\lim_{\xi\to\infty} v(\xi) = 0$, and $\lim_{\xi\to-\infty} v(\xi) = v_0$. As $\epsilon \to 0$, n follows $n_{\xi\xi} - (\chi v_\xi n)_\xi = 0$. Integrating this equation, we have $n_\xi - \chi v_\xi n = C_0$. As $\xi \to \pm\infty$, $n_\xi \to C_0$, since $v_\xi \to 0$. For large $|\xi|$, $n_\xi \approx C_0$. Integrating one more time, then for large $|\xi|$ we have $n \approx C_1\xi + C_0$ where C_0 and C_1 are integral constants. However, for any non–zero constant C_0, a different sign of ξ generates a negative population for the predators, i.e. if $C_0 > 0$, then for negative large ξ, n becomes negative. Thus, C_0 must be zero. We now have $n_\xi - \chi v_\xi n = 0$ for all ξ and $n_\xi = 0$ for large $|\xi|$. Isolating n on the left side and v on the right side, we have

$$\frac{1}{n}n_\xi = \chi v_\xi. \tag{5.83}$$

This can be integrated directly with respect to ξ so that

$$\ln(n(\xi)) - \ln(n(-\infty)) = \int_{-\infty}^{\xi} \chi v_\xi d\xi = \chi(v(\xi) - v(-\infty)), \tag{5.84}$$

Since $n(-\infty) = n_0$, a constant to be determined, we have
$n(\xi) = n_0 \exp(\chi(v(\xi) - v_0))$. Thus, we have a single equation for v,

$$v_{\xi\xi} + v\left(f(v) - \frac{n_0 \exp(\chi(v(\xi) - v_0))}{v}h(v)\right) = 0, \tag{5.85}$$

where the boundary conditions are: $\lim_{\xi\to\pm\infty} v_\xi(\xi) = 0$, $\lim_{\xi\to\infty} v(\xi) = 0$, and $\lim_{\xi\to-\infty} v(\xi) = g^{-1}(n_0) = v_0$. Multiplying equation (5.85) by $dv/d\xi$, and integrating with respect to ξ from $-\infty$ to ∞ gives us

$$\int_{-\infty}^{\infty} \left\{ \frac{d^2v}{d\xi^2} + v\left(f(v) - \frac{n_0 \exp(\chi(v(\xi) - v_0))}{v} h(v) \right) \right\} \frac{dv}{d\xi} d\xi = 0. \tag{5.86}$$

The first term is integrated directly and the second term is done by using a change of variables from ξ to v, to get

$$\frac{1}{2}\left(\frac{dv}{d\xi}\right)^2 \Big]_{-\infty}^{\infty} + \int_0^{v_0} v\left(f(v) - \frac{n_0 \exp(\chi(v - v_0))}{v} h(v) \right) dv = 0. \tag{5.87}$$

Applying the boundary conditions and $n_0 = g(v_0)$ yields

$$\int_0^{v_0} v\left(f(v) - \frac{g(v_0) \exp(\chi(v - v_0))}{v} h(v) \right) dv = 0, \tag{5.88}$$

which determines v_0 consistent with a stationary solution.

Right-hand outer solutions. We now consider equations (5.79)–(5.80) setting $\epsilon = 0$ so that v and n satisfy

$$0 = v(f(v) - \frac{n}{v} h(v)), \tag{5.89}$$

$$0 = n_{xx} - (\chi v_x n)_x + \gamma n(h(v) - \delta). \tag{5.90}$$

From equation (5.89), $v = 0$ or $n = g(v) = \frac{vf(v)}{h(v)}$. Since we are looking for right–hand outer solutions, we here focus on $v = 0$ so that in equation (5.90) v_x becomes zero and we get

$$n_{xx} - \gamma\delta n = 0, \tag{5.91}$$

with boundary conditions: $\lim_{x\to\infty} n(x) = 0$ and $n(0) = n_1 = n_0 \exp(-\chi v_0)$. This equation (5.91) is the same as (D.11). Therefore after applying boundary conditions we get

$$n(x) = n_1 \exp(-\sqrt{\gamma\delta}x), \text{ or equivalently } \frac{dn}{dx}(0) = -n_0 \exp(-\chi v_0)\sqrt{\gamma\delta}. \tag{5.92}$$

Left–hand outer solutions. We now consider the other outer layer. Recall that without prey–taxis, in the transition layer n was constant so that equation (D.13) played the role of a boundary condition to find left–hand outer solutions. However, the prey–taxis term makes the procedure of matching the solutions more complicated. Here we consider the conserved flux in the transition layer so that $(\frac{dn}{dx} - \chi n\frac{dv}{dx})\Big|_{x=0} = (\frac{dn}{dx} - \chi n\frac{dv}{dx})\Big|_{x=\infty} = (\frac{dn}{dx})\Big|_{x=\infty} = -n_0 \exp(-\chi v_0)\sqrt{\gamma\delta}$. The last equality comes from matching the inner solution and the outer solution of the transition layer and the right hand outer solution. $n = g(v)$ is put into equation (5.80) to get

$$n_{xx} - (\chi v_x n)_x + \gamma n(h(g^{-1}(n)) - \delta) = 0, \tag{5.93}$$

with boundary conditions: $n(0) = n_0$, $\lim_{x\to-\infty} n(x) = n_s$, $(\frac{dn}{dx} - \chi n\frac{dv}{dx})\Big|_{x=0} = -n_0 \exp(-\chi v_0)\sqrt{\gamma\delta}$, and $\frac{dn}{dx}(-\infty) = 0$, which satisfy the conservation of flux in the transition layer.

Multiplying equation (5.93) by $dn/dx - \chi n dv/dx$, and integrating with respect to x from $-\infty$ to 0 we find

$$\int_{-\infty}^{0} \{n_{xx} - (\chi n v_x)_x + \gamma n(h(g^{-1}(n)) - \delta)\} \left(\frac{dn}{dx} - \chi n \frac{dv}{dx}\right) dx = 0. \tag{5.94}$$

As we did for the analysis in the transition layer, the first term is integrated directly and the second term is done by using a change of variables from ξ to n, to get

$$\frac{1}{2}\left(\frac{dn}{dx} - \chi n \frac{dv}{dx}\right)^2 \Big]_{-\infty}^{0} + \int_{n_s}^{n_0} \gamma n(h(g^{-1}(n)) - \delta)\left(1 - \chi \frac{n}{g'(g^{-1}(n))}\right) dn = 0. \tag{5.95}$$

With the change of n with v in some part of the above expression, the second part is turned into

$$\int_{v_s}^{v_0} \gamma g(v)(h(v)g'(v) - h(v)\chi g(v) + \delta \chi g(v))dv - \int_{n_s}^{n_0} \gamma \delta n dn. \tag{5.96}$$

Applying the boundary conditions to equation (5.95) and $n_0 = g(v_0)$ yields

$$\begin{aligned}
&\gamma \int_{v_0}^{v_s} g(v)h(v)g'(v)dv + \gamma\chi \int_{v_0}^{v_s} g^2(v)(\delta - h(v))dv \\
&\quad = -\gamma\delta \frac{(n_0^2 - n_s^2)}{2} + \frac{1}{2}\left(\frac{dn}{dx} - \chi n \frac{dv}{dx}\right)^2 \Big]_{x=0} \\
&\quad = \gamma\delta \frac{(g^2(v_s) - g^2(v_0))}{2} + \frac{1}{2} g^2(v_0) \exp(-2\chi v_0)\gamma\delta,
\end{aligned}$$

which gives a condition that the left– and right– hand outer solutions match at n_0 if and only if

$$\begin{aligned}
&\int_{v_0}^{v_s} v f(v) g'(v) dv + \chi \int_{v_0}^{v_s} g^2(v)(\delta - h(v))dv = \\
&\quad \delta \frac{(g^2(v_s) - g^2(v_0))}{2} + \frac{1}{2} g^2(v_0) \exp(-2\chi v_0)\delta,
\end{aligned}$$

after γ is canceled from both sides.

Thus, we have the following two conditions in order for zero wave speed solutions and those conditions restrict the values of v_0, δ, and χ.

$$\int_0^{v_0} v\left(f(v) - \frac{g(v_0)\exp(\chi(v - v_0))}{v} h(v)\right) dv = 0, \tag{5.97}$$

$$\begin{aligned}
&\int_{v_0}^{v_s} v f(v) g'(v) dv + \chi \int_{v_0}^{v_s} g^2(v)(\delta - h(v))dv = \\
&\quad \delta \frac{(g^2(v_s) - g^2(v_0))}{2} + \frac{1}{2} g^2(v_0) \exp(-2\chi v_0)\delta.
\end{aligned} \tag{5.98}$$

If χ is zero, then conditions (5.97)–(5.98) reduce to conditions (5.69)–(5.70). It is noted that for the diffusion–only case the predator density is constant in the transition layer, but including prey–taxis allows the predator density to vary in the transition layer. Therefore when we match the right–hand and left–hand outer solutions we need some adjustment.

Second, we consider $\chi(v) = \frac{b}{v}$ as the form of prey–taxis and the outcome for the stopping conditions. We follow a similar procedure as before. Then from the transition layer analysis, we have

$$\int_0^{v_0} v\left(f(v) - \frac{g(v_0)}{v}h(v)\left(\frac{v}{v_0}\right)^b\right)dv = 0. \tag{5.99}$$

In the transition layer the predator–prey relationship is

$$n = n_0\left(\frac{v}{v_0}\right)^b, \tag{5.100}$$

and as $v \to 0$, we have $n \to 0$. Thus the right–hand outer solution is

$$n(x) = 0, \text{ or equivalently } \frac{dn}{dx}(0) = 0. \tag{5.101}$$

For the left–hand outer solution, we can follow similar steps as before. Conservation of flux across $n = n_0$ gives $\frac{dn}{dx} - \frac{b}{v}\frac{dv}{dx}n]_{(v,n)} = (v_0, n_0) = \frac{dn}{dx} - \frac{b}{v}\frac{dv}{dx}n]_{(v,n)} = (0,0)$. Since $\frac{dn}{dx} = 0$ at $(v,n) = (0,0)$, we need to find $\frac{b}{v}\frac{dv}{dx}n]_{(v,n)} = (0,0)$. As $v \to 0$, we first compute $\frac{1}{v}\frac{dv}{dx}$ from equations (5.79) and (5.100). If $h(0) = 0$, then the linearization of equation (5.79) with n given in equation (5.100) near $v = 0$ is

$$0 = \epsilon v_{xx} + f(0)v. \tag{5.102}$$

Multiplying both sides by v_x and integrating it leads to

$$C = \epsilon\frac{v_x^2}{2} + f(0)\frac{v^2}{2}, \tag{5.103}$$

with integral constant C. We apply the boundary condition, that is, $v = 0$ and $v_x = 0$, then we have $C = 0$. Rearranging the above equation gives

$$\frac{v_x}{v} = \pm\sqrt{\frac{-f(0)}{\epsilon}}. \tag{5.104}$$

Since ϵ is a constant, $\frac{b}{v}\frac{dv}{dx}n \to 0$ as $(v,n) \to (0,0)$. Indeed, zero flux occurs across $n = n_0$. Then the matching procedure between right–hand and left–hand outer solutions gives

$$\int_{v_0}^{v_s} vf(v)g'(v)dv + b\int_{v_0}^{v_s}\frac{g^2(v)}{v}(\delta - h(v))dv = \delta\frac{(g^2(v_s) - g^2(v_0))}{2}. \tag{5.105}$$

In this section, we found that when there is an Allee effect of the prey the predator may stop the prey spread. We considered this problem with two prey sensitivity functions, $\chi(v) = \chi$ and $\chi(v) = \frac{b}{v}$. Then we found two necessary conditions (5.97)–(5.98) for stopping the prey spread.

5.4 Discontinuous Travelling Wave Solution

In this section we take a look at the case that prey are immobile and predators take mainly directional movement with weak diffusion. We modify the model, which Pettet and Mcelwain [75] considered, with a nonconstant prey sensitivity $\chi(v) = \frac{b}{v}$. When an approximate

model with the assumption of no diffusion is considered, we look for the existence of discontinuous solutions. Then we put the diffusion term back and consider the role of the diffusion term with respect to discontinuous solutions. This problem originated from wound healing. Macrophage generates growth factors (prey) and endothelial cells (predator) eat growth factors. Understanding this model will give an insight how the wound heals and give a guideline for more efficient wound healing.

5.4.1 Traveling Wave Analysis

In this section, we begin travelling wave analysis with the phase plane analysis. Here we consider the following system

$$v_t = v(f(v) - \frac{n}{v}h(v)), \tag{5.106}$$

$$n_t = \epsilon n_{xx} - (\chi(v)v_x n)_x + \gamma n(h(v) - \delta), \tag{5.107}$$

where $f(v) = 1 - v$, $h(v) = v$, and $\chi(v) = b/v$ are mainly considered. Here it is assumed that the prey have a negligible ability of movement and predators are able to move directly towards high prey density. In addition, predators are assumed to have small diffusion-induced dispersal. As $\epsilon \to 0$, we have approximate equations as follows

$$v_t = v(1 - v - n), \tag{5.108}$$

$$n_t = -(\frac{b}{v}v_x n)_x + \gamma n(v - \delta). \tag{5.109}$$

With travelling coordinate, $z = x - ct$ with wave speed c, the system becomes

$$-cv_z = v(1 - v - n), \tag{5.110}$$

$$-cn_z = -(\frac{b}{v}v_z n)_z + \gamma n(v - \delta). \tag{5.111}$$

Thus v_z is isolated as $v_z = -\frac{v(1-v-n)}{c}$. Substituting this result into equation (5.111), we have

$$-cn_z = \frac{b}{c^2}nv(1 - v - n) + \frac{b}{c}(1 - v - 2n)n_z + \gamma n(h(v) - \delta). \tag{5.112}$$

Here we put n_z terms together into the left hand side as follows

$$-(c + \frac{b}{c}(1 - v - 2n))n_z = \frac{b}{c^2}nv(1 - v - n) + \gamma n(v - \delta). \tag{5.113}$$

When $c + \frac{b}{c}(1 - v - 2n) = 0$, equation (5.113) becomes singular. Thus the curve $c + \frac{b}{c}(1 - v - 2n) = 0$ becomes a barrier so that phase plane trajectories cannot cross this curve. The coexistence steady state of equations (5.106) and (5.107) is

$$(v_s, n_s) = (\delta, 1 - \delta). \tag{5.114}$$

Depending on where the coexistence lies, we may not expect a continuous connection between the prey-only state $(v, n) = (1, 0)$ and the coexistence state $(v_s, n_s) = (\delta, 1 - \delta)$ (see Figure (5.9)). When the coexistence state is located below the wall of singularity, i.e. $K = \frac{c^2}{b} > 1 - \delta$, there may be a continuous connection from the prey-only state to the

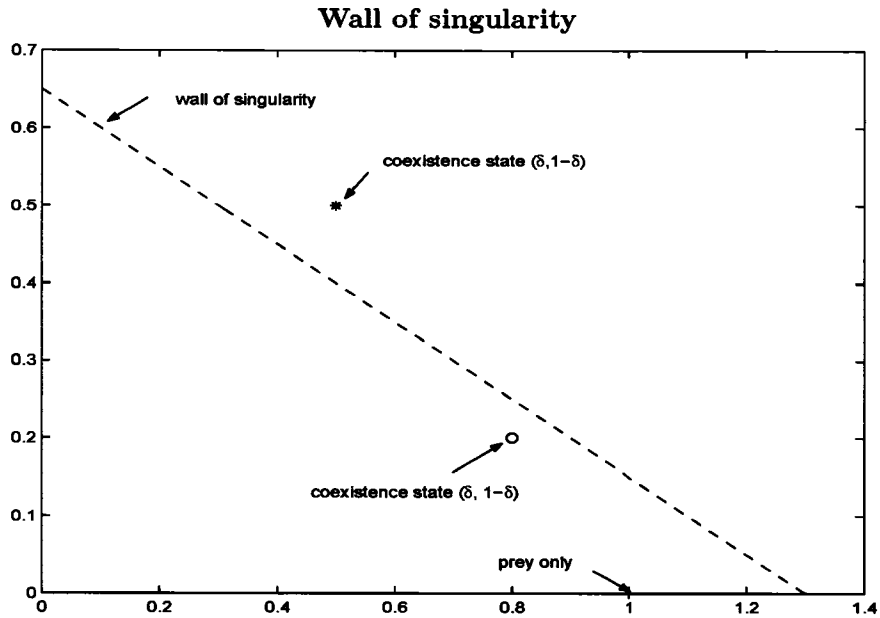

Figure 5.9: Wall of singularity $n = \frac{K+1-v}{2}$ is drawn with two possible locations of coexistence states. $K = 0.3$ and two $\delta = 0.5$ and $\delta = 0.8$.

coexistence state, however when the coexistence state is located above the wall of singularity, i.e. $K < 1 - \delta$, there will be no continuous connection from the prey-only state to coexistence since trajectories cannot cross the wall of singularity. One exception to this is when the n nullcline, $\frac{b}{c}nv(1-v-n)+\gamma n(h(v)-\delta) = 0$, intersects the singular curve. This intersection point is called the 'hole in the wall' (see [75] for detail). Thus the hole in the wall is the intersection point(s) of the following two curves

$$c + \frac{b}{c}(1 - v - 2n) = 0 \tag{5.115}$$

$$\frac{b}{c^2}nv(1-v-n)+\gamma n(v-\delta) = 0, \tag{5.116}$$

equivalently

$$n = \frac{K+1-v}{2} \tag{5.117}$$

$$n = 1 - v + \frac{K\gamma(v-\delta)}{v}. \tag{5.118}$$

Since an equation collapsed from equations (5.117)–(5.118) becomes a quadratic equation, there may be no intersection, one intersection, or two intersections depending on the parameter K. The number of intersections can be computed from the number of solutions of

$$\frac{K+1-v}{2} = 1 - v + \frac{K\gamma(v-\delta)}{v}, \tag{5.119}$$

or equivalently

$$v^2 + (K - 1 - 2K\gamma)v + 2K\gamma\delta = 0. \tag{5.120}$$

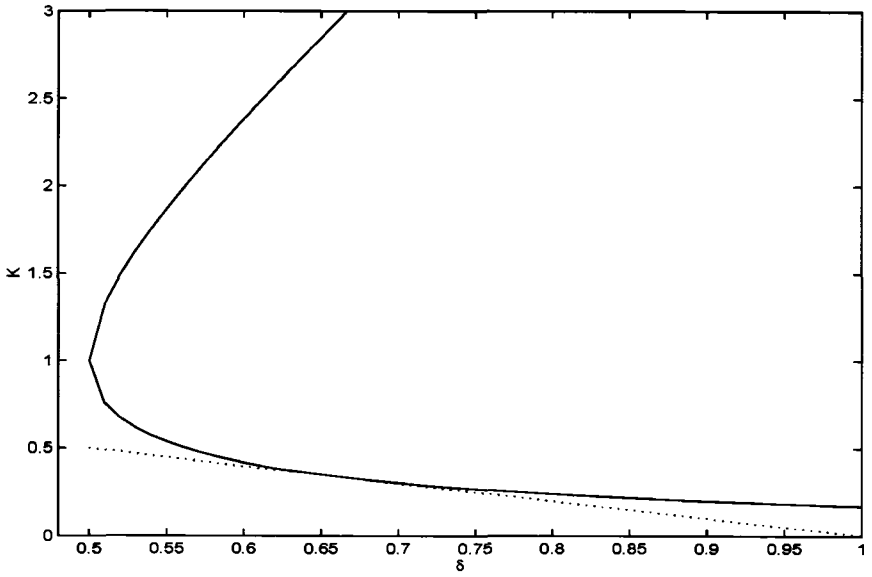

Figure 5.10: Determinant curve, equation (5.122) shown in dashed line and $K = 1 - \delta$ is shown in dotted line with $\gamma = 1$.

The condition for two intersections is when v has two roots, i.e.

$$(K - 1 - 2K\gamma)^2 - 8K\gamma\delta > 0, \tag{5.121}$$

similarly the condition for one intersection is

$$(K - 1 - 2K\gamma)^2 - 8K\gamma\delta = 0, \tag{5.122}$$

and the condition for no intersection

$$(K - 1 - 2K\gamma)^2 - 8K\gamma\delta < 0. \tag{5.123}$$

Here we assume $\gamma = 1$ for the simplicity of analysis. On the right side of the curve (see Figure 5.10), there is no intersection, i.e. no hole in the wall. On the curve, there is one intersection, i.e. one hole in the wall. On the left side of the curve, there are two intersections, i.e. two holes in the wall. Thus when $K < 1 - \delta$ there are always two holes, but when $K > 1 - \delta$ three cases may occur; no hole, one hole, or two holes.

The v and n values of the hole in the wall then are respectively

$$V_H = \frac{K+1}{2} \pm \frac{\sqrt{1 + 2K + K^2 - 8K\delta}}{2} \tag{5.124}$$

$$N_H = \frac{K+1}{4} \mp \frac{\sqrt{1 + 2K + K^2 - 8K\delta}}{4}. \tag{5.125}$$

When there are two holes, if $\delta > \frac{1}{2}$, one v-value of two holes is larger than 1 and the other is less than 1. If $\delta < \frac{1}{2}$, then both v-values of two holes are less than 1. Recall that $(v, n) = (1, 0)$ is the prey–only steady state. When there is no continuous connection from

the prey-only state to coexistence due to the wall of singularity, we may have a discontinuous connection of two states.

The v–intersections of n–nullcline (5.118) are

$$V_{n\text{–nullcline}} = \frac{K+1}{2} \pm \frac{\sqrt{1+2K+K^2-4K\delta}}{2}. \tag{5.126}$$

The v–intersection of n–nullcline , $V_{n\text{–nullcline}} = \frac{K+1}{2} + \frac{\sqrt{1+2K+K^2-4K\delta}}{2}$ is larger than 1. It is also seen that v–values of the holes in the wall are located between the two v–intersections of n–nullcline (5.118).

In this section, we began with considering the travelling wave coordinates, and converted a system of two PDEs into a system of two ODEs for the phase plane analysis. However, we found 'the wall of singularities', which prohibits us from doing the phase plane analysis. The existence of the singular barrier may require a discontinuous solution. Hence, we will consider shock conditions next.

5.4.2 Shock Conditions

Here we consider the possibilty of a discontinous connection from the prey-only state to the coexistence state via transforming equations (5.108) and (5.109) into a non–linear hyperbolic system. When $K < 1-\delta$, there is no continuous connection between the coexistence steady state and the prey–only steady state due to the singular barrier lying between those two steady states. Thus we cannot use phase plane analysis. Instead, we view the model in the form of a hyperbolic system. To do so, we introduce a new variable $w = v_x$. Then equations (5.108) and (5.109) turn into

$$v_t = v(1-v-n), \tag{5.127}$$

$$n_t = -\chi'(v)w^2 n - \chi(v)w_x n - \chi(v)wn_x + \gamma n(v-\delta) \tag{5.128}$$

$$w_t = w - 2vw - wn - vn_x, \tag{5.129}$$

which can be expressed in matrix form as follows

$$\frac{\partial}{\partial t}\begin{bmatrix} v \\ n \\ w \end{bmatrix} + \begin{bmatrix} 0 & 0 & 0 \\ 0 & \chi(v)w & \chi(v)n \\ 0 & v & 0 \end{bmatrix} \frac{\partial}{\partial x}\begin{bmatrix} v \\ n \\ w \end{bmatrix} = \begin{bmatrix} v(1-v-n) \\ \gamma n(v-\delta) - \chi'(v)w^2 n \\ w - 2vw - wn \end{bmatrix} \tag{5.130}$$

Provided $w > 0$, there are three real distinct eigenvalues, i.e. $\lambda_1 = \frac{\chi(v)w}{2} - \frac{\sqrt{\chi^2(v)w^2+4v\chi(v)n}}{2}$ $< \lambda_2 = 0 < \lambda_3 = \frac{\chi(v)w}{2} + \frac{\sqrt{\chi^2(v)w^2+4v\chi(v)n}}{2}$ so that equations (5.127–5.129) are a strictly hyperbolic system. Thus system (5.130) allows shocks in any of the three characteristic fields.

We are looking for travelling wave solutions moving at a positive speed $c > 0$ so that the jump occurs in the λ_3 field. In order to find jump conditions, equation (5.130) is now changed in the conservative form as follows

$$\frac{\partial}{\partial t}\begin{bmatrix} v \\ n \\ w \end{bmatrix} + \frac{\partial}{\partial x}\begin{bmatrix} 0 \\ \chi(v)wn \\ -v(1-v-n) \end{bmatrix} = \begin{bmatrix} v(1-v-n) \\ \gamma n(v-\delta) \\ 0 \end{bmatrix} \tag{5.131}$$

For $\bar{U} = (v, n, w)$, the system is now in the hyperbolic system form of $\bar{U}_t + \bar{A}_x = \bar{C}$. Rankine–Hugoniot jump condition in the kth field is

$$[\bar{U}]s_k = [\bar{A}]$$

where $[\bar{U}]$ denotes the jump in $\bar{U}$ and s_k the shock speed. Applying the jump condition for $\lambda_3 > 0$, then we have

$$[v]s_3 = 0, \tag{5.132}$$

$$[n]s_3 = [\chi(v)wn] = \chi(v)[wn] \tag{5.133}$$

$$[w]s_3 = -[v(1-v-n)] = v[n], \tag{5.134}$$

with $[v] = V_L - V_R$. We assume travelling wave solutions so that positive speed, $c > 0$ leads to $[v] = 0$, that is, $V_L = V_R$. With $w = v_z = -\frac{v(1-v-n)}{c}$ and $s_3 = c$, equation (5.133) is $[n]c = -\frac{\chi(v)}{c}v[(1-v-n)n]$, which is expanded as $(N_L - N_R)c = -\frac{\chi(v)}{c}v((1-v) - (N_L + N_R))(N_L - N_R)$. Thus if $N_L \neq N_R$, for $v = V_L = V_R$ we have the jump condition

$$N_L + N_R = 1 - v + \frac{c^2}{\chi(v)v} = 1 - v + K \tag{5.135}$$

with $\chi(v) = \frac{b}{v}$ and $K = \frac{c^2}{b}$. Indeed, it is noted that the average of N_L and N_R is located on the wall of singularity, i.e. $\frac{N_L+N_R}{2} = \frac{1-v+K}{2}$. Equation (5.134) always holds.

Uniqueness of the discontinuous wave solution can be shown by the Lax entropy condition. A jump in the kth field is admissible only if

$$\lambda_k(\bar{U}_L) > s_k > \lambda_k(\bar{U}_R).$$

Equation (5.133) and $w = -\frac{v(1-v-n)}{c}$ give the shock speed

$$s_3 = \frac{\chi(V)W_R}{2} + \frac{\sqrt{\chi^2(V)W_R^2 + 4V\chi(V)N_L}}{2},$$

and eigenvalue λ in the 3rd field is

$$\lambda_3 = \frac{\chi(v)w}{2} + \frac{\sqrt{\chi^2(v)w^2 + 4v\chi(v)n}}{2},$$

which yields

$$\lambda_3(\bar{U}_L) = \frac{\chi(V)W_L}{2} + \frac{\sqrt{\chi^2(v)W_L^2 + 4V\chi(V)N_L}}{2},$$

$$\lambda_3(\bar{U}_R) = \frac{\chi(V)W_R}{2} + \frac{\sqrt{\chi^2(v)W_R^2 + 4V\chi(V)N_R}}{2}.$$

Therefore a jump in the 3rd field is admissible since

$$\lambda_3(\bar{U}_L) > s_3 > \lambda_3(\bar{U}_R),$$

provided that $N_L > N_R$, which leads to $W_L > W_R$ from the relation $w = -\frac{v(1-v-n)}{c}$.

Here we found the necessary conditions for the existence of a discontinuous travelling wave solution. The shock speed was computed. We will consider the proof of the existence of a discontinuous solution.

5.4.3 Existence of Traveling Waves

Here we consider the existence of traveling wave solutions as K varies given δ. For each parameter space, we investigate travelling wave solutions. We begin with the existence of continuous wave solutions connecting the coexistence state $(v_s, n_s) = (\delta, 1-\delta)$ and the prey–only state $(v, n) = (1, 0)$ of an ODE system (5.110) and (5.113).

Linear stability analysis says that the prey–only state $(v, n) = (1, 0)$ is a saddle as long as $\delta < 1$. Thus there is one stable manifold and one unstable manifold. The stable manifold is tangent to an eigenvector $(\frac{1}{2-\delta}, 1)$, which lies above the v–nullcline $n = 1 - v$, corresponding to a negative eigenvalue at prey–only steady state $(v, n) = (1, 0)$.

The Jacobian matrix of equations (5.110) and (5.113) at the coexistence state $(v_s, n_s) = (\delta, 1-\delta)$ is

$$\mathbf{J} = \begin{bmatrix} \delta & \delta \\ \frac{(1-\delta)(\delta-K)}{K-1+\delta} & \frac{(1-\delta)\delta}{K-1+\delta} \end{bmatrix} \tag{5.136}$$

The trace of $\mathbf{J}$ is

$$\mathrm{tr}(\mathbf{J}) = \frac{\delta K}{K-1+\delta}, \tag{5.137}$$

and the determinant of $\mathbf{J}$

$$\det(\mathbf{J}) = \frac{\delta(1-\delta)K}{K-1+\delta}. \tag{5.138}$$

If $\det(\mathbf{J}) < 0$, that is, $K < 1-\delta$, the system (5.110) and (5.113) has a saddle at the coexistence state $(v_s, n_s) = (\delta, 1-\delta)$. When $K > 1-\delta$, the trace of $\mathbf{J}$ is positive and $\mathrm{tr}(\mathbf{J})^2 - 4\det(\mathbf{J})$ is

$$\mathrm{tr}(\mathbf{J})^2 - 4\det(\mathbf{J}) = \frac{\delta K(5K\delta - 4K + 4 - 8\delta + 4\delta^2)}{(K-1+\delta)^2}, \tag{5.139}$$

in which the $5K\delta - 4K + 4 - 8\delta + 4\delta^2$ term determines the sign of $\mathrm{tr}(\mathbf{J})^2 - 4\det(\mathbf{J})$. That is, if $K \geq -\frac{(1-\delta)^2}{5\delta-4}$, $\mathrm{tr}(\mathbf{J})^2 - 4\det(\mathbf{J})$ is non–negative so that the coexistence state is an unstable node. If $K < -\frac{(1-\delta)^2}{5\delta-4}$, then $\mathrm{tr}(\mathbf{J})^2 - 4\det(\mathbf{J})$ is negative so that the coexistence state is an unstable spiral.

In Figure 5.9, when the coexistence state is below the singular barrier, i.e. $K > 1-\delta$, it is noted that the coexistence state is an unstable spiral or node. On the other hand, when the coexistence state is above the singular barrier, i.e. $K < 1-\delta$, the coexistence state is seen to be a saddle.

First of all, we consider a node(or spiral)–saddle connection, i.e. $K > 1-\delta$. When there is no hole in the wall, Figure 5.11 shows a typical feature of the phase plane of equations (5.110) and (5.113). We follow the proof of the existence of a traveling wave connection in [20]. The prey–only steady state $(v, n) = (1, 0)$ is a saddle, so there is a unique trajectory T landing on $(1, 0)$ via a stable manifold. We follow this trajectory T back into the region PAB bounded by P–A line (a part of the v–nullcline), A–B line, and P–B curve (a part of the n–nullcline). Then it must either lead to a steady state in the closed region PAB or cross the boundary.

First, in the closed region PAB, there are only two steady states, the prey–only steady state and the coexistence state. Since vector fields in the closed region push the trajectory T increasing along the v axis and decreasing along the n axis, it is easily checked that the trajectory T originally did not leave the prey–only steady and returns the prey–only steady,

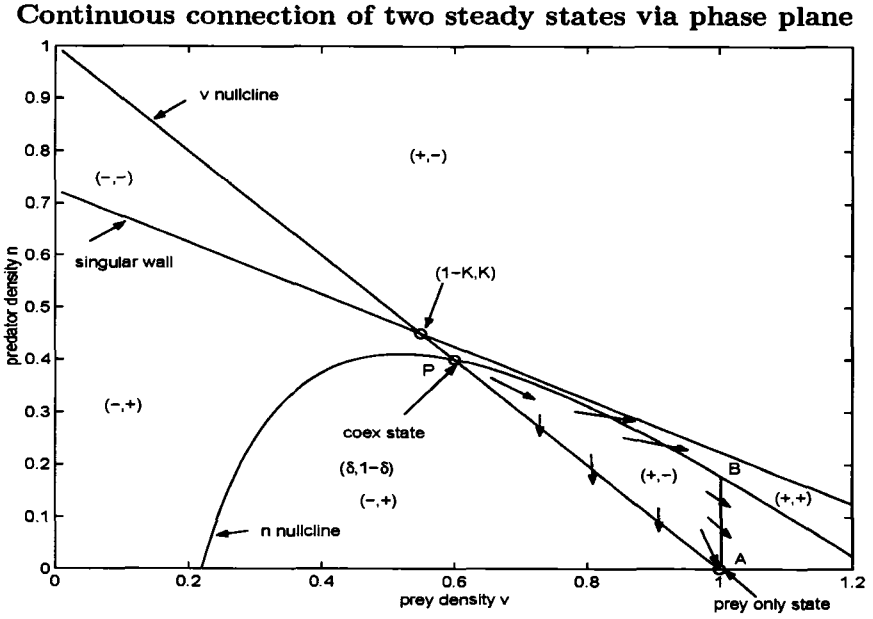

Figure 5.11: Coexistence state is located below the wall of singularity and an unstable node. $K = 0.45$ and $\delta = 0.6$ are used to demonstrate a continuous connection from the coexistence steady state to the prey–only steady state. Vector fields are shown in terms of $+$ and $-$.

i.e. no homoclinic orbit. Thus if any, we would follow the trajectory T back to another steady state, that is, the coexistence state.

Second, we can exclude the situation that the backward trajectory T does not cross the boundary. From vector fields, v is strictly increasing on the trajectory T. Therefore T cannot come through the side AB. In addition, n is decreasing and v is increasing in the closed region PAB, so all trajectories approaching the line PA approach from the left. Therefore T cannot get back to this line PA. Similarly, so all trajectories approaching the curve PB approach from the left. If all n values of PB are smaller than that of the coexistence state, i.e. $K < \delta$, T cannot get back to this curve PB. With $K > 1 - \delta$, we have $\delta > 0.5$. specifically Figure 5.12 shows that $K < \delta$ guarantees that the coexistence steady state is an unstable node. Therefore one place the trajectory T possibly leads to is the coexistence state and we have the existence of a wave connection.

So far, we considered the one of seven cases with $K > 1 - \delta$, i.e. G region in Figure 5.12). In region A, there are two holes, the coexistence state is an unstable spiral, and n values of PB near the coexistence state is bigger than one of the coexistence state. In region B, there is no hole, the coexistence state is an unstable spiral, and n values of PB near the coexistence state is bigger than the n value of the coexistence state. In region C, there is no hole, the coexistence state is an unstable node, and n values of PB near the coexistence state is bigger than that of the coexistence state. In region D, there are two holes, the coexistence state is an unstable node, and n values of PB near the coexistence state are bigger than that of the coexistence state. In region E, there are two holes, the coexistence state is an unstable node, and all n values of PB near the coexistence state are smaller than the one of the coexistence state. In region F, there is no hole, the coexistence

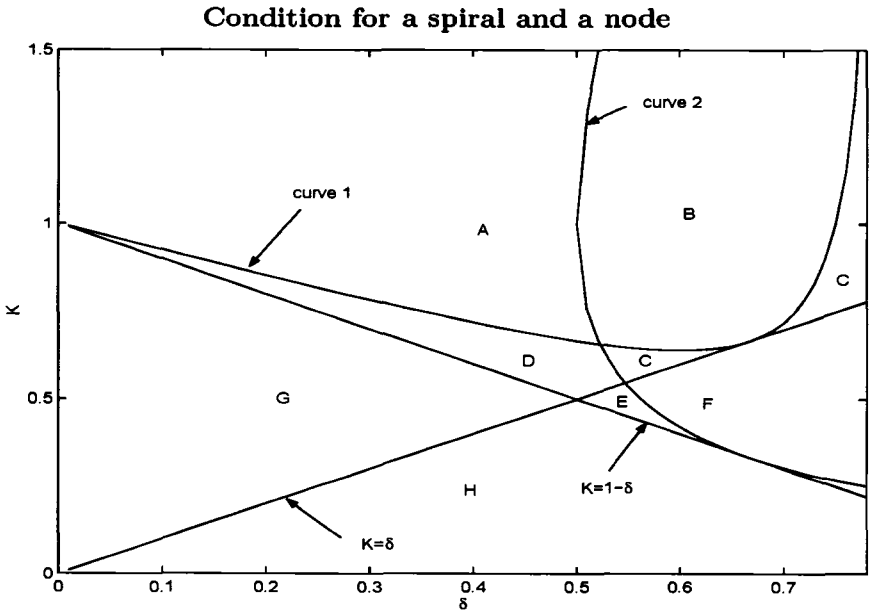

Figure 5.12: Curve 1 and curve 2 denote $K = -\frac{4(1-\delta)^2}{5\delta-4}$ and $\delta = \frac{(1+K)^2}{8K}$, respectively.

state is an unstable node, and all n values of PB near the coexistence state are smaller than that of the coexistence state.

With $K < 1 - \delta$, in region G, there are two holes, the coexistence state is a saddle, and n values of PB near the coexistence state is bigger than the coexistence state value. In region H, there are two holes, the coexistence state is a saddle, and all n values of PB near the coexistence state are smaller than the coexistence state value. Next, we consider the case that n values of PB near the coexistence state is bigger than one of the coexistence state, i.e. $K > \delta$. Figure 5.12 indicates that the coexistence state is either an unstable spiral or else an unstable node. Unless there is a limit cycle around the coexistence state, the trajectory T possibly leads to the coexistence state, but more work is needed. Figure 5.13 demonstrate phase plane, in which the vector fields around the coexistence state show a spiral behaviour.

The proof of the other cases of the existence of continuous or discontinuous travelling wave solutions and their uniqueness needs to be studied. We also need to show whether a travelling wave solution is uniquely determined for given parameters b and δ. If the wave speed c is uniquely determined, K is fixed, so we can easily determine whether the solution is continuous or discontinuous. For that, we need to do intense simulations.

We did numerical experiments where the wave speed is uniquely determined given δ and b and prey sensitivity function $\chi(v) = \frac{b}{v}$. First, we chose $\delta = 0.5$ and found the wave speed $c = 0.4$ and $K = 0.16$. Thus the solution is discontinuous as shown in Figure 5.14. However, more simulations need to be done for various parameter space.

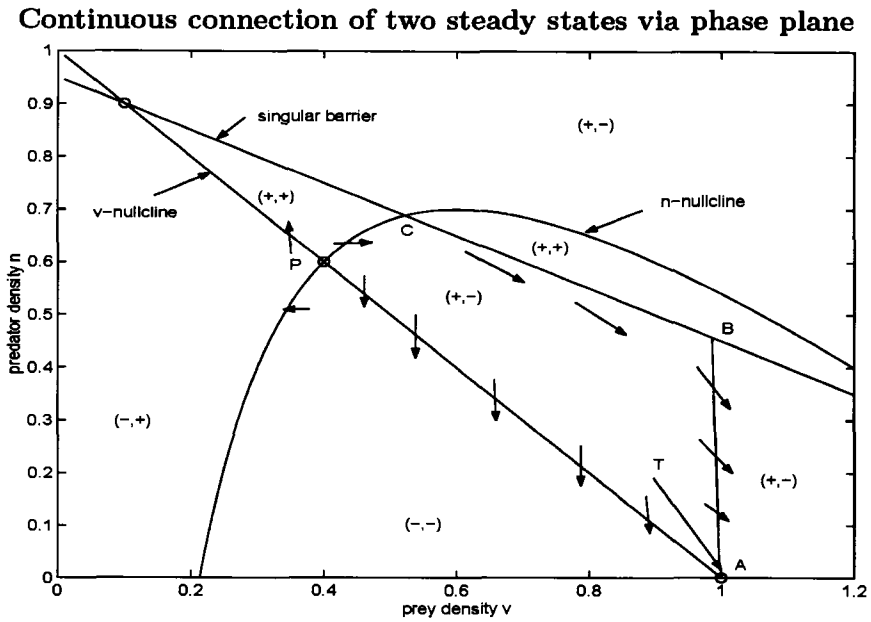

Figure 5.13: Coexistence state is located below the wall of singularity and an unstable spiral. $K = 0.9$ and $\delta = 0.4$ are used to demonstrate a continuous connection from the coexistence steady state to the prey–only steady state. Vector fields are shown in terms of $+$ and $-$.

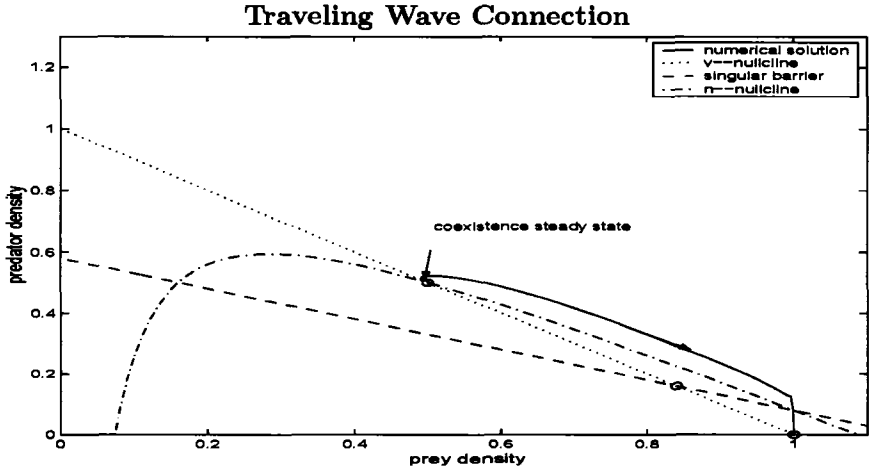

Figure 5.14: When $\delta = 0.5$, numerical solution computed wave speed as $c = 0.4$, so $K = 0.16 < 1 - \delta = 0.5$. Singular barrier, v– and n– nullclines are drawn together. $dx = 0.01$, $dt = 0.005$, and $t = 5$ are considered. NT scheme is used for the simulation.

5.4.4 Full Model

Now we look at the full equations (5.107)–(5.107) and consider the role of a diffusion process in a discontinuous travelling wave solution. For that, we consider an inner expansion around the singular barrier. With travelling coordinate, $z = x - ct$, the equations (5.107)–(5.107) are transformed to

$$-cv_z = v(f(v) - \frac{n}{v}h(v)), \tag{5.140}$$

$$-cn_z = -(\chi(v)v_z n)_z + \gamma n(h(v) - \delta) + \epsilon n_{zz}, \tag{5.141}$$

or equivalently

$$-cv_z = v(1 - v - n), \tag{5.142}$$

$$-cn_z = \frac{1}{c}(\chi(v)v(1 - v - n)n)_z + \gamma n(v - \delta) + \epsilon n_{zz}, \tag{5.143}$$

With $\chi(v) = \frac{b}{v}$, equations (5.142–5.142) are

$$v_z = -\frac{v(f(v) - \frac{n}{v}h(v))}{c}, \tag{5.144}$$

$$-(c + \frac{b}{c}(1 - v - 2n))n_z = \frac{b}{c^2}nv(1 - v - n) + \gamma n(v - \delta) + \epsilon n_{zz}. \tag{5.145}$$

Here we consider the inner expansion of equations (5.144–5.145) around the singular barrier with $z - z_0 = \epsilon\xi$ so that

$$v_\xi = -\epsilon\frac{v(f(v) - \frac{n}{v}h(v))}{c}, \tag{5.146}$$

$$-(c + \frac{b}{c}(1 - v - 2n))n_\xi = \epsilon\frac{b}{c^2}nv(1 - v - n) + \epsilon\gamma n(v - \delta) + n_{zz}. \tag{5.147}$$

With regular expansion of v and n, i.e.

$$v = v_0 + \epsilon v_1 + \mathcal{O}(\epsilon^2) \tag{5.148}$$

$$n = n_0 + \epsilon n_1 + \mathcal{O}(\epsilon^2), \tag{5.149}$$

the leading order terms are calculated as

$$-cv_{0\xi} = 0 \tag{5.150}$$

$$-(c + \frac{b}{c}(1 - v_0 - 2n_0))n_{0\xi} = n_{0\xi\xi}. \tag{5.151}$$

Therefore $v_0 =$ constant and $n_{0\xi\xi} + (c + \frac{b}{c}(1 - v_0 - 2n_0))n_{0\xi} = 0$. The last equation is integrated as $n_{0\xi} - \frac{b}{c}n_0^2 + (c + \frac{b}{c}(1 - v_0))n_0 + A = 0$ with integral constant A. We can isolate $n_{0\xi}$ so that $n_{0\xi} = \frac{b}{c}n_0^2 - (c + \frac{b}{c}(1 - v_0))n_0 + A$. Depending on b, c, and A, there may be two equilibrium points, one equilibrium point, or none (see Figure 5.15). If there are two equilibrium points, let $N_L = n_0^2$, $N_R = n_0^1$, then $\frac{n_0^1+n_0^2}{2}$ is the extremum of the quadratic, which lies on the singular barrier since $q(n_0) = \frac{b}{c}n_0^2 - (c + \frac{b}{c}(1 - v_0))n_0 + A$ and $q'(n_0) = 2\frac{b}{c}n_0 - (c + \frac{b}{c}(1 - v_0))$ so that $q'(n_0) = 0$ gives rise to $n_0 = \frac{K+1-v}{2} = \frac{n_0^1+n_0^2}{2}$.

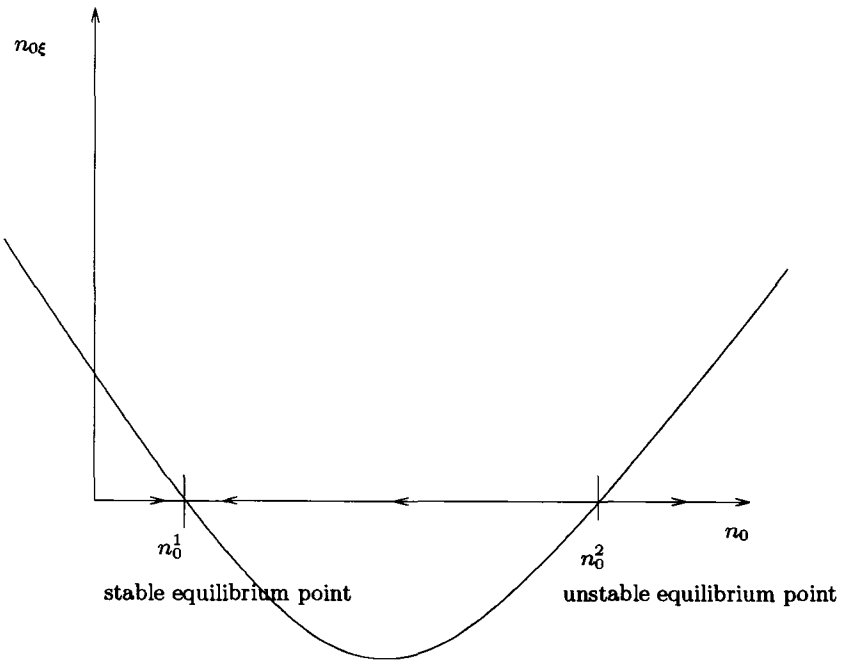

Figure 5.15: Two discrete points are smoothly connected through inner expansion.

Figures 5.16 and 5.17 demonstrate the situation that introduced predators spread into the area in which prey density reaches its full carrying capacity so that the predator and prey density approach the coexistence steady state. In other words, the prey–only steady state, $(v, n) = (1, 0)$, is connected to the coexistence steady state, $(v, n) = (\delta, 1 - \delta)$. Figure 5.16 demonstrates a discontinuous connection between the prey–only steady state and the coexistence steady state. In Figure 5.17 those two steady states are connected smoothly by the help of a diffusion process.

In this section, we applied a prey–taxis model to wound healing. In particular, we considered the case that prey (growth factors) are immobile and predators (endothelial cells) take mainly directional movement with weak diffusion. Without diffusion, the prey–taxis model exhibits rich possibilities of a discontinuous travelling wave solution. Even though we found some necessary conditions for the existence of a discontinuous solution and computed a shock speed, more work needs to be done to understand the mechanisms for wound healing.

5.5 Comparison of the Wave Speeds for Resting Models

In this section we take into account the wave speeds for the resting models in Section 3.6. Here we consider two states, moving and resting states. In a moving state, there are two subgroups as before, right–moving and left–moving species. Then we investigate the spread rate of the total population and compare the result with that found from other approaches.

The classic diffusion–reaction model is

$$\frac{\partial n}{\partial t} = D\frac{\partial^2 n}{\partial x^2} + F(n), \tag{5.152}$$

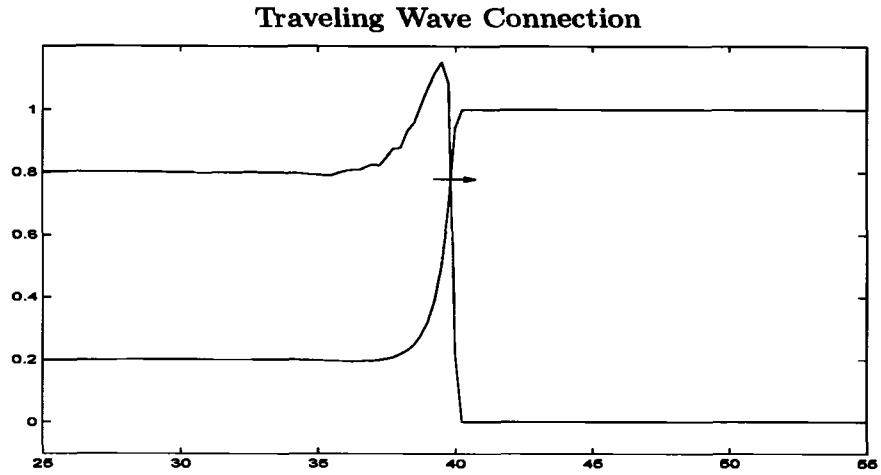

Figure 5.16: From the left predators invade rightward to the area in which prey dominate upto its full capacity. $\epsilon = 0$.

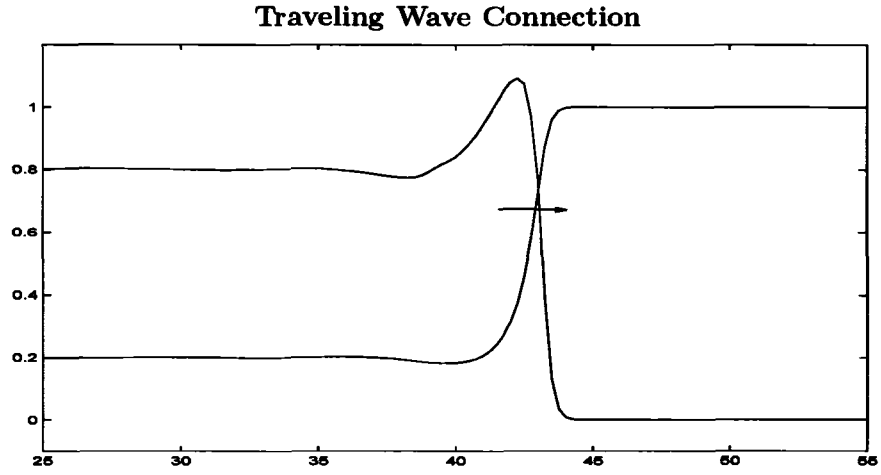

Figure 5.17: From the left predators invade rightward to the area in which prey dominate upto its full capacity. $\epsilon = 0.1$.

where D is a diffusion rate and $F(n)$ the population dynamics. In particular, when the population growth function $F(n)$ is logistic growth, i.e. $F(n) = \gamma_0 n(1-n/K)$ with intrinsic growth rate γ_0 and carrying capacity K, equation (5.152) is the well-known Fisher equation [57, 68, 72]. The wave speed c of the Fisher equation asymptotically converges to the minimum wave speed, $c^2 = 4\gamma_0 D$.

When a population's dispersal shows a correlated random walk rather than random walk, the population dynamics can be eventually combined with telegraph dispersal as follows

$$\frac{\partial n}{\partial t} = -\frac{1}{2r}\frac{\partial^2 n}{\partial t^2} + \frac{u^2}{2r}\frac{\partial^2 n}{\partial x^2} + \frac{1}{2r}\frac{\partial F(n)}{\partial t} + F(n), \tag{5.153}$$

where r is an individual's turning rate and u an individual's speed [32]. The diffusion process (5.152) is the limit of the telegraph process (5.153) as r and u go to ∞ while $\frac{u^2}{2r}$ goes to a constant, say $D = \frac{u^2}{2r}$. When the intrinsic growth rate γ_0 is relatively small compared to the turning rate r, the wave speed was computed in [39] as $c^2 = \frac{8\gamma_0 r}{(\gamma_0+2r)^2}u^2$. When we then consider the diffusion process as a limit of the telegraph process, the diffusion rate D is equivalent to $D = \frac{u^2}{2r}$, which allows us to compare the wave speeds for diffusion–reaction (5.152) and telegraph–reaction (5.153) models with the ratio

$$\frac{c_{\text{tele}}}{c_{\text{diff}}} = \frac{1}{(\gamma_0/2r+1)} < 1, \tag{5.154}$$

where c_{diff} and c_{tele} are the wave speeds of diffusion–reaction (5.152) and telegraph–reaction (5.153) models, respectively [39]. Since the wave speed for the telegraph–reaction (5.153) model was computed under the restriction of relatively small γ_0 compared to r, the comparison ratio (5.154) is close to 1. In addition, as a limit of the telegraph related wave speed, the diffusion related wave speed leads to a slight overestimate.

In the classic Fisher equation (5.152), individuals move randomly without having a rest, which excludes the situation that sometimes individuals take a rest for various reasons such as handling food. In [59], Lewis and Schmitz consider two subgroups. The first group is a subgroup in the moving state with diffusion process and the second one is one in the resting state allowing only local dynamics with a moving subgroup. They consider population spread with the following model,

$$\frac{\partial n}{\partial t} = D\frac{\partial^2 n}{\partial x^2} - \alpha n + \beta q - \mu n \tag{5.155}$$

$$\frac{\partial q}{\partial t} = \alpha n - \beta q + \gamma_0 q(1 - q/K), \tag{5.156}$$

where $q(x,t)$ is a population density in the resting state, α is a transition rate from moving to resting, β is a transition rate from resting to moving, and μ is a death rate of the individuals in the moving state. Reproduction is assumed to occur only in the resting state, but death occurs in both the moving and resting states.

In particular, when γ_0 is very small, the transition rates α and β are equal, and $\mu = 0$, the minimum wave speed of the total population, say $a = n + q$, was computed in [59] as $c^2 = \gamma_0 D$ (see also [25]). Recall that D can be approximated as $D = \frac{u^2}{2r}$ (see [39] and section 3.4).

In equation (5.155), the dispersal term of the moving population is determined by a diffusion process. Now we consider the case that a correlated random walk is the primary

dispersal mechanism. Section 3.6.4 deals with the similar situation with models (5.155)–(5.156), that is, where a correlated random walk is the primary dispersal mechanism with reproduction in the resting state and death in the moving state. If the resting population shows logistic growth, we have

$$\frac{\partial n^+}{\partial t} + u\frac{\partial n^+}{\partial x} = -\alpha(V,S)n^+ + \frac{\beta(S)}{2}q - rn^+ + rn^- - \mu n^+, \tag{5.157}$$

$$\frac{\partial n^-}{\partial t} - u\frac{\partial n^-}{\partial x} = -\alpha(V,S)n^- + \frac{\beta(S)}{2}q + rn^+ - rn^- - \mu n^-, \tag{5.158}$$

$$\frac{\partial q}{\partial t} = \alpha(V,S)(n^+ + n^-) - \beta(S)q + \epsilon^2 F(q), \tag{5.159}$$

with $F(q) = \gamma_1 q(1 - q/K)$. When the death rate of the moving group is zero, i.e. $\mu = 0$, the resting and moving groups are combined via rescaling to lead to the total population spatial dynamics of the diffusion–advection–reaction equation (see section 3.6.3 for details),

$$a_\tau = \left(\frac{u^2}{(\alpha+2r)}\frac{\beta}{\beta+\alpha}a_\xi + \frac{u^2}{(\alpha+2r)}\left(\frac{\beta}{\beta+\alpha}\right)_\xi a\right)_\xi + F(a), \tag{5.160}$$

where a is the total population and $F(a) = \gamma_1 \frac{\alpha}{\beta+\alpha}a\left(1 - \frac{\alpha}{\beta+\alpha}a/K\right)$.

We now compare the wave speed of (5.160) with that of (5.155)–(5.156).

First, we consider the case that the transition rates α and β are equal and constant as Lewis and Schmitz did in [59] and as shown in equations (5.155)–(5.156). Then equation (5.160) leads to a diffusion–reaction equation as follows

$$a_\tau = \left(\frac{u^2}{2(\alpha+2r)}a_\xi\right)_\xi + F(a), \tag{5.161}$$

since $\left(\frac{\beta}{\beta+\alpha}\right)_\xi = 0$ and $\frac{\beta}{\beta+\alpha} = \frac{1}{2}$. We now recover the original scales, i.e. $\tau = \epsilon^2 t$ and $\xi = \epsilon x$ to get

$$a_t = \frac{u^2}{2(\alpha+2r)}a_{xx} + \epsilon^2 F(a), \tag{5.162}$$

which is the form of the Fisher equation. Now the diffusion coefficient is $D = \frac{u^2}{2(\alpha+2r)}$ and the intrinsic growth rate is $\frac{\gamma_0}{2}$ with $\gamma_0 = \epsilon^2\gamma_1$. Here the diffusion coefficient is determined by the turning rate r and the transition rate α, which were disregarded when the diffusion coefficient was originally calculated as $D = \frac{u^2}{2r}$. However, $D = \frac{u^2}{2(\alpha+2r)}$ does not contradicted with $D = \frac{u^2}{2r}$ at all. We revisit equations (5.157)–(5.159) with the same rescaling in Section 3.6. The leading term of q is $q_0 = \frac{\alpha}{\beta}n_0$, which we put into equations (5.157) and (5.158) to get leading terms of the right and left moving groups, n_0^+ and n_0^-. With the original coordinates, we have

$$\frac{\partial n_0^+}{\partial t} + u\frac{\partial n_0^+}{\partial x} = -\alpha(V,S)n_0^+ + \frac{\alpha(V,S)}{2}(n_0^+ + n_0^-) - rn_0^+ + rn_0^- - \mu n_0^+, \tag{5.163}$$

$$\frac{\partial n_0^-}{\partial t} - u\frac{\partial n_0^-}{\partial x} = -\alpha(V,S)n_0^- + \frac{\alpha(V,S)}{2}(n_0^+ + n_0^-) + rn_0^+ - rn_0^- - \mu n_0^-, \tag{5.164}$$

which are rearranged with the additional assumption $\mu = 0$ as follows

$$\frac{\partial n_0^+}{\partial t} + u\frac{\partial n_0^+}{\partial x} = -(r + \frac{\alpha(V,S)}{2})n_0^+ + (r + \frac{\alpha(V,S)}{2})n_0^-, \tag{5.165}$$

$$\frac{\partial n_0^-}{\partial t} - u\frac{\partial n_0^-}{\partial x} = (r + \frac{\alpha(V,S)}{2})n_0^+ - (r + \frac{\alpha(V,S)}{2})n_0^-. \tag{5.166}$$

Thus the turning rate here is $r + \frac{\alpha(V,S)}{2}$ and twice the turning rate is $2r + \alpha(V,S)$, which explains why $D = \frac{u^2}{2(\alpha+2r)}$. Therefore, the minimum wave speed of the model of (5.155)–(5.156) is $c^2 = \frac{u^2}{(\alpha+2r)}\gamma_0$. It is interesting to note that the intrinsic growth rate of the total population is half that of the resting group. Also, the diffusion coefficient here is slightly different from that derived in [59], i.e. the diffusion coefficient of the total population is the half that of moving group $D = \frac{u^2}{2r}$, which is independent of the transition rate α. We label the wave speed from equations (5.155) and (5.156) $c_{\text{m–diff}}$ and that from equations (5.157)–(5.159) $c_{\text{m–hyper}}$, where "m" denotes multiple states of a species. The comparison between the two wave speeds is shown by the ratio

$$\frac{c_{\text{m–hyper}}}{c_{\text{m–diff}}} = \sqrt{\frac{1}{1+\alpha/2r}} < 1. \tag{5.167}$$

If the turning rate r is very big compared to the transition rate α, then $c_{\text{m–diff}}$ becomes approximately the same as $c_{\text{m–hyper}}$, i.e. $c_{\text{m–diff}} \approx c_{\text{m–hyper}}$. Thus the ratio $\frac{\alpha}{2r}$ is an important factor that makes two models different. As a limit of $c_{\text{m–hyper}}$, $c_{\text{m–diff}}$ leads to a slight overestimate. Thus we may interpret $c_{\text{m–diff}}$ as a special case of $c_{\text{m–hyper}}$. Likewise, the models of (5.155)–(5.156) are a special case of the resting models in section 3.6.

We considered the case of $\alpha = \beta$ and $\mu = 0$. We now release these restrictions for the more general case of α, β, and μ in equations (5.155) and (5.156). Then the total population equation of combined moving and resting groups is obtained in [34] as follows

$$a_t = \left(\frac{\beta}{\beta+\alpha}Da_x + D\left(\frac{\beta}{\beta+\alpha}\right)_x a\right)_x + F(a), \tag{5.168}$$

where a is the total population and $F(a) = \gamma_0\frac{\alpha}{\beta+\alpha}a\left(1 - \frac{\alpha}{\beta+\alpha}a/K\right) - \mu\frac{\beta}{\beta+\alpha}a$.

Likewise, equations (5.157)–(5.159) lead to

$$a_t = \left(\frac{u^2}{(\alpha+2r)}\frac{\beta}{\beta+\alpha}a_x + \frac{u^2}{(\alpha+2r)}\left(\frac{\beta}{\beta+\alpha}\right)_x a\right)_x + F(a). \tag{5.169}$$

If α and β are constant and $D = \frac{u^2}{2r}$, the comparison between the two wave speeds is the same as (5.167), i.e. $\frac{c_{\text{m–hyper}}}{c_{\text{m–diff}}} = \sqrt{\frac{1}{1+\alpha/2r}} < 1$. Figure 5.18 shows that the ratio of wave speeds of the two resting models, (5.155)–(5.156) and (5.157)–(5.159), decreases from 1 to 0.817 as the ratio α/r increases from 0 to 1. Thus an increased transition rate, given a fixed turning rate, reduces the invasion speed of a species with the resting and moving states compared to that of a species only with the moving state. From equation (5.169) the diffusion coefficient is $D = \frac{u^2}{(\alpha+2r)}\frac{\beta}{\beta+\alpha}$. If α is big, in other words, moving individuals take

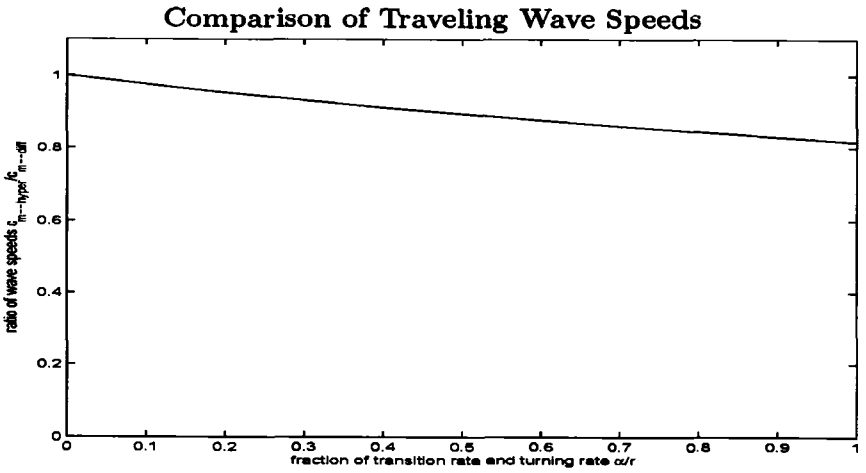

Figure 5.18: A ratio of wave speeds of two resting models, (5.155)–(5.156) and (5.157)–(5.159), decreases as a α/r ratio increases

a rest very often, so the diffusion rate decreases. Alternatively, small β, which means that resting organisms rarely launch into the moving state, reduces the diffusion rate of the total population.

This result has important implication for interpreting model prediction. For examples, Holmes [39] calculated turning rates from diffusion rates and moving speeds. Kareiva and Odell computed the moving speed of ladybugs by using a diffusion rate and a turning rate estimated from field data. However, those turning rates, which Holmes found, may consist of both turning rate and transition rates as $D = \frac{u^2}{2(\alpha+2r)}$, and as a result, those turning rates may be an overestimate. Likewise excluding the transition rates between resting and moving subgroups may lead to an underestimate of the population moving speed.

A comparison of the wave speeds for diffusion–reaction and telegraph–reaction models, which was studied using empirical data in [39], indicates that the wave speed difference between the two models is at most 7.3 %, and that the wave speed for diffusion–reaction model is a slight overestimate. However, comparison of the wave speeds for diffusion–reaction (5.155) and (5.156) and hyperbolic–reaction (5.157)–(5.159) models of moving and resting subgroups predicts that the wave speed difference between the two models may increase depending on the transition rates between the moving and resting states. Indeed, the main difference between those two models is that the wave speed for hyperbolic–reaction models of moving and resting subgroups also depends on the transition rates between the moving and resting states, whereas the wave speed for diffusion–reaction models of moving and resting subgroups is independent of these transition rates.

Invasion speeds of cabbage butterflies were computed in [39]. Holmes considered two populations with three or seven generations per year and an adult life expectancy of 10 or 20 days, respectively. For the first group with 3 generations per year and a 10 day life expectancy, the diffusion coefficient is $D = 3.87$ km^2/yr and an individual's moving speed is $u = 21$ km/yr. Because the intrinsic growth rate of cabbage butterflies is relatively small compared to the diffusion coefficient (9.0 per year vs. 3.87 km^2/yr), the derivations of the invasion speeds for diffusion–reaction and hyperbolic–reaction models of moving and resting

subgroups are valid. We apply these results to diffusion–reaction and hyperbolic–reaction models of moving and resting subgroups.

First we consider the model (5.155)–(5.156). Since $D = 3.87$ km^2/yr applies to the total population, the actual diffusion coefficient for the moving population is twice that, i.e. $D_{\text{moving}} = 2D = 7.74$ km^2/yr (see [59]). From the diffusion approximation that $D_{\text{moving}} = \frac{u^2}{2r}$, we can compute the turning rate $r = 28.49$ /yr which can be converted into 9.5 per generation or 0.95 per day. However, it has been reported that in a single day the butterflies tend to move in straight lines and they only change directions from one day to the next, so the turning rate 0.95 per day seems to be an overestimate (A turning rate of 0.5 might be more reasonable since on each new day an individual butterfly picks a new direction randomly (0.5)).

Now we consider the hyperbolic–reaction model of moving and resting subgroups, and take the limit approximation (5.162). Here the diffusion coefficient $D = \frac{u^2}{2(\alpha+2r)}$ and the individual moving speed u gives $\alpha+2r = 56.98$ per year or 1.9 per day. With the assumption that the turning rate $r = 0.5$, we come to the conclusion that the transition rate $\alpha = 0.9$ per day. If we consider a 10 day life span, there are only 9 new days, so 4.5 turns per generation may be expected and the transition rate $\alpha = 10$ per generation is obtained. Converting these data to a daily scale gives us Figure 5.19. We consider 15 and 30 time (day) units, representing a butterfly population with 3 generations per year and a 10–day adult life expectancy. Thus, the wave solutions project the butterfly spread for one year. Figure 5.19 shows that the approximate model (5.169) is an overestimate of the full model (5.157)–(5.159).

The second butterfly population with 7 generations per year and a 20 day adult life expectancy gives the diffusion coefficient $D = 18.05$ km^2/yr and an individual moving speed $u = 98$ km/yr. With these results, the turning rate of the diffusion–reaction model of moving and resting subgroups is $r = 19.00$ per generation or $r = 0.95$ per day, which is almost the same result as for the first butterfly population. For the hyperbolic–reaction model of moving and resting subgroups, the transition rates are 1.0 per day with the same assumption of the turning rate $r = 0.45$.

So far, we considered the diffusion coefficient of the resting models, with which the reproduction function determines the wave speed of the population. We now consider the reproduction function $F(a)$ in the approximate model (5.168). Recall that $F(a) = \gamma_0 \frac{\alpha}{\beta+\alpha} a \left(1 - \frac{\alpha}{\beta+\alpha} a/K\right) - \mu \frac{\beta}{\beta+\alpha} a$. The intrinsic growth rate is now $\frac{\gamma_0\alpha-\mu\beta}{\beta+\alpha}$. The bigger α tends to increase the intrinsic growth rate and the bigger β tends to decrease that.

It is interesting to note that a resting model may be thus able to explain the appearance of Allee effect. Here for the simplicity of example, we assume that K is very big so that we can disregard the term of $\frac{\alpha}{\beta+\alpha} a/K$. In addition, we assume that the death rate μ is a function of a. With $\mu = \frac{r_0\alpha+A-(1+A)a+a^2}{\beta}$ for some positive constant A, the local population

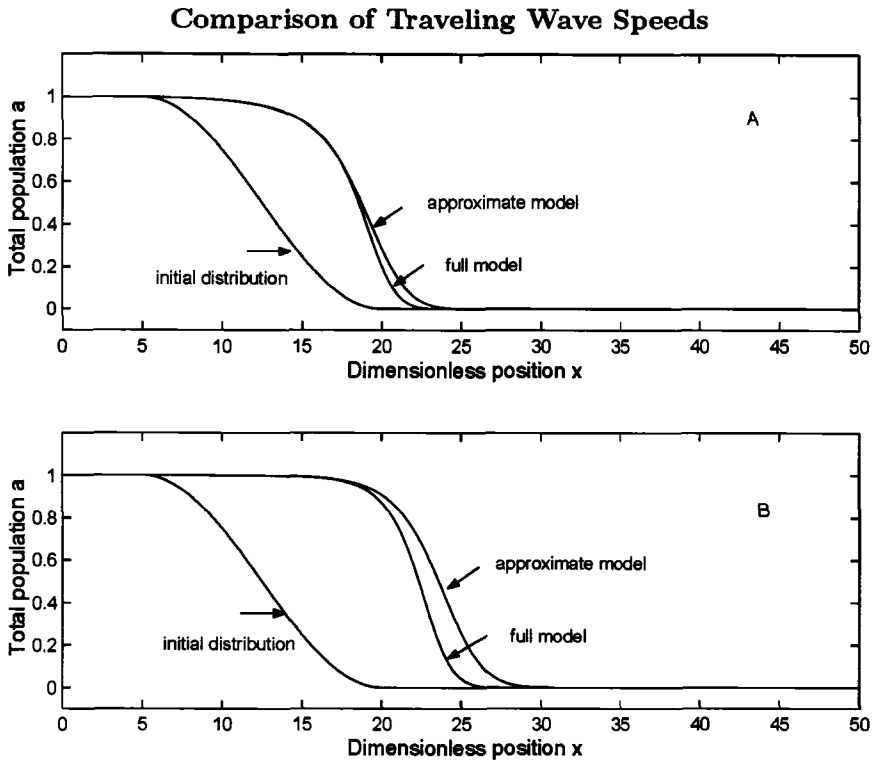

Figure 5.19: Traveling wave solutions to full model (5.157)–(5.159) and approximate model (5.169), with butterfly data. $\alpha = \beta = 1$ per day, $u = 0.7$ km per day, $r = 0.45$ per day, $\gamma_0 = 0.3$ per day. A, 15 days after release; B, 30 days after release.

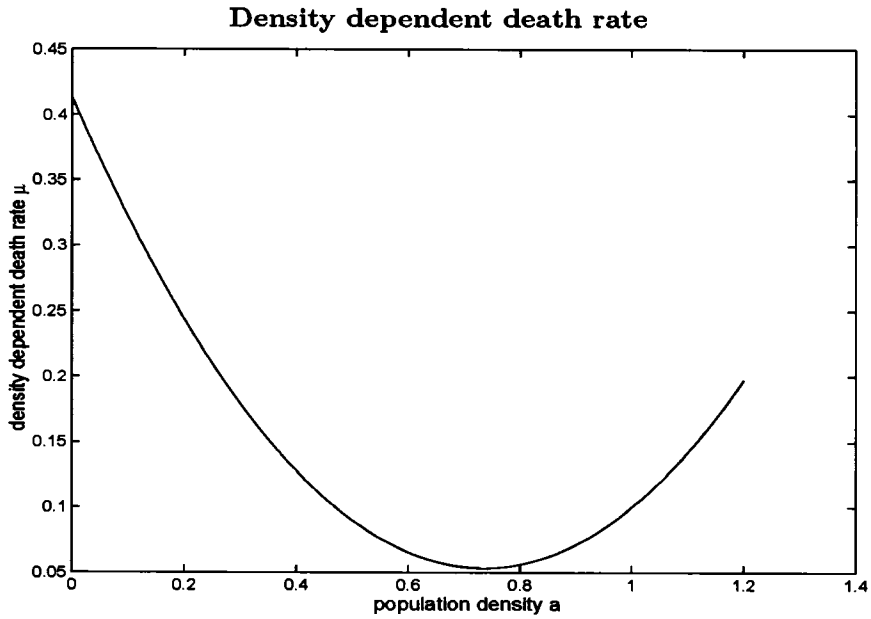

Figure 5.20: Density dependent death rate $\mu = \frac{0.62-1.47a+a^2}{1.5}$ is plotted.

function $F(a)$ is now

$$F(a) = \frac{a}{\alpha+\beta}(r_0\alpha - \mu\beta) \tag{5.170}$$

$$= \frac{a}{\alpha+\beta}(r_0\alpha - (r_0\alpha + A - (1+A)a + a^2)) \tag{5.171}$$

$$= \frac{a}{\alpha+\beta}(-A + (1+A)a - a^2) \tag{5.172}$$

$$= \frac{a}{\alpha+\beta}(1-a)(a-A). \tag{5.173}$$

in which an intrinsic growth rate is negative, i.e. $-\frac{A}{\alpha+\beta}$ even though at $a = 0$, a death rate $\mu = \frac{r_0\alpha+A}{\beta}$ is smaller than r_0 for big β, i.e $\beta > \alpha + \frac{A}{r_0}$. Here we demonstrate how an Allee effect may occur and how it acts in the full model (5.157)–(5.159) and an approximate model (5.169). To do so, we use, for example, $K = 1$ and $\mu = \frac{0.7-1.55a+a^2}{1.5}$. Figure 5.20 shows one candidate function of the death rate $\mu(a)$, which determines that the population has a high death rate at low and high densities and a low death rate at intermediate density. Here the intrinsic growth rate of the resting group is $\gamma_0 = 0.6$, which is bigger than the death rate of moving group $\mu = 0.47$, at $a = 0$. This could represent, for example, efficient group defence but also greater disease spread at high density. Thus the population may have a lower death rate at intermediate density, which may represent the optimal size of the population. Figure 5.21 demonstrates traveling wave solutions to full model (5.157)–(5.159) and approximate model (5.169). At 15 and 60 time units after release, the approximate model still shows forward spreading due to small A. In contrary, the full model shows much slower spreading. It is also noted that even if the population spreads forward in the approximate model, it may retreat in the full model.

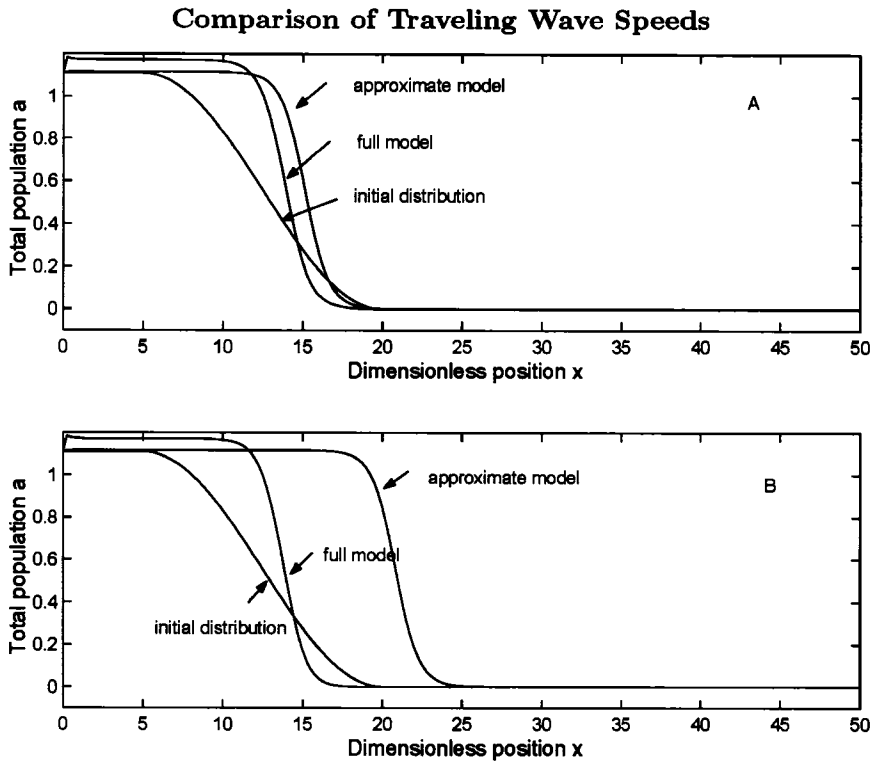

Figure 5.21: Traveling wave solutions to the full model (5.157)–(5.159) and the approximate model (5.169), showing an Allee effect. $\alpha = 0.5$ $\beta = 1.5$ $u = 0.7$, $r = 0.45$, $A = 0.4$, $\gamma_0 = 0.6$. A, 15 time units after release; B, 60 time units after release.

When there are two states, moving and resting, the spread rate of the total population decreases not only as the turning rates increase but also as the transition rates increase. Moreover, an Allee effect may occur due to the different transition rates between the moving and resting states, which reminds us of diffusion–induced instability. Without exchanging two states, there is no Allee effect shown, but with exchanging two states, there may be an Allee effect occurred.

5.6 Summary

In this Chapter, we considered travelling wave solutions to prey–taxis models. In Sections 5.1–5.3, we considered a predator–prey system given by

$$v_t = \epsilon v_{xx} + v(f(v) - \frac{n}{v}h(v)), \tag{5.174}$$

$$n_t = n_{xx} - (\chi(v)v_x n)_x + \gamma n(h(v) - \delta), \tag{5.175}$$

where $\epsilon \ll 1$.

In Sections 5.1–5.2, we considered logistic growth and various functional responses: type I and II functional responses as well as ratio dependent functional responses. We used linear analysis to investigate whether the predator may slow down and stop prey spread. It was shown that without an Allee effect, the predator with any type of functional response cannot stop prey spread. However, it was seen that the predator with ratio dependent functional responses can slow down the prey spread. We found that prey–taxis is not involved in this slowing down phenomenon.

In Section 5.3, we considered an Allee effect in the prey growth term and derived the conditions for stopping the prey spread with prey taxis. For $\chi(v) = \chi$ the conditions are

$$\int_0^{v_0} v\left(f(v) - \frac{g(v_0)\exp(\chi(v - v_0))}{v}h(v)\right)dv = 0, \tag{5.176}$$

$$\int_{v_0}^{v_s} vf(v)g'(v)dv + \chi\int_{v_0}^{v_s} g^2(v)(\delta - h(v))dv = \delta\frac{(g^2(v_s) - g^2(v_0))}{2} + \frac{1}{2}g^2(v_0)\exp(-2\chi v_0)\delta. \tag{5.177}$$

If χ is zero, then conditions (5.176)–(5.177) reduce to conditions (5.69)–(5.70) that Lewis and Owen [72] found.

In Section 5.4, we considered that the prey have no mobility and the predator motility is determined by a directional movement and small diffusion.

$$v_t = v(f(v) - \frac{n}{v}h(v)), \tag{5.178}$$

$$n_t = \epsilon n_{xx} - (\chi(v)v_x n)_x + \gamma n(h(v) - \delta), \tag{5.179}$$

where $f(v) = 1 - v$, $h(v) = v$, and $\chi(v) = b/v$. We first considered an approximate model with $\epsilon = 0$ and found this approximate model may have a discontinuous travelling wave solution under shock conditions. The shock speed was calculated. Regions for a continuous

wave and a discontinuous wave were considered. The diffusion coefficient ϵ played the role in connecting a discontinuous solution smoothly.

In Section 5.3, we considered the wave speeds for the resting models in Section 3.6. Furthermore, we compared the results with those Lewis and Schmitz found in [59]. The comparison between the two wave speeds was shown by the ratio

$$\frac{c_{\text{m-hyper}}}{c_{\text{m-diff}}} = \sqrt{\frac{1}{1+\alpha/2r}} < 1, \tag{5.180}$$

with a turning rate r and a transition rate α. It was also noted that the different transition rates between the moving and resting states produce an Allee effect to the total population.

The significance of this chapter is as follows. With prey–taxis an Allee effect is a necessary factor for the predator to stop the prey spread. Ratio dependent functional responses enable predators to slow down the prey spread but not stop it. In the last section we found that an Allee effect may occur under certain circumstances independent of the difficulty of finding a mate. Hence, when we attempt to control pest, it needs to be studied how we can generate an artificial Allee effect for the pest, because an Allee effect is a necessary factor for the predator to stop the prey spread.

Chapter 6

Pattern Formation

In this chapter we investigate the potential of spatial pattern formation for predator–prey taxis model (5.3)–(5.4). For the predator–prey systems with diffusion, it is noted in the book of Okubo [70] that an Allee effect and a density dependent death rate of the predator are necessary to generate spatial patterns. Jorné [43] argued that the inclusion of species migration (advection) as an additional transport process may increase the possibility of pattern formation. In this chapter we investigate pattern formation induced by dispersal terms for the spatio–temporal predator–prey taxis system (3.126)–(3.127). Furthermore, we consider the role of the prey taxis term as an initiator or an inhibitor of spatial patterns.

6.1 Pattern Formation in Prey Taxis Systems

The ability of the predator–prey taxis system (3.126)–(3.127) to exhibit a spatial pattern crucially depends on the parameter functions $h(v)$ (or $h(v,n)$ for ratio dependent functional responses), $\delta(n)$, and $f(v)$. Thus we study various typical cases separately. An overview of the cases and the corresponding results is given in Table 6.1.

In this section we focus on constant $\chi(v) = \chi$. The predator–prey taxis system derived in Section 3.7 reads

$$v_t = \epsilon v_{xx} + v(f(v) - \frac{n}{v}h(v)), \tag{6.1}$$

$$n_t = n_{xx} - (\chi v_x n)_x + \gamma n(h(v) - \delta(n)), \tag{6.2}$$

on an interval $[0, L]$ with homogeneous Neumann boundary condition given by

$$v_x(0,t) = 0, \quad v_x(L,t) = 0, \quad n_x(0,t) = 0, \quad n_x(L,t) = 0. \tag{6.3}$$

We first consider (6.1)–(6.2) for the general $f(v)$, $h(v)$, and $\delta(n)$, and study the specific functional forms later. We assume that a non–trivial coexistence steady state (v_s, n_s) exists.

We first investigate the stability of the coexistence equilibrium with respect to spatially homogeneous perturbations. For that we set all spatial derivatives in (6.1)–(6.2) equal to zero and linearize about (v_s, n_s)

$$V_t = (v_s f'(v_s) + f(v_s) - n_s h'(v_s))V - h(v_s)N \tag{6.4}$$

$$N_t = \gamma n_s h'(v_s)V + \gamma(h(v_s) - \delta(n_s) - \delta'(n_s))N, \tag{6.5}$$

Section	functional response $h(v)$ or $h(v,n)$	death rate $\delta(n) = \delta + \nu n$	prey growth $f(v)$	pattern formation
6.1.1	Type I	constant	logistic	no
6.1.2	Type II	constant	logistic	no
6.1.3	Type I	density dependent	logistic	no
6.1.4	Type I	density dependent	Allee	yes, with diffusion
6.1.5	Type I	density dependent	Allee	yes, with taxis and diffusion
6.1.6	linear ratio	constant	logistic	no
6.1.7	hyperbolic ratio	constant	logistic	yes, with taxis and diffusion

Table 6.1: The possibility of pattern formation is considered in spatial predator–prey system (3.126)–(3.127) with various functional responses, h, prey population dynamics, f, and predator death rates, δ. We study Type I functional response of the form $h(v) = v$, Type II functional response of the form $h(v) = \frac{(\alpha+1)}{\alpha+v}v$, linear ratio functional response of the form $h(v,n) = \nu_0\frac{v}{n}$, and hyperbolic ratio functional response of the form $h(v,n) = \frac{\mu v}{dn+v}$. Constant death rate means $\delta(n) = \delta$ and density dependent death rate means $\delta(n) = \delta + \nu n$. In the logistic growth rate, we have $f(v) = 1 - v$, and for an Allee effect we have $f(v) = K(1-v)(v-a)$. The parameters α, ν_0, μ, d, ν, K, and a are all positive constants.

where $|N|, |V| \ll 1$. Thus, we have

$$\begin{pmatrix} V_t \\ N_t \end{pmatrix} = \begin{pmatrix} (v_s f'(v_s) + f(v_s) - n_s h'(v_s)) & -h(v_s) \\ \gamma n_s h'(v_s) & \gamma(h(v_s) - \delta(n_s) - \delta'(n_s)) \end{pmatrix} \begin{pmatrix} V \\ N \end{pmatrix}. \tag{6.6}$$

We look for solutions in the form

$$V, N \propto \exp(\lambda t), \tag{6.7}$$

where λ is the eigenvalue. Negative real parts of λ imply that the steady state (v_s, n_s) is linearly stable. Substitution of (6.7) into (6.8) gives

$$\begin{vmatrix} (v_s f'(v_s) + f(v_s) - n_s h'(v_s)) - \lambda & -h(v_s) \\ \gamma n_s h'(v_s) & \gamma(h(v_s) - \delta(n_s) - \delta'(n_s)) - \lambda \end{vmatrix} = 0. \tag{6.8}$$

Hence, the eigenvalues λ satisfy the following quadratic equation

$$\lambda^2 - (A + D)\lambda + AD - BC = 0, \tag{6.9}$$

where

$$\begin{aligned} A &= (v_s f'(v_s) + f(v_s) - n_s h'(v_s)) \\ B &= -h(v_s) \\ C &= \gamma n_s h'(v_s) \\ D &= \gamma(h(v_s) - \delta(n_s) - \delta'(n_s)). \end{aligned} \tag{6.10}$$

To investigate pattern formation induced by spatial movement, we assume that (v_s, n_s) is linearly stable for the purely kinetic equations (no spatial terms).

Assumption:

$$A + D < 0, \quad AD - BC > 0, \tag{6.11}$$

which guarantee linear stability, that is, $Re(\lambda) < 0$.

Now, we consider the full reaction–taxis–diffusion system (3.126)–(3.127) and again linearize about the homogeneous coexistence steady state, (v_s, n_s),

$$V_t = \epsilon V_{xx} + (v_s f'(v_s) + f(v_s) - n_s h'(v_s))V - h(v_s)N \tag{6.12}$$

$$N_t = N_{xx} - \chi n_s V_{xx} + \gamma n_s h'(v_s)V + \gamma(h(v_s) - \delta(n_s) - \delta'(n_s))N, \tag{6.13}$$

where $|N|, |V| \ll 1$. Here, we consider the small perturbation of n and v so that the product of two small terms, $V_x N_x$ and $V_x V_x$, can be disregarded. Therefore, we have the following linearized system

$$\begin{pmatrix} V_t \\ N_t \end{pmatrix} = \begin{pmatrix} A + \epsilon \frac{\partial^2}{\partial x^2} & B \\ C - \chi n_s \frac{\partial^2}{\partial x^2} & D + \frac{\partial^2}{\partial x^2} \end{pmatrix} \begin{pmatrix} V \\ N \end{pmatrix} = 0. \tag{6.14}$$

We look for solutions of the form

$$V, N \propto \exp(\lambda t + ikx), \tag{6.15}$$

where V and N satisfy zero flux boundary conditions (6.3) on the interval $[0, L]$. Substitution into (6.14) gives the dispersion relation between eigenvalues λ and wavenumber k. The dispersion relation $\lambda(k)$ gives the growth rate of the corresponding mode. The eigenvalues λ are determined by the roots of the characteristic polynomial

$$\begin{vmatrix} A - \epsilon k^2 - \lambda & B \\ C + \chi n_s k^2 & D - k^2 - \lambda \end{vmatrix} = 0, \tag{6.16}$$

which can be simplified as follows

$$\lambda^2 - M_1(k^2)\lambda + M_2(k^2) = 0, \tag{6.17}$$

where

$$M_1(k^2) = A + D - (1 + \epsilon)k^2, \tag{6.18}$$

and

$$M_2(k^2) = AD - BC + \epsilon k^4 - (A + \epsilon D + B\chi n_s)k^2, \tag{6.19}$$

with A, B, C and D defined in equations (6.10). Nonnegative ϵ and k^2 guarantee $M_1(k^2) \leq A + D < 0$ for all k, so the only way $\lambda(k^2)$ can be positive is the case that $M_2(k^2) < 0$ for some k^2. Hence a necessary condition for pattern formation is $A + \epsilon D + B\chi n_s > 0$.

In the following subsections we consider specific choices for the functional responses, h, the death rate of the predator, δ, and the growth of the prey, f.

6.1.1 Type I Functional Response, Constant Predator Death Rate and Logistic Growth

In this subsection we consider $f(v) = 1 - v$, $h(v) = v$, and $\delta(n) = \delta$. The coexistence steady state is $(v_s, n_s) = (\delta, 1 - \delta)$, which is biologically relevant for $0 \leq \delta < 1$. Then A, B, C and D defined in equations (6.10) are as follows

$$A = -\delta, \quad B = -\delta, \quad C = \gamma(1 - \delta), \quad D = 0, \tag{6.20}$$

and $M_1(k^2)$ and $M_2(k^2)$ are now

$$M_1(k^2) = -\delta - (1 + \epsilon)k^2 \tag{6.21}$$

$$M_2(k^2) = \delta\gamma(1 - \delta) + \epsilon k^4 + (\delta + \delta\chi n_s)k^2. \tag{6.22}$$

We note that $M_2(k^2) > 0$ for all k, hence the homogeneous steady state is linearly stable.

Lemma 6.1 *Assume $f(v) = 1 - v$, $h(v) = v$, and $\delta(n) = \delta$, then no pattern formation occurs about the coexistence steady state, $(v_s, n_s) = (\delta, 1 - \delta)$ for the system (6.1)–(6.2).*

In Figure 6.1 we use $\chi = 6.5$ and random initial conditions. The solution approximates the coexistence equilibrium $(v_s, n_s) = (0.75, 0.25)$ for $t \to \infty$. Thus Figure 6.1 confirms Lemma 6.1.

Although not treated analytically, we tested a nonconstant prey–sensitivity $\chi(v) = \frac{b}{v}$. Also here initial perturbations are damped and (v_s, n_s) is stable (see Figure 6.2)

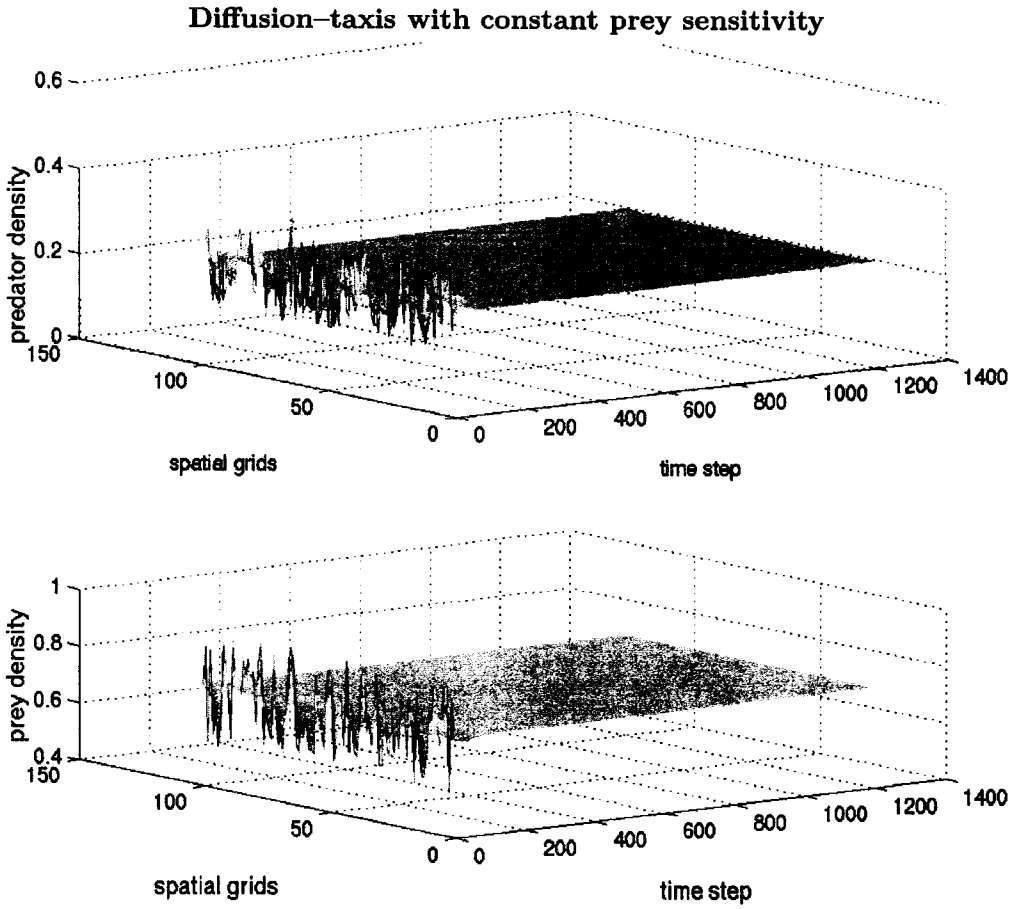

Figure 6.1: Coexistence steady state is shown to be asymptotically stable for the system (6.1–6.2) with $\chi = 6.5$, $f(v) = 1 - v$, $h(v) = v$, and $\delta = 0.75$. Spatial grid size is $dx = 0.25$, and time step $dt = 0.05$ with 60 time units. Here the coexistence steady state is $(v_s, n_s) = (0.75, 0.25)$.

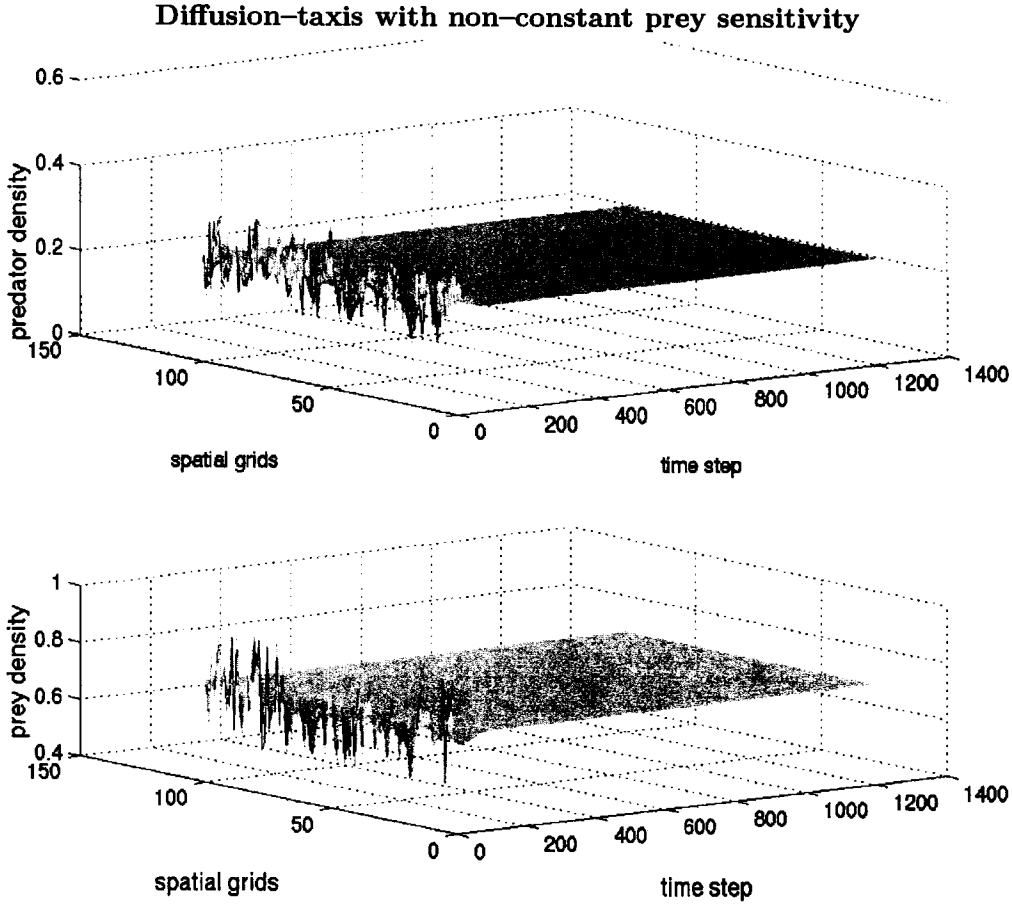

Figure 6.2: Coexistence steady state is shown to be asymptotically stable for the system (6.1)–(6.2) with $\chi(v) = \frac{6.5}{v}$, $f(v) = 1 - v$, $h(v) = v$, and $\delta = 0.75$. Spatial grid size is $dx = 0.25$, and time step $dt = 0.05$ with 60 time units. Here the coexistence steady state is $(v_s, n_s) = (0.75, 0.25)$.

6.1.2 Type II Functional Response, Constant Predator Death Rate and Logistic Growth

We now consider type II functional response, $h(v) = \frac{(\alpha+1)}{\alpha+v}v$ as in Lewis and Owen [72], $\delta(n) = \delta$, and $f(v) = 1 - v$. Thus the coexistence steady state is $(v_s, n_s) = (\frac{\delta\alpha}{(1+\alpha-\delta)}, \frac{(1+\alpha)\alpha(1-\delta)}{(1+\alpha-\delta)^2})$, which is biologically relevant for $0 \leq \delta < 1$. In this case

$$A = -\frac{\delta(\alpha - 1 + \delta)}{(1 + \alpha - \delta)}, \quad B = -\delta, \quad C = \gamma(1 - \delta), \quad D = 0, \tag{6.23}$$

and $M_1(k^2)$ and $M_2(k^2)$ are now

$$M_1(k^2) = -\frac{\delta(\alpha - 1 + \delta)}{(1 + \alpha - \delta)} - (1 + \epsilon)k^2 \tag{6.24}$$

$$M_2(k^2) = \delta\gamma(1 - \delta) + \epsilon k^4 + (\delta + \delta\chi n_s)k^2. \tag{6.25}$$

We note that $M_2(k^2) > 0$ for all k, hence the homogeneous steady state is linearly stable.

Lemma 6.2 *Assume $f(v) = 1-v$, $h(v) = \frac{(\alpha+1)}{\alpha+v}v$, and $\delta(n) = \delta$, then no pattern formation occurs about the coexistence steady state, $(v_s, n_s) = (\frac{\delta\alpha}{(1+\alpha-\delta)}, \frac{(1+\alpha)\alpha(1-\delta)}{(1+\alpha-\delta)^2})$ for the system (6.1)-(6.2).*

It is noted that type II functional response does not play any role for pattern formation versus type I. Figure 6.3 shows a numerical solution with $\chi = 6.5$ and randomly chosen initial distribution. We observe that the coexistence equilibrium $(v_s, n_s) = (0.6, 0.2667)$ is stable.

6.1.3 Type I Functional Response, Density Dependent Predator Death Rate and Logistic Growth

We now include competition in the predator death rate, so the predator death rate is $\delta(n) = \delta+\nu n$. In addition, we consider type I functional response, $h(v) = v$ and $f(v) = 1-v$. Thus the coexistence steady state is $(v_s, n_s) = (\frac{\delta+\nu}{1+\nu}, \frac{1-\delta}{1+\nu})$, which is biologically relevant for $0 \leq \delta < 1$. In this case

$$A = -\frac{\delta + \nu}{1 + \nu}, \quad B = -\frac{\delta + \nu}{1 + \nu}, \quad C = \gamma\frac{1 - \delta}{1 + \nu}, \quad D = -\nu\gamma\frac{1 - \delta}{1 + \nu}, \tag{6.26}$$

and $M_1(k^2)$ and $M_2(k^2)$ are now

$$M_1(k^2) = A + D - (1 + \epsilon)k^2 \tag{6.27}$$

$$M_2(k^2) = AD - BC + \epsilon k^4 - (A + \epsilon D + B\chi n_s)k^2. \tag{6.28}$$

We find $A < 0$ and $D < 0$ for biologically relevant δ, which result in $A + D < 0$. Moreover, $B < 0$ and $C > 0$ give rise to $AD - BC > 0$. In addition, $A < 0$,$D < 0$, $B < 0$, and $AD - BC > 0$ give $M_2(k^2) = AD - BC + \epsilon k^4 - (A + \epsilon D + B\chi n_s)k^2 > 0$ for all k. Hence we note that $M_2(k^2) > 0$ for all k, hence the homogeneous steady state is linearly stable.

Lemma 6.3 *Assume $f(v) = 1-v$, $h(v) = v$, and $\delta(n) = \delta+\nu n$, then no pattern formation occurs about the coexistence steady state, $(v_s, n_s) = (\frac{\delta+\nu}{1+\nu}, \frac{1-\delta}{1+\nu})$ for the system (6.1)-(6.2).*

Figure 6.4 shows a numerical solution with $\chi = 6.5$ and randomly chosen initial distribution. We observe that the coexistence equilibrium $(v_s, n_s) = (0.792, 0.208)$ is stable.

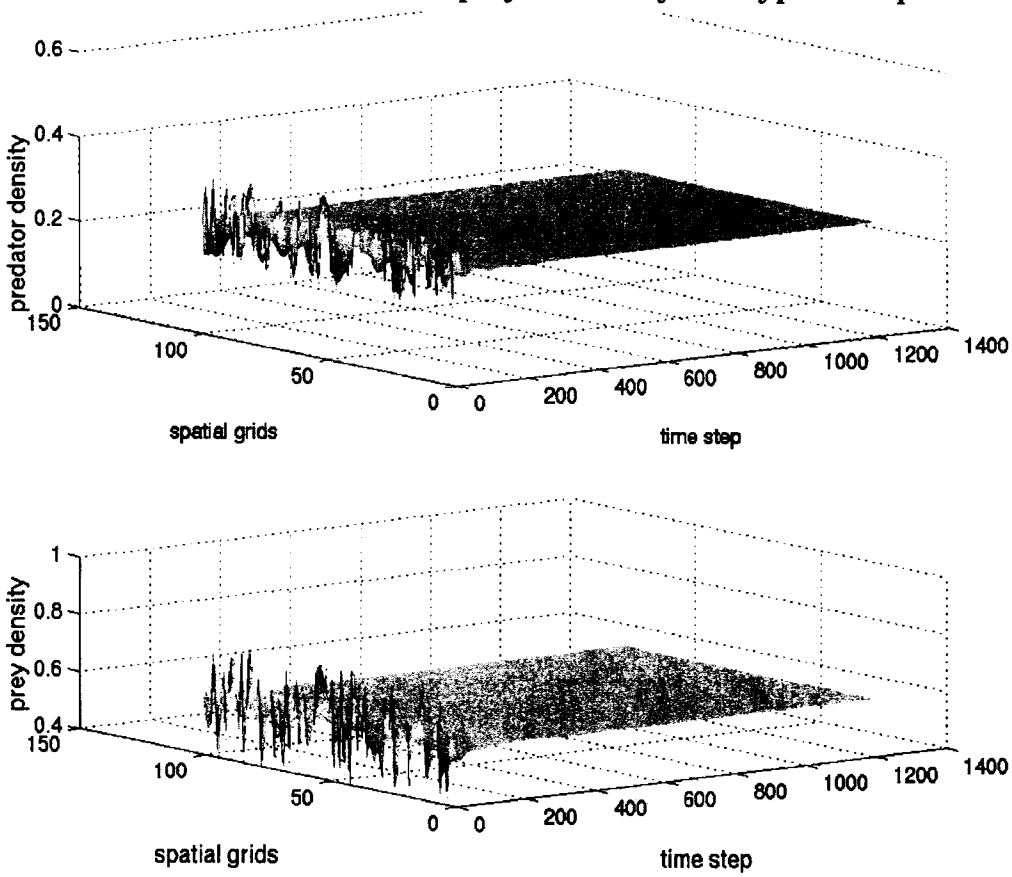

Figure 6.3: Coexistence steady state is shown to be asymptotically stable for the system (6.1)–(6.2) with $f(v) = 1 - v$, $\chi = 6.5$, $h(v) = v\frac{\alpha+1}{\alpha+v}$, and $\delta = 0.9$. Spatial grid size is $dx = 0.25$, time step $dt = 0.05$, and $\alpha = 0.2$ with 60 time units. Here the coexistence steady state is $(v_s, n_s) = (0.6, 0.2667)$.

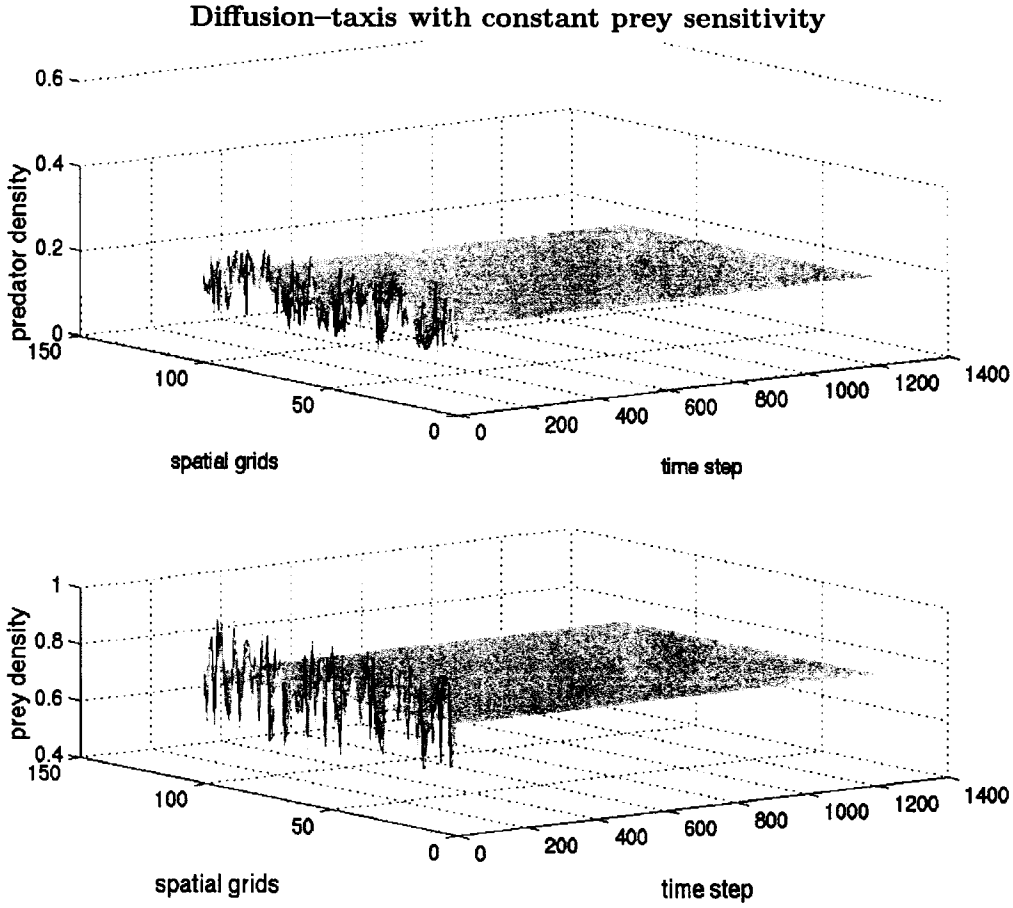

Figure 6.4: Coexistence steady state is shown to be asymptotically stable for the system (6.1)–(6.2) with $\chi = 6.5$, $f(v) = 1 - v$, $h(v) = v$, and $\delta(n) = 0.75 + 0.2n$. Spatial grid size is $dx = 0.25$, time step $dt = 0.2$, and $\gamma = 1$ with 60 time units. Here the coexistence steady state is $(v_s, n_s) = (0.792, 0.208)$.

6.1.4 Type I Functional Response, Density Dependent Predator Death Rate and Allee Effect with Diffusion Only

In this subsection we consider an Allee effect on the prey population dynamics $f(v) = K(1-v)(v-a)$ with $0 < a < 1$ and $K = \frac{4}{(1-a)^2}$, $h(v) = v$, $\delta(n) = \delta + \nu n$, and without taxis, i.e. $\chi = 0$ and $\nu \geq 0$ is a constant parameter. Here the parameter a is a threshold, below which the prey population declines Okubo et al. [70] argued that a predator–prey model with dispersal may generate diffusion driven instability if the mortality of the predator depends on the population density and the per–capita growth rate of the prey is determined by an Allee effect. Note that the trivial steady state $(v,n) = (0,0)$ is locally stable because for $(v,n) = (0,0)$ the characteristic polynomial (6.8) has two negative eigenvalues, $\lambda = -\gamma\delta$ and $\lambda = -Ka$. We assume biologically relevant parameters region $0 < \delta < 1$ and $a < 1$. For the prey–only steady state $(v,n) = (1,0)$ the characteristic polynomial (6.8) has one positive eigenvalue $\lambda = \gamma(1-\delta)$ and one negative eigenvalue $\lambda = -K(1-a)$.

For the homogeneous coexistence steady state (v_s, n_s), we find

$$A = Kv_s(1+a-2v_s), \quad B = -v_s, \quad C = \gamma n_s, \quad D = -\gamma n_s \nu, \tag{6.29}$$

and $M_1(k^2)$ and $M_2(k^2)$ are given by

$$M_1(k^2) = A + D - (1+\epsilon)k^2 \tag{6.30}$$

$$M_2(k^2) = AD - BC + \epsilon k^4 - (A + \epsilon D + B\chi n_s)k^2. \tag{6.31}$$

It is noted that the sign of A depends on the sign of $1+a-2v_s$. We here set $\bar{v} = \frac{1+a}{2}$. Hence, when $v_s > \bar{v}$, A is negative and when $v_s < \bar{v}$, A is positive. Recall that the coexistence steady state (v_s, n_s) comes from the intersection of the two nullclines: $v - \delta - \nu n = 0$ and $K(1-v)(v-a) - n = 0$ (see Figure 6.5).

First, we consider $v_s > \frac{1+a}{2}$. Since $v_s > \bar{v}$ we find that at $v = \bar{v}$ the v–nullcline is above the n–nullcline. This means that $K(1-\bar{v})(\bar{v}-a) > \frac{\bar{v}-\delta}{\nu}$, which translates into the condition

$$a + 1 < 2(\delta + \nu). \tag{6.32}$$

For this case we prove stability.

Lemma 6.4 *Assume that $h(v) = v$, $\delta(n) = \delta + \nu n$, $f(v) = K(1-v)(v-a)$, and $\chi = 0$. If $a + 1 < 2(\delta + \nu)$, then no pattern formation occurs about the coexistence steady state, (v_s, n_s) for the system (6.1)–(6.2).*

Proof. The condition $a + 1 < 2(\delta + \nu)$ implies that $v_s > \frac{1+a}{2}$. Hence $A < 0$. In addition, we find $B < 0$, $C > 0$, and $D < 0$ and $A < 0$, $B < 0$, and $D < 0$ imply $M_2(k^2) = AD - BC + \epsilon k^4 - (A\epsilon + D + B\chi n_s)k^2 > 0$ for all real k. Hence, we cannot expect diffusion–taxis driven instability about the coexistence steady state.□

In Figure 6.5 it is noted that v_s should be between a and 1, i.e. $a < v_s < 1$, otherwise n_s is negative. In Lemma 6.4, we considered that $v_s > \frac{1+a}{2}$ and found no pattern. Thus we now consider $a < v_s < \bar{v} = \frac{1+a}{2}$. First we investigate how many v_s may exist between a and $\bar{v}$, and then we find conditions for the existence of v_s between a and $\bar{v}$.

The v vaules for the coexistence steady state are obtained from

$$K(1-v)(v-a) = \frac{v-\delta}{\nu}, \tag{6.33}$$

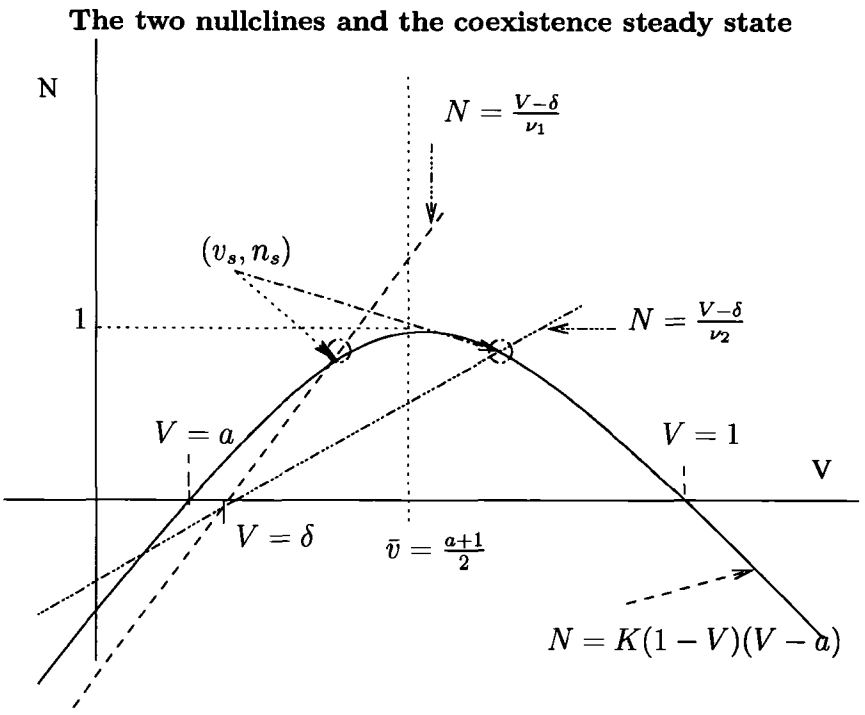

Figure 6.5: The v–nullcline $N = K(1-V)(V-a)$ is shown as a solid curve. For two values of ν we show the corresponding n–nullcline, $N = \frac{V-\delta}{\nu}$ as a dashed line and a dash–dotted line. The equilbrium (v_s, n_s) is the intersection of the nullclines. We have chosen two values of ν so that $v_s < \bar{v}$ for ν_1 and $v_s > \bar{v}$ for ν_2 with $\nu_1 < \nu_2$.

which is a quadratic equation, so there are up to two real roots v depending on the parameters a, ν, and δ. Equation (6.33) is rearranged as follows

$$K\nu v^2 - (K\nu(1+a) - 1)v + K\nu a - \delta = 0. \tag{6.34}$$

When $a < \delta$, Figure 6.5 shows that equation (6.34) has two real roots. Here $V = \delta$ is a x–intersection of the n–nullcline and $V = a$ is a x–intersection of the v–nullcline. One root is bigger than a and the other is less than a. Thus, for the root less than a, n_s would be negative, which is not biologically relevant. Hence, when $a < \delta$ equation (6.34) has one biologically relevant root. In addition, $v_s < \bar{v}$ leads to

$$a > 2(\delta + \nu) - 1. \tag{6.35}$$

Therefore, for

$$2(\delta + \nu) - 1 < a < \delta, \tag{6.36}$$

the biologically relevant coexistence state exists and its v value is located between $\delta < v_s < \bar{v}$.

When $a > \delta$, we may expect two positive roots from equation (6.34). For that, $K\nu a > \delta$ and $K\nu(1+a) > 1$ are required, in addition to the positive discriminant $(K\nu(1+a)-1)^2 - 4K\nu(K\nu a - \delta)$. The discriminant implies $a < 4\nu + 1 - 4\sqrt{\nu - \nu\delta}$. However, the assumption $K\nu a > \delta$ implies $a > \frac{2\nu+\delta-2\sqrt{\nu^2+\delta\nu}}{\delta}$, which contradicts $a < 4\nu + 1 - 4\sqrt{\nu - \nu\delta}$, because $\frac{2\nu+\delta-2\sqrt{\nu^2+\delta\nu}}{\delta} \geq 4\nu + 1 - 4\sqrt{\nu - \nu\delta}$. Thus we cannot have two positive roots. In sum, in order to have a biologically relevant coexistence steady state we found conditions (6.36). Under assumption (6.36) the biologically relevant solution of (6.34) is given by

$$v_s = \frac{K\nu + K\nu a - 1 + \sqrt{K^2\nu^2a^2 + (-2K\nu - 2K^2\nu^2)a + K^2\nu^2 + 1 - 2K\nu + 4K\nu\delta}}{2K\nu}. \tag{6.37}$$

The discriminant in (6.37) is zero for

$$\underline{v} = \frac{K\nu + K\nu a - 1}{2K\nu} = \frac{1+a}{2} - \frac{1}{2K\nu}. \tag{6.38}$$

(6.37) and (6.38) give a condition for the existence of the coexistence steady state,

$$v_s \geq \underline{v} = \frac{1+a}{2} - \frac{(1-a)^2}{8\nu}, \tag{6.39}$$

which will be used to show that $AD - BC > 0$, whenever v_s exists.

We find $A > 0$ from the condition $v_s < \frac{1+a}{2}$ (6.36). Additionally. from (6.29) we find $B < 0$, $C > 0$, and $D < 0$. The stability conditions require that $A + D < 0$ and $AD - BC > 0$. The condition $A + D < 0$ leads to a condition

$$A + D = Kv_s(1 + a - 2v_s) - \gamma n_s\nu \tag{6.40}$$

$$= Kv_s(1 + a - 2v_s) - \gamma(v_s - \delta) < 0, \tag{6.41}$$

which with $n_s\nu = v_s - \delta$ is rearranged as

$$Kv_s(1 + a - 2v_s) < \gamma(v_s - \delta). \tag{6.42}$$

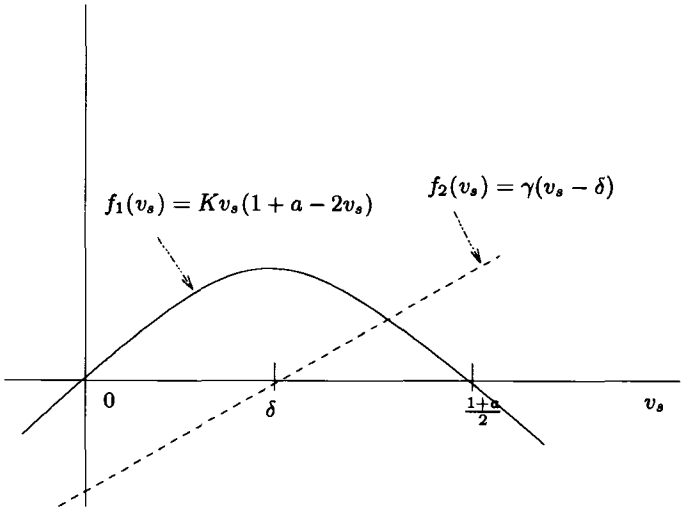

The existence of positive v_s

Figure 6.6: Plot of the left and right hand sides of (6.42) as function of v_s. The region of $A + D < 0$ is where the dashed line lies above the curve.

In Figure 6.6 we plot the left and right hand sides of (6.42). As γ varies from zero to infinity, the intersection of $Kv_s(1 + a - 2v_s)$ and $\gamma(v_s - \delta)$ changes from $v_s = \frac{1+a}{2}$ to $v_s = \delta$. Given a value for v_s we can always choose γ small enough such that condition (6.42) is not true. Thus γ should be greater than a minimum value, γ_0. Here $\gamma_0 = \frac{Kv_s(1+a-2v_s)}{v_s - \delta}$ where v_s is computed in (6.37). Therefore for $\gamma > \gamma_0$, we have $A + D < 0$.

Thus a biologically relevant v_s is in the interval

$$\max\left(\delta, \frac{1+a}{2} - \frac{(1-a)^2}{8\nu}\right) \leq v_s < \frac{a+1}{2}. \tag{6.43}$$

We found that (6.43) holds under assumption (6.36).

Theorem 6.1 *Assume that $h(v) = v$, $\delta(n) = \delta + \nu n$, $f(v) = K(1-v)(v-a)$, and $\chi = 0$. If a satisfies condition (6.36), then (i) the coexistence steady state (v_s, n_s) exists, (ii) $AD - BC > 0$, (iii) if in addition, there exists $\epsilon_1 > 0$ such that for each $\epsilon < \epsilon_1$ there exists an nonempty interval $[k_1, k_2]$ of unstable modes, so we may expect diffusion driven instability about the coexistence steady state, (iv) if $\epsilon > \epsilon_1$, then (v_s, n_s) is linearly stable.*

Proof. (i) It was shown that condition (6.36) implies the existence of a unique positive root v_s. (ii) When a positive v_s exists, v_s satisfies condition (6.43). Now we consider the condition for $AD - BC > 0$.

$$AD - BC \tag{6.44}$$
$$= -Kv_s(1 + a - 2v_s)\gamma n_s \nu + \gamma n_s v_s \tag{6.45}$$
$$= \gamma n_s v_s (1 - K\nu(1 + a - 2v_s)) > 0, \tag{6.46}$$

which holds if $v_s > \frac{1+a}{2} + \frac{1}{2K\nu}$. Indeed, this is true by condition (6.43). Therefore $AD - BC$ is always positive under the assumption of the existence of a coexistence steady state. (iii) $M_1(k^2)$ and $M_2(k^2)$ are now

$$M_1(k^2) = A + D - (1 + \epsilon)k^2, \tag{6.47}$$

and

$$M_2(k^2) = (-\epsilon k^2 + A)(-k^2 + D) - BC, \tag{6.48}$$

with $A = Kv_s(1 + a - 2v_s)$, $B = -v_s < 0$, $C = \gamma n_s > 0$ and $D = -\gamma n_s \nu < 0$.

$A + D < 0$ guarantees $M_1(k^2) = A + D - (1 + \epsilon)k^2 < 0$. Hence instability can only occur if $M_2(k^2)$ is negative for some real k. $M_2(k^2)$ is rearranged as $AD - BC + \epsilon k^4 - (A + D\epsilon)k^2$. If $\epsilon \geq 1$, then $D < 0$ gives $A + D\epsilon \leq A + D < 0$, hence $M_2(k^2)$ is always positive, which results in no diffusion–driven instability for $\epsilon \geq 1$. Therefore ϵ should be strictly less than 1. Indeed, setting $\epsilon_0 = \frac{Kv_s(1+a-2v_s)}{\gamma(v_s-\delta)}$, for $\epsilon < \epsilon_0$, we have $A + D\epsilon > 0$ and $M_2(k^2)$ can be negative for some k.

Setting $T = k^2$, $M_2(T) = 0$ may have two roots (see Figure 6.7)

$$T_{1,2} = \frac{Kv_s(1 + a - 2v_s) - \epsilon\gamma n_s v_s \mp \sqrt{P}}{2\epsilon}, \tag{6.49}$$

with $P = K^2v_s^2 + 2K^2v_s^2a + 2Kv_s\epsilon\gamma n_s\nu - 4K^2v_s^3 + K^2v_s^2a^2 + 2Kv_sa\epsilon\gamma n_s\nu - 4K^2v_s^3a + \epsilon^2\gamma^2n_s^2\nu^2 - 4\epsilon\gamma n_s\nu Kv_s^2 + 4K^2v_s^4 - 4\epsilon v_s\gamma n_s$. Then critical T_c is

$$T_c = \frac{Kv_s(1 + a - 2v_s) - \epsilon\gamma n_s v_s}{2\epsilon}, \tag{6.50}$$

for $P = 0$. For $P \geq 0$, $k_{1,2}$ are real numbers. $P = 0$ is a quadratic equation with respect to ϵ. Hence $P = 0$ has two roots ϵ_1 and ϵ_2 with $\epsilon_1 < \epsilon_2$ such that for $\epsilon < \epsilon_1$ or $\epsilon > \epsilon_2$ there exist real k_1 and k_2 with $k_1 < k_2$. These ϵ_1 and ϵ_2 are found by the quadratic formula. Moreover, it is seen that $\epsilon_2 > \epsilon_0 > \epsilon_1$. Thus for $\epsilon < \epsilon_1$ there exist real k_1 and k_2. For unstable modes $k \in [k_1, k_2]$ with $k_1 = \sqrt{T_1}$ and $k_2 = \sqrt{T_2}$, eigenvalues λ are given by $\lambda = \frac{M_1(k^2) \pm \sqrt{M_1(k^2)^2 - 4M_2(k^2)}}{2}$. Hence, for $k_1 < k < k_2$, we have $\mathrm{Re}(\lambda) > 0$ and we may expect diffusion driven instability about the coexistence steady state (see also [81]).

(iv) if $\epsilon > \epsilon_1$, then $M_2(k^2)$ is always positive for all k. Hence we cannot expect diffusion driven instability about the coexistence steady state.□

Segel and Jackson ([81]) also considered diffusion driven instability in a predator–prey interaction . They used $\delta(n) = \nu n$ and $f(v) = 1 + Kv$, and found the wavelength of the instability (see also [70] for general discussion on diffusion driven instability in a predator–prey interaction).

In particular, for $\epsilon \ll 1$, we can approximate two values of k^2, say k_1^2 and k_2^2, so that for $k_1 < k < k_2$, $M_2(k^2)$ is negative. To find k_1 and k_2 we set $T = k^2$ and $M_2(T) = 0$,

$$\epsilon T^2 - (A + \epsilon D)T + AD - BC = 0. \tag{6.51}$$

Letting $\epsilon = 0$, equation (6.51) has a unique solution, $T = \frac{AD-BC}{A}$, which is positive due to $A > 0$ and $AD - BC > 0$. To find a second root for $\epsilon \ll 1$ we use a rescaling, $T = \frac{T_0}{\epsilon} + T_1 + \cdots$. Plugging this rescaling into the equation (6.51), we have the leading term as follows

$$T_0^2 - AT_0 = 0. \tag{6.52}$$

Thus nonzero $T_0 = A$ leads to $T \approx \frac{A}{\epsilon}$. With small ϵ, it is seen that $\frac{A}{\epsilon} > \frac{AD-BC}{A}$. The equation (6.51) is quadratic with positive leading coefficient and two positive roots. Therefore for $\frac{AD-BC}{A} < T < \frac{A}{\epsilon}$, $M_2(T)$ is negative.

For example, we consider an interval $[0, L]$ with homogeneous Neumann boundary condition given by (6.3). If $k^n = \frac{n\pi}{L}$ in $[k_1, k_2]$ of (6.49) with positive integer n, then pattern

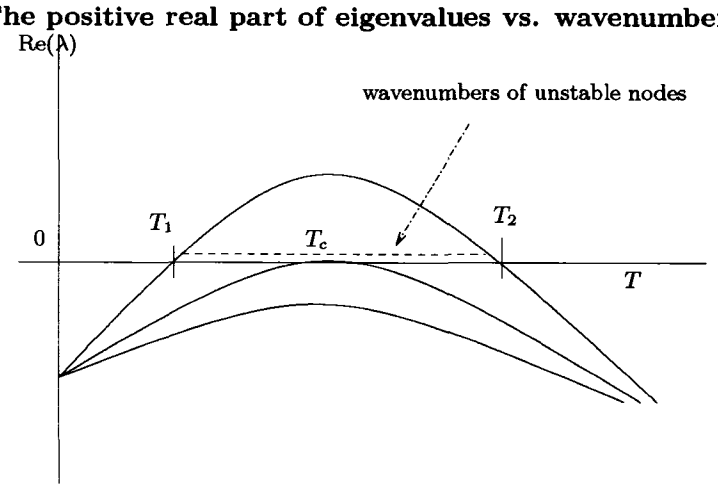

Figure 6.7: Plot of the eigenvalue $\lambda(k^2)$ as a function of T with $T = k^2$.

formation occurs. Thus we can calculate a minimum domain size for pattern formation. Since $k_1 < k_n < k_2$, we substitute $k_n = \frac{n\pi}{L}$ and rearrange the inequality with respect to L. Then we have

$$\frac{n\pi}{k_2} < L < \frac{n\pi}{k_1}, \tag{6.53}$$

which should hold for some n. Therefore, the minimum length for possible instabilities is $L^* = \frac{\pi}{k_2}$, and for $L < \frac{\pi}{k_2}$, we cannot expect pattern formation.

In Figure 6.8 we show phase portraits of the predator–prey system (6.1)–(6.2) without dispersal terms. As γ increases, the coexistence steady state bifurcates from an unstable spiral to a stable spiral. From simulations with various γ, it is noted that an unstable limit cycle occurs for a certain range of γ. When γ is smaller than the lower bound of this range, the coexistence steady state is an unstable spiral. When γ is bigger than the upper bound of the range, the coexistence steady state is a stable spiral with nonempty basin of attraction. Figure 6.9 shows that the stable coexistence steady state without dispersal terms becomes unstable if diffusion terms are introduced. As a result patterns are generated.

6.1.5 Type I Functional Response, Density Dependent Predator Death Rate and Allee Effect with Diffusion and Prey Taxis

Now we consider the reaction–diffusion–taxis system (6.1)–(6.2) for $\chi \neq 0$. $f(v) = K(1-v)(v-a)$ with $0 < a < 1$ and $K = \frac{4}{(1-a)^2}$, $h(v) = v$, and $\delta(n) = \delta + \nu n$. We have shown in the previous subsection that for $\chi = 0$ pattern formation may occur. In this subsection we consider how the conditions of pattern formation change if χ is introduced.

Lemma 6.5 *Assume a, δ, and ϵ satisfy instability conditions of Theorem 6.1 Then there exists a $\chi^* = \frac{Kv_s(1+a-2v_s)+\epsilon\gamma(v_s-\delta)}{v_s n_s}$ such that the coexistence steady state (v_s, n_s) for system (6.1)–(6.2) is linearly stable for each $\chi > \chi^*$. For $\chi < \chi^*$ there exists an interval $[k_1, k_2]$ of unstable modes.*

Proof. $M_1(k^2)$ and $M_2(k^2)$ are now

$$M_1(k^2) = A + D - (1+\epsilon)k^2, \tag{6.54}$$

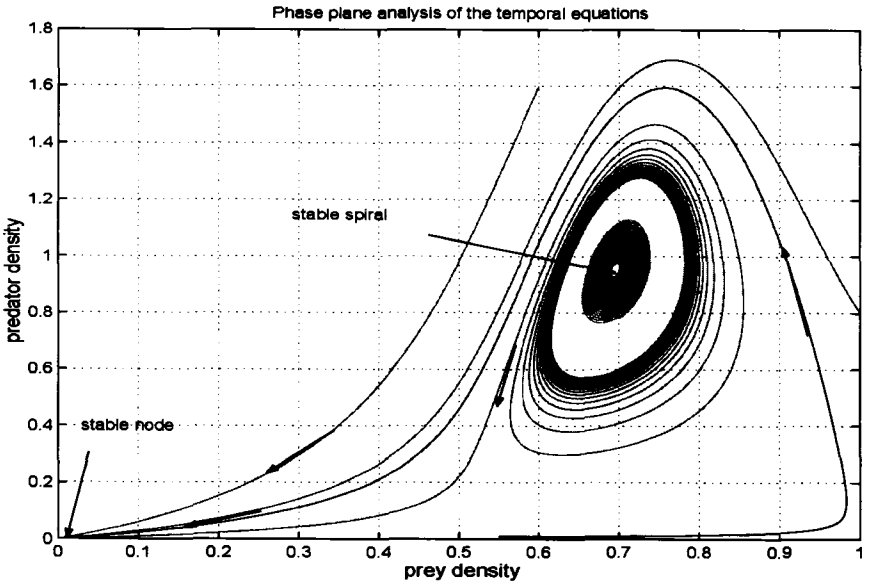

No dispersal

Figure 6.8: Coexistence steady state is shown to be locally asymptotically stable for system (6.1)–(6.2) without dispersal terms and with $f(v) = 16(1-v)(v-0.5)$, $h(v) = v$, and $\delta(n) = 0.6 + 0.1n$. Time step is $dt = 0.01$ and $\gamma = 13$. Here the coexistence steady state is $(v_s, n_s) = (0.695, 0.952)$.

and

$$M_2(k^2) = AD - BC + \epsilon k^4 - (A + \epsilon D + B\chi n_s)k^2, \tag{6.55}$$

where A, B, C, and D are defined in (6.48). Here $M_1(k^2)$ is the same as in the case of diffusion–only (6.47) so that it is negative for all k. But $M_2(k^2)$ is different by the term $B\chi n_s$. Setting $M_2(k^2) = 0$ and $T = k^2$, we obtain after rearrangements

$$\epsilon T^2 - (A + \epsilon D)T + AD - BC = B\chi n_s T. \tag{6.56}$$

Figure 6.10 shows three typical situations of intersections of the left hand and the right hand sides of equation (6.56). In the diffusion–only case, we saw that there may be two roots, T_1 and T_2, of $\epsilon T^2 - (A+\epsilon D)T + AD - BC = 0$ under the conditions that $A + \epsilon D > 0$. Between $T_1 < T < T_2$, $\epsilon T^2 - (A + \epsilon D)T + AD - BC$ is negative. $T_1 = k_1^2$ and $T_2 = k_2^2$. In order for $M_2(T)$ to be negative, the left hand side of equation (6.56) should be less than the right hand of the equation (6.56). In Figure 6.10, the region $T_3 < T < T_4$ where the solid curve is below the dashed line makes $M_2(T)$ negative. As we can see in Figure 6.10, T_3 is always greater than T_1 and T_4 smaller than T_2 for positive χ. As χ gets bigger, the slope of the line of the right hand side of equation (6.56) is steeper so that for $\chi > \chi^*$ there will be no intersection of the curve and the line (see Figure 6.10). In that case, $M_2(k^2)$ is always non negative, which leads to negative eigenvalues and to stability. In Theorem 6.1, for $\chi = 0$ we found a threshold of $\epsilon_0 = \frac{Kv_s(1+a-2v_s)}{\gamma(v_s-\delta)}$. For $\chi \neq 0$, the threshold for pattern formation is $\epsilon_1 = \frac{Kv_s(1+a-2v_s)-v_s\chi n_s}{\gamma(v_s-\delta)} \leq \epsilon_0$. Thus as χ gets bigger, ϵ_1 requires smaller value ϵ for pattern formation.□

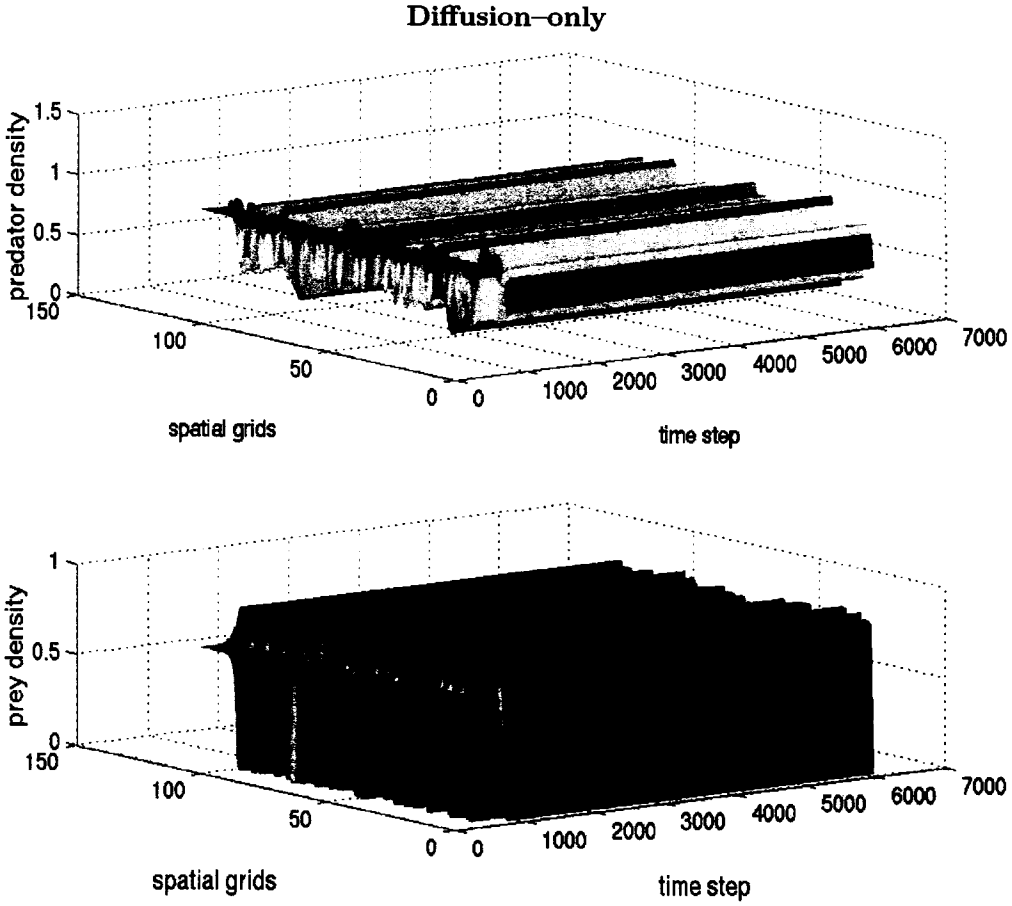

Figure 6.9: Coexistence steady state is shown to be locally unstable for system (6.1)–(6.2) with $\chi(v) = 0.0$, $f(v) = 16(v - 0.5)(v - 1)$, $h(v) = v$, and $\delta(n) = 0.6 + 0.1n$. Spatial grid size is $dx = 0.25$, time step $dt = 0.01$, and $\gamma = 14$ with 60 time units. Here the coexistence steady state is $(v_s, n_s) = (0.695, 0.952)$.

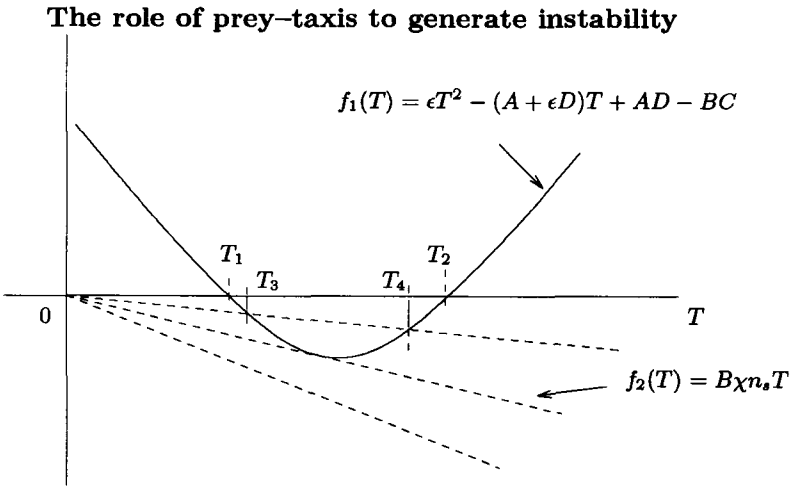

Figure 6.10: Plot of the left and right hand sides of equation (6.56) as a function of T with $T = k^2$. The solid curve is from the left hand side of equation (6.56) and the dashed lines are from the right hand side of equation (6.56). As χ varies, the number of intersection changes from zero to two. Note that B is negative.

Therefore prey–taxis tends to reduce the occurrence of dispersal–induced instability. Furthermore, it is noticed that predator diffusion is crucial to dispersal–induced instability. Prey–taxis pushes predators into high prey density area, otherwise predators move opposite direction. Thus, prey–taxis seems to reduce predator diffusion. In prey only situation, prey diffusion is considered as a rate of making heterogeneous prey distribution homogeneous. Prey–taxis seems to make this process faster. Thus,prey diffusion seemingly increases due to prey–taxis. When prey diffusion is large enough, we may not expect pattern formation from Theorem 6.1.

Figure 6.8 shows that the coexistence steady state for the spatially homogeneous predator–prey system (6.1)–(6.2) without dispersal terms is stable. In Figure 6.9, introducing the diffusion term generates patterns. Figure 6.11 shows that when we introduce a large prey–taxis term patterns disappear.

6.1.6 Linear Ratio Dependent Functional Response, Constant Predator Death Rate and Logistic Growth

We now consider the linear ratio dependent functional response, $h(v,n) = \nu_0 \frac{v}{n}$ with $f(v) = 1 - v$ and $\delta(n) = \delta$ and ν_0 is a constant parameter. Thus the coexistence steady state is now $(v_s, n_s) = (1 - \nu_0, \frac{\nu_0}{\delta}(1 - \nu_0))$, which is biologically relevant for $0 \leq \nu_0 < 1$. In this case

$$A = -(1 - \nu_0), \quad B = 0, \quad C = \gamma\nu_0, \quad D = -\delta, \tag{6.57}$$

and $M_1(k^2)$ and $M_2(k^2)$ are now

$$M_1(k^2) = A + D - (1 + \epsilon)k^2, \tag{6.58}$$

$$M_2(k^2) = AD - BC + \epsilon k^4 - (A + \epsilon D + B\chi n_s)k^2. \tag{6.59}$$

We observe that $A < 0$,$D < 0$, $B = 0$, $AD - BC > 0$, and $M_2(k^2) = AD - BC + \epsilon k^4 - (A + \epsilon D + B\chi n_s)k^2 > 0$ for all k. Hence the homogeneous steady state is linearly stable.

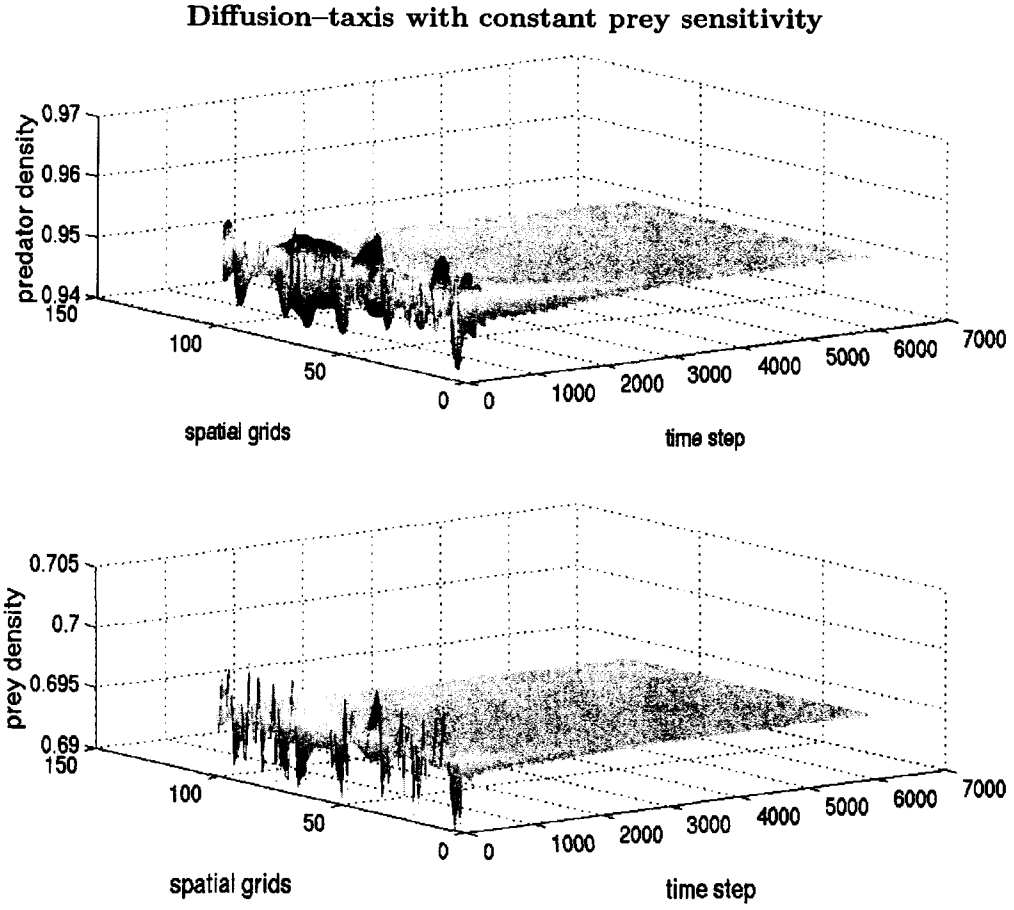

Figure 6.11: Coexistence steady state is shown to be locally asymptotically stable for system (6.1)–(6.2) with $\chi(v) = 6.5$, $f(v) = 16(v - 0.5)(v - 1)$, $h(v) = v$, and $\delta(n) = 0.6 + 0.1n$. Spatial grid size is $dx = 0.25$, time step $dt = 0.01$, and $\gamma = 14$ with 60 time units. Here the coexistence steady state is $(v_s, n_s) = (0.695, 0.952)$.

Lemma 6.6 *Assume* $f(v) = 1 - v$, $h(v) = \nu_0 \frac{v}{n}$, *and* $\delta(n) = \delta + \nu n$, *then no pattern formation occurs about the coexistence steady state,* $(v_s, n_s) = (1-\nu_0, \frac{\nu_0}{\delta}(1-\nu_0))$ *for system (6.1)-(6.2).*

6.1.7 Hyperbolic Ratio Dependent Functional Response, Constant Predator Death Rate and Logistic Growth

We now consider hyperbolic ratio dependent functional response, $h(v,n) = \frac{\mu v}{dn+v}$ with $f(v) = 1 - v$ and $\delta(n) = \delta$, and $\mu \geq 0$ and $d \geq 0$ are constants. Thus the coexistence steady state in this case is $(v_s, n_s) = (\frac{(d-\mu+\delta)}{d}, \frac{(d-\mu+\delta)(\mu-\delta)}{d^2\delta})$, which is biologically relevant for $\delta < \mu < d + \delta$. In this case, we have

$$A = -\frac{(d\mu - \mu^2 + \delta^2)}{d\mu}, \quad B = -\frac{\delta^2}{\mu}, \quad C = \frac{(\mu-\delta)^2}{d\mu}\gamma, \quad D = -\frac{\delta(\mu-\delta)}{\mu}\gamma, \tag{6.60}$$

and $M_1(k^2)$ and $M_2(k^2)$ are now

$$M_1(k^2) = A + D - (1+\epsilon)k^2, \tag{6.61}$$

$$M_2(k^2) = AD - BC + \epsilon k^4 - (A + \epsilon D + B\chi n_s)k^2. \tag{6.62}$$

In this case pattern formation is possible.

We now consider conditions that $A + D < 0$ and $AD - BC > 0$. For $A < 0$, it is seen that $A + D < 0$ and $AD - BC > 0$. For $A > 0$, $AD - BC = \frac{(\mu-\delta)(d-\mu+\delta)\delta}{\mu d}\gamma$ is positive due to the fact of $\delta < \mu < d + \delta$. However, $A + D < 0$ is not always true. Since A is independent of γ for the fixed parameters μ, d, and δ and the magnitude of D is linearly increasing as γ gets bigger, $A + D$ changes its sign over γ from positive to negative. That is, for $\gamma > -\frac{(d\mu-\mu^2+\delta^2)}{d(\mu-\delta)\delta}$, $A + D$ becomes negative. Thus $\gamma > \gamma_0$, with $\gamma_0 = -\frac{(d\mu-\mu^2+\delta^2)}{d(\mu-\delta)\delta} > 0$, implies that $A + D < 0$.

Lemma 6.7 *Assume* $f(v) = 1-v$, $h(v) = \frac{\mu v}{dn+v}$, $\delta(n) = \delta$, *and* $\chi = 0$. *(i) If* $(d\mu-\mu^2+\delta^2) > 0$, *no pattern formation occurs about the coexistence steady state,* (v_s, n_s) *for system (6.1)-(6.2).*
(ii) Assume $(d\mu-\mu^2+\delta^2) < 0$. *If there exists* $\epsilon_1 > 0$ *such that for each* $\epsilon < \epsilon_1$ *there exists an nonempty interval* $[k_1, k_2]$ *of unstable modes, so we may expect diffusion driven instability about the coexistence steady state, (iii) in case (ii) if* $\epsilon > \epsilon_1$, *then* (v_s, n_s) *is linearly stable.*

Proof. (i) First, $(d\mu - \mu^2 + \delta^2) > 0$ implies $A < 0$. In addition, we find $B < 0$, $C > 0$, and $D < 0$. Thus $M_1(k^2) \leq A + D < 0$ for all k, so the only way $\lambda(k^2)$ can be positive is the case that $M_2(k^2) < 0$ for some k^2. Since $B < 0$, $A < 0$, and $D < 0$, we find

$$M_2(k^2) = AD - BC + \epsilon k^4 - (A + \epsilon D)k^2 > 0. \tag{6.63}$$

Hence, we cannot expect diffusion–taxis driven instability about the coexistence steady state.

(ii) Second, we consider $(d\mu - \mu^2 + \delta^2) < 0$, which gives $A > 0$. However, it is seen that $AD - BC > 0$. In addition, for $\gamma > \gamma_0$, it is straightforward to show that $A + D < 0$, which implies that $M_1(k^2) = A + D - (1 + \epsilon)k^2$ is still negative. However, $M_2(k^2) = \epsilon k^4 - (A + \epsilon D)k^2 + AD - BC$ could be negative if $A + \epsilon D$ is positive. Indeed, when ϵ is less than $\epsilon_0 = -\frac{(d\mu-\mu^2+\delta^2)}{d\gamma(\mu-\delta)\delta}$, $A + \epsilon D$ is positive. Thus $M_2(k^2)$ can be negative. With the same

steps in Theorem 6.1, we can find k_1 and k_2 with $k_{1,2}^2 = (\mu^2 - d\mu - \delta^2 - \epsilon d\mu\gamma\delta + \epsilon d\gamma\delta^2 \mp \sqrt{G_0 + G_1\epsilon + G_2\epsilon^2})/(2\epsilon d\mu)$ where

$$G_0 = (-d\mu + \mu^2 - \delta^2)^2 \tag{6.64}$$

$$G_1 = 2d(\mu - \delta)\gamma\delta(\mu^2 - d\mu - 2\mu\delta + \delta^2) \tag{6.65}$$

$$G_2 = \gamma^2\delta^2 d^2(\mu - \delta)^2. \tag{6.66}$$

For $G_0 + G_1\epsilon + G_2\epsilon^2 \geq 0$, $k_{1,2}$ are real numbers. It is seen that $G_0 > 0$ and $G_2 > 0$. However, G_1 is not always positive. The discriminant is now $G_1^2 - 4G_0G_2 = 4d^2\mu\gamma^2\delta^3(\mu - \delta)^3(d - \mu + \delta) > 0$ for the biologically relevant $\delta < \mu < d + \delta$. Hence, there exist ϵ_1 and ϵ_2 with $\epsilon_1 < \epsilon_2$ such that for $\epsilon < \epsilon_1$ or $\epsilon > \epsilon_2$ there exist real k_1 and k_2 with $k_1 < k_2$. $\epsilon_{1,2} = \frac{-G_1 \mp \sqrt{G_1^2 - 4G_0G_2}}{2G_2}$. Moreover, it is seen that $\epsilon_2 > \epsilon_0 > \epsilon_1$. Thus for $\epsilon < \epsilon_1$ there exist real k_1 and k_2. Furthermore, for $k_1 < k < k_2$ we have $\mathrm{Re}(\lambda) > 0$ and we may expect diffusion driven instability about the coexistence steady state.

(iii) If $\epsilon > \epsilon_1$, then $M_2(k^2)$ is positive for all k. Hence we cannot expect diffusion driven instability about the coexistence steady state.□

Alonso et al. [3] also considered a hyperbolic ratio dependent functional response for pattern formation by using numerical exploration of the parameter space.

Now we can follow the argument of the case including an Allee effect. Thus the reaction–diffusion system may show diffusion–driven instability depending on parameters μ, d, δ, γ, and ϵ. Furthermore, prey–taxis term tends to limit the occurrence of dispersal–driven instability (see subsection 6.1.5 for the full argument).

In Figure 6.12 we show phase portraits of the predator–prey system (6.1)–(6.2) with hyperbolic ratio functional response and without dispersal terms. As γ increases, the coexistence steady state bifurcates from an unstable spiral to a stable spiral. Figure 6.13 demonstrates that the stable coexistence steady state without dispersal terms becomes unstable if diffusion terms are introduced. As a result patterns are generated. Figure 6.14 shows that when we introduce a large prey–taxis term patterns eventually disappear.

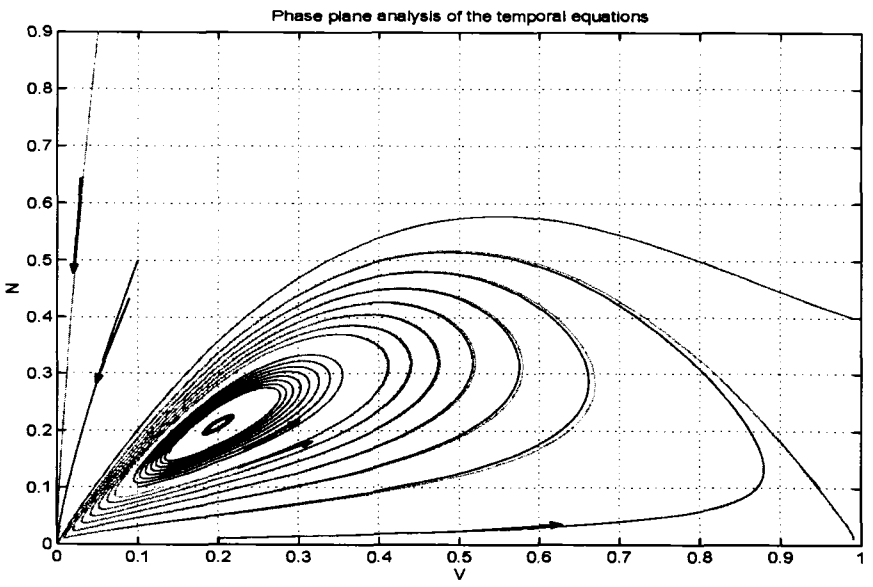

No dispersal

Figure 6.12: Coexistence steady state is shown to be locally asymptotically stable for system (6.1)–(6.2) without dispersal terms and with $h(v,n) = \frac{0.8v}{0.05n+v}$, $f(v) = 1 - v$, and $\delta(n) = 0.76$. Time step is $dt = 0.005$, and $\gamma = 15$. Here the coexistence steady state is $(v_s, n_s) = (0.2, 0.211)$.

6.2 Global Stability

In the previous section, we showed that without both the Allee effect and the density dependent predator death rate, diffusion and prey-taxis do not change the local stability of the coexistence steady state. We choose one of the cases without pattern formation to study the global stability of (v_s, n_s). We consider $f(v) = 1 - v$, $h(v) = v$, $\delta(n) = \delta + \nu n$, and $\chi(v) = \frac{b}{v}$ for the spatially homogeneous case of system

$$v_t = \epsilon v_{xx} + v(f(v) - \frac{n}{v}h(v)), \tag{6.67}$$

$$n_t = n_{xx} - (\chi v_x n)_x + \gamma n(h(v) - \delta(n)). \tag{6.68}$$

on an interval $\Omega = [0, L]$ with homogeneous Neumann boundary conditions given by

$$v_x(0,t) = 0, \quad v_x(L,t) = 0, \quad n_x(0,t) = 0, \quad n_x(L,t) = 0. \tag{6.69}$$

Lyapunov function,

$$\tilde{V} = \int_{v_s}^{v} \frac{\tilde{v} - v_s}{\tilde{v}} d\tilde{v} + \int_{n_s}^{n} \frac{\tilde{n} - n_s}{\gamma \tilde{n}} d\tilde{n}, \tag{6.70}$$

has been used to show the global stability. We will show that $V(v,n) = \int_\Omega \tilde{V}(v,n)dx$ is a Lyapunov functional for the full spatially dependent problem (6.67)–(6.68).

Theorem 6.2 *For $f(v) = 1 - v$, $h(v) = v$, $\delta(n) = \delta + \nu n$, and $\chi(v) = \frac{b}{v}$, in the case of boundary condition (6.69), we assume that $4\epsilon\gamma > \frac{n_s}{v_s}b^2$. Then there exist positive invariant*

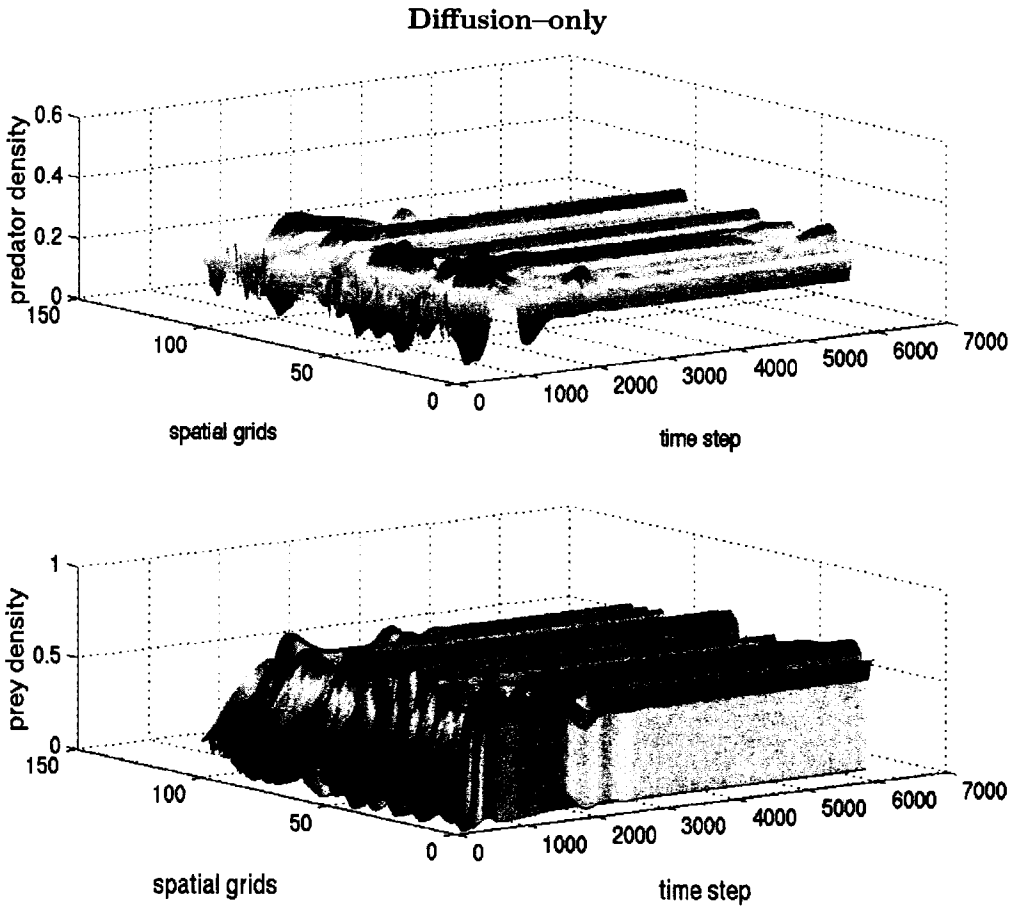

Figure 6.13: Coexistence steady state is shown to be locally unstable for system (6.1)–(6.2) with $h(v,n) = \frac{0.8v}{0.05n+v}$, $f(v) = 1 - v$, and $\delta(n) = 0.76$ and with $\chi(v) = 0.0$. Spatial grid size is $dx = 0.25$, time step $dt = 0.01$, and $\gamma = 15$. Here the coexistence steady state is $(v_s, n_s) = (0.2, 0.211)$.

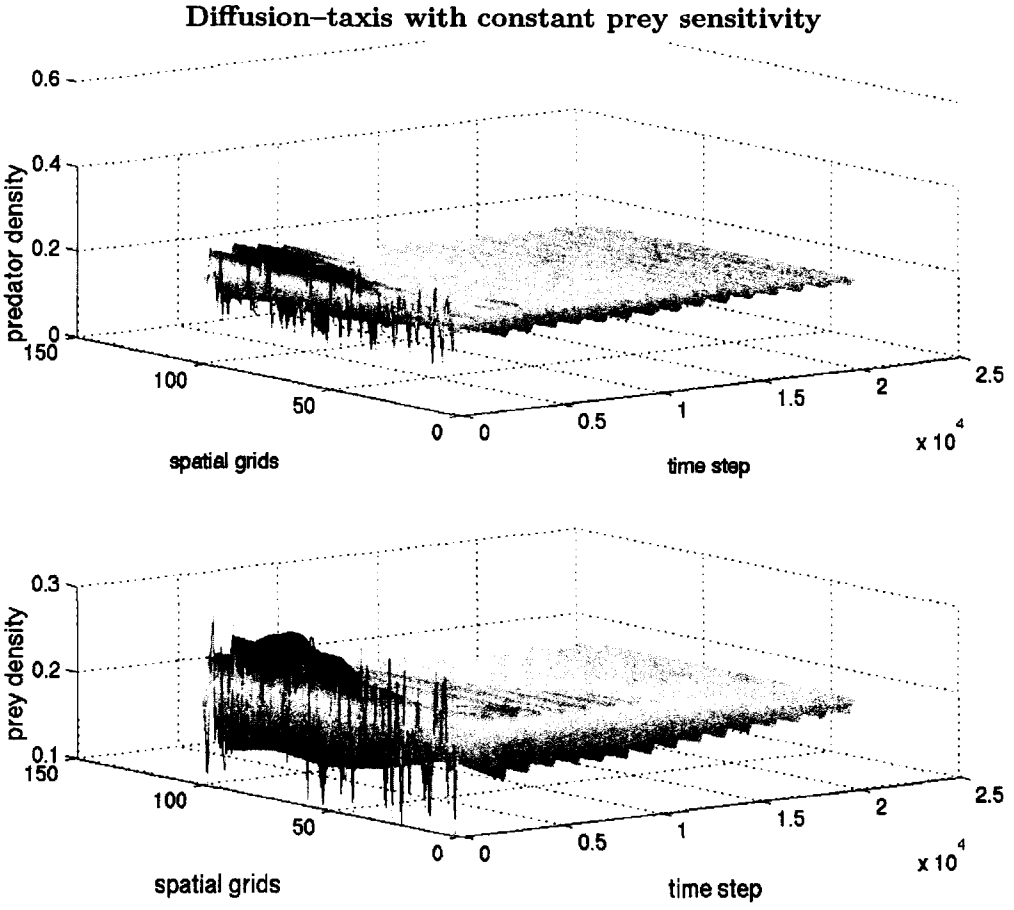

Figure 6.14: Coexistence steady state is shown to be locally asymptotically stable for system (6.1)–(6.2) with $h(v,n) = \frac{0.8v}{0.05n+v}$, $f(v) = 1 - v$, and $\delta(n) = 0.76$ and with $\chi(v) = 6.5$. Spatial grid size is $dx = 0.25$, time step $dt = 0.01$, and $\gamma = 15$. Oscillations are eventually seen to be damped out. Here the coexistence steady state is $(v_s, n_s) = (0.2, 0.211)$.

sets N_L such that for all $(v,n) \in N_L$ the functional, $V(v,n)$, defined in (6.70) is a Lyapunov functional for system (6.1)-(6.2). For $4\epsilon\gamma > b^2\frac{n_s}{v_s}$, $V(v,n) \to 0$ as $t \to \infty$, so $(v,n) \to (v_s,n_s)$, and the coexistence steady state is asymptotically stable.

Proof. Setting $N_L = \{(v,n)|V(v,n) \leq L\}$ for L large enough, then we claim that the level sets N_L are positive invariant. When $(v,n) = (v_s,n_s)$, $V(v,n)$ becomes zero due to $\tilde{V} = 0$. Otherwise, $\tilde{V}$ is positive in N_L because for $v > v_s$ and $n > n_s$, $\frac{v-v_s}{v}$ and $\frac{n-n_s}{\gamma n}$ are positive, respectively and for $v < v_s$ and $n < n_s$, $\frac{v-v_s}{v}$ and $\frac{n-n_s}{\gamma n}$ are negative respectively. Hence the functional, $V(v,n)$ is bounded below. Since $\tilde{V} = v - v_s\ln(v) - v_s + v_s\ln(v_s) + \frac{n-n_s\ln(n)-n_s+n_s\ln(n_s)}{\gamma}$, it is straightforward to see that $\lim_{v\to 0,n\to 0} V(v,n) = \infty$ and $\lim_{v\to\infty,n\to\infty} V(v,n) = \infty$. Since $\frac{\partial V(v,n)}{\partial v} = \int_\Omega \frac{v-v_s}{v}dx$ and $\frac{\partial V(v,n)}{\partial n} = \int_\Omega \frac{n-n_s}{\gamma n}dx$, $V(v,n)$ is continuously differentiable for $v,n > 0$. The next step is showing that for $(v,n) \in N_L$ dV/dt is negative definite for a certain parameter space.

$$\begin{aligned} dV/dt &= \int_\Omega \frac{d\tilde{V}(v,n)}{dt}dx \\ &= \int_\Omega \frac{v-v_s}{v}\dot{v} + \frac{n-n_s}{\gamma n}\dot{n}dx \\ &= \int_\Omega \frac{v-v_s}{v}v_{xx} + (v-v_s)(f(v)-n)dx \\ &+ \int_\Omega \frac{n-n_s}{\gamma n}(\epsilon n_{xx} - (\chi(v)v_x n)_x) + (n-n_s)(v-\delta-\nu n)dx. \end{aligned} \tag{6.71}$$

We arrange the right hand side of this equation into two parts; one including the local dynamics and the other on including the dispersal terms. First we look at local dynamics

$$\begin{aligned} &\int_\Omega (v-v_s)(f(v)-n) + (n-n_s)(v-\delta-\nu n)dx \\ &= \int_\Omega (v-v_s)(f(v)-n_s+n_s-n) + (n-n_s)(v-\delta-\nu n)dx \\ &= \int_\Omega (v-v_s)(f(v)-n_s) + (n-n_s)(v-\delta-\nu n-v+v_s)dx \\ &= \int_\Omega (v-v_s)(f(v)-f(v_s)) + (n-n_s)(v_s-\delta-\nu n)dx \end{aligned}$$

(see [7] for the case of a constant death rate of the predator). Here $(v-v_s)$ and $(f(v)-f(v_s))$ have the opposite sign with $f(v) = 1-v$ so that $(v-v_s)(f(v)-f(v_s))$ is negative. Similarly, $(n-n_s)$ and $(v_s-\delta-\nu n)$ have the opposite sign due to $(v_s-\delta-\nu n) = \nu(n_s-n)$. Therefore $\int_\Omega (v-v_s)(f(v)-n) + (n-n_s)(v-\delta-\nu n)dx$ is negative unless $(v,n) = (v_s,n_s)$. We now take into account the dispersal term of (6.71) by using integration by parts with zero flux

boundary condition

$$\begin{aligned}
&\int_\Omega \frac{v-v_s}{v}v_{xx} + \frac{n-n_s}{\gamma n}(\epsilon n_{xx} - (\chi(v)v_x n)_x)dx \\
&= \frac{v-v_s}{v}v_x + \frac{n-n_s}{\gamma n}(\epsilon n_x - \chi(v)v_x n)\Big|_{\partial\Omega} \\
&- \int_\Omega \Big(\frac{v-v_s}{v}\Big)_v (v_x)^2 + \epsilon\Big(\frac{n-n_s}{\gamma n}\Big)_n (n_x)^2 - \Big(\frac{n-n_s}{\gamma n}\Big)_n \chi(v) n v_x n_x dx \\
&= -\int_\Omega \Big(\frac{v-v_s}{v}\Big)_v (v_x)^2 + \epsilon\Big(\frac{n-n_s}{\gamma n}\Big)_n (n_x)^2 - \Big(\frac{n-n_s}{\gamma n}\Big)_n \chi(v) n v_x n_x dx \\
&= -\int_\Omega \frac{v_s}{v^2}(v_x)^2 + \epsilon\frac{n_s}{\gamma n^2}(n_x)^2 - \frac{n_s}{\gamma n}\chi(v) v_x n_x dx \\
&= -\int_\Omega X^T A X dx,
\end{aligned}$$

where $X = \begin{pmatrix} v_x \\ n_x \end{pmatrix}$ and $A = \begin{pmatrix} \frac{v_s}{v^2} & -\frac{n_s}{2\gamma n}\chi(v) \\ -\frac{n_s}{2\gamma n}\chi(v) & \epsilon\frac{n_s}{\gamma n^2} \end{pmatrix}$. Thus the matrix A is symmetric. Hence if A is positive definite, all eigenvalues of the matrix A are positive. Here $\mathrm{tr}(A) = \frac{v_s}{v^2} + \epsilon\frac{n_s}{\gamma n^2}$ is positive. Thus a positive determinant $\Delta(A) = \frac{v_s}{v^2}\epsilon\frac{n_s}{\gamma n^2} - \frac{n_s^2}{4\gamma^2 n^2}\chi(v)^2$ guarantees two positive eigenvalues for the matrix A. As a result, for $(v,n) \in N_L$ $\frac{dV}{dt} < 0$. Hence the level sets N_L are positive invariant. With the specific example of $\chi(v) = \frac{b}{v}$, we have the condition for positive eigenvalues that $4\epsilon\gamma > \frac{n_s}{v_s}b^2$. For the special case of $\chi(v) = 0$, i.e. diffusion–only case, the matrix A is always positive definite for N_L. Therefore the functional $V(v,n)$ is shown to be a Lyapunov functional under the condition specified above.□

6.3 Summary

In this chapter we considered pattern formation for a predator–prey taxis model of reaction–diffusion–advection type given by

$$v_t = \epsilon v_{xx} + v(f(v) - \frac{n}{v}h(v)), \tag{6.72}$$

$$n_t = n_{xx} - (\chi(v)v_x n)_x + \gamma n(h(v) - \delta(n)) \tag{6.73}$$

with a constant prey sensitivity, i.e. $\chi(v) = \chi$. We considered various reaction terms: for h including type I and II functional responses as well as ratio dependent functional responses. We considered constant and density dependent death rate δ of the predator, and a logistic growth or an Allee effect in the prey growth term.

The combination of a type I functional response, a constant death rate of the predator, and a logistic growth rate of the prey was shown in Section 6.1.1 to not generate a spatial pattern. In Section 6.1.2, a type I functional response was replaced with a type II functional response, however this combination also failed to show a spatial pattern. In Section 6.1.3 a density dependent death rate of the predator was studied instead of a constant death rate. The combination of a type I functional response, a density dependent death rate of the predator, and a logistic growth rate of the prey cannot produce a spatial pattern. An Allee effect was considered in Sections 6.1.4 and 6.1.5 instead of a logistic growth rate of the prey. In these cases, pattern formation occurs for certain parameter values (Theorem

6.1). However, in general we observed that a prey taxis term stabilizes the coexistence steady state of system (6.72)–(6.73) (Lemma 6.5). In Section 6.1.6 a linear ratio functional response was considered. The combination of a linear ratio functional response, a constant death rate of the predator, and a logistic growth rate of the prey was shown to not generate patterns. However, in Section 6.1.7 it is seen that a hyperbolic ratio functional response can lead to pattern formation (Lemma 6.7). In summary, the following functional forms support spatial pattern formation:
— a hyperbolic ratio dependent functional response, $h(v,n) = \frac{\mu v}{dn+v}$
— a density dependent death rate, e.g. $\delta(n) = \delta + \nu n$ and an Allee effect, e.g. $f(v) = K(1-v)(v-a)$.

For the global stability of the coexistence steady state, in Section 6.2 we considered the case of Section 6.1.3. We derived a Lyapunov functional and proved the existence of invariant regions. Moreover, the global stability of the coexistence steady state follows (Theorem 6.2).

The significance of this chapter is that prey–taxis is a process that makes the coexistence of predator–prey interactions stabilized. In other words, prey–taxis plays a role in homogeneous environments. In the long run, it tends to carve heterogeneous environments into homogeneous environments. At an initial pest onset, prey–taxis helps predators to move towards high prey density. Hence, when pesticides are used at this moment, pesticides need to be selected carefully. Otherwise, pesticides would kill all predators before prey would be controlled. As a result, there will be more severe pest onset following. In particular, we found that a combination of an Allee effect of the prey and a density dependent death rate of the predator generates spatial patterns. In this case, due to spatial patterns prey exhibit the local onset and predators patrol high prey density areas. If pesticides expel predators, the local prey onset will be the global onset.

Chapter 7

Concluding Remarks

The response of living organisms to the environment relies on two basic instincts; living and death instincts. Individuals move toward where they increase a chance of living and move away from high predation risk.

The purpose of this research was to investigate how predators actively react to the spatial configuration of the prey on the landscape rather than passively respond relying on predator's random movement. To this end, the level of predator satiation was assumed to mediate the prey–taxis process such that predators search more actively in high prey density areas. Subsequently we incorporated the concept of prey–taxis into spatial predator–prey dynamics to understand the underlying mechanisms for predator dispersal towards high prey density. Then we explored how these mechanisms generate spatial patterns in predator–prey interactions.

In Chapter 2, we derived a predator–prey satiation model, which consists of five equations. The complete predator–prey satiation model consists of three components: a pair of hyperbolic equations for the predator movement model, a pair of hyperbolic equations for the spatio–temporal satiation dynamics, and the prey model. Lastly, the turning rates of the predator, which depend on the satiation level, was obtained using a Poisson process. The system of five equations is not amenable to analysis, so we considered simplification.

In Chapter 3, we investigated approximations of the predator–prey satiation model, which resulted in a prey–taxis model. The prey–taxis model consists of two components; the spatial predator dynamics and the spatial prey dynamics. A pair of hyperbolic equations for the predator movement model and a pair of hyperbolic equations for the spatio–temporal satiation dynamics were collapsed into a parabolic equation for the spatial predator dynamics. In addition to analyzing the resulting system, numerical solutions also provide some insight into the prey–taxis model, so we considered numerical methods next.

In Chapter 4, we discussed numerical methods for simulations of the prey–taxis model. Fractional step methods were described as the framework for simulations. For each case of the diffusion, advection, and reaction terms, the Crank–Nicolson scheme, the Nessyahu–Tadmor scheme, the second–order explicit Runge–Kutta method were considered respectively. In the next two chapters, we analyzed prey–taxis models to investigate spatial patterns; for a large spatial scale, we considered travelling wave solutions and for a small scale, we studied pattern formation.

Owen and Lewis [72] found predators may not slow down prey spread without an Allee effect in the prey dynamics by means of linear analysis and singular perturbation analysis.

In Chapter 5, we derived the conditions for the predator to stop the prey spread with prey–taxis incorporated. A ratio–dependent functional response was not previously considered but we included it here. We also considered a special case of the predator–prey model with prey–taxis, in which the predator diffusion rate is small and the prey do not have spatial mobility. Then we found the condition for a discontinuous travelling wave solution without predator diffusion. Here the so called 'Hole in the Wall' appears. Subsequently the full model with small predator diffusion was investigated and compared with the approximate model without predator diffusion. We also considered traveling wave speeds to the resting models and found that the spread rate of the total population depends on a turning rate, transition rates between moving and resting states, moving speed, and an intrinsic growth rate.

In Chapter 6, we found that the following functional forms support spatial pattern formation: a hyperbolic ratio dependent functional response, a density dependent death rate, and an Allee effect. A diffusion process tended to induce instability. In contrast, we observed that a prey–taxis term stabilizes the coexistence steady state of prey–taxis models.

The significance of this study is two–fold; first, this research refreshes a prey–taxis concept in predator–prey interactions. We investigated the derivation of a prey–taxis model, and opened possibilities of various forms of prey–taxis models. Hence, this research may lead to active studies on prey–taxis in predator–prey dynamics. Second, understanding prey–taxis can be applied for biological control strategies.

Investigating travelling waves enables us to understand how the prey population can be controlled by the predator released as biological control agents. A specialist and a generalist predator are said to show Type II and Type III different functional responses respectively [92]. Hence understanding the mechanism of the predator response to spatial prey density helps us to select a proper control agent. In addition, we may be able to diagnose the sources of failure and success in biological control campaigns. As a result, we could suggest management possibilities that are likely to be successful.

Prey–taxis models can be applied to medical applications. For instance, a wound healing model was considered in Chapter 5 and we considered a discontinuous travelling wave solution. Understanding this model will give an insight how the wound heals and give a guideline for more efficient wound healing. Adding strong prey–taxis seems to speed up wound healing (prey–taxis may be correlated with wave speed), but more work is required.

Studying pattern formation provides ideas of a critical domain size and a maximum population for persistence of the prey population. This has applications to the problem of the pest population at a refuge level (Ecological control strategy : When and where to release biological control agents to reduce the pest population).

This thesis can be broadened in three directions; first, modelling with different functional responses and satiation dynamics, extending the models to two dimensions and considering more than two species; second, validation of models with field data; and third, analysis of two dimensions models. We discuss more details of future directions in the next section.

Future directions

When we formulated the predator-prey satiation model in Chapter 2 and the prey–taxis model in Chapter 3, we considered a Type II functional response. The selection of functional responses affects not only the population growth of the predator but also the satiation dynamics, which may result in different prey sensitivity $\chi(v)$. For instance, it is noted that prey sensitivity can be negative for a type IV functional response. This negative

prey sensitivity may generate spatial patterns without an Allee effect. It is noted that some predators prefer attacking a particular size of prey group [50], which may support a type IV functional response.

Mobile species may show different functional responses from Holling type functional responses. Vucetich et al. [98] compared three types of killing rates of wolf predation: prey dependent, predator–prey ratio dependent, and prey and predator dependent killing rates. They indicated that in the wolf–moose interaction, ratio dependent killing rates show a better fit than other types (see also [92] for more explanation). We may incorporate satiation dynamics into deriving ratio dependent functional responses. Here the growth of satiation depends on predator and prey densities and the level of satiation. Hence, we will have a different type of prey sensitivity.

Simple predator–prey interactions may not be enough to explain the diversity and complex webs of interactions so that higher order interactions have been emphasized (Kareiva [45]). Losey and Denno [63] studied the aphid anti–predator defensive behaviours. The most popular method adapted by aphids is dropping from plants and fleeing from the primary habitat in which they reside. Generally, their dropping rate is proportional to their population density and predator size, and inversely proportional to the habitat quality. After dropping from the plant, prey need to overcome desiccation, starvation and ground–foraging predators before prey settle down on new plants. Losey and Denno [61] compared the dropping tendency of two aphid species according to their abilities such as relocating speed and off–plant survival. Foliar-foraging and ground-foraging predators have different abilities to attack prey, i.e. different moving speed and prey–sensitivity. Losey and Denno [62] found the synergistic effects on regulating prey density from the positive interactions of foliar-foraging and ground-foraging predators compared to their individual effect on suppressing aphid populations. Hence, it is worth considering a model of two predators and one prey for investigating biological control strategies.

The modelling framework in Chapters 2 and 3 could be modified to investigate the effect of prey defences. Prey tend to adjust their relative position to the predator to reduce predation risk [27, 67, 96, 97]. We may apply the concept of prey–taxis to prey escape response to predator density. It may refer to predator–taxis. For instance, crayfish (prey) exhibit different activities depending on the presence of a predator (bass). An increased predation risk restricts crayfish foraging and increases anti–predator behaviour such as shelter seeking [22, 30].

For predator–prey interactions, satiation dynamics are determined by the predator's satiation level and prey density. We may develop this idea further, and show that satiation dynamics may be used to classify types of species interactions. If the satiation level of one species is independent of the satiation level of the other but depends on the other's density, then the interaction is classified as predator–prey. If the satiation level of one species positively correlates with the satiation level of the other but is independent of the other's density, then the interaction is mutualism. If the satiation level of one species negatively correlates with the satiation level of the other's density but is independent of the other's density, then the interaction is classified as competition. Thus the concept of prey–taxis may be applied to various other phenomena in ecology. In particular, interspecific interactions of competition are a matter of obtaining resource (prey). Hence, we may incorporate prey–taxis into competitive interactions and consider the role of prey–taxis in winning strategies to obtain more resource (prey) and in dominating the other competitor. We may also

consider the role of prey–taxis in mutualism models. Here the satiation dynamics may be related to mutualism.

Results in this thesis were obtained theoretically. Hence, the next step should be validating prey–taxis model with field data. For that, we may collect data from the literature. To do field experiments, we need to investigate a field experimental design (see Appendix B for example).

The modelling framework in this thesis is based on a one–dimensional landscape. In two dimensions chemotaxis models with spatial patterns have been considered [94, 95, 16]. With a two–dimensional prey–taxis model we may explain various spatial patterns from phytoplankton and zooplankton interactions. The phytoplankton shows vertical and horizontal spatial distributions in response to physical processes such as upwelling, thermoclines and eddies [87]. On the other hand, the mechanisms of spatial pattern formation of the zooplankton, which are foraging on the phytoplankton, are not explained well with only physical processes. Various biological approaches have been contributed to indicate the characteristic features of the spatial structure of the zooplankton with respect to the spatial structure of the phytoplankton. Steele and Henderson [85, 86] studied spatially homogeneous nutrient-plant-herbivore models with deterministic phytoplankton growth rates and stochastic zooplankton mortality in which trajectories can approach limit cycles. Steele and Henderson [87] added the same diffusion terms to the zooplankton and the phytoplankton for the spatial variation. They considered a logistic growth for the prey and a type III functional response, and allowed stochastic effects on the predator mortality. Here, the zooplankton–phytoplankton model, with diffusion coefficients determined by the water currents and a nonlinear reaction term including a stochastic element, showed the spatially and temporally complex structure. Rothschild and Osborn [78] studied the effects of small scale turbulence on the predator–prey contact rate, which is determined by the product of the prey density and the effects of the predator–prey motility and the mean square turbulent velocity. The active and passive motilities of each species increase the contact rate. At different spatial and temporal scales, different types of interactions may occur.

The existence of travelling wave solutions to predator–prey models has been considered by many authors [68]. However, the existence of travelling wave solutions to prey–taxis models has not been considered. The sufficient conditions for the existence of discontinuous travelling wave solutions were considered in Chapter 5. However, the proof of the existence of such solutions and their uniqueness has not been completed. It will be a challenge to prove the existence of travelling wave solutions and their uniqueness to prey–taxis models.

There are various methods that can be used to show the existence of such a heteroclinic connection; we single out two approaches: 1. the Conley connection index (topological method), and 2. analyzing the property of trajectories of the ODE system with Wazewski's theorem.

The basic steps involved in proofs by using the Conley index theory are as follows. First, construct a homotopy of the four-dimensional system to a system with an invariant two-dimensional subsystem on which the dynamics are those of the standard one–species problem. Second, prove the existence of a wave speed for which the heteroclinic orbit occurs in the two-dimensional subsystem. Third, construct a homotopy back to the original problem, and last conclude that for some wave speed the heteroclinic orbit persists and hence the travelling wave exists for the original problem. To construct a homotopy, two (Conley index) or three (connection index) invariant sets should be defined. The Conley

index is associated with isolated (maximal) invariant sets in some compact neighborhood N (isolating neighborhood). A suitable isolating neighborhood N allows the connection index and Conley index to be defined. Since the index is invariant under continuation (homotopy invariant index), the equations are deformed to a simpler case where the index is nontrivial. This implies the existence of an orbit which stays in the isolating neighborhood for all time [12, 84]. For instance, using the Conley index approach Mischaikow and Reineck [66] proved the existence of various types of travelling waves solutions to reaction-diffusion equations which model two-species predator-prey nonlinear interactions. These include the existence of bistable waves (providing a transition between two stable steady states), Fisher waves (providing a transition from an unstable steady state to a stable steady state), higher-dimensional analogue ($n-$dimensional system) of Fisher waves, which all correspond to heteroclinic orbits in a four-dimensional system of ordinary differential equations. Moreover they find homoclinic travelling waves (often called a travelling pulse or a solitary pulse: providing a transition starting and ending at the same steady state), using the Conley index, continuation arguments, and the connection matrix and transition matrix theory. When prey dynamics are regulated by an Allee effect, predator-prey systems with constant diffusion terms for both species have a unique travelling wave solution. Gardner [21] showed the existence of such travelling wave solutions by using a connection index argument (see Conley and Smoller [12, 84] for details).

For the second approach, a particular Wazewski set is constructed and then the Wazewski theorem and the Lasalle Invariance Principle indicate that a positive orbit approaches the co-existence equilibrium after it leaves the saddle point through the unstable manifold (see Appendix A for more details). As an example of the second approach, Dunbar used Wazewski's theorem [17, 18, 19]. He demonstrated the existence of various travelling wave trains (travelling wave solutions which show periodic behaviours) and travelling front solutions for a diffusive predator-prey system by using shooting techniques, invariant manifold theory, and the qualitative theory of ordinary differential equations. By modifying Dunbar's methods, Huang [40] extended Dunbar's results to the case that the prey has a diffusion term as well. When a Hopf bifurcation occurs in the reaction term, the existence of the connection orbit from the saddle point (prey only at its carrying capacity) to the limit cycle around the coexistence equilibrium is shown in a similar way [19].

The concluding chapter began with addressing the goal of this research. Then the results of the thesis were presented by chapters. Subsequently the contributions of this thesis to research community were presented and further research directions were described.

We conclude this thesis with contemplating the goal of this thesis and its potential extensions. The purpose of this research was to investigate the mechanisms of spatial predator–prey interactions. Our perspective on predator–prey interactions was not that predator–prey interactions occur by chance but that predator–prey interactions are generated by the active foraging behaviours of predators. In previous predator–prey models, this perspective was disregarded. In contrast, we considered satiation dynamics and turning rates of the predator to understand predator–prey interactions. In particular, the level of the predator's satiation related to prey density was considered as a key factor to determine predator–prey interactions. Hence, understanding the key factor leads to understanding the interactions, which are seemingly complex. This approach enables us to understand underlying mechanisms causing phenomena. We conjecture that our approach may be used more widely to understand ecological phenomena such as animal learning behaviours and

evolution in ecology. Moreover, the mechanisms for formulating habits and dispositions of an individual could be derived. The mechanisms of the evolution of virulence would be understood in this perspective.

Appendix A

Definitions and Theorems

A.1 Notation and Units

The following notation and units for the variables are used in this thesis.
(Units: L – length, T – time, N – number, and N–D – nondimsensional.)

Definition (Wazewski set [12]) Let Γ be a topological space and let R denote the real numbers. Let a continuous function from $\Gamma \times R \rightarrow \Gamma$ be denoted by $(\gamma, t) \rightarrow \gamma \cdot t$. This function is called a flow on Γ if the following conditions are satisfied for all $\gamma \in \Gamma$ and $s, t \in R$:
(a) $\gamma \cdot 0 = \gamma$
(b) $\gamma \cdot (s + t) = (\gamma \cdot s) \cdot t$
For $\Gamma' \subset \Gamma$ and $R' \subset R$, let $\Gamma' \cdot R'$ be the set of points $\gamma \cdot t$ such that $\gamma \in \Gamma'$ and $t \in R'$.

Definition Given $W \subset \Gamma$, let W^o be the set of points $\gamma \in W$ such that , for some positive t,$\gamma \cdot t \notin W$. For $y_0 \in W^o$, define $T(y_0) = sup\{s : y_0 \cdot [0, s] \subseteq W\}$. $T(y_0)$ is called an exit time. Let W^- be the set of points $\gamma \in W$ such that, for any positive t, $\gamma \cdot [0, t) \not\subset W$. The set W^- is contained in W^o and is called the exit set of W. The set W is called a **Wazeski set** if the following conditions are satisfied:
(a) If $\gamma \in W$ and $\gamma \cdot [0, t] \subset \mathrm{cl}(W)$, then $\gamma \cdot [0, t] \subset W$,
(b) W^- is closed relative to W^o.
Definition: A subset A of a topological space X is a **strong deformation retract** of X if there is a continuous function $r : X \times [0, 1] \rightarrow X$ such that: (1) for $x \in X$, $r(x, 0) = x$ and $r(x, 1) \in A$; and (2) for $x \in A$ and $\sigma \in [0, 1]$, $r(x, \sigma) = x$. The function r is called a **strong deformation retraction.**

Theorem If W is a Wazeski set then W^- is strong deformation retract of W^o and W^o is open relative to W.
Wazeski Theorem shows that if W is a Wazeski set and W^- is not strong deformation retract of W then $W \backslash W^o$ is not empty, i.e. there exist solutions which stay in W for all positive time.

Theorem (Invariance Principle) Let V be a real-valued function and let $U \equiv \{x \in R^2 : V(x) < k\}$, where k is a real number. Suppose further that V is continuous on the closure $\bar{U}$ of U and C^1 on U with $\dot{V}(x) \leq 0$ for $x \in U$. Consider the subset S of $\bar{U}$ defined

$+/-$	positive/ negative direction moving [N–D]
u	speed at which a predator travels [L/T]
$V(x,t)$	prey density [N/L]
$n^+(x,t)$	right–moving predator density [N/L]
$n^-(x,t)$	left–moving predator density [N/L]
$n(x,t)$	total predator density $(= n^+(x,t) + n^-(x,t))$ [N/L]
$r = R(S)$	direction–reversal probability per unit time for predator [1/T]
$S(x,t)$	degree to which a predator is satiated($[0,1]$) [N–D]
K	max density of prey [N/L]
$\mathbf{J}_P$	flux density of predators [N/T]
$S_0 = S_0(V)$	steady–state value of S [N–D]

Table A.1: Notation and units of the predator–prey–satiation model

by $\equiv \{x \in \bar{U} : \dot{V}(x) = 0\}$ and let M be the largest invariant set in S. Then every positive orbit that starts in U and remains bounded has its $\omega-$ limit set in M. [26]

Poincaré–Bendixson Theorem [26, 74, 89]. Suppose that $x' = f(x)$ is a planar system with a finite number of equilibrium points. If the positive orbit $\gamma^+(x^0)$ of x^0 is bounded, then one of following is true:

- The ω-limit set $\omega(x^0)$ is a single point $\bar{x}$ which is an equilibrium point and $\varphi(t, x^0) \to \bar{x}$ as $t \to +\infty$.
- $\omega(x^0)$ is a periodic orbit Γ and either $\gamma^+(x^0) = \omega(x^0) = \Gamma$ or else $\gamma^+(x^0)$ spirals with increasing time toward Γ on one side of Γ.
- $\omega(x^0)$ consists of equilibrium points and orbits whose α- and ω- limit sets are the equilibrium points.

Appendix B

Literature review

In this appendix, two prey–taxis related articles are reviewed.

Using spatially explicit models to characterize foraging performance in heterogeneous landscapes

Grünbaum [23] focused on the predator dispersal term without predator population dynamics. He computed two statistical indicators ; one is the expected payoff of satiety per predator per unit of time and the other is the travel time statistic of how quickly predator find and aggregate around a prey, and how quickly they get to homogeneous predator distribution.

He began with the following master equation for the predator redistribution

$$\frac{\partial P}{\partial t} = \frac{\partial}{\partial x}\left(D\frac{\partial P}{\partial x} - UP\right), \tag{B.1}$$

where $P(t,x)$ is the predator density at time t and position x, D is the diffusion coefficient of predators, and U describes the directional movement of predators due to external stimulus. The diffusion coefficient D is assumed to vary in space. The advection term, U, is presented as $U = \chi\frac{\partial V}{\partial x}$ with prey density $V(t,x)$. χ is a taxis coefficient.

The equilibrium solution of equation B.1 was computed with reflecting boundary conditions for both predator and prey populations,

$$0 = \frac{\partial}{\partial x}\left(D\frac{\partial P}{\partial x} - \chi\frac{\partial V}{\partial x}P\right),$$

where both sides are integrated

$$c = D\frac{\partial P}{\partial x} - \chi\frac{\partial V}{\partial x}P,$$

with c for integral constant. Reflecting boundary conditions justify $c = 0$ so that predator density distribution is computed explicitly,

$$P(x) = P_0\rho(V(x)), \rho(V) = \exp\left(\int_{V_1}^{V}\frac{\chi(V')}{D(V')}dV'\right),$$

where P_0 is a constant determining the total predator population, and V_1 is prey density. With the result of predator distribution, the expected payoff is calculated

$$\bar{S} = \frac{\int_0^L S(V(x))P(x)dx}{\int_0^L P(x)dx} = \frac{\int_0^L S(V(x))\rho(V(x))dx}{\int_0^L \rho(V(x))dx},$$

with 0 the left end location of the domain, L the right end location of the domain and S a satiation function of V.

The expected time, $\bar{T}$, to reach a resource peak is an estimate of the travel time taken by a predator that starts from a low-resource area to make its way to a resource center. $\bar{T}$ is a useful indicator of how long it takes the forager distribution to reach equilibrium, so it can help determine how long the expected payoff experiment should run. For the computation of $\bar{T}$, the left boundary has a constant flux condition (foragers are added at the low-resource end), and the right boundary has a zero-density condition (foragers that reach the resource peak are removed). The equilibrium forager distribution is then calculated with the following steps; since P is zero on the right end due to the zero–density condition, that is, $P(L) = 0$, $c = D(L)\frac{\partial P}{\partial x}|_{x=L}$. After rearranging the equation, we have

$$\frac{1}{P}\partial P = \frac{c}{DP}\partial x + \frac{\chi}{D}\partial V,$$

which can be integrated as

$$\ln P(x) - \ln P(0) = \int_0^x \frac{c}{DP}dx' + \int_{V(0)}^{V(x)} \frac{\chi}{D}dV'.$$

With moving $\ln P(0)$ to the right side and removing 'ln', then we have

$$P(x) = P(0)\rho(V(x)) \exp \int_0^x \frac{c/P_0}{\rho(V(x'))D(V(x'))}dx',$$

but this result is not the same as the author's calculation

$$P(x) = P_0\rho(V(x)) \int_x^L \frac{1}{\rho(V(x'))D(V(x'))}dx'. \tag{B.2}$$

And the travel time statistic is

$$\bar{T} = \int_0^L \rho(V(x)) \int_x^L \frac{1}{\rho(V(x'))D(V(x'))}dx'dx,$$

with the resource distribution fixed in time. Even though the travel time statistic can be expressed only with predator distribution, $\bar{T} = \frac{\int_0^L P(x)dx}{P_0}$, how the travel time statistic was computed in the original article is not clear.

Grünbaum applied the expected time statistic and pay–off statistic to aphids and lady-birds interaction according to the data by Kareiva and Odell. The diffusion coefficient, $D = \frac{u^2}{3}\tau$, and prey–taxis coefficient, $\chi = -\frac{u^2}{2}\frac{d\tau}{dV}$, were used to calculate the specific pay–off and travel time statistic, where $\tau = \frac{1}{R(S(V))}$ (remark: $D = \frac{u^2}{2R(S_0(V))}$ and $\chi = -\frac{u^2 dR(S(V))}{R(S_0(V))(2R(S_0(V))-\partial f/\partial S[S_0(V),V])}$). In this case, $\rho(V) = \exp(\int_{V(0)}^{V} -\frac{3}{2\tau}d\tau) = \tau(V)^{-3/2} - \tau(V(0))^{-3/2} = R(S(V))^{3/2} - R(S(V(0)))^{3/2} = R(S(V))^{3/2}$ with the implicit assumption of $R(S(V(0))) = 0$. Therefore, the expected payoff is as follows

$$\bar{S} = \frac{\int_0^L S(V(x))R(S(V(x)))^{3/2}dx}{\int_0^L R(S(V(x)))^{3/2}dx}.$$

Using $\rho(V)D(V) = R(S(V))^{3/2}\frac{u^2}{3}\tau = \frac{u^2}{3}R(S(V))^{1/2}$, the expected travel time is

$$\bar{T} = \frac{3}{u^2}\int_0^L (R(S(V(x)))^{3/2}\int_x^L R(S(V(x')))^{-1/2}dx')dx.$$

For a simulation, he used

$$S(V) = \frac{0.85V}{V_0 + V}, V_0 = 107m^{-1}.$$

He introduced a family of turning rates ($R(S) = 3.19+7.43(\frac{S-S_0}{0.85-S_0})^\lambda$ with $S_0 = 0.0379$), which has one free parameter (λ) except for satiation variable. If the turning threshold (one parameter) is changed, the turning rate $R(S)$ shows different qualities. Grünbaum computed different turning thresholds , the expected payoff (in the ladybug case, it is satiety) for foraging strategy, and mean time to reach resource. He then compared the success of two predator species who used different foraging strategies, due to different turning thresholds. He says the significance of the turning threshold in that ladybirds tend to remain in aphid patches above the threshold and leave patches below the threshold. Thus the turning threshold, λ, is highlighted as the essential link between the ladybirds' area–restricted search and the patching–leaving criteria from foraging theory. He used simulations to show the effects of the turning threshold. He said that comparing behavioral thresholds in different species of predators may provide important insights into the ecological circumstances that give one species a competitive advantage over another.

In sum, Grünbaum worked on the results of steady state solutions of predator dynamics and did some simulations of prey–predator dynamics without predator population dynamics.

Models for predator–prey systems at multiple scales

Out of Kareiva and Odell's models [46] Cantrell and Cosner [9] focused on the migration effects of the predator on the persistence of the prey with the assumption that the prey population and the predator population experience space and time on quite different scales; The time scale for predator dispersal is very fast, the time scales for prey dispersal and reproduction are moderately fast, the time scale for prey dispersal is relatively slow. These assumptions are based on the phenomenon that the predator and the prey recognize the environment in different ways; Relatively high motility of the predator helps it experience the environment as the collection of patches. With these assumptions, Cantrell and Cosner did not need to use prey–taxis term and diffusion term in the predator dynamics. The prey–taxis term and diffusion term were excluded, and they could focus only on emigration and immigration of predator between patches as a dispersal for the predator. It is assumed that prey move slowly and do not jump between patches. Thus, only prey equations have diffusion term, which is different from the articles that exclude prey diffusion and include only predator diffusion for the simplicity of analysis. It is assumed that the predator aggregation response is so rapid that the predator number is immediately adjusted to prey densities. Thus, quasi–steady-state assumptions are used to incorporate the predator population dynamics into the prey population equations. Instead of considering the predator dynamics, Cantrell and Cosner focused on the prey persistence by the relationship between patch size and prey density due to the presence of predators.

They consider two cases in that the total predator population , saying C, is finite or unlimitedly supplied. For the finite case,

$$C = P_A + \sum_{n=1}^{N} P_n,$$

where P_A is the number of predators in the air, P_n is the number of predators on nth patch, and N is the total number of patches. For the unlimited supply of predators, $P_A =$ constant.
The master equations are

$$\begin{aligned}\frac{dP_n}{dt} &= I_n P_A - E_n P_n, \\ \frac{\partial v_n}{\partial t} &= D\left(\frac{\partial^2 v_n}{\partial x^2} + \frac{\partial^2 v_n}{\partial y^2}\right) + r\left(1 - \frac{v_n}{K}\right) v_n - c\left(\frac{P_n}{l_n^2}\right) v_n,\end{aligned}$$

where $0 < x < l_n$, $0 < y < l_n$ for the domain and $v_n(x, y, t) = 0$ for $x = 0, l_n$, $y = 0, l_n$. The nth patch is considered as a squared area, i.e. $l_n^2 = A_n =$ area of the nth patch. v_n is the prey density on the nth patch. The parameters I_n and E_n describe the per capita immigration and emigration rates on the nth patch.

The choices of hypotheses which are most crucial in determining the qualitative structure and properties of their models are the choices between finite and unlimited predator populations and between dependence on purely geometric factors and dependence on prey densities in the per capita immigration and emigration rates I_n and E_n . For the immigration and emigration rate of the predator, Cantrell and Cosner considered two aspects: the one is the size of the patch, and the other is the average prey density with finite and infinite supply of predator from the air.

The focus was on examining the effects of changing the size of patches on the prey persistence of the models. In their models the coupling between patches occurs only in the equations for the predator populations, and those are coupled only in the case where the total predator population is finite.

Unlimited supply of predators with immigration and emigration depending only on geometric effects

Under the quasi–steady state assumption for predator dynamics, $I_n P_A - E_n P_n = 0$, $P_n = \frac{I_n P_A}{E_n}$ is calculated and prey dynamics is described as

$$\frac{\partial v_n}{\partial t} = D\left(\frac{\partial^2 v_n}{\partial x^2} + \frac{\partial^2 v_n}{\partial y^2}\right) + r\left(1 - \frac{v_n}{K}\right) v_n - c\left(\frac{P_A(I_n/E_n)}{l_n^2}\right) v_n. \tag{B.3}$$

The immigration and emigration rates are assumed to be $I_n = i l_n^p$ and $E_n = e l_n^q$ for constants i, e, p, and q. The specific hypothesis is that $p = 2$ and $q = -1$, since the patch size is considered to be the main factor of the immigration rate as randomly falling out of sky on the patch, and the perimeter/area ratio is reasonably assumed to be the main factor of the emigration rate. A patch shape is assumed to be a square for the simplicity of analysis.

Most of the effects of the patch size on the prey in their models depend on the following result.

Theorem B.1 Let D, R, and B be positive constants. The model

$$\frac{\partial v}{\partial t} = D\left(\frac{\partial^2 v}{\partial x^2} + \frac{\partial^2 v}{\partial y^2}\right) + Rv - Bv^2$$

for $0 < x < l$, $0 < y < l$, $t > 0$, $v = 0$ for $x = 0, l$, $y = 0, l$
has a unique equilibrium $v^*(x, y)$ with $v^*(x, y) > 0$ for $0 < x < l$ and $0 < y < l$ and with

$v \to v^*$ as $t \to \infty$ if $v(x,y,0) \geq 0$, $v(x,y,0) \not\equiv 0$, provided

$$R - (2\pi^2 D/l^2) > 0. \tag{B.4}$$

The equilibrium $v^*(x,y)$ increases for each (x,y) if R is increased. If B.4 does not hold, then all positive solutions approach zero as $t \to \infty$.
Remark: $\pi^2 D/l^2$ is the principal eigenvalue for $-D(\frac{\partial^2}{\partial x^2} + \frac{\partial^2}{\partial y^2})$.

Since there is no coupling between patches in prey equations, n can be deleted for the simplicity of calculation. If we change the equation B.3 in the form of Theorem B.1., we have

$$\frac{\partial v}{\partial t} = D\left(\frac{\partial^2 v}{\partial x^2} + \frac{\partial^2 v}{\partial y^2}\right) + rv - \frac{rv^2}{K} - cP_A(i/e)l^{p-q-2}v$$

for $0 < x < l$, $0 < y < l$, $t > 0$, $v = 0$ for $x = 0, l$, $y = 0, l$.
The quantity corresponding to R in Theorem B.1. is

$$R = r - cP_A(i/e)l^{p-q-2};$$

The inequality corresponding to B.4 and characterizing when the prey can persist is

$$r - cP_A\frac{i}{e}l^{p-q-2} - \frac{2\pi^2 D}{l^2} > 0, \text{ or equivalently } r > cP_A\frac{i}{e}l^{p-q-2} + \frac{2\pi^2 D}{l^2}. \tag{B.5}$$

If l is too large, then $l^{p-q-2} \to \infty$ given by $p - q - 2 > 0$. Too small l turns the left hand size into infinity due to l^{-2} term. This case thus yields a maximum patch size which will sustain a prey equilibrium as well as the usual minimum patch size.

Finite predator supply with immigration and emigration depending only on geometric effects

Using $I_n P_A = i l_n^p P_A = i(C - \sum_{k=1}^N P_k) l_n^p$, the model becomes

$$\begin{aligned}
\frac{dP_n}{dt} &= i(C - \sum_{k=1}^{N} P_k)l_n^2 - (el_n^{-1})P_n, \\
\frac{\partial v_n}{\partial t} &= D\left(\frac{\partial^2 v_n}{\partial x^2} + \frac{\partial^2 v_n}{\partial y^2}\right) + r\left(1 - \frac{v_n}{K}\right)v_n - c\left(\frac{P_n}{l_n^2}\right)v_n,
\end{aligned}$$

where $0 < x < l_n$, $0 < y < l_n$ for the domain and $v_n(x,y,t) = 0$ for $x = 0, l_n$, $y = 0, l_n$. This system is coupled in the predator equations, which are independent of the prey.

With the quasi–steady–state assumption, the number of predators on the nth patch is calculated as $P_n = \frac{icCl_n^{p-q-2}}{i\sum_{k=1}^N l_k^{p-q} + e}$. Thus prey equations become

$$\frac{\partial v_n}{\partial t} = D\left(\frac{\partial^2 v_n}{\partial x^2} + \frac{\partial^2 v_n}{\partial y^2}\right) + rv_n - \frac{rv_n^2}{K} - \left(\frac{icCl_n^{p-q-2}}{i\sum_{k=1}^N l_k^{p-q} + e}\right)v_n$$

for $0 \leq x \leq l_n$, $0 \leq y \leq l_n$, $v_n(t,x,y) = 0$ for $x = 0, l_n$, $y = 0, l_n$, $n = 1, ..., N$.

$$\frac{\partial v_n}{\partial t} = D\left(\frac{\partial^2 v_n}{\partial x^2} + \frac{\partial^2 v_n}{\partial y^2}\right) + rv_n - \frac{rv_n^2}{K} - \left(\frac{icCl_n^{p-q-2}}{i\sum_{k=1}^N l_k^{p-q} + e}\right)v_n$$

for $0 \leq x \leq l_n$, $0 \leq y \leq l_n$, $v_n(t,x,y) = 0$ for $x = 0, l_n$, $y = 0, l_n$, $n = 1, ..., N$.
For each n, the quantities corresponding to B and R in Theorem B.1. are

$$B = r/K, \; R = R_n = r - \frac{icCl_n^{p-q-2}}{i\sum_{k=1}^{N} l_k^{p-q} + e},$$

the inequality corresponding to B.4 and characterizing when the prey can persist is

$$r > \frac{icCl_n^{p-q-2}}{i\sum_{k=1}^{N} l_k^{p-q} + e} + (2\pi^2 D/l^2). \tag{B.6}$$

In this case, it was shown that there would be a maximum patch size which could sustain a prey population.

For the density–dependent model, the total prey population on patch n at time t was used for the average prey density on the nth patch. $V_n = \int_0^{l_n}\int_0^{l_n} v_n(x,y,t)dxdy$ = total prey population on patch n at time t. The basic form of the predator equations in the density-dependent model is

$$\frac{dP_n}{dt} = I_n P_A - l_n^2 E_n P_n / V_n.$$

It is assumed that predator aggregation occurs at a much faster rate than prey dispersal and dynamics, which yields the quasi-steady state.

$$P_n = (I_n P_A / E_n l_n^2) V_n,$$

which changes prey dynamics as

$$\frac{\partial v_n}{\partial t} = D\left(\frac{\partial^2 v_n}{\partial x^2} + \frac{\partial^2 v_n}{\partial y^2}\right) + r\left(1 - \frac{v_n}{K}\right)v_n - c\left(\frac{I_n P_A}{E_n l_n^4}\right)v_n V_n.$$

Unlimited supply of predators with immigration and emigration depending only on geometric effects and the prey density

With the assumptions of $I_n = il_n^2$ and $E_n = e/l_n$, the predator population was calculated with a quasi-steady-state assumption;

$$P = (i/e)P_A l^{p-q-2} V.$$

Since the unlimited predator case generates a decoupled case, n is ommited for the simplicity of analysis. Thus the prey equation is

$$\frac{\partial v}{\partial t} = D\left(\frac{\partial^2 v}{\partial x^2} + \frac{\partial^2 v}{\partial y^2}\right) + r\left(1 - \frac{v}{K}\right)v - c(i/e)P_A l^{p-q-2} V v, \tag{B.7}$$

where zero density boundary conditions are used. Due to the V term in equation B.7, Theorem 3.1. cannot be applied to this case so that Cantrell and Cosner [9] introduced some other theorems for the condition of prey persistence due to the predator presence. In this case they showed that there must be an inverse relation between patch size and average prey density V.

Finite predator supply with immigration and emigration depending on geometric effects and the prey density

With the assumptions of $I_n = il_n^2$ and $E_n = e/l_n$, the predator equations become

$$\begin{aligned}\frac{dP_n}{dt} &= il_n^2 P_A - el_n P_n/V_n \\ &= i\left(C - \sum_{k=1}^{N} P_k\right) l_n^2 - el_n P_n/V_n.\end{aligned}$$

The quasi-steady state assumption then yields

$$\frac{\partial v_n}{\partial t} = D\left(\frac{\partial^2 v_n}{\partial x^2} + \frac{\partial^2 v_n}{\partial y^2}\right) + r\left(1 - \frac{v_n}{K}\right) v_n - \frac{cP_n^*(V1, ..., V_n)}{l_n^2} v_n,$$

where $P_n^*(V1, ..., V_n)$ are the solutions of $0 = i(C - \sum_{k=1}^{N} P_k) l_n^2 - el_n P_n/V_n$ in terms of the average prey density in each patch.

For this scenario, Cantrell and Cosner considerd a single patch case and many patches case. In the single patch case, it is shown that a maximum prey population will occur for some finite patch side, l, and the population will be smaller on the patches of larger size. In the case of many patches, the similar result may occur according to parameter values.

In sum, Cantrell and Cosner were concerned with the persistence of the prey population due to the migration of the predator without predator mobility on each patch, which is not quite related with what this thesis is interested in. Nonetheless, the methods that were used to find the patch size for the prey persistence would be applied to consider the biological control in this thesis.

Appendix C

Numerical Codes

In this appendix, we introduce numerical codes for the spatio–temporal predator–prey–taxis system (3.126)–(3.127). In particular, we focus on the codes for the advection term. Because RK2 scheme and Crank–Nicolson scheme are well known, we do not include those codes in this appendix. Among the numerical schemes for the advection term, the code for N–T scheme will be presented written in MATLAB. This code is for one species and was used for computing numerical solutions to Burgers' equation in Section 4.2 and in Figures 4.1. However, this code is easily extended for two species by modifying the flux function.

function n = ntmethod1d(a,dt,dx,q,theta);

%% NT Scheme
%% a: old data of a species, nstar: midpoint valuse $n_i^{j+1/2}$
%% n: updated data of a species
%% dx : spatial grid size, dt : time step
%% theta gives a choice of minmod
%% q : number of grid cells
%% f is a flux function
e=0.5*(dt)/dx;

%% finding a_x at $t = t^j$ and $x = x_i$
for i=2:q;
a_x(i)=rminmod(a(i+1),a(i),a(i-1),theta)/(dx);
end
a_x(1)=0; a_x(q+1)=0; %% on the boundary
%% finding f_x at $t = t^j$ and $x = x_i$
for i=2:q
f_x(i)=rminmod(f(a(i+1)),f(a(i)),f(a(i-1)),theta);
end
f_x(1)=0; f_x(q+1)=0; %% on the boundary
%% computing the midpoint value $n_i^{j+1/2}$
for i=1:q+1;
nstar(i)=a(i)-0.25 e f_x(i);
end
%% updating data

```
for i=2:q;
n(i)=0.5(a(i+1)+a(i))+0.125*dx*(a_x(i)-a_x(i+1))-e*(f(nstar(i+1))-f(nstar(i)));
end
n(1)=a(1); n(q+1)=a(q+1); %BC
function x=rminmod(X,Y,Z,theta)
%%minmod limiter
a=X-Y;
b=X-Z;
c=Y-Z;
if a>0 & b>0 & c>0
x=min(min(theta*a,0.5*b),theta*c);
elseif a<0 & b<0 & c < 0
x=max(max(theta*a,0.5*b),theta*c);
else
x=0;
end
```

Appendix D

Singular Perturbation Analysis of the Wavefront

In this appendix, a singular perturbation analysis of the wavefront, which Owen and Lewis ([72]) used, is described in detail. We consider the temporal steady state for system (5.3)–(5.4) with $\chi = 0$ and the zero wave speed $c = 0$ given by

$$0 = \epsilon v_{xx} + v\left(f(v) - \frac{n}{v}h(v)\right), \tag{D.1}$$

$$0 = n_{xx} + \gamma n(h(v) - \delta). \tag{D.2}$$

Transition layer. Rescaling the spatial coordinate to $\xi = \frac{x}{\sqrt{\epsilon}}$, equations (D.1)–(D.2) are written as

$$0 = v_{\xi\xi} + v\left(f(v) - \frac{n}{v}h(v)\right), \tag{D.3}$$

$$0 = n_{\xi\xi} + \epsilon\gamma n(h(v) - \delta), \tag{D.4}$$

which is the stationary front solutions of (5.3)–(5.4). In addition, the boundary conditions are: $\lim_{\xi\to\pm\infty} v_\xi(\xi) = 0$, $\lim_{\xi\to\infty} v(\xi) = 0$, and $\lim_{\xi\to-\infty} v(\xi) = v_0$. As $\epsilon \to 0$, the n equation ends up with $n_{\xi\xi} = 0$. Integrating this twice, n satisfies $n = C_0\xi + C_1$ where C_1 and C_2 are integral constants. We are looking for nonnegative predator population, $n \geq 0$. Since for large $|\xi|$ non–zero C_0 eventually make a negative population for the predator, C_0 should be zero and then the predator population is constant in the region of this transition layer, saying $n = n_0$. Thus, we have a single equation for v only,

$$v_{\xi\xi} + v\left(f(v) - \frac{n_0}{v}h(v)\right) = 0, \tag{D.5}$$

where the boundary conditions are: $\lim_{\xi\to\pm\infty} v_\xi(\xi) = 0$, $\lim_{\xi\to\infty} v(\xi) = 0$, and $\lim_{\xi\to-\infty} v(\xi) = g^{-1}(n_0) = v_0$. Multiplying equation (D.5) by $dv/d\xi$, and integrating with respect to ξ from $-\infty$ to ∞ gives us

$$\int_{-\infty}^{\infty}\left\{\frac{d^2v}{d\xi^2} + v\left(f(v) - \frac{n_0}{v}h(v)\right)\right\}\frac{dv}{d\xi}d\xi = 0. \tag{D.6}$$

The first term is integrated directly and the second term is done by using a change of variables from ξ to v, to get

$$\frac{1}{2}\left(\frac{dv}{d\xi}\right)^2\Big]_{-\infty}^{\infty} + \int_0^{v_0} v\left(f(v) - \frac{n_0}{v}h(v)\right)dv = 0. \tag{D.7}$$

Applying the boundary conditions and $n_0 = g(v_0)$ yield

$$\int_0^{v_0} v\left(f(v) - \frac{g(v_0)}{v}h(v)\right)dv = 0, \tag{D.8}$$

which determines v_0 consistent with a stationary solution.

Right–hand outer solutions. We now consider equations (D.1)–(D.2) setting $\epsilon = 0$ so that v and n satisfy

$$0 = v\left(f(v) - \frac{n}{v}h(v)\right), \tag{D.9}$$

$$0 = n_{xx} + \gamma n(h(v) - \delta). \tag{D.10}$$

From equation (D.9), $v = 0$ or $n = g(v)$. Since we are looking for right–hand outer solutions, we here focus on $v = 0$ so that in equation (D.10) we get

$$n_{xx} - \gamma\delta n = 0, \tag{D.11}$$

with boundary conditions: $\lim_{x\to\infty} n(x) = 0$ and $n(0) = n_0$. The general solution of (D.11) is

$$n(x) = A\exp(\sqrt{\gamma\delta}x) + B\exp(-\sqrt{\gamma\delta}x). \tag{D.12}$$

With the boundary conditions, we have

$$n(x) = n_0\exp(-\sqrt{\gamma\delta}x), \text{ or equivalently } \frac{dn}{dx}(0) = -n_0\sqrt{\gamma\delta}. \tag{D.13}$$

Left–hand outer solutions. We now consider the other outer layer. Recall that in the transition layer n = constant so that equation (D.13) plays the role of a boundary condition to find left–hand outer solutions. Now $n = g(v)$ is substituted into equation (D.10) to get

$$n_{xx} - \gamma n(h(g^{-1}(n)) - \delta) = 0, \tag{D.14}$$

with boundary conditions: $n(0) = n_0$, $\lim_{x\to-\infty} n(x) = n_s$, $\frac{dn}{dx}(0) = -n_0\sqrt{\gamma\delta}$, and $\frac{dn}{dx}(-\infty) = 0$. Multiplying equation (D.14) by dn/dx, and integrating with respect to x from $-\infty$ to 0 we find

$$\int_{-\infty}^{0}\left\{\frac{d^2n}{dx^2} + \gamma n(h(g^{-1}(n)) - \delta)\right\}\frac{dn}{dx}dx = 0. \tag{D.15}$$

As we did for the analysis in the transition layer, the first term is integrated directly and the second term is done by using a change of variables from ξ to n, to get

$$\frac{1}{2}\left(\frac{dn}{dx}\right)^2\Big]_{-\infty}^{0} + \int_{n_s}^{n_0}\gamma n(h(g^{-1}(n)) - \delta)dn = 0. \tag{D.16}$$

Applying the boundary conditions and rearranging equation (D.16) yield

$$\int_{n_s}^{n_0}\gamma n h(g^{-1}(n))dn = -\frac{1}{2}\left(\frac{dn}{dx}\right)^2\Big|_{x=0} + \int_{n_s}^{n_0}\gamma n\delta dn \tag{D.17}$$

$$= -\frac{1}{2}\gamma\delta n_0^2 + \frac{1}{2}\gamma\delta n_0^2 - \frac{1}{2}\gamma\delta n_s^2, \tag{D.18}$$

which gives a condition that the left– and right– hand outer solutions match at n_0 if and only if

$$\int_{n_0}^{n_s} nh(g^{-1}(n))dn = \frac{1}{2}\delta n_s^2, \tag{D.19}$$

which can be translated in terms of v as follows

$$\int_{v_0}^{v_s} vf(v)g'(v)dv = \frac{1}{2}\delta g(v_s)^2, \tag{D.20}$$

by using a change of variable with $n = g(v)$. Thus we have the following two conditions in order to have zero wave speed solutions and those conditions restrict the values of v_0 and δ.

$$\int_0^{v_0} v\left(f(v) - \frac{g(v_0)}{v}h(v)\right)dv = 0, \tag{D.21}$$

$$\int_{v_0}^{v_s} vf(v)g'(v)dv = \frac{1}{2}\delta g(v_s)^2. \tag{D.22}$$

Bibliography

[1] W. C. Allee, O. Park, A. E. Emerson, and T. Park. *Principles of animal ecology.* Saunders Co., Philadelphia, 1949.

[2] M. B. Allen and M. B. Eli. *Numerical Analysis for Applied Science.* Wiley–Interscience, New York, 1998.

[3] D. Alonso, F. Bartemeus, and J. Catalan. Mutual interference between predators can give rise to turing spatial patterns. *Ecology*, 83:28–34, 2002.

[4] T. M. Apostol. *Mathematical Analysis.* Addison-Wesley Pub. Co., Waltham, Mass., 2 edition, 1974.

[5] P. Auger, R. B. de la Parra, S. Morand, and E. Sanchez. A predator–prey model with predators using hawk and dove tactics. *Math. Biosc.*, 177&178:185–200, 2002.

[6] W. E. Boyce and R. C. Di Prima. *Elementary Differential Equations and Boundary Value Problems.* John Wiley & Sons, Inc, New York, 7 edition, 2003.

[7] N. F. Britton. *Reaction–Diffusion Equations and Their Applications to Biology.* Academic Press, London, 1986.

[8] K. P. Burnham and D. A. Anderson. *Model selection and inference : a practical information-theoretic approach.* Springer Verlag, New York, 1998.

[9] R. S. Cantrell and C. Cosner. Models for predator–prey systems at multiple scales. *SIAM Rev.*, 38:256–286, 1996.

[10] R. S. Cantrell and C. Cosner. A comparison of foraging strategies in a patchy environment. *Math. Biosc.*, 160:25–46, 1999.

[11] N. Cappuccino. Comparative population dynamics of two goldenrod aphids: Spatial patterns and temporal constancy. *Ecology.*, 68:1634–1646, 1987.

[12] Charles Conley. *Isolated Invariant Sets and the Morse Index*, volume No. 38 of *Conf. Board Math. Sci.* Amer. Math. Soc., Providence, RI, 1978.

[13] C. Cosner, D. L. DeAngelis, J. S. Ault, and D. B. Olson. Effects of spatial grouping on the functional response of predators. *Theor. Popul. Biol.*, 56(1):65–75, 1999.

[14] M. J. Crawley. *Natural Enemies: The Population Biology of Predator, Parasites and Disease.* Blackwell Scientific Publications, Oxford, 1992.

[15] A. F. G. Dixon. *Insect Predator–Prey Dynamics: Ladybird Beetles and Biological Control.* Cambridge University Press, Cambridge, 2000.

[16] Y. Dolak and T. Hillen. Cattaneo models for chemosensitive movement numerical solution and pattern formation. *J. Math. Biol.*, 46:153–170, 2003.

[17] S. R. Dunbar. Travelling wave solutions of diffusive lotka-volterra equations. *J. Math. Biol.*, 17:11–32, 1983.

[18] S. R. Dunbar. Traveling wave solutions of diffusive lotka-volterra equations: a heteroclinic connection in r^4. *Trans. Amer. Math. Soc.*, 286:557–594, 1984.

[19] S. R. Dunbar. Traveling waves in diffusive predator-prey equations: periodic orbits and point-to periodic heteroclinic orbits. *SIAM J. Appl. Math.*, 46:1057–1078, 1986.

[20] P. Fife. *Mathematical aspects of reacting and diffusing systems. Lecture notes in biomathematics v. 28.* Springer Verlag, New York, 1979.

[21] R. Gardner. Existence of traveling wave solutions of predator-prey systems via the connection index. *SIAM J. Appl. Math.*, 44:56–79, 1984.

[22] J. E. Garvey, R. A. Stein, and H. M. Thomas. Assessing how fish predation and interspecific prey competition influence a crayfish assemblage. *Ecology*, 75(2):532–547, 1994.

[23] Daniel Grunbaum. Using spatially explicit models to characterize foraging peformance in heterogeneous landscapes. *Am. Nat.*, 151:97–115, 1998.

[24] K. P. Hadeler. Reaction transport systems in biological modelling. In *In Capasso, V. and Diekman, O., editors, Mathematics inspired by biology, Lect. Notes Math. 1714*, pages 95–150. Springer Verlag, Heidelberg, 1999.

[25] K. P. Hadeler and M. A. Lewis. Spatial dynamics of the diffusive logistic equation with sedentary component. *Canadian Applied Math. Quarterly*, 10:473–500, 2002.

[26] J. Hale and H Koçak. *Dynamics and Bifurcations.* Springer–Verlag, New York, 1991.

[27] W. D. Hamilton. Geometry for the selfish herd. *J. Theor. Biol.*, 31:295–311, 1971.

[28] P. Hartman. *Ordinary Differential Equations.* John Wiley & Sons, Inc, New York, 1964.

[29] M. P. Hassell. *Arthropod Predator–Prey Systems.* Princeton University Press, New Jersey, US., 1978.

[30] A. M. Hill and D. M. Lodge. Replacement of resident crayfishes by an exotic crayfish: The roles of competition and predation. *Ecological Applications*, 9(2):678–690, 1999.

[31] T. Hillen. A turing model with correlated random walk. *J. Math. Biol.*, 35:49–72, 1996.

[32] T. Hillen. Invariance principles for hyperbolic random walk systems. *J. Math. Anal. and Appl.*, 210:360–374, 1997.

[33] T. Hillen. Hyperbolic models for chemosensitive movement. *Math. Models Methods Appl. Sci.*, 12(7):1007–1034, 2002.

[34] T. Hillen. Transport equations with resting phases. *Euro. J. Appl. Math.*, 14:613–636, 2003.

[35] T. Hillen and A. Stevens. Hyperbolic models for chemotaxis in 1–d. *Nonlinear Analysis: Real World applications*, 1.3:409–433, 2000.

[36] C. S. Holling. The components of predation as revealed by a study of samll mammal predation of the european pine sawfly. *Canadian Entomologist*, 91:293–320, 1959a.

[37] C. S. Holling. Some characteristics of simple types of predation and parasitism. *Canadian Entomologist*, 91:385–398, 1959b.

[38] C. S. Holling. The functional response of predators to prey and its role in mimicry and population regulation. *Mem. Entomol. Soc. Can.*, 45:1–60, 1965.

[39] E. E. Holmes. Are diffusion models too simple? a comparison with telegraph models of invasion. *Am. Nat.*, 142:779–795, 1993.

[40] J. Huang, G. Lu, and S. Ruan. Existence of traveling wave solutions in a diffusive predator-prey model. *J. Math. Biol.*, 46:132–152, 2003.

[41] Y. Huang. *The Interplay of Migration and Population Dynamics in a Patchy World.* PhD thesis, Utrecht University, Utrecht, Netherlands, 2003.

[42] J. M. Jeschke, M. Kopp, and R. Tollrian. Predator functional responses: discriminating between handling and digesting prey. *Ecol. Mono.*, 72(1):95–112, 2002.

[43] Jacob Jorné. The effects of ionic migration on oscillations and pattern formation in chemical systems. *J. Theor. Biol.*, 43:375–380, 1974.

[44] P. Kareiva. Population dynamics in spatially complex environments: theory and data. *Philos. Trans. Roy. Soc. Ser. B, London*, 330:175–190, 1990.

[45] P. Kareiva. Higher order interactions as a foil to reductionist ecology (special feature). *Ecology*, 75:1527–1528, 1994.

[46] P. Kareiva and G. Odell. Swarms of predators exhibit 'preytaxis' if individual predators use area–restricted search. *Am. Nat.*, 130:233–270, 1987.

[47] E. F. Keller and L. A. Segel. Initiation of slime mold aggregation viewed as an instability. *J. Theor. Biol.*, 26:399–415, 1970.

[48] E. F. Keller and L. A. Segel. Travelling bands of chemotatic bacteria: A theoretical analysis. *J. Theor. Biol.*, 30:235–248, 1971.

[49] Mark Kot. *Elements of Mathematical Ecology.* Cambridge university press, Cambridge, 2001.

[50] J. Krause and J. J. Godin. Predator preferences for attacking particular prey group sizes: onsequences for predator hunting success and prey predation risk. *Anim. Behav.*, 50:465–473, 1995.

[51] A. Kurganov and E. Tadmor. New high resolution central schemes for nonlinear conservation laws and convection–diffusion equations. *J. Comput. Phys.*, 160:214–282, 2000.

[52] K. A. Landman, G. J. Pettet, and D. F. Newgreen. Chemotactic cellular migration: smooth and discontinuous travelling wave solutions. *SIAM J. Appl. Math.*, 63:1666–1681, 2003.

[53] K. A. Landman, G. J. Pettet, and D. F. Newgreen. Mathematical models of cell colonization of uniformly growing domains. *Bull. math. Biol.*, 65:235–262, 2003.

[54] R. J. LeVeque. *Numerical Methods for Conservation Laws.* Birkhauser, Basel, 1992.

[55] R. J. LeVeque. *Finite Volume Methods for Hyperbolic Problems.* Cambridge University Press, Cambridge, 2002.

[56] M. A. Lewis. Spatial coupling of plant and herbivore dynamics: The contribution of herbivore dispersal to transient and persistent 'waves' of damage. *Theor. Pop. Biol.*, 45:277–312, 1994.

[57] M. A. Lewis and P. Kareiva. Allee dynamics and the spread of invading organisms. *Theor. Pop. Biol.*, 43(2):141–157, 1993.

[58] M. A. Lewis and J. D. Murray. Modelling territoriality and wolf–deer interactions. *Nature*, 366:738–740, 1993.

[59] M. A. Lewis and G. Schmitz. Biological invasion of an organism with separate mobile and stationary states: modeling and analysis. *Forma*, 11:1–25, 1996.

[60] X. Liu and E. Tadmor. Third order nonoscillatory central scheme for hyperbolic conservation laws. *Numer. Math.*, 79:397–425, 1998.

[61] J. E. Losey and R. F. Denno. Interspecific variation in the escape responses of aphids: Effect on risk of predation from foliar–foraging and ground–foraging predators. *Oecologia*, 115:245–252, 1998.

[62] J. E. Losey and R. F. Denno. Positive predator–predator interactions: Enhanced predation rates and synergistic suppression of aphid populations. *Ecology*, 79:2143–2152, 1998.

[63] J. E. Losey and R. F. Denno. The escape response of pen aphids to foliar–foraging predators: factors affecting dropping behaviour. *Eco. Entom.*, 23:53–61, 1998c.

[64] B. Marchant. *Modelling Cell Invasion.* PhD thesis, University of Oxford, Oxford, UK, 1999.

[65] J. A. J. Metz and M. W. Sabelis. Scaling properties of satiation–based functional responses. metz@rulsfb.leidenuniv.nl, 2003.

[66] K. Mischaikow and J. F. Reineck. Travelling waves in predator-prey systems. *SIAM J. Math. Anal.*, 24:1179–1214, 1993.

[67] T.L. Morton, J. Haefner, V. Nugala, R. D. Decino, and L. Mendes. The selfish herd revisited: Do simple movement rules reduce relative predation risk. *J. Theor. Biol.*, 167:73–79, 1994.

[68] J. D. Murray. *Mathematical Biology.* Springer Verlag, New York, 1989.

[69] H. Nessyahu and E. Tadmor. Non–oscillatory central differencing for hyperbolic conservation laws. *J. Comput. Phys.*, 87:408–463, 1990.

[70] A. Okubo and S. A. Levin. *Diffusion and ecological problems: new perspectives.* Springer Verlag, New York, 2 edition, 2000.

[71] A. Okubo, P. K. Maini, M. H. Williamson, and J. D. Murray. On the spatial spread of the grey squirrel in britain. *Proc. R. Soc. Lond. B*, 238:113–125, 1989.

[72] M. R. Owen and M. A. Lewis. How predation can slow, stop or reverse a prey invasion. *Bull. Math. Biol.*, 63:655–684, 2001.

[73] J. K. Parrish and L. Edelstein-Keshet. Complexity, pattern, and evolutionary trade–offs in animal aggregation. *Science*, 284:99–101, 1999.

[74] L. Perko. *Differential Equations and Dynamical Systems.* Springer–Verlag, New York, 2 edition, 1996.

[75] D. L. Pettet, G. J.and McElwain and J. Norbury. Lotka-volterra equations with chemotaxis: Walls, barriers and travelling waves. *Math. Appl. Med. Biol.*, 17:395–413, 2000.

[76] G. H. Pyke. Are animals efficient harvesters? *Anim. Behav.*, 26:241–250, 1978.

[77] G. H. Pyke. Optimal foraging theory; a critical review. *Journal of Plankton Research*, 14:157–172., 1984.

[78] B. J. Rothschild and T. R. Osborn. Small-scale turbulence and plankton contact rates. *Journal of Plankton Research*, 10:465–474., 1988.

[79] L. A. Segel. Incorporation of recepter kinetics into a model for bacterial chemotaxis. *J. Theor. Biol.*, 57:23–42, 1976.

[80] L. A. Segel. Mathematical models for celluar behavior. In *Studies in Mathematical Biology (vol 15 I)*, pages 156–190. Mathematical Association of America, 1978.

[81] L.A. Segel and J. Jackson. Dissipative structure: an explanation and an ecological example. *J. Theor. Biol.*, 37:545–559, 1972.

[82] A. Sih. Optimal foraging: partial consumption of prey. *Am. Nat.*, 116:281–290, 1980.

[83] G. D. Smith. *Numerical Solution of Partial Differential Equations: Finite Difference Methods.* Oxford University Press, Oxford, 3 edition, 1985.

[84] J. Smoller. *Shock Waves and Reaction–Diffusion Equations.* Springer Verlag, New York, 2 edition, 1994.

[85] J. H. Steele and E. W. Henderson. A simple plankton model. *Am. Nat.*, 117:676–691., 1981.

[86] J. H. Steele and E. W. Henderson. The role of predation in plankton models. *Journal of Plankton Research*, 14:157–172., 1992a.

[87] J. H. Steele and E. W. Henderson. A simple model for plankton patchiness. *Journal of Plankton Research*, 14:1397–1403., 1992b.

[88] J. C. Strikwerda. *Finite Difference Schemes and Partial Differential Equations.* Wadsworth, Inc., California, 1989.

[89] S. H. Strogatz. *Nonlinear Dynamics and Chaos : With Applications to Physics, Biology, Chemistry, and Engineering.* Reading, Mass. : Addison–Wesley Pub., Cambridge, Massachusetts, 1994.

[90] P. Turchin and P. Kareiva. Aggregation in aphids varians: An effective strategy for reducing predator risk. *Ecology.*, 70:1008–1016, 1989a.

[91] Peter Turchin. *Quantitative Analysis of Movements: Measuring and Modeling Population Redistribution in Animals and Plants.* Sinauer Associates, Sunderland, Mass., 1998.

[92] Peter Turchin. *Complex Population Dynamics.* Princeton University Press, Princeton and Oxford, 2003.

[93] R. Tyson, S. R. Lubkin, and J. D. Murray. A minimal mechanism for bacterial pattern formation. *Proc. Roy. Soc. London*, 266:299–304, 1999.

[94] R. Tyson, S. R. Lubkin, and J. D. Murray. Model and analysis of chemotactic bacterial patterns in a liquid medium. *J. Math. Biol*, 38:359–375, 1999.

[95] R. Tyson, L. G. Stern, and R. J. LeVeque. Fractional step methods applied to a chemotaxis model. *J. Math. Biol.*, 41:455–475, 2000.

[96] S. V. Viscido, M. Miller, and D. S. Wethey. The response of a selfish herd to an attack from outside the group perimeter. *J. Theor. Biol.*, 208:315–328, 2001.

[97] S. V. Viscido and D. S. Wethey. Quantitative analysis of fiddler crab flock movement: evidence for 'selfish herd' behaviour. *Anim. Behav.*, 63:735–741, 2002.

[98] J. A. Vucetich, R. O. Peterson, and C. L. Schaefer. The effect of prey and predator densities on wolf predation. *Ecology*, 83(11):3003–3013, 2002.

[99] P. J. Wangersky. Lotka–volterra population models. *Ann. Rev. ecol. Syst.*, 9:189–218, 1978.

[100] E. Zauderer. *Partial Differential Equations of Applied Mathematics.* Wiley-interscience, New York, 2 edition, 1989.